DISSERTATION

CONTROL OF POLYMER NETWORK STRUCTURE AND DEGRADATION

Submitted by

Ima Yaghoubi Rad

Department of Chemical and Biological Engineering

In partial fulfillment of the requirements

For the Degree of Doctor of Philosophy

Colorado State University

Fort Collins, Colorado

Fall 2017

Doctoral Committee:

Advisor: Matthew J. Kipper
Co-Advisor: Jeffrey W. Stansbury

Susan P. James
Travis S. Bailel

ABSTRACT

CONTROL OF POLYMER NETWORK STRUCTURE AND DEGRADATION

This thesis presents work performed evaluating controlled degradation in polymeric networks via incorporation of nanogels either as precursor or as a component of pseudo-interpenetrating polymeric networks. These polymeric crosslinked nanoparticles have applications in drug/gene delivery, cell imaging, and inert or functional prepolymer nano-fillers, therefore controlling their molecular weight (size) and structural properties are mandatory requirements. In addition to the primary effects of reactant selection on the nanogel formation, the solvent used and the agitation rate can provide additional parameters to control nanogel size.

This work also develops a practical understanding of polymer characteristics and degradation kinetics of networks constructed from reactive nanogels with regio-specifically degradable linkages. Analogous non-degradable control structures are also prepared for each experimental condition. Clear, monolithic photopolymers are prepared from 50 wt% solvent-based dispersions of the reactive nanogels. The results of equilibrium swelling, mass loss, and compressive modulus (dry/swollen) demonstrate interplay between hydrophilic/hydrophobic effects, labile linkage location, and the crosslinking density that appears to dominate many of predicted property trends. The introduction of hydrolytically degradable linkages (PLA) into the internal crosslink structure of the nanogel promotes greater hydrophobic character compared to PLA

placement in external reactive side chains. Consequently, nanogel-based networks with shorter hydrophilic crosslinker and lower crosslinker concentration show lower mass swelling rate, higher Tg, and lower compressive modulus reduction. Nanogels unlock an immense potential in designing superior alternatives for accepted materials with significantly reduced network heterogeneity compared to conventional hydrogels, which ultimately appoint them as novel candidates for controlled drug delivery and tissue engineering applications. Another part of this work demonstrates the effects of nano-scale pre-crosslinked hydrophobic particles as additive to model labile monomer on hydrolytic degradation. The modification of hydrolytically vulnerable polymers through the intimate integration of secondary networks based on styrenic nanogel structures is intended to reduce or even eliminate hydrolytic degradation potential. Nanogel addition at any level produces reduction in network swelling and mass loss proportional to nanogel content. The flexural modulus and ultimate transverse strength of nanogel-loaded resin monomer (TEGDMA) does not change compared to neat resin homopolymer as one control material in addition to the homopolymer of PEG_{2000}PLADMA, which includes polylactic acid segments in the crosslinks. The use of a monomer-swollen highly crosslinked hydrophobic nanogel offers a versatile platform from which hydrolytic and potentially enzymatic degradation can be suppressed in a variety of applications such as polymer-based dental restoratives while retaining resin formulation, handling and mechanical properties.

Some of the most important challenges in processing high performance materials are their high viscosity and limited solubility as a result of high molecular weight, intermolecular interactions, and rigid monomeric structure. Alternatively, high strength

thermoset materials formed by ambient photopolymerization are limited in their performance by incomplete, vitrification-limited conversion, and relatively low glass transition temperature. In non-biological applications, significant effort has been focused on improving processing techniques and advanced machinery, and notably trivial attention has been paid to upgrade molecular structure of the resins. On the other hand, in biological applications photocuring is the perfect choice since applying high temperatures is practically impossible. As a result, another objective of this work was to develop an alternative photocurable material with enhanced processability, yet retaining thermal and mechanical properties of conventional resins. The average diameter of these polymeric particles is less than 20 nm with glass transition temperatures greater than 200 °C. These paradoxical properties trace back to molecular-level rearrangements of the same monomeric building blocks used in current thermoplastic/thermoset resins.

ACKNOWLEDGEMENTS

This is the best opportunity to thank and express my gratitude, in writing, to many wonderful individuals who have instructed and supported me throughout this journey.

First and foremost, I would like to thank my advisor and mentor, **Dr. Jeff Stansbury**, Professor and Associate Dean for Research at UC Anschutz, School of Dental Medicine. I sincerely appreciate all his contributions of time, vast knowledge, wisdom, novel ideas, and funding to make my PhD experience productive and stimulating. Observing his humble and graceful leadership has taught me lifetime lessons on empowering human resources and effective problem solving not only in research but also in life. His lab has always been an ultimate scientific playground for numerous students and postdocs to perform outstanding research. It is a great honor to be his PhD student.

I wish to thank my co-advisor, **Dr. Matt Kipper**, Associate Professor of CBE department at CSU, for accepting me into the graduate program and his team. He has been a great source of knowledge and guidance throughout my PhD. For him, my progress and success had the same priority as his main students. Being exposed to his fascinating research projects helped me to obtain a broader perspective towards the importance of material science in tissue engineering applications. Thanks to my committee members, **Dr. Sue James**, Professor and Department Head of ME, and **Dr. Travis Bailey**, Associate Professor of CBE department at CSU, for sharing their invaluable expertise. I truly appreciate the help obtained from incredible staff and faculty members at CSU and UC Anschutz, who instructed and trained me in different techniques and instruments and allowed me to use their facilities. These include: **Dr. Devatha Nair**,

Dr. Clifton Carey from School of Dental Medicine at UC Anschutz; **Dr. Jiancheng Liu** and **Dr. Parag Shah** from CBE department at UC Boulder; **Dr. Roy Geiss**, **Dr. Pat McCurdy**, and **Dr. Ellen Brennan-Pierce** from Central Instrument Facility at CSU; **Steven Lewis** and **Matt Barros** from Stansbury laboratory at UC Anschutz. I recognize the support and help received from all members of CBE department at CSU and School of Dental Medicine at UC Anschutz, in particular **Dr. David Dandy**, **Claire Lavelle**, and **Laurine Szymanski**. I also thank Colorado State University, University of Colorado, National Institutes of Health, and taxpayers for financing the research presented here.

Special thanks go to my dear colleagues and friends for helping me with research and supporting me mentally and emotionally through these years, in particular **Dr. Valéria Bisinoto Gotti**, **Dr. Bruna Fronza**, **Dr. Sara Darvishi**, **Dr. Maciej Podgórski**, **Kristin Simboski**, **Rebecca Roberts**, **Danielle Jones**, **Whitney Setterberg, Mahin** and **Essi Shahmardian**, **Shahriar Shahmardian**, **Farid** and **Golnar Babazadeh**, **Sheida** and **Dr. Mahmoud Azimi**, **Giti** and **Dr. Mona Mirsiaghi**, **Massi** and **John Gray**, **Nasrin** and **Farhad Zandi**, **Mahsa** and **Dr. Ali Tasdighi**.

Finally, everlasting gratitude goes to my beloved husband **Dr. Kamran Eftekhari Shahroudi**, my lovely parents and siblings **Shirin**, **Javad**, **Ava**, and **Pouya Yaghoubi Rad**, and my beautiful grandmother **Zara Nategh** for their unconditional love, endless support, and encouragement to pursue my dreams. Also, a very special bless goes to my late uncle **Hamed Yaghoubi** for being the greatest chemical engineer role model I have ever known.

DEDICATION

For my beloved Kamran
my best friend, my happiness, and my source of energy

and

my lovely parents
Shirin & Javad

TABLE OF CONTENTS

CHAPTER 1

INTRODUCTION

1.1. Motivation

Based on extensive research in the past few decades since the introduction of reproducible and predictable drug-release concept by Alejandro Zaffaroni (a pharmaceutical chemist) and Judah Folkman (a medical doctor at Harvard University) in the late 1960s (Hoffman, 2013), polymeric nano/micro particle delivery systems have emerged as the preferred drug carriers over conventional methods in terms of targeted and controlled delivery superiority. In this regard, polymeric nanoparticles have additional advantages compared to microparticle counterparts such as limited dose-induced toxicity, higher surface to volume ratio for multi-conjugation and hindering burst release, and ability to carry small molecules (i.e. chemotherapeutic agents). Yet, there are still major challenges to be addressed including their size and surface chemistry optimization for deep tissue (i.e. tumor) penetration, as Langer et al. have predicted in 2014: *"The future research should focus on intracellular delivery".* Systematic introduction of biodegradable linkages to the structure of the polymeric carrier for utilizing diffusion, as the main mass transport mechanism in a more controlled fashion, is another important factor in designing modern drug delivery systems (Mitragotri, 2014). Tuning the elasticity and stiffness of the polymeric nanoparticles is another challenge that needs particular attention, for instance, cell internalization favors stiffness, on the other hand, prolonged blood circulation favors elasticity, therefore a facile synthetic route that allows to adjust elastic properties without

changing the monomeric constituents and increasing the optimal size is highly beneficial (Anselmo, 2017). Degradable tissue scaffold engineering is another biomedical field that controlled-degradation plays a crucial role for successful tissue regeneration and elimination of the unfavorable scaffold removal procedure. The rate of scaffold degradation not only should match the rate of tissue formation, but also should be designed in a way that maintains the scaffold mechanical integrity until the formed tissue is structurally robust. Current approaches in forming degradable scaffolds include *in situ* free-radical polymerization (particularly photopolymerization as a preferred route) of vinyl-functionalized PEG-*co*-PLA copolymers. In spite of its popularity, the crosslinked scaffolds suffer from a marked level of heterogeneity in their crosslinking density distribution in a length scale of 10-100 nm, which ultimately results in much lower mechanical properties and unpredictable catastrophic degradation.

Any proposed solution for the aforementioned challenges is subjected to a stringent FDA approval limitation, therefore a novel class of nano polymers that are processable, soluble in aqueous media, more biologically active (size in the lower end of nanometer scale), can be used as precursors for macroscopic network formation with decreased level of heterogeneity, display variable physiochemical properties, and only uses PEG, PLA, or other extensively tested polymers (i.e. PGA, PCL) will be in the front row to be commercialized (Manavitehrani, 2016).

1.2. Free-Radical Polymerization

Free-radical polymerization is by far the most widely used process for forming polymeric materials. Free radicals are readily produced from a variety of convenient initiation schemes and as neutral reactive species, they are compatible with a tremendous range of predominantly vinyl-based monomers. Initiation of polymerization is highly efficient in this chain growth process, where the π-bond of carbon-carbon double bond in vinyl monomers is opened homolytically by a reactive radical species to create a new radical, followed by the addition of many monomers to that center by a chain-type kinetic mechanism, until polymer growth is terminated at some point by destruction of the reactive center. The average degree of polymerization depends on the frequency of addition steps relative to termination steps. High-molecular-weight polymer is produced immediately, and the molecular weight of polymer product is only modestly affected before reaching high extents of conversion. Radical chain polymerization is a chain reaction consisting of a sequence of four steps, initiation, propagation, chain transfer, and termination, which all can proceed and compete simultaneously. An important characteristic of free-radical polymerization is the onset of autoacceleration (Trommsdorff effect), which is due to decreased rate of termination relative to propagation that overcomes the expected reduction in rate, linked with decreasing reactive group concentration as monomer is consumed (Odian, 2004; Hiemenz, 2007).

1.2.1. Thermal Initiation

Polymerization through thermal decomposition of an initiator to produce radicals is a common strategy employed to induce radical polymerization. Peroxides, hydroperoxides, and related structures are regularly used as thermal initiators due to the

inherent weakness of the O-O bond. Alternatively, azo compounds, such as 2,2'-azobisisobutyronitrile (AIBN), also serve as another generally used class of thermal initiators. The homolytic dissociation of AIBN results in formation of 2 identical radicals and nitrogen molecule (Eq. 1.1),

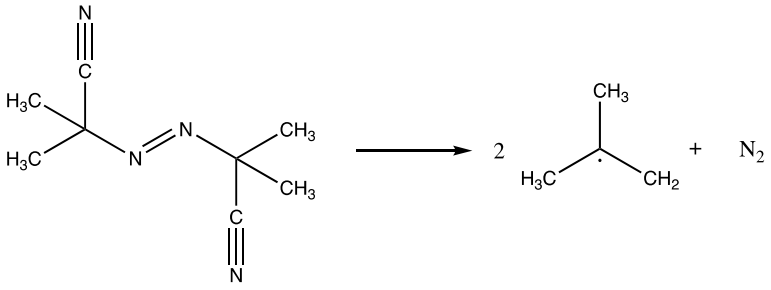

(1.1)

The C-N bond dissociation energy is high (~290 kJ/mol), but the driving force for homolysis of AIBN is the formation of highly stable nitrogen molecule. The half-life ($t_{1/2}$) of AIBN at 50, 70, and 100 °C is 74 h, 4.8 h, and 7.2 min, respectively, thus if extended reaction times at high temperatures are required to achieve high conversion, it would be necessary to add additional AIBN during the reaction, or alternatively select from a wide variety of commercial initiators that provide well controlled radical production rates from over a large range of temperatures. The monomer impurities such as peroxides with weak O-O bond can also create radicals via thermal homolysis and initiate polymerization (i.e. styrene, methyl methacrylate). In thermolysis the two radicals are produced in a solvent cage that promotes direct recombination, thus their diffusion out of the cage is a rate-limiting step for producing the effective chain-initiating radicals IM□ (the cage effect is the result of formation of 2 radicals at once regardless of the energy source). By increasing the viscosity during the course of polymerization, the lifetime of radicals in the solvent

cage increases, leading to higher probability of radical-radical recombination. For AIBN, *f* (initiator efficiency) in the polymerization of styrene decreases from 0.75 at conversions up to 30% to 0.20 at 90-95% conversion (Odian, 2004; Hiemenz, 2007). Important applications of thermal radical polymerization are solution polymerization of micro- (Oh, 2009) and nano-gels (Liu, 2012, 2014), thermosetting polymers (Pascault, 2002), and surface-initiated coating (Huang, 2001).

1.2.2. Photochemical Initiation

Photochemical polymerizations occur when radicals are produced by light irradiation (i.e. ultraviolet, visible) as the energy source. There are two basic types of radical initiation via photochemical processes. In type I, the photoinitiator absorbs the energy of the photons (excitation step) and consequently decomposes into at least two radicals, which may differ in their initiating efficiency. For type II initiators, a photosensitizer absorbs the energy, then it interacts with the second compound (either by energy transfer or redox reaction) to form radicals (Odian, 2004). The type I is typically used for UV and type II for visible light initiation where the lower energy photons may not be sufficiently energetic to promote direct homolysis of an initiator (Kim, 2009; Chatani, 2014).

According to the Jablonski diagram, when photon(s) is absorbed by a molecule (i.e. photoinitiator), a valence electron from its ground state (S_0) is promoted to its singlet excited state (S_1). From this point on, the excited electron can either relax and deactivate to (S_0) through heat dissipation and/or fluorescence (radiative decay), or alternatively go to a lower energy excited state (T_1) by changing its spin angular momentum (intersystem crossing). From the longer-lived triplet state (T_1), the free radical can either deactivate

through heat dissipation, another radiative decay process called phosphorescence, transfer its energy to another molecule (i.e. type II), or alternatively react with monomer to promote the desired photo-activated polymerization process (chatani, 2014). The efficiency of initiation reaction is governed by both primary radical production and first monomer addition to the primary radical (initiating radical formation). Our main focus here will be on the type I radical initiation. For a photon to be absorbed by the initiator: (i) the spectral emission of the light source and the absorption spectra of the photoinitiator must overlap, and (ii) the absorbed photon must have sufficient energy to cause the desired reaction (Chatani, 2014).

Photopolymerization has several advantages compared to other types of radical polymerizations due to spatial (i.e. confined to specific regions) and temporal (i.e. on and off switch) controllability, fast initiation rate due to different radical formation processes compared to thermal initiation, ambient temperature curing, and solvent-free formulations, which is highly desirable in terms of economic and environmental aspects.

The significant disadvantage of photopolymerization is that the penetration of light through optically thick, opaque or colored materials is low, and it may yield a gradient in reation rates that can in turn introduce a structure/property gradient throughout the bulk of the material. Thus, photopolymerization is best suited for transparent surfaces or relatively thin films, although light penetration potential is significantly altered by the wavelength of light being transmitted as well. Also, since oxygen is extremely reactive with free radicals, oxygen inhibition manifests its presence on any exposed surface layer of a polymerization (thickness of the inhibited layer depends on the viscosity and the rate of the polymerization reaction relative to the rate of oxygen diffusion). For instance, this

inhibition causes a tacky top layer in dental restorations. Photopolymerization is widely used in ultrafast drying of varnishes, printing inks, coatings, adhesives, photoimaging, photolithography, holography, 3D printing, curing dental restorations, nanogel synthesis, and biomaterials (Odian, 2004; Moraes, 2011). There are some serious concerns raised regarding bio-applications of photopolymerization due to the adverse effects of UV or even visible light on cells. This is largely addressed by selecting lower energy visible or even near-infrared wavelengths with appropriate initiating systems, or by using efficient UV initiators that can provide adequate polymerization activity with the application of brief, low irradiance UV irradiation.

1.2.3. Bulk Polymerization

Bulk polymerization is the simplest method for polymerizing neat monomer or comonomer mixtures with minimum contamination. It has commercially been used for polymerization of ethylene, styrene, methyl methacrylates and many others, yet its applicability at industrial scale for production of thick parts is highly limited, due to several disadvantages: (i) it requires careful temperature control due to the exothermic polymerization reaction and the thermal insulation properties of polymers that result in ineffective heat dissipation, (ii) gel effects and high viscosity even at low conversions, (iii) needs powerful stirring equipment due to (i) and (ii) problems, (iv) degradation and discoloration due to local hot spots, (v) increased rate of chain transfer to polymer, which causes branching and ultimately alters the properties of the final product (broader molecular distribution), (vi) in the case of bulk crosslinking polymerization, hot spots can occur due to extensive localized cyclizations, which consequently results in heterogeneous crosslinking distribution, and much lower mechanical properties (Ahmed,

2015), and (vii) in the case of uncontrolled autoacceleration, it can lead to disastrous reactions. Bulk polymerization is considered one type of homogeneous polymerization, yet during the reaction it can turn into a heterogeneous type due to low solubility of the polymer product in the initial monomer media. On the other hand, it is suitable for bench-scale research, coatings, composite materials such as dental restorations, high performance materials (i.e. thermoplastics, thermosets) (Pattanayak, 2005), optical materials (Lü, 2006), ring-opening polymerization of lactones (Albertsson, 2003), and *in situ* formation of hydrogels (Ahmed, 2015).

1.2.4. Solution Polymerization

Solution polymerization of a monomer in a solvent has major advantages over bulk polymerization: (i) solvent dilutes the media and lowers the viscosity, thus stirring is much easier, and (ii) solvent acts as a heat sink and conductor to reduce the exotherm effects, thus thermal control is dramatically improved (Matyjaszewski, 2002; Odian, 2004). The common problems with solution polymerization are the compatibility of solvent-monomer and solvent-polymer, chain transfer to solvent, impurities, and separation of the polymeric products from the solvent. The solution polymerization can be performed either in homogeneous or heterogeneous form, as will be discussed in the next two sections.

The most important requirement for homogeneous solution polymerization is that the initiator, all monomers, and the formed polymer product should be soluble or a stable dispersion in the reaction medium (Qiu, 2001). The molecular weight of the particle is controlled by chain transfer concentration, initiator concentration, temperature, and solvent to monomer ratio. In the case of free-radical crosslinking, the sol fraction is also soluble in the medium, therefore it is not trapped inside the particle network, and the

material is porous due to the swollen state of the particles. In industrial-scale, solution polymerization is generally chosen when the polymer solutions are used directly as the final product (i.e. solvent-based coatings).

In heterogeneous solution polymerization, the compatibility of monomer-solvent and polymer-solvent is not the first requirement anymore, thus the limitation on the choice of monomer and solvent is no longer valid, particularly for polymerization in aqueous medium, which is highly desirable in an industrial scale (Qiu, 2001). There are four types of heterogeneous solution polymerizations: suspension, emulsion, dispersion, and precipitation. Heterogeneous polymerization processes occur in a two-phase system in which the monomer(s) and/or polymer products are in the form of fine dispersion in an immiscible medium. Our focus here is particularly on emulsion polymerization, which is based on emulsifying the insoluble/partially soluble monomer(s) in a solvent (i.e. colloidal dispersions) and transforming it to polymer particles.

The main components in emulsion polymerization are the monomer(s), dispersing medium (i.e. water), emulsifier (surfactant), and medium-soluble initiator. For instance, if the dispersing medium is water, then the surfactants are arranged as micelles with their hydrocarbon portion pointed towards the interior of the micelle and their ionic ends outward toward the aqueous phase. Small portion of the monomers enter into water and the micelles, and the major portion (>95%) is dispersed as monomer droplets with size range of 10^3-10^5 nm. Since the initiator is water-soluble, then primary radicals are generated in the aqueous phase. The nucleation (formation of initiating radicals) also happens in the aqueous phase by reaction between primary radical and solubilized monomer molecule, then the initiating radical enters into the micelle (reaction site), where

diffusion is the rate limiting process, as a consequence the concentration of radicals inside each micelle is much lower than the homogeneous solution. Therefore, high molecular weight polymers are obtained in each micelle at the same time that the overall reaction rate is high as well due to large number of micelles. During the reaction, the monomer droplets provide monomer molecules in the aqueous phase, which ultimately end up in the micelles, yet there are almost no reaction happening inside the monomer droplets themselves. The size of the polymer particles depends on many factors such as the agitation rate, surfactant and initiator concentration, solubilized monomer concentration, and reaction temperature since increasing the temperature increases the nucleation rate and ultimately reduces particle size (Arshady, 1992; Tobita, 1992, 2000; Odian 2004).

One of the main physical advantages of this type of polymerization is that the product (latex) can be used directly without further separations (when monomer droplets are fully consumed). It also has a significant advantage in terms of polymerization kinetics, which is the ability to simultaneously attain both high molecular weights and high reaction rates. Some of the disadvantages of emulsion polymerization are particle stabilization and size control particularly when particles with less than 100 nm are desirable, particle instability (coagulation) at high crosslinker concentrations, surfacnt removal, and surfactant critical temperature (Odian, 2004).

1.3. Crosslinked Polymeric Networks

To form a crosslinked polymer (3-D network) via free-radical polymerization, it is necessary to have at least one divinyl monomer known as the crosslinker (Dušek, 2000). A crosslinked polymer is a material in which polymer chains are linked together via

covalent bonds (crosslinkers) to create a single molecule with an infinite molecular weight (Hiemenz, 2007). Elastomers and thermosets are subclasses of 3-D polymeric networks. The former has relatively low crosslinking density (number of crosslinks per unit volume) and undergoes glass transition below room temperature, thus it is a deformable and soft solid (i.e. rubber band). The latter, on the other hand, is a non-defomable polymer network with high crosslinking density and high glass transition temperature (i.e. dental restorations).

A crosslinked network structure has different elements (Dušek, 2000; Hiemenz, 2007): (i) strand, is a segment of polymer chain that begins from one junction and ends at another without any junctions in between, and (ii) junction, is a crosslink that not only connects two polymer chains (backbone) but also is connected to the rest of the network. The functionality of a junction is equal to the number of strands diverging from it, which depends on different factors such as functionality of the crosslinker, the reactivity of the functional groups, and crosslinker concentration. Although, secondary cyclizations are responsible for multi-strand junctions or super junctions, here we have to note that not all junctions are active, only junctions with functionality of 3 are considered active, less than 3 is considered inactive since the chains can relax under deformation, and more than 3 chains, is considered active but their contribution is equivalent to one active junction (Dobson, 1965). Dangling end, is a section of the polymer backbone that starts from the last junction and does not end with another junction (it dangles), therefore each backbone chain has 2 dangling chain ends, and since they are only attached to the network from one end, they have enough degrees of freedom (conformations) to relax over time under stress, therefore they dissipate the elastic energy and do not contribute to the equilibrium

elasticity of the network (they are considered as network defects). Loop, is a section of the backbone chain that begins and ends at the same junction, which is the result of primary cyclizations (Matsumoto 1995), and since they can partially relax under stress, they are also considered as network defects. Sol fraction is another component of a crosslinked network that includes the trapped oligomers, free monomers, and/or solvent. The sol fraction is extractable after immersing the network in a good solvent, and is an intrinsic characteristic of crosslinked networks via free-radical polymerization. The gel effect is another important property of a crosslinked network, which is the result of autoacceleration onset and diffusion-controlled termination by combination (Dušek, 2000). At gel point, covalent bonds are percolated from one end to the other end of the sample container without interruption and the resulting gel is insoluble in any solvents (Matsumoto, 1995; Hiemenz 2007).

The random nature of free-radical polymerization creates a lot of complexity by forcing each active polymer chain to experience a different history of crosslinking and cyclization, which results in the formation of a crosslinking density distribution in the network. Flory-Stockmayer's gelation theory predicts the gel point (the extent of reaction at the onset of infinite network formation) of an ideal network, by assuming equal reactivity for all vinyl groups in the system, all double bonds react independently, and no cyclization reactions in finite polymer chains. However, the gel point is substantially delayed (~1-3 orders of magnitude) in real crosslinked polymers, when the concentration of di- or multi-vinyl monomer exceeded even fractions of 1 mol%. This non-ideality arises from (i) the increased reactivity of pendant double bonds compared to monomers at lower conversions due to their higher local concentration compared to that of in solution or bulk,

and close proximity to the active center (controlled by chain segment statistical conformation), and (ii) decreased reactivity of pendant double bonds at higher conversions due to steric suppression or thermodynamic excluded volume effect. The combination of these effects gives rise to the formation of primary and secondary intramolecular cyclizations, creating loops and multiple crosslinks, respectively. As it was mentioned before, loops and multiple crosslinks are considered network defects (ineffective crosslinks) (Dušek, 1984), since they consume pendant double bonds but do not contribute to the formation of infinite network, although in terms of storing elastic energy, the contribution of multiple crosslinks is considerable compared to loops (Tobita, 1992; Matsumoto, 1995, 1999; Funke, 1998; Dušek, 2000; Hiemenz, 2007).

In bulk crosslinking, as soon as a primary radical propagates through the nearest monomers, extensive local cyclizations begin, which ultimately results in the formation of dispersed highly compact nanogel clusters at the early stages of reaction (stiff segments of the network), then macroscopic gelation occurs by a lower concentration of crosslinks between the dispersed still-growing nanogels/microgels (softer segments of the network reside between the microgel domains), since steric hindrance and excluded volume effects make the interior pendant double bonds much less accessible, therefore the final network possesses a pronounced heterogeneous spatial distribution of crosslinks in the length scale of 10-100 nm (Leicht, 1981; Dušek, 2000; Di Lorenzo, 2015). Furthermore, the degree of heterogeneity increases by higher ratio of divinyl to monovinyl monomer, divinyl reactivity, swelling (excluded volume effect), and temperature. This nanostructural heterogeneity in real crosslinked networks manifests itself in substantial behavioral and property deviations from an ideal network described by Flory, such as heterogeneous

swelling ratios, which is higher than predicted by Flory-Rehner equation, and much lower elastic and elongation properties compared to the prediction of rubber elasticity theory (Flory, 1985; Hiemenz, 2007; Di Lorenzo, 2015). The schematic presentation of a heterogeneous crosslinked network is shown in Fig. 1.1.

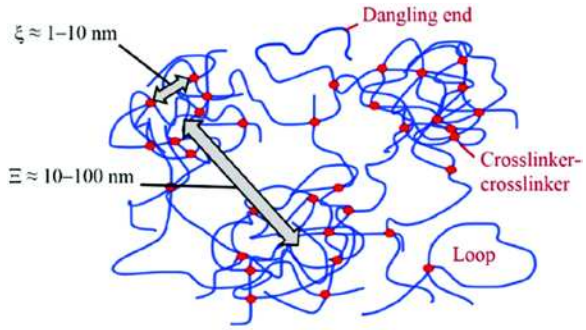

Figure 1.1. Heterogeneous crosslinked network via free-radical polymerization of di- or multi-functional monomers; ξ and Ξ represent a typical mesh size and a typical length scale of spatial distribution of crosslinking density (Adapted from Di Lorenzo et al. 2015).

1.3.1. Methacrylate and Styrenic Monomers

Methacrylate monomers are the building blocks of various polymeric materials, either as homopolymer (i.e. poly(methyl methacrylate) (PMMA)), or as copolymers (i.e. poly(methyl methacrylate-*co*-styrene)). Methyl methacrylate is the most common of the methacrylate ester monomers, since its homopolymer (PMMA) and copolymers have been used in numerous applications such as aircraft windows, lenses, bathtubs, optical fibers, dentures, dental filling materials, and contact lenses (hard and soft). PMMA has high strength, high dimensional stability (rigid polymer backbone), optical clarity, and weatherability. It is also resistant to impact, chemicals (i.e. organic solvents), and relatively high temperatures (Davy, 1997; Odian, 2004). Methacrylate polymers can be produced via bulk polymerization (i.e. casting process) to obtain rigid materials, or via solution and emulsion polymerization for nonrigid applications. Divinyl methacrylates

such as bisphenol A glycidyl methacrylate (BisGMA), urethane dimethacrylate (UDMA), triethyleneglycol dimethacrylate (TEGDMA), and 2-hydroxyethyl methacrylate (HEMA) are extensively used in dental (Stansbury, 1990; Ge, 2005; Cramer, 2011) and biomedical applications (i.e. bone cements) (Davy 1997) due to their excellent mechanical properties, rapid free-radical polymerization (i.e. photopolymerization), and relatively low cytotoxicity (Yoshii, 1997), yet they suffer from a very large volume contraction (shrinkage), unless they are modified (Ge, 2005), incomplete conversion due to their vitrified/glassy network structure, water uptake, and acid/base- and enzyme-catalyzed hydrolysis due to their inherent structural ester groups (Santerre, 1999; Ferracane, 2006; Hennink, 2012).

While polystyrene is a commodity polymer, majority of higher-performance styrenic polymers are copolymers or blends due to the brittle, low impact resistance of polystyrene. Some of the notable styrenic copolymer materials are: SBR (styrene-*co*-1,3-butadiene rubbers) used in tires, and latex paints; high-impact polystyrene (HIPS); and crosslinked styrene-*co*-divinylbenzene materials used in size-exclusion chromatography and ion-exchange resins (Odian, 2004). Due to the hydrophobic character of styrene (all-carbon structure), it has been copolymerized with hydrophilic methacrylates (i.e. HEMA) to control water uptake and wettability (Okano, 1978). Styrene is also used as a comonomer in conjugation with natural polymers (i.e. polysaccharides) to control their biodegradability (i.e. resistance to enzymatic attacks) (Dizge, 2009; Hernandez, 2011; Ahmed, 2015). Poly(styrene-*b*-isobutylene-*b*-styrene) (Quatromer^{TM}) has been proposed to be used in trileaflet heart valve due to its oxidative stability, hemocompatability, and mechanical durability (Gallocher, 2006; Harm, 2014; Brubert, 2016).

1.3.2. Copolymerization of Methacrylic and Styrenic Monomers

Mayo et al. showed (1944) that in free-radical copolymerization of styrene and methyl methacrylate at 60 °C in benzene with 0.1 mol% of benzoyl peroxide, the reactivity ratios of both radicals are independent of the monomer mixture, the extent of conversion, the rate of polymerization, and the presence or absence of benzoyl peroxide as initiator. They showed that styrene and methacrylate radicals, both have significant preference to undergo crossover to add to methyl methacrylate and styrene monomers, respectively, with the final product of random copolymer tending towards an alternating structure (Kotani, 1998; Gao, 2011). They also observed that this preference was strongly dependent on the nature of the initiator (Mayo, 1944; Gao, 2011). For instance, when they used stannic chloride (an initiator for cationic polymerization) instead of benzoyl peroxide, the product was almost exclusively polystyrene, which is due to higher electron donating effect of benzene ring in styrene compared to that of methyl group in methyl methacrylate (Mayo, 1944; Odian, 2004). Styrene is distinctive as one of relatively few monomers that can be polymerized by either anionic, cationic or radical polymerization mechanisms. Scott et al. (2002, 2008) has demonstrated a class of impressive high-performance styrene/methacrylate copolymer known as vinyl ester, based on the copolymerization of BisGMA and styrene.

1.3.3. Interpenetrating Polymer Networks

Interpenetrating polymer networks (IPN) refer to polymeric materials that consists of two polymers, each in an interwoven crosslinked form with the other network. The IPN morphology can display varying degrees of heterogeneity. There are two main classes of IPNs, (i) simultaneous IPN, when the mixture of both monomers are polymerized and

crosslinked simultaneously, and (ii) sequential IPN, when polymer I is crosslinked first, then its network is swollen by monomer II, and afterwards monomer II is crosslinked (Sperling, 1981). One of the important applications of interpenetrating polymer networks is IPN composite hydrogels based on natural and synthetic polymers. These hydrogels are able to respond rapidly to 2 or 3 external stimuli, display superior mechanical properties (i.e. ionic IPNs), promote multi-component drug delivery, and have a high adsorption capacity and reusability (Matricardi, 2013; Dragan, 2014). The initial stage of IPN formation (mixing the monomers or swelling the first network with the second monomer) must be thermodynamically feasible (interaction parameter $\chi < 0$) to avoid gross phase separation, yet after the IPN is formed, any further microphase separation is extremely limited due to high viscosity and the high level of physical entanglements between two networks (Lipatov, 2007).

1.4. Degradable Hydrogels

Hydrogels are highly water-swollen 3-D polymeric networks consisting of physical and/or covalent crosslinks that resemble biological tissues, thus due to their biomimetic character they are highly desirable in biomedical applications. The covalent crosslinking in hydrogels can be obtained by radical polymerization (i.e. photopolymerization), chemical reactions of complementary groups such as amine-carboxylic acid or isocyanate-OH/NH_2, high-energy radiation (i.e. gamma, electron beam) to create radicals, or crosslinking via enzymes (Hennink, 2012). Physical crosslinking can be introduced by: (i) ionic interactions, (ii) hydrogen bonding, (iii) hydrophobic interactions, (iv) crystallinity, (v) polymer chains entanglements, and (vi) combination of two or more of the aforementioned interactions (Raemdonck, 2009; Hennink, 2012; Hoffman, 2013). The

main advantage of physical crosslinking is that the use of toxic agents (i.e. initiators) is avoided, although the hydrogel stability is strongly dependent on the environmental conditions and any equilibrium processes. Therefore, physical crosslinked hydrogels are prone to leakage and loosing any loaded drug or other molecules with poor control even before reaching their intended target.

On the other hand, among the chemical crosslinking mechanisms, the radical polymerization and high-energy radiation are fast and can be done in biocompatible conditions, although when the latter process is used, the tissue need to be soaked with antioxidant due to the high concentration of generated radicals, therefore, the radical polymerization route remains as a desirable alternative. Photopolymerization particularly has superior advantages over thermal radical polymerization due to spatial and temporal control including rapid on-demand curing under ambient conditions. Hydrogels can be classified as non-degradable or degradable, and the latter has several sub-classes, including hydrolytically or enzymatically degradable hydrogels. Our focus here is on degradable hydrogels crosslinked via free-radical polymerization of mono- and di-vinyl monomers with imbedded hydrolytically labile groups. It is important to reiterate that crosslinked hydrogels via free-radical polymerization are intrinsically heterogeneous, as it was discussed earlier. However, in applications based on diffusion of a rigid nanoparticles or flexible linear chains through a non-degradable hydrogel system, different heterogeneity levels have shown no significant effect on diffusion time if it is measured on the micro-scale and beyond (Di Lorenzo, 2014; Walta, 2017), although this is not true for degradable hydrogels. The main applications of degradable hydrogels are in controlled drug delivery and tissue engineering scaffolds, since degradable hydrogels

not only can carry drugs or other molecular cargo based on physical interactions, but also the drug molecules can be covalently attached to the hydrogel network and be released through connecting bond cleavage. In addition, the need to invasively remove the tissue scaffold in bioengineering applications is eliminated by using degradable hydrogels.

The rate of scaffold degradation should ideally mirror the rate of new tissue formation but this is a significant problem especially if a certain threshold mechanical preoperty target must be maintained. This application-based tuning of the type and rate of degradation, nature and size of the degradation by-products, and the guarantee of mechanical properties as degradation proceeds has introduced new challenges in this field. The most studied degradable hydrogels are the free-radical crosslinked networks of B-A-B block copolymers of polyethylene glycol (PEG) (A) and polylactide (PLA) (B) with (meth) acrylate end-functionalities. Other approaches have used thiol-ene polymerizations, star polymers as macromers along with several other approaches that can accommodate relatively dilute aqueous solution polymerization conditions to yield water-swollen gels with adequate properties. PEG and PLA have been used successfully in number of validated implants and are safe, non-toxic, biocompatible, and FDA approved (Drury, 2003). They degrade into natural metabolites such as lactic and glycolic acids, and are excreted from the body through the kidneys (Hoffman, 2013). The main purpose of adding degradability character to hydrogels is to gain more control over the drug release profile and rate of scaffold elimination instead of only relying on diffusion, but hydrogels of crosslinked B-A-B copolymers suffer from an uncontrolled instant dissolution of the network after less than 60% mass loss, known as the onset of reverse gelation (Metters *Polym* 2000, *Phys Chem* 2000; Mason, 2001; Anseth, 2002; Bryant,

2004; Papadopoulos, 2011). The onset of reverse gelation has also been observed for radical-initiated crosslinked hydrogels with photodegradable moieties (Fairbanks, 2011; Azagarsamy, 2014). The reverse gelation onset is the result of non-systematic degradation, or in other words deviating from ideal degrading network. The network structure associated with hydrogels formed under fairly dilute conditions is expected to be far from ideal due to enhanced level of cyclization. A more comprehensive definition of this phenomenon can be extracted from delayed gelation in real networks compared to ideal networks. Flory's theory predicts a much lower conversion at the onset of gelation, therefore reverse gelation should occur very late during the course of degradation (i.e. at ~98% mass loss), but instead when it happens at a mass loss of around 60%, we can confidently call it premature reverse gelation. This disparity indirectly indicates that the actual gelation during polymerization has happened at ~40% conversion in these networks, which confirms the high level of cyclization and network heterogeneity. Another important disadvantage is the release of non-degradable high molecular weight poly(meth)acrylate chains. Crosslinked hydrogels made via free-radical polymerization with A-B-A copolymer with acrylate end-functionalities did not display the onset of reverse gelation and mass loss followed a sustained rate (Clapper, 2007) although they still exhibit high molecular weight non-degradable by-products of the degradation. Therefore, these results indicate that new degradable materials with novel design and more controlled-properties with PEG, PLA, PCL or other FDA approved polymers (i.e. 2-hydroxyethyl methacrylate HEMA) as their building blocks are highly necessary, and could potentially be brought to market in less time and lower cost than a counterpart polymeric material with "untested" status (Hoffman, 2013).

1.4.1. Hydrolytically and Enzymatically Degradable Hydrogels

Hydrogels with imbedded repeating ester groups in their structures (i.e. PLA) are able to degrade and eventually dissolve by two mechanisms: hydrolysis and enzymolysis of their backbone chains, crosslinkers, or side chains (Hoffman, 2013), although light irradiation can also initiate degradation in hydrogels with labile groups such as nitrobenzyl (Kloxin, 2009; Griffin, 2012). Hydrolysis is an acid/base-catalyzed chemical reaction that cleaves the susceptible linkages, where resonance-stabilized intermediates are possible, and transforms the ester molecule to carboxylic acid and alcohol. The molecular and structural factors affecting hydrolysis are: (i) bond stability, which decreases with higher stability of the intermediates (i.e. anhydrides, esters), (ii) hydrophobicity, which controls the concentration of bound water especially in the bulk, and ultimately affects the hydrolysis kinetics, (iii) polymer morphology such as crystallinity or porosity, which controls the concentration of unbound water, and further controls the diffusion rate of degraded by-products, (iv) glass transition temperature, which defines the range of elasticity, and further controls the equilibrium swelling ratio, and (v) molecular weight and molecular weight distribution (Hiemenz, 2007; Hoffman, 2013). On the other hand, the kinetic rate of hydrolysis is directly governed by temperature, ester group concentration, bound water concentration, and H^+ or OH^- concentration. Enzymes are globular proteins consisting of large molecules with high molecular weights (10,000-400,000 g/mol), as a result enzymatic degradation almost always begins at the surface unless a polymer offers interconnected pores that are of sufficient size for the enzyme to penetrate the bulk (Mochizuki, 1997). The first requirement for enzymatic degradation of polymers to occur is that the polymer chains must be flexible enough to fit into the active sites of the enzyme

(lock and key action), and this can occur either at random points along the polymer chain, or at the ends. For instance, the stereochemical conformation has dramatic effect on the rate of enzymatic degradation of PLA (the highest for D,L-PLA) (Cai, 1996; Mochizuki 1997). The other factors affecting the rate of enzymatic degradation are: crystallinity (hindering effect), balanced amphiphilic structures (enhancing effect), decreased mobility and free volume (hindering effect), and higher crosslink density (hindering effect) (Cai, 1996; Mochizuki, 1997; Ferracane, 2006). The order of enzymatic degradation in polyesters is as follows: aliphatic > heterocyclic > aromatic, in fact aromatic polyesters hardly degrade and among aliphatic polyesters a polymer with lower melting point generally degrades faster (Mochizuki, 1997; Marten, 2005). Research has shown clear evidence of enzymatic degradation of dental restorations as a result of esterases activities in oral environment at a minimal level of enzyme concentrations (Santerre, 2001; Ferracane, 2006; De Munck, 2009), and also high spontaneous metastasis in tumor cells with greatest level of collagen (i.e. type IV) degrading enzymes (Liotta, 1980; Kessenbrock, 2010).

1.4.2. Bulk and Surface Erosion

Hydrolysis is not a surface limited degradation mechanism since the bulk of hydrogels are swollen with water as well, but enzymatic degradation leads to surface erosion, and the percent of mass loss has a direct correlation with the surface area, and enzyme and ester concentrations (Cai, 1996; Mochizuki, 1997; Drury, 2003). The term erosion is used when a material loses mass, it can either happen through dissolution (i.e. sugar cube) or degradation, but erosion and degradation are not necessarily synchronized, a material can be degraded but does not lose mass due to factors such as

diffusion-controlled mass loss in highly crosslinked networks. In bulk erosion, the rate of water penetration into the network exceeds the rate at which the polymer is transformed into water-soluble material(s), therefore the water uptake in bulk-eroding materials includes the whole volume of the network. Cracks and fractures are typical signs of bulk erosion, and ultimately transform the polymer into pieces, which promote uncontrollability. In general, PLA (hydrophobic) is a bulk-eroding polymer particularly when it is copolymerized with PEG (hydrophilic), although the rate of water uptake depends on the interplay between their degree of hydrophilicity and hydrophobicity, which further are length dependent. Therefore, the B-A-B copolymer networks are bulk eroding unless more hydrophobic polymers are used instead of PLA such as polyanhydrides to obtain surface eroding materials (Uhrich, 1999). However, any bulk eroding material has a critical thickness, which beyond that it practically becomes a surface eroding device (Von Burkersroda, 2002). In surface erosion, the rate at which the polymer is transformed into water-soluble material(s) has to be fast relative to the rate of water penetration into the network, therefore the polymer becomes thinner with time but it retains its structural/mechanical integrity throughout most of the erosion process (Hoffman, 2013).

1.5. Nanogel Engineering

If relatively hydrophilic in nature, nanogels are hydrogels in nano-scale. However, nanogels have additional properties compared to hydrogels due to their extreme dimensions. They have high surface to volume ratio along with counterintuitive high loading/swelling capacity, high stability (particularly covalently crosslinked nanogels), high responsiveness to external stimuli (i.e. pH, temperature), and tunable hydrophilic/hydrophobic character and mesh size, which ultimately allow them to swell not only in aqueous solutions, but also in compatible organic solvents and monomers (Kabanov, 2009; Xia, 2013).

The covalently crosslinked nanogels via free-radical polymerization have dense core structure, which relatively restricts the post-modifications mainly to their surface, since surface functional groups accessibility is very important either for further crossliking the nanogels as precursors for macroscopic network formation (Dailing, 2013), or fast response to external stimuli (Funke, 1998). Their compact core is due to extensive primary and secondary cyclizations as a result of their very short active chains and intrinsic kinetic behavior of free-radical polymerization (Funke, 1998; Liu, 2012). Nanogels synthesized in heterogeneous colloidal environments can be more versatile in terms of monomer composition than the ones produced in homogeneous solutions (Kabanov, 2009), yet the former route yields much larger particles even with microemulsion techniques (10-50 nm) (Odian, 2004; Kabanov, 2009). The important applications of active and non-active nanogels are: binding component of coatings, carriers for biochemical and pharmaceutical compounds (covalently and/or physically bonded), and fillers for reinforcing plastics and dental restorations (Funke, 1998). The superiority of

nanogels in drug delivery applications is due to their ability to deliver very small drugs such as anticancer and antiviral agents in a distribution-controlled fashion due to their cell permeability (Uhrich, 1999; Kabanov 2009).

Our group has developed variety of nanogels for different dental material applications such as reducing polymerization-induced volumetric shrinkage and stress, mechanical property and water-compatibility improvement, and drug release (Morães, 2011, 2012; Liu, 2012, *Polym Chem* 2014, *Dent Mater J* 2014; Dailing, 2014, 2015; Saraswathy, 2016). These nanogels are highly crosslinked globular networks generally below 10 nm in diameter. They are synthesized in homogeneous solutions via thermally- or photochemically-induced free-radical polymerization of at least a di-vinyl and a monovinyl monomer. High concentration of chain transfer agent (i.e. 2-mercaptoethanol) controls the nanoscale size of the particles by shortening their active chain lengths and promoting extensive primary and secondary cyclizations. The degree of heterogeneity in free-radical crosslinked nanogels is reduced to molecular-scale due to their total nano-scale size. Nanogels like microgels are considered soft colloidal particles and their behavior is in a range between hard-sphere and ultra-soft colloids (i.e. star polymers with small number of arms), therefore their average interparticle distance can be smaller than the particle diameter, which is stabilized via steric hindrance (repulsive in nature) (Hiemenz, 1997; Heyes, 2009). Due to this soft-repulsive interaction, nanogels can compress or interpenetrate to a certain degree, called dense-packing regime, which leads to interesting structural and dynamical properties. Their level of compressibility depends on crosslinking density and nanogel-solvent or nanogel-monomer interactions, which is controlled by their monomeric constituents (Di Lorenzo, 2013). In dense-packing regime,

where nanogels are overlapped beyond the volume fractions of close-packing limit for hard-spheres, they become immobilized and resemble the properties of elastic macroscopic gels. By choosing monomers with secondary functional groups, the nanogels can be further post-functionalized to transform into an active particle, or in other words, a macromolecule precursor for further macroscopic network formation. The combination of dense-packing and crosslinking between overlapped nanogels result in the formation of a macroscopic network that its degree of heterogeneity (both intraparticle and interparticle) is reduced to molecular-scale without changing the polymerization mechanism (i.e. controlled-radical polymerization, step-growth polymerization).

1.6. Research Aims

The heterogeneous structure of crosslinked networks of di- and multi-vinyl monomers via free-radical polymerization was soon recognized after Flory developed his fundamental gelation theory, due to the drastic discrepancy between measured properties of the real network and that of predicted by Flory's model. Karel Dušek by introducing the revolutionary Gel Collapse phenomenon started a new chapter in polymer science (Bohdanecký, 2000), and portrayed the localized microgel formation as the root cause of this intrinsic heterogeneity. However, the actual length scale of inhomogeneity could not be seen and measured until instruments such as AFM, small angle X-ray and neutron scattering clearly showed the nanometer scale of highly crosslinked domains and their distribution (Di Lorenzo, 2015). This fundamental new knowledge was a great encouragement to explore the following research questions:

- Is it possible to reduce heterogeneity by incorporating nanogels into the network structure without altering the polymerization mechanism?

- How the global minimum of heterogeneity is achieved in nanogel-based networks?
- Does nanogel-based network obtain improved properties?

To answer these questions, the following specific aims are explored:

I. Investigate the effects of solvent-monomer interaction and agitation rate as synthesis parameters on the size and structural properties of the nanogels synthesized by free-radical polymerization of a divinyl monomer (EGDMA or UDMA) with a monovinyl monomer (IBMA).

II. Investigate the swelling properties, mechanical properties, and mass loss in amphiphilic hydrolytically degradable hydrogels, constructed from crosslinking of densely packed degradable active nanogel precursors differing in amphiphilicity, crosslinking density, and location of the labile groups (imbedded in the crosslinker, side chains, or both). Investigate the evolution of molecular weight between crosslinks during degradation based on rubber elasticity theory and equilibrium swelling theory (Flory-Rehner equation) with Gaussian and non-Gaussian chain conformation assumptions.

III. Investigate the effect of hydrophobic nanogels (styrene and divinylbenzene with two different molar concentrations) and their loading levels on swelling ratios and mass loss of hydrolytically degradable divinyl monomer/nanogel pseudo-IPN.

IV. Investigate the properties of high glass transition temperature nanogel and its effect on mechanical behavior of a TEGDMA/nanogel pseudo-IPN.

1.7. Organization of Dissertation

Each of the previously mentioned specific aims is addressed in the subsequent chapters of this thesis. A brief description of each chapter is given below:

Chapter 1. *"Introduction"* A literature review is provided in this chapter with a focus on nanogel engineering to control polymer degradation. This chapter presents an overview of thermally- and photochemically-initiated free-radical polymerizations in bulk and solution. It then compares the important aspects of homogeneous and heterogeneous solution polymerization. It provides a detailed differentiation between ideal and real crosslinked networks via free-radical polymerization, and also focuses on methacrylic and styrenic monomers as the most important sub-classes of vinyl monomers, and pseudo-IPN as a practical route to introduce multiple functionalities to a crosslinked polymer system. The most relevant degradation mechanisms and mass erosions in biomedical devices and drug carriers are also discussed. The chapter finalizes with how nanogel engineering has improved and can continue improving current challenges regarding free-radical crosslinked networks.

Chapter 2. *"Parameters Influencing Nanogel Structure and Properties during Homogeneous Solution Polymerization"* In this chapter the importance of controlling the molecular weight (size) and properties of nanogels is discussed by focusing on the influence of solvent nature and its concentration, reactant selection, as well as agitation rate. In this investigation, two different nanogel systems in terms of the internal crosslinker structures (urethane dimethacrylate: UDMA or ethylene glycol dimethacrylate: EGDMA) are studied. The divinyl monomers are reacted with isobornyl methacrylate (IBMA) in a chain transfer dominated, free radical homogeneous solution polymerization and the outcome of altered agitation rate is fully discussed. Triple detector gel permeation chromatography (GPC) is utilized to evaluate the number- and weight-averaged molecular weights, hydrodynamic radius, and polydispersity index. The effect of agitation

rate on the kinetics of polymerization is also qualitatively discussed. This study shows that depending on the choice of reactants and solvent, the potential for significant variation in critical polymer structure and properties is certainly present. This chapter fulfills research aim I.

Chapter 3. *"Use of Nanogel-Based Polymer Construction to Regio-Specifically Control Network Degradation"* This chapter develops a practical understanding of polymer characteristics and degradation kinetics of networks constructed from reactive nanogels with regio-specifically degradable linkages. Design and characterization of nanogel-based hydrogels on the copolymerization of poly(ethylene glycol dimethacrylate) with 2-hydroxyethyl methacrylate (PEG-HEMA) and these same comonomers with 2-methoxyethyl methacrylate (PEG-HEMA-MEMA) is investigated based on structural location of hydrolytically degradable poly(lactic acid) (PLA) linkages. The results of equilibrium swelling, mass loss, and compressive modulus (dry/swollen) demonstrate an interplay between hydrophilic/hydrophobic effects associated with PEG-PLA linkages, PLA location, and the crosslinking density that appear to dominate many of predicted property trends. Consequently, nanogel-based networks with shorter PEG and lower crosslinker concentration showed lower mass swelling rate, higher Tg, and lower compressive modulus reduction. This chapter fulfills research aim II.

Chapter 4. *"Suppression of Hydrolytic Degradation in Labile Polymer Networks via Integrated Styrenic Nanogels"* This chapter demonstrates the effects of nano-scale pre-crosslinked hydrophobic particles as additive to model labile monomer on hydrolytic degradation. The modification of hydrolytically vulnerable polymers through the intimate integration of secondary networks based on styrenic nanogel structures (divinylbenzene-

co-styrene) was intended to reduce or even eliminate hydrolytic degradation potential. Nanogel is added to labile macromer (PEG_{2000}PLADMA) and to triethylene glycol dimethacrylate (TEGDMA) with nanogel reactivity, mass swelling ratio, mass loss, residual mass, contact angle, viscosity and mechanical properties evaluation. Nanogel addition at any level produces reduction in network swelling and mass loss proportional to nanogel content. The flexural modulus and ultimate transverse strength of nanogel-loaded TEGDMA does not change compared to neat TEGDMA homopolymer. The use of a monomer-swollen highly crosslinked hydrophobic nanogel offers a versatile platform from which hydrolytic and potentially enzymatic degradation can be suppressed. This chapter fulfills research aim III.

Chapter 5. *"Nanogels with High Glass Transition Temperature"* This chapter investigates an alternative (nanogel) to conventional thermosetting resins, with enhanced processability, yet retaining desired thermal and mechanical properties. The average diameter of the polymeric nanogels is less than 20 nm, yet they possess glass transition temperature greater than 200 °C. These paradoxical properties trace back to micro-structural rearrangements of the same monomeric building blocks in current thermoset resins. This chapter fulfills research aim IV.

Chapter 6. *"Conclusions and Future Work"* In this chapter the conclusion of all the work done in this thesis will be presented along with possible future studies.

CHAPTER 2

PARAMETERS INFLUENCING NANOGEL STRUCTURE ANDPROPERTIES DURING HOMOGENEOUS SOLUTIONPOLYMERIZATION

2.1. Introduction

Nanotechnology as an interdisciplinary branch of science has enabled the creation of a variety of molecular-manufacturing platforms. In polymer science, nanogels have been used in many application areas but rarely as material additives or the primary components of new materials. Due to their nano-scale size and extensive options for processing, nanogels have served different functions such as nano-carriers in spatial and temporal controlled drug delivery (Asadi, 2011), cell imaging (Wu, 2010), gene delivery (Mintzer, 2009) and as high performance reactive fillers (Rouzeau, 2007). In dental materials for instance, nanogels have been used to generically achieve significant reductions in polymerization shrinkage and stress (Moraes, 2011), while also improving mechanical properties of composite restoratives and dental adhesive formulations (Liu, 2012).

As a basic definition, nanogels are dispersible intramolecular crosslinked macromolecules less than 100 nm in size (Dailing, 2013). There are quite ranges of synthetic and structural approaches used to prepare nanogel materials. In this case we are designing nanogels with intentionally short primary chains that are interconnected by

multiple crosslinks to allow internal free volume as well as high degrees of network-based branching (Graham, 1998). This class of polymers is synthesized based on at least one mono-vinyl monomer and one di-vinyl (or multi-vinyl) monomer as a crosslinker (Rouzeau, 2007). Solvent-modified crosslinking polymerizations routes (Dvorakova, 2010) can be performed in either homogeneous (e.g. solution polymerization) or heterogeneous (e.g. emulsion polymerization) modes. Here, the focus is on relatively concentrated free radical-initiated, homogeneous solution polymerization due to facile one-pot synthesis and the diversity of applicable monomers and other reagents.

Controlling nanogel size, particularly involving a homogeneous polymerization process, is very important due to the potential for macrogelation during the synthesis (Rouzeau, 2007). The average molecular weight of a nanogel affects many of its physical and mechanical properties such as viscosity, density, surface to volume ratio, and modulus (Dailing, 2013). Steric stabilization contributes to the control of nanogel size during synthesis (Graham, 1998). In order to control the size, different approaches can be incorporated (Rouzeau, 2007; Dvorakova, 2010; Liu, 2014): i) the use of reactors with nanoscale size restrictions, ii) dilution of the reacting medium to modify the relative ratio of cyclization to effective crosslinking, iii) addition of chain transfer agent or controlled radical polymerization approaches to manipulate primary chain length, iv) selection of a solvent with appropriate solubility parameter, and v) crosslinking monomer content. In particular, a high concentration of crosslinking monomer typically has a detrimental effect on the stability of the growing nanogel particles since it reduces the extent of solvated polymer chains and loops responsible for stabilizing the nanogel particles and also promotes macrogelation.

In this study, we demonstrate the effect of solvent and stirring rate on free radical homogeneous solution polymerization applied to nanogel particle formation. The effect of stirring rate on polymer size has been extensively studied for heterogeneous solution polymerization (e.g. emulsion polymerization) (Jalil, 1990; Sánchez, 2008) but its effect on homogeneous reaction regimes has been relatively neglected. In batch reactors, agitation is important since it provides heat dissipation capability as well as reaction mixture homogeneity (Erdoğan, 2002). The effects of solvents and agitation rate on reaction kinetics and structure/property relationships developed during nanogel synthesis of are presented in this study.

2.2. Materials and Methods

Isobornyl methacrylate (IBMA) (Tokyo Chemical Industry Co., Ltd.), urethane dimethacrylate (UDMA) (Sigma Aldrich), and ethylene glycol dimethacrylate (EGDMA) (Sigma Aldrich) were used as monomers. 2-Mercaptoethanol (ME) (Sigma Aldrich) and 1-dodecanethiol (DDT) (Sigma Aldrich) were used as chain transfer agents. Thermal initiator was 2,2'-azobisisobutyronitrile (AIBN) (Sigma Aldrich). 2,6-Di-tert-butyl-4-methylphenol (BHT) (Sigma Aldrich) was used as inhibitor. Toluene (Fisher Scientific, Certified ACS), hexane (Fisher Scientific, Certified ACS), methyl ethyl ketone (Fisher Scientific), and tetrahydrofuran (OmniSolv) were the solvents. All materials were used as received.

2.2.1. Nanogel Synthesis

Two different nanogels were synthesized in equivalent 100 mL round bottom flasks (stir bar 25 mm Long x 8 mm Diameter) via free radical solution polymerization. EGDMA and UDMA were used separately as di-vinyl crosslinkering monomers (30 mol%). IBMA

was added to each flask as the mono-vinyl monomer (70 mol%). ME (20 mol%) and DDT (20 mol%) were added as chain transfer agents to control average primary chain length in the nanogel structures. AIBN (1 wt% relative to monomer mass) was used as a thermal initiator. A two-fold excess of toluene (relative to monomer mass) was added as reaction solvent. Also, another set of nanogel from IBMA and UDMA was synthesized in methyl ethyl ketone as solvent. The polymerization reactions were carried out at 80 °C (oil bath temperature) under ambient atmosphere for each stirring rate (0, 200, and 400 rpm). The reactions proceeded at constant bath temperature for 1 h. Mid-IR spectroscopy (Nexus 670, Nicolet, Madison, WI) was used to evaluate the conversion of methacrylate double bonds (based on C=C peak area at 1637 cm^{-1} relative to the C=O absorbance at 1720 cm^{-1}). The clear reaction mixture was held at room temperature for 30 min followed by drop-wise precipitation in a four-fold excess (relative to reaction solution volume) of hexane. The precipitate was then re-dispersed in acetone and after a trace amount of BHT as inhibitor, the acetone was removed under high vacuum. A white powder (isolated nanogel) was obtained after complete removal of the solvent under reduced pressure. Structures of the monomers used are shown in Table 2.1.

Table 2.1. Structure of monomers.

IBMA	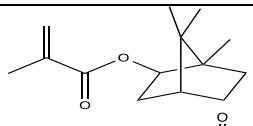
EGDMA	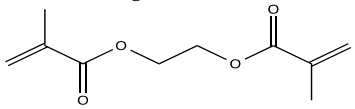
UDMA	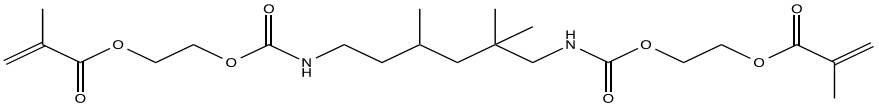

2.2.2. Nanogel Characterization

Triple detector (differential refractive index, viscosity, light scattering) gel permeation chromatography (GPC; Viscotek, Houston, TX) with a series of four columns spanning molecular weights of 10^4-10^7 was used to characterize the nanogel particles in tetrahydrofuran (THF) as eluant. Molecular weight (M_w) (based on right/low angle light scattering detection calibrated with a 65 kDa poly(methyl methacrylate) standard), hydrodynamic radius (R_h), polydispersity index (PDI), and Mark-Houwink parameter (MH-*a*) were all determined from the GPC analysis.

2.2.3. Reynolds Number Calculation

By analogy our nanogel synthesis was carried out in an unbaffled batch stirred tank reactor (100 mL round bottom flask) with a flat paddle stirrer (stir bar; length = 2.5 cm). By using Eq 2.1 (Doran, 1995) and assuming that the density and viscosity of the reaction mixture are equal to those of pure solvent at 80 ^oC we could estimate the Reynolds number (Re) at each stirring rate (0, 200, 400 rpm) (i.e. the density and viscosity of toluene at 80 ^oC and ambient pressure are 809.808 kg m^{-3} and 0.26 mNs m^{-2}, respectively) (McLinden, 2008; Sinnott, 2009).

$$\mathbf{Re = ND^2\rho/\mu} \qquad (2.1)$$

N: Stirrer Speed

D: Stir Bar Length

ρ: Solution Density

μ: Solution Viscosity

2.2.4. Statistical Analysis

Analysis of Variance (one-way) was performed in conjunction with multiple pair-wise by comparisons using Tukey-Kramer Tests for assignment of significant differences between means.

2.3. Results and Discussion

2.3.1. Flow Regime Determination

The calculated Reynolds numbers for stirring rate of 0, 200, and 400 rpm revealed three different flow regimes (Table 2.2). Flow regimes at 0, 200, and 400 rpm were laminar, transient, and fully developed turbulent, respectively. In laminar flow, the shear rate increases linearly with increasing the stirrer speed (Eq 2.2) but in turbulent regime the rate of increase is higher and it is non-linear (Eq 2.3) (Doran, 1995). In non-Newtonian fluids (e.g. polymer solutions) increasing the shear rate causes a shear thinning effect, which aligns the particle structure to the shear field (Sánchez Pérez, 2006). This alignment behavior involves not only polymer chains but also applies to the deformable, globular nanogel particles.

$$\gamma = \text{constant} \cdot N \quad \text{(Laminar Flow)} \tag{2.2}$$

$$\gamma = \text{constant} \cdot N^{3/2} \quad \text{(Turbulent Flow)} \tag{2.3}$$

Table 2.2. Reynolds number and flow regime associated with each stirring rate.

Stirring Rate [rpm]	Reynolds Number	Flow Regime
0	0	Re < 10: Laminar
200	6500	Re < 10^4: Transient
400	13000	Re > 10^4: Turbulent

2.3.2. Reaction Kinetics

In an agitated vessel the apparent diffusion layer thickness (h) for spherical particles is inversely correlated with agitation rate through Ranz-Marshall correlation (Eq 2.4-5) where r is the particle radius and Sh is Sherwood number (Ma, 2013), which is directly correlated with agitation rate through Reynolds number (Re). Nanogels are not hard sphere particles but rather soft, porous structures with reactions going on internally as well as externally. By using the Ranz-Marshal equation we have simplified nanogel characteristic to hard sphere behavior:

$$h = 2r / Sh \tag{2.4}$$

$$Sh = 2 + 0.6\, Re^{1/2}\, Sc^{1/3} \tag{2.5}$$

$$Sc\ (Schmidt\ Number) = \mu / \rho D_{AB} \tag{2.6}$$

It is evident that increasing the agitation rate decreases the apparent diffusion layer thickness so diffusivity is enhanced. Now we focus on the effect of agitation rate on the free radical polymerization kinetics. The kinetics of free radical polymerization with chain transfer agent can be summarized into four reactions (Hiemenz, 2007): i) homolytic thermal decomposition of the azo-compound initiator (I) followed by radical functionality transfer to monomers; ii) propagation of polymer chains; iii) chain transfer (which also involves a re-initiation step); and iv) termination. We limit our discussion by assuming that only homolytic decomposition rate of the initiator as well as its efficiency *f*, and termination rate are diffusion-controlled and consequently are affected by the viscosity of the medium at any stage and the rate of agitation.

Thermolysis of azo compounds generates nitrogen gas and two identical radicals (Eq 2.7). Any means that promotes radical diffusion out of the solvent cage will reduce

the recombination probability, so as a consequence, the efficiency *f* increases. On the other hand, stirring increases the dissolved oxygen content for any reaction run open to the air, which is the case in the nanogel synthesis procedure used here. In principle, higher dissolved oxygen content may counter the potential higher efficiency by consumption of the initiating radicals particularly at low conversion where the solution viscosity is low and oxygen diffusion is relatively high; however, the high thiol concentrations used here would be expected to minimize the inhibitory effects of oxygen (O'Brien, 2006). While not measured directly here, based on the preceding assumptions, the overall effect of increasing the stirring rate might be expected to yield a higher initiation rate and initiating radical concentration. The higher number of initiating radicals decreases the active chain length, although to a lesser extent than the effects associated with the chain transfer agents used here. Eq 2.7 and Eq 2.8 show the decomposition reaction of an azo compound and initiation rate with k_d as the decomposition rate constant.

$$I \rightarrow 2I^* + N_2 \tag{2.7}$$

$$R_i = 2\, f\, k_d\, [I] \tag{2.8}$$

In radical polymerization, the termination rate, especially by combination, is diffusion-controlled due to the high reactivity of the free radicals. By increasing the stirring rate and increasing the diffusion rate as a result the termination rate would increase. For methacrylate polymers, both combination and disproportionation contribute to termination with disproportionation favored (Ma, 2013). Radical termination rate can be determined by Eq. 2.9, where k_t is the rate constant, which is equal to the diffusion rate of reactive polymers into the same solvent cage (Hiemenz, 2007). The increase in termination rate

delays the autoacceleration effect and as a result would be expected to lead to lower conversion as a function of reaction time (Ma, 2013).

$$R_t = 2k_t [P^*]^2 \quad (2.9)$$

2.3.3. Conversion

An increase in the stirring rate did not change the final conversion for the IBMA:UDMA(70:30) nanogel synthesized in toluene (Fig 2.1A) but the IBMA:EGDMA(70:30) nanogel (also synthesized in toluene) was affected (Fig 2.1B). The NH bond in UDMA is effective hydrogen bonding donor but ineffective hydrogen bonding acceptor (Lemon, 2007). For the IBMA:UDMA(70:30) monomer mixture in toluene, which promotes hydrogen bonding due to its lack of donor/acceptor contribution, the urethane NH can hydrogen bond with the urethane carbonyl sites on UDMA as well as the methacrylate ester carbonyls in both UDMA and IBMA. These intra- and inter-molecular hydrogen bonding interactions in IBMA/UDMA adopt continually changing equilibrium conformations throughout all stages of the polymerization reaction. Heating impacts both the intra- and inter-molecular hydrogen bonding but primarily the latter due to the increased intermolecular spacing (Lemon, 2007). In the IBMA:EGDMA monomer mixture, the physical hydrogen bonding interactions do not exist as there is no donor functionality involved. Based on Eq 2.10 for degree of conversion *P* in radical polymerization, we can conclude that either the rate of propagation is not affected by stirring rate, therefore the unchanged conversion is an indication of an unchanged termination rate, or both propagation and termination are affected in similar fashion.

$$P = R_p / (R_p + R_t) \quad (2.10)$$

The effect of hydrogen bonding counteracts the stirring rate increase to promote diffusion. In IBMA:EGDMA(70:30) nanogel, where there is no hydrogen bonding present, the statistical result showed no difference between the final conversions when the stirring rate increased from 0 to 200 rpm but when it was further increased to 400 rpm there was 30% reduction in final conversion. This result is aligned with our kinetics analysis, which predicted higher termination rate for higher agitation rate and thus lower conversion. The termination rate could be enhanced based on greater macroradical mobility and increased dissolved oxygen.

(A)

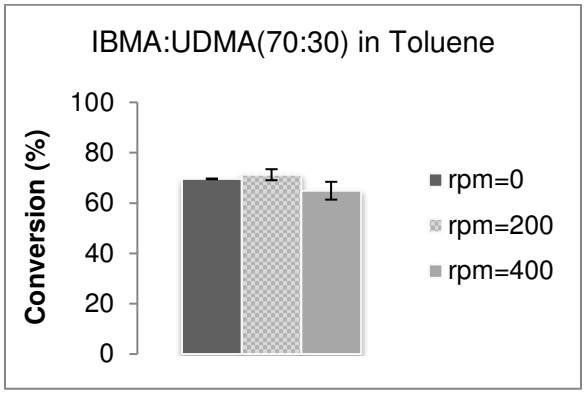

(B)

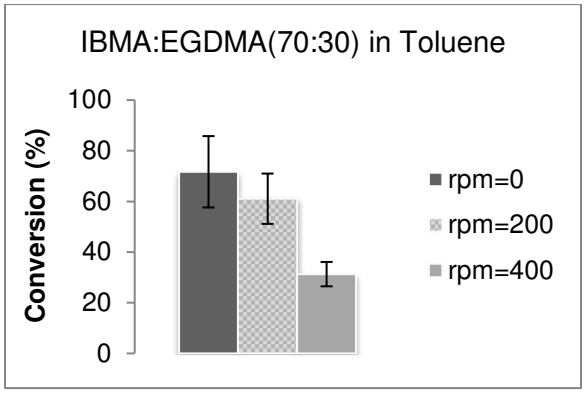

Figure 2.1. (A) Conversion of IBMA:UDMA(70:30) in Toluene (*p*-level = 0.15); (B) Conversion of IBMA:EGDMA(70:30) in Toluene (*p*-level = 0.03).

We also studied the effect of solvent on reaction kinetics and size of the IBMA:UDMA(70:30) nanogel synthesized in toluene and MEK (Fig 2.2 A-B). Addition of hydrogen bonding acceptor group in the solvent disrupts extended UDMA hydrogen bonding and promotes the more uniform dispersion of comonomers in the reaction mixture. The effect of increasing the stirring rate is evident in the more sluggish conversion development at higher rpm value (400 rpm) for nanogels in both solvents, but in terms of final conversion as in the previous result, there is no statistically significant difference between reactions at 0, 200, and 400 rpm (p-level between groups > 0.05) in toluene and MEK.

The comparison of early-stage conversion at different stirring rates (measured at 10 min) between IBMA:UDMA(70:30) nanogel synthesized in toluene and MEK reveals that the double bond conversion is higher for the nanogel in MEK at the stirring rates under study. The slower rate of conversion in a hydrogen bonding disruptive solvent is an indication of a barrier for active site transfer throughout the reaction solution. In toluene the effective UDMA concentration is locally higher and these regions would be expected to polymerize more rapidly at first. This would also lead to initially denser polymer structure. The residual IBMA would have to react in a depleted UDMA environment and this would slow down the late-stage process. Based on this observation we also expect to see lower molecular weight nanogel particles synthesized in MEK.

(A)

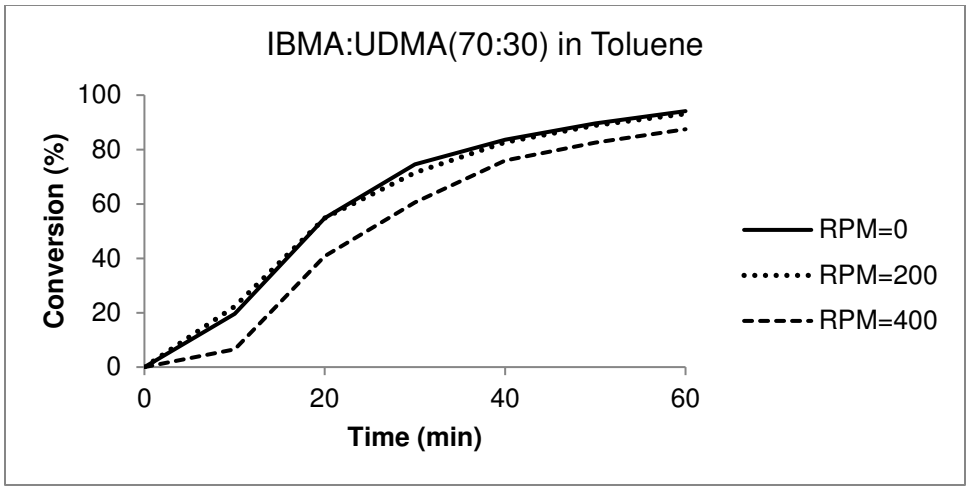

(B)

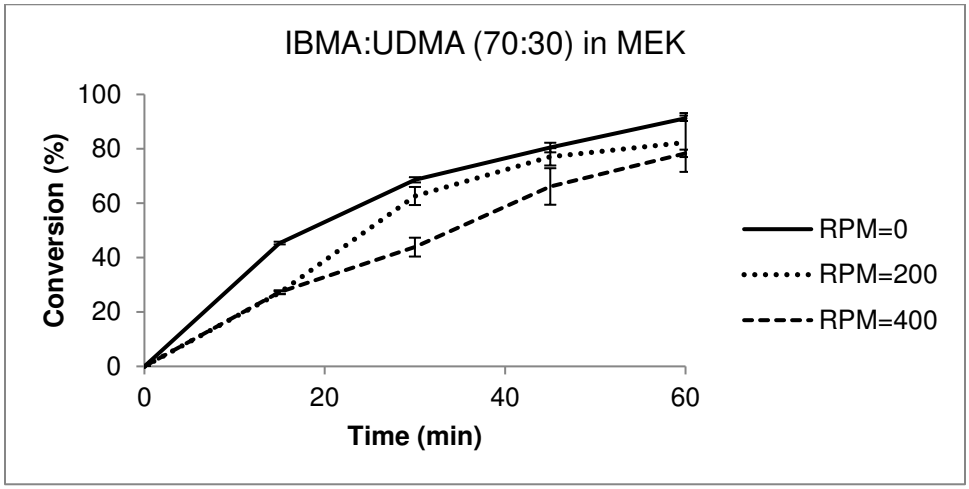

Figure 2.2. (A) Conversion vs. time for IBMA:UDMA(70:30) in Toluene; (B) Conversion vs. time of IBMA:UDMA(70:30) in MEK at different stirring rates (0, 200, 400).

2.3.4. Molecular Weight and Polydispersity Index

In termination by disproportionation, the weight average degree of polymerization $(N_w)_d$ can be obtained by Eq 2.11 (Hiemenz, 2007) and since final conversion (*P*) has not changed for IBMA:UDMA(70:30) nanogel synthesized under different conditions in toluene we can conclude that $(N_w)_d$ and M_w would not change. Fig 2.4 A shows that final molecular weights at different stirring rates are not statistically different but on the other hand, Fig 2.3A indicates a more sluggish *P* and molecular weight development throughout the course of reaction for nanogel synthesized at stirring rates of 200 and 400 rpm (Fig

2.3A only shows one run of reaction). The rise in molecular weight is dependent on conversion-driven consumption of both free monomers and pendant groups but also based on nanoparticle growth associated with capture of oligomers and other nascent particles.

$$(N_w)_d = 1 + P/1 - P \quad (2.11)$$

For IBMA:UDMA(70:30) nanogel synthesized in MEK (Fig 2.3B), there is a dramatic difference in the development of molecular weight and the final value of M_w. Also, we observed a significant decrease in M_w when the nanogel is synthesized in MEK, which confirms our earlier prediction. In this case, the lower final conversion and delay in autoacceleration at higher stirring rate affected the final molecular weights of the nanogels.

In the IBMA:EGDMA(70:30) nanogel synthesized in toluene, increasing the stirring rate decreased the final molecular weight of the nanogel particles but did not change the PDI (Fig 2.4 B). The trends in molecular weight followed the conversion trend in this nanogel system. This result agrees with our earlier prediction based on the change in the reaction kinetics. The potential combined effects of higher initiating radicals and shorter active chain length with higher termination rate and lower conversion would be expected to produce a lower molecular weight.

(A)

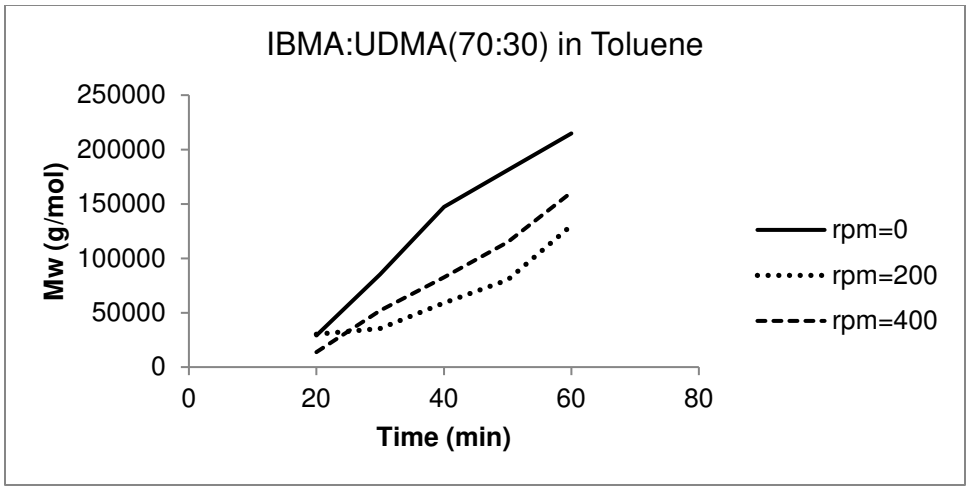

(B)

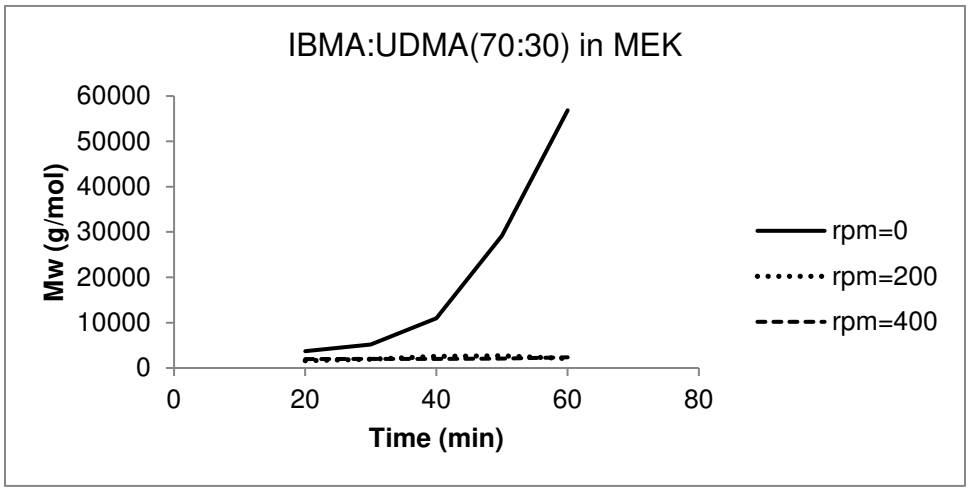

Figure 2.3. Weight average molecular weight vs. time at different stirring rates (0,200,400 rpm) for IBMA:UDMA(70:30) nanogel synthesized in MEK.

In the IBMA:UDMA(70:30) nanogel synthesized in toluene, an increase in the stirring rate from 0 to 200 did not impose any statistical difference on the polydispersity index (PDI) but when the stirring rate was further increased the PDI decreased (Fig 2.4A). This trend was also observed for IBMA:UDMA(70:30) nanogel synthesized in MEK (Fig 2.4C). We should also acknowledge that the PDIs observed for this nanogel system are significantly higher than that expected for the formation of chain-transfer mediated primary chains but here, the nanogel particles represent statistical distributions of these covalently interconnected oligomeric chains. The decrease in heterogeneity of particle

size distribution even though the degree of conversion remained basically unchanged may indicate that there is a difference between monomer addition rather than addition of branched oligomers at higher stirring rates. At high rpm, the interaction number between particle and oligomer may be higher but the interaction time may be reduced.

An increase in the stirring rate did not affect the hydrodynamic radius (R_h) in the IBMA:UDMA(70:30) nanogel synthesized in toluene (Fig 2.5A). Unchanged R_h was expected since conversion and M_w did not change either. In the IBMA:EGDMA(70:30) nanogel, increasing the stirring rate from 0 to 200 rpm did not affect the R_h but further increasing it to 400 rpm decreased the R_h (Fig 2.5B). These results are all in agreement with the conversion and M_w trends observed. Also, in the case of IBMA:UDMA(70:30) nanogel synthesized in MEK, increasing the stirring rate decreased the hydrodynamic radius of the particles (Fig 2.5C), which also is in agreement with molecular weight trends.

(A)

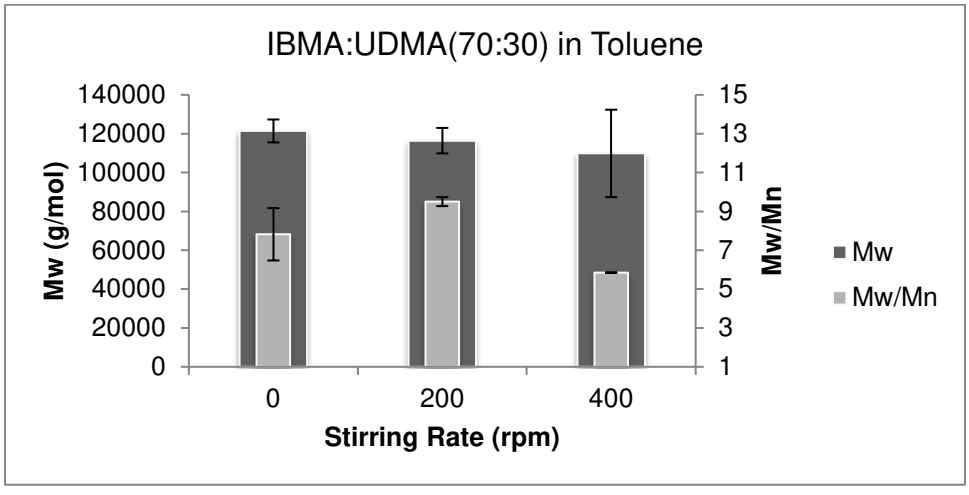

(B)

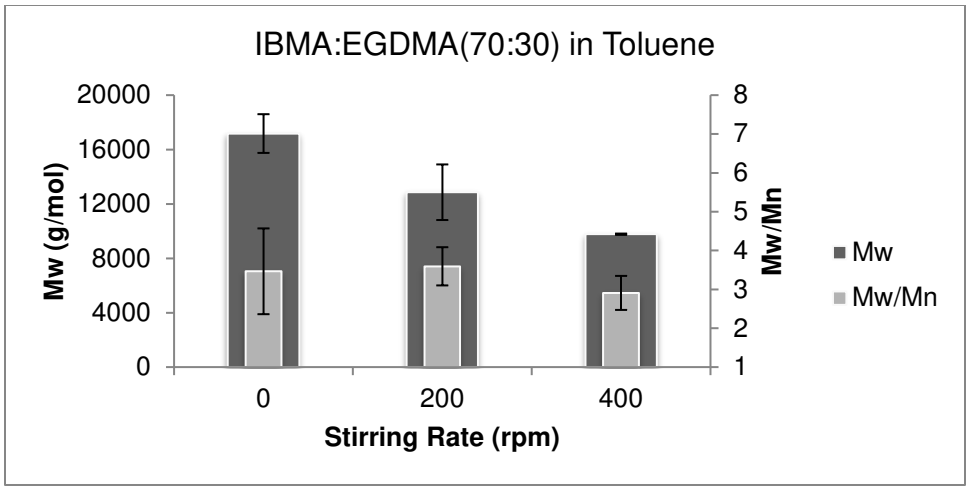

(C)

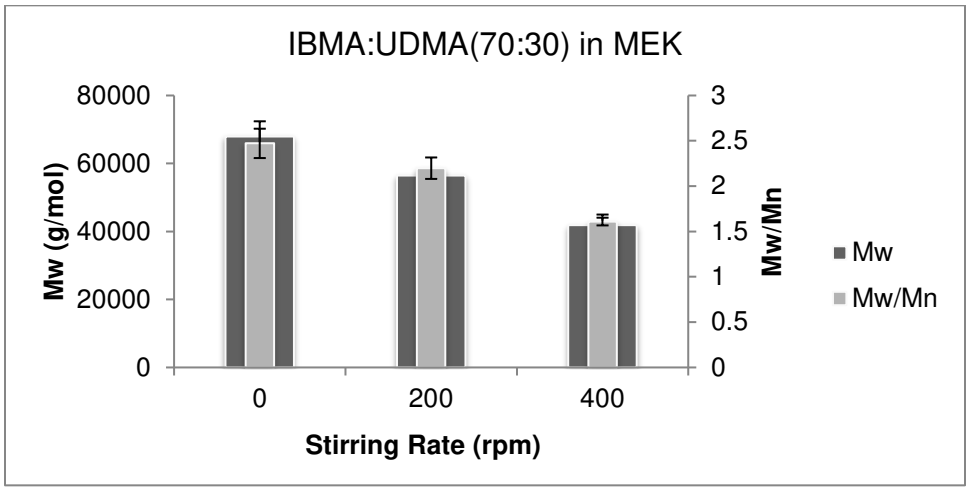

Figure 2.4. Molecular weights and PDI vs. Stirring Rate for: (A) IBMA:UDMA(70:30) in Toluene (*p*-levels between groups for M_w and PDI were 0.73 and 0.04, respectively); (B) IBMA:EGDMA(70:30) in Toluene (*p*-levels between groups for M_w and PDI were 0.01 and 0.64, respectively); (C) IBMA:UDMA(70:30) in MEK (*p*-levels between groups for M_w and PDI were 0.00 and 0.00, respectively).

(A)

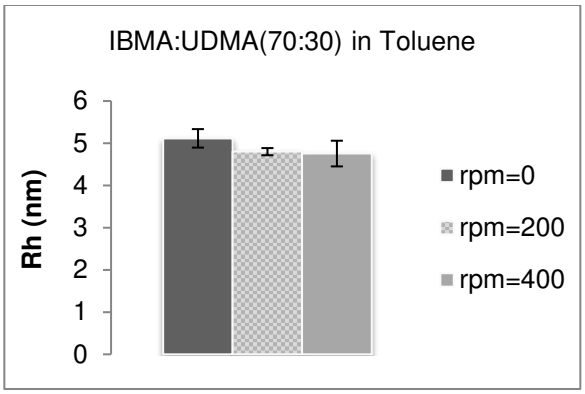

(B)

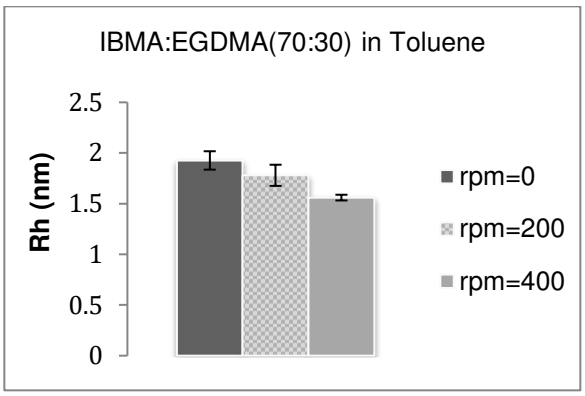

(C)

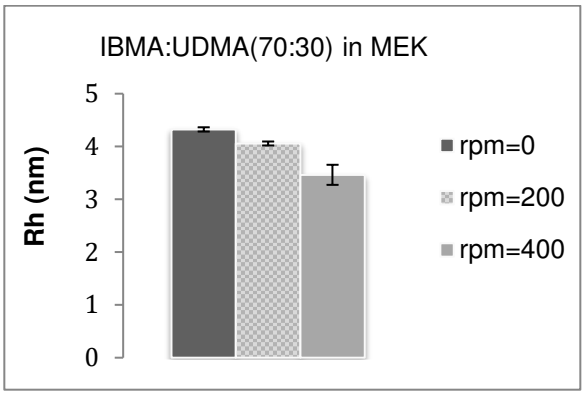

Figure 2.5. Hydrodynamic radius (R_h) vs Stirring Rate of: (A) IBMA:UDMA(70:30) in Toluene (*p*-level between groups = 0.34); (B) IBMA:EGDMA(70:30) in Toluene (*p*-level between groups = 0.02); (C) IBMA:UDMA(70:30) in MEK (*p*-level = 0.00).

2.3.5. MH-a Value

The average of *a*-exponent of Mark-Houwink equation (MH-*a*) was equal to or less than 0.314 for all the nanogels, which confirms the relatively spherical, globular geometry of these particles (Table 2.3). Higher rpm increased the *a*-value in the

IBMA:UDMA(70:30) nanogel synthesized in toluene, which is an indication of a slightly less spherical structure in this case. Higher stirring rate will result in much higher shear rate in turbulent flow regime (400 rpm), which was predicted earlier in this paper and as a result, particles can experience the shear thinning effect which aligns and deforms the particle structure to the shear field. Increasing the stirring rate did not change the *a*-value in the IBMA:EGDMA(70:30) nanogel, which might be attributed to the difference in the structures of the short/stiff divinyl crosslinker EGDMA and the more extended and flexible UDMA. Also, MH-*a* value statistically did not change in IBMA:UDMA(70:30) nanogel synthesized in MEK, which is an indication of different particle alignment in this case that eliminates the shear thinning effect. This new alignment might be explained by new-formed hydrogen bonding with the solvent molecules due to increased shear.

Table 2.3. MH-*a* values for nanogels synthesized in Toluene and MEK at different stirring rates.

	RPM = 0	RPM = 200	RPM = 400	*p*-level between groups
IBMA:UDMA(70:30) in MEK	0.223 ± 0.007	0.193 ± 0.020	0.146 ± 0.060	0.10
IBMA:UDMA(70:30) in Toluene	0.253 ± 0.001	0.279 ± 0.021	0.314 ± 0.023	0.09
IBMA:EGDMA(70:30) in Toluene	0.164 ± 0.059	0.103 ± 0.019	0.120 ± 0.063	0.36

2.4. Conclusions

Two nanogels were synthesized with different dimethacrylate monomers, one with UDMA a hydrogen bonding donor/acceptor and the other with EGDMA where hydrogen bonding was effectively absent. The effect of stirring rate as an operational condition was investigated in free-radical solution polymerization on nanogel conversion, molecular weight, hydrodynamic radius, polydispersity, and *a*-value of Mark-Houwink equation.

Increasing the stirring rate did not change the conversion, molecular weight or hydrodynamic radius in the IBMA:UDMA(70:30) nanogel synthesized in a hydrogen bonding promoter solvent (toluene). In MEK, which intervenes in the monomer/polymer hydrogen bonding, increasing the stirring rate decreased M_w and R_h. With the IBMA:EGDMA(70:30) nanogel prepared in toluene, increasing the stirring rate decreased the nanogel conversion rate, molecular weight, and hydrodynamic radius while the PDI and MH-*a* value did not change. Even though the effect of stirring rate in a free radical solution polymerization is generally not considered, this study showed that depending on the choice of reactants and solvent, the potential for significant variation in critical polymer structure and properties is certainly present.

CHAPTER 3

USE OF NANOGEL-BASED POLYMER CONSTRUCTION TO REGIO-SPECIFICALLY CONTROL NETWORK DEGRADATION

3.1. Introduction

Amphiphilic degradable hydrogels have been the focus of much research due to their biomimetic and biocompatibility characteristics. Two fields of engineered tissue scaffold removal (Anseth, 2013) and controlled drug delivery (Uhrich, 1999) have benefited tremendously from advances in designing new degradable hydrogel systems (Fu, 2010). Extensive work in fabrication of biodegradable hydrogels include crosslinked network construction via radical polymerization from different combinations of amphiphilic block copolymers of polyethylene glycol (PEG) as the hydrophilic segment and polylactide (PLA) as the hydrophobic hydrolytically degradable segment with (meth) acrylate end functionalities (Metters, *Polym* 2000; Clapper, 2007; Papadopoulos, 2011). Both of these polymer chains (PEG and PLA) are biocompatible and FDA approved (Lee, 2006). Adding PEG of sufficient length to the copolymer chain enables a high degree of swelling (Metters, *J Phys Chem B* 2000; Tessmar, 2007) and hydrophobic PLA on the other hand, not only improves the mechanical properties but also adds the biodegradability character to the system. Degradation of PLA and PEG yield lactic acid and glycolic acid, which are both native compounds (Foster, 1880) that can be metabolized and excreted completely from the body (Middleton, 2000; Lee, 2006; Yu, 2012).

Combinatorial effect of PEG and PLA in the copolymer by changing their structural order, and molar ratios have enabled scientists to manipulate several properties of the hydrogel network such as permeability, degradation rate, and mechanical integrity (Metters, *Polym* 2000; Clapper, 2007). The macroscopic gel preparation via free-radical crosslinking of bi- or multi-functional monomers/oligomers is favorable due to its simplicity, yet it comes with fundamental drawbacks that should be taken into account based on hydrogel application. These gels exhibit pronounced degree of nano-structural heterogeneity in a form of spatial distribution of crosslinks on 10-100 nm length scale, they also display significant range of defects such as dangling chain ends, loops (primary cyclization), sol fraction, and super-crosslinks (close-spaced crosslinks) (Duešk, 2000; Di Lorenzo, *Polym Chem* 2015). Super-crosslinks are highly crosslinked local domains, which are the result of intramolecular crosslinking (secondary cyclization), yet their ability to contribute to elasticity of the network and store elastic energy is equivalent to a single effective crosslink, therefore the elastic moduli of a real network is significantly lower by a denominator factor of 5-1000 compared to an ideal network predicted by rubber elasticity theory (Di Lorenzo, *Polym Chem* 2015). The formation of highly crosslinked domains occurs at low conversion, when spatially distributed nanogel clusters are created by exhausting the accessible interior dangling double bonds. The final macroscopic network is formed at higher conversions, from the onset of gelation and beyond until vitrification, through less number of crosslinks interconnecting the clusters.

This topological heterogeneity manifests itself further when the gel is swollen in a solvent, typically in the form of uneven swelling ratios between highly and loosely crosslinked domains, where typically the former swells less than the latter, although more

hydrophilic moieties are able to alter this classification regardless of the degree of crosslinking. On the other hand, the heterogeneous swelling in hydrolytically degradable gels induce limited control over degradation variables such as time, nature of degradation by-products, and type of degradation (bulk vs. surface). Additional degree of heterogeneity associated with amphiphilic PEG-*co*-PLA gels also may arise as a result of self-assembly of hydrocarbon backbone of poly(meth)acrylate chains, whereby the regional swelling dispersity widens.

Desired molecular weight of polymeric by-products in biological applications is less than 30 kg/mol, otherwise they can not be excreted through the kidneys (Tessmar, 2007) yet in these gels one of the by-products of degradation is non-degradable high molecular weight (long) poly(meth)acrylate chains with highly branched dangling side chains (Metters, *J Phys Chem B*, *Polym* 2000). Furthermore, transition from bulk to surface eroding material demands substitution of PLA with more hydrophobic monomers such as polyanhydrides and polyorthoesters (Middleton, 2000), as the interplay between the rate of water penetration to the network and polymer conversion rate to water-soluble materials determines the type of degradation (Middleton, 2000). In highly swollen gels of this kind when hydrophilicity of PEG segment is distinctly dominant compared to hydrophobicity of PLA segment (longer PEG and shorter PLA), the erosion of the network is controlled by bulk degradation, whereas in low or moderately swollen gels the heterogeneous distribution of swelling ratios might induce both types of erosions in tandem.

These hydrogels also exhibit a pronounced onset of reverse gelation (burst effect) at certain point during degradation when un-eroded mass becomes instantly soluble in the solvent. The onset of reverse gelation is attributed to the deviation from systematically (homogeneous) degrading ideal network. The critical degradation conversion (P_c) associated with reverse gelation, is elegantly formulated by Anseth et al. (Eq 3.1) (Metters, *J Phys Chem B* 2000) based on statistical-kinetic model of an ideal network defined by Flory (Hiemenz, 2007). In this equation, increasing the number of crosslinks per kinetic chain (N), increases P_c and delays the onset of reverse gelation, yet what is not captured in this correlation is the effectiveness of the crosslinks to hold the network together (Metters, *J Phys Chem B* 2000). In other words, more sustained rate of mass loss (higher degree of linearity vs. time) at any theoretical N value is dependent on the total number of effective crosslinks embedded in N. Increasing the crosslinker concentration only creates more heterogeneous network (Di Lorenzo, *Polym Chem* 2015), hence for delaying or even eliminating the onset of reverse gelation, the number of effective crosslinks (N_e) should approach the number of crosslinks in an ideal network ($N_e \rightarrow N$) or should be maximized ($N_e \rightarrow \infty$), respectively.

$$P_c = 1 - (\frac{2}{N})^{1/2} \quad (3.1)$$

As it was mentioned earlier, the length scale of heterogeneity in free-radical crosslinked networks of di- or multi-vinyl monomers is 10-100 nm, therefore any modification to reduce the macroscopic heterogeneity should target this size range. By taking this argument as first criteria, along with preserving both the synthesis simplicity and approved monomer palettes, a bottom-up approach yielding scaled-down heterogeneity (< 10 nm) in individual building blocks, offers a promising refinement.

Majority of biodegradable polymeric nanoparticles are formulated through a self-assembly process using block-copolymers with different hydrophilicity, which spontaneously assemble into a core-shell structures (Kim, 2003; Rijcken, 2005; Chu, 2006; Tessmar, 2007; Asadi, 2011; Wang, 2012) yet they suffer to fulfill several requirements such as stability in blood stream, novel functionality for further bioconjugation, diameter less than 100 nm, which facilitates cellular uptake, and enhanced mechanical properties, since there is no crosslinking involved in the formation of the nano-structure (Oh, 2008; Wang, 2012).

Matyjaszewski et al. have developed a low crosslinked (crosslinker concentration = 2.6 mol%), 110-120 nm size range nanogel by copolymerizing poly(ethylene oxide) dimethacrylate (PEODM) as the crosslinker agent with oligo(ethylene oxide) monomethyl ether methacrylate ($OEO_{300}MA$) as the monofunctional monomer via inverse miniemulsion Atom Transfer Radical Polymerization (ATRP) as a precursor for forming a hybrid enzymatic degradable hydrogel with degradable S_2 linkages attached to the nanogel surface (Bencherif, 2009). The two-phase characteristic of miniemulsion polymerization is the first limiting factor on the choice of compatible monomers from already limited selection of biocompatible and approved materials. The second issue is the size of droplets and their stability in the continuous phase, besides droplet size range (30-500 nm) defines the minimum achievable size for nanogels (Landfester, 2001). To attain stable droplets the amount of surfactant and costabilizer, the amount of energy used in homogenization process (ultrasonication), and the reaction temperature are significantly important factors and have to be well adjusted (Landfester, 2001; Odian, 2004). The other limitation is the use of a non-radical forming reducing agent instead of

a conventional radical initiator (Activator Generated by Electron Transfer AGET ATRP). In addition to the complexity of reaction mixture, in miniemulsion crosslinking polymerization when the mole fraction of divinyl to monovinyl monomer increases, the polymer particles coagulate during the early stage of reaction (Tobita, 2000; Odian, 2004), therefore producing nanogel particles with high crosslinking density and size less than 100 nm becomes practically impossible (the mechanical properties of the control hydrogel did not change after modification with 1, 5, and 10% wt/v nanogel loading due to low crosslink density).

In this work, we introduce polymeric globular nanogels with tunable size well below 100 nm with large surface to volume ratio that are novel candidates for multivalent bioconjugation either on their surface or their interior, which make them ideal for drug delivery applications or precursors for tissue scaffold (Dailing, 2013). This unique approach utilizes free radical solution (homogeneous) polymerization as a simple route to synthesize wide range of polymeric nanoparticles for variety of applications such as shrinkage stress reduction and enhanced mechanical properties in dental materials, surface morphology modification for polymer gradient materials, and precursors for macroscopic network formation (Moraes, *Dent Mater* 2011, *J Dent Res* 2012; Liu, 2012, 2014; Dailing, 2013; Gotti, 2016). Nanogels are formed by free-radical polymerization of at least a di-vinyl and a mono-vinyl monomer in a relatively concentrated solution (good solvent) in the presence of an initiator and chain transfer agent. With this approach: i) larger selection of monomers are applicable, ii) highly crosslinked nanogels (<< 100 nm) are easily attainable, in fact increasing the crosslinker concentration creates more compact particles (Funke, 1998), iii) stable one-phase reaction eliminates the requisite

for surfactant and monomer droplet formation, therefore polymerization site shrinks to the size of a swollen monomer, iv) instead of coagulation that happens at early stage of minimemulsion polymerization, microgel formation as a result of macroradicals crosslinking, happens at high conversions in homogeneous solution polymerization (late stage of reaction), and v) the kinetic chain length is controlled and reduced by the concentration of chain transfer agent to maintain the nanoscale dimension of the growing particle, additional branching is also introduced to the nanogel structure (Hiemenz, 2007).

It is important to mention that the distribution of crosslinks in the nanogel is not homogeneous either since primary cyclization and intramolecular crosslinking are favored at early stages of reaction (the local concentration of pendant vinyl groups inside a macroradical coil is much higher than their overall concentration in the mixture), but then cyclizations are replaced by intermolecular crosslinking due to steric and excluded volume effects, as a result the degree of crosslinking decreases outward. The remarkable phenomenon in nanogel formation is the reduced level of heterogeneity to sub-nano scale, even though the nanoscopic network still has defects such as loops, dangling chains, and super-crosslinks. The sol fraction is soluble in reaction solvent and is separated from nanogel particles after precipitation step. Furthermore, when high concentration of purified active nanogels (> 50 wt%) is dispersed in a good solvent, a continuous phase of overlapped swollen nanogels (confluent or densely packed) is created, where nanogel-nanogel interactions are immobilized through steric stabilization in the overlapped volume (Hiemenz, 1997). The continuous phase is then fixed in place by radical crosslinking (photo-polymerization) and a uniform macroscopic network with reduced level of heterogeneity is created that its mechanical properties are in quantitative

agreement with theory of rubber elasticity (Di Lorenzo, *Colloid Polym Sci*, 2013). Due to nanogels overlapping, unreacted nanogels, dangling nanogels, and loops has low probability (Di Lorenzo, *ACS Macro Lett* 2015), although multiple crosslinking can occur beween adjacent nanogels. It is important to note that pre-defined distance between vinyl groups in active nanogels increases the number of effective crosslinks in the final macroscopic network (Di Lorenzo, *Colloid Polym Sci*, *ACS Macro Lett* 2015). This contribution investigates the following hypotheses for further insight into degradable hydrogels: 1) hydrolytically degradable nanogel precursors (<< 100 nm), overlapped beyond percolation threshold, are able to create macroscopic degradable network with decreased level of heterogeneity compared to conventional crosslinked networks, and 2) the type of macroscopic erosion can be pre-modulated by the location of hydrolytically labile linkages in the nanogel structure. Amphiphilic degradable active nanogels were synthesized with secondary methacrylate functionalization, enabling them to create a secondary crosslinked network. The degradation of the hydrogels was investigated based on structural location of PLA linkages. A series of nanogels were synthesized according to several experimental variables: 1) addition of degradable lactide linkage to i) crosslinker structure within the nanogel (bulk degradation), and/or ii) side chain structure (surface degradation); 2) two different molar percentages of the crosslinker (10 mol%, 50 mol%); 3) three different molecular weight PEGs (600, 2000, and 4600 g/mol); and 4) mono-functional biocompatible monomers (Abraham, 2005; Tanaka, 2010; Johnson, 2012), 2-hydroxyethyl methacrylate (HEMA) and 2-methoxyethyl methacrylate (MEMA). The analysis of the nanogel structures is performed in terms of molecular weight (M_w), degree of branching (MH-*a*), polydispersity index (PDI), and glass transition temperature

(T_g). The macroscopic hydrogels underwent hydrolytic degradation and experimental/observational results are presented in terms of equilibrium water uptake (%W), mass loss (%), mechanical property (compressive modulus K), and pH value. These nanogels propose invaluable possibilities in tissue engineering and controlled drug delivery.

3.2. Materials and Methods

3.2.1. Materials

Polyethylene glycol (M_w = 600 g/mol) (PEG_{600}) (Sigma Aldrich), polyethylene glycol (M_w = 2000 g/mol) (PEG_{2000}) (Sigma Aldrich), polyethylene glycol (M_w = 4600 g/mol) (PEG_{4600}) (Sigma Aldrich), hydroxyethyl methacrylate (HEMA) (ESSTECH), ethylene glycol methyl ether methacrylate (MEMA) (Sigma Aldrich), 3,6-dimethyl-1,4-dioxane-2,5-dione (D,L Lactide) (Sigma Aldrich), 2-isocyanatoethyl methacrylate (IEM) (TCI) were used as monomers. The thermal initiator was 2,2'-azobisisobutyronitrile (AIBN) (Sigma Aldrich). 1-Dodecanethiol was the chain transfer agent and 2,2-dimethoxy-2-phenylacetophenone (DMPA) (Sigma Aldrich) was used as photo initiator. Dibutyltin dilaurate (Sigma Aldrich) was the catalyst. Butylated hydroxytoluene (BHT) was added as an inhibitor. Methyl ethyl ketone (MEK) (Fisher Scientific) and hexane (Fisher Chemical) were used as solvents. All the materials were used as received. For cell biocompatibility study, Minimum Essential Medium (MEM), 10000 international unit (IU)/mL penicillin, and 10000 µg/mL streptomycin antibiotic solutions were purchased from Gibco Life Technologies. Fetal bovine serum (FBS) was purchased from Sigma-Aldrich.

3.2.2. Non-Degradable Monomers Synthesis

For non-degradable crosslinker PEGDMA synthesis, methacrylate functionality was added to both sides of PEG (600, 2000, 4600 g/mol). PEG and IEM with 1 to 2 molar ratio were added to 6-fold excess of methylene chloride relative to monomer mass. The catalyst (dibutyltin dilaurate) (0.2 wt% relative to monomer mass) was added to the mixture, and reaction was carried out under ambient condition for 48 hours. The reaction reached 100% conversion and methacrylate functionalized PEG was precipitated out by drop-wise addition of the mixture to 10-fold excess of hexane (relative to mixture volume). The monomer was re-dispersed in acetone and inhibitor amount of BHT was added to the solution before removing the solvent (acetone) under high vacuum. The other non-degradable monomers (HEMA and MEMA) were used as received.

3.2.3. Degradable Monomer Synthesis

Degradable crosslinkers were synthesized by adding one PLA block on each side of the PEG via ring-opening polymerization reaction of lactide with PEG (Sawhney, 1993), and further functionalization of PLA-PEG-PLA copolymer on both sides with methacrylate groups PEGPLADMA (MA-PLA-PEG-PLA-MA). PEG to lactide molar ratio was 1 to 4.5. To avoid oxidation, mixture was under N_2 purge 30 minutes prior to reaction till the end. Reaction temperature was 140 ^oC. After almost 30 minutes the lactide was melted, then catalyst (dibutyltin dilaurate) (0.2 wt% relative to monomer mass) was added to the reaction mixture. N_2 was continuously purging throughout the reaction time. After 4 h of reaction the mixture was cooled down to room temperature before exposing it to oxygen, then the unreacted lactide was removed via Kugelrohr Distillation Apparatus (BÜCHI) under high vacuum at 180 ^oC. IEM and 2-fold (relative to mass) of DCM was added to the

product (PLA-PEG-PLA), then the catalyst (dibutyltin dilaurate) (0.2 wt% relative to monomer mass) was added to the mixture. The molar ratio of PLA-PEG-PLA to IEM was 1 to 2. After the reaction reached 100% conversion at room temperature, drop-wise precipitation step in 10-fold excess of hexane (relative to volume) was performed to purify the product from unreacted species. Degradable side-chain monomer HEMA-PLA was also synthesized following the same procedure. HEMA to lactide molar ratio was 1 to 2.

3.2.4. Nanogel Synthesis

All nanogels were synthesized via free radical solution polymerization. The non-degradable nanogel batch included PEGDMA (10, 50 mol%) as primary crosslinker, HEMA (45, 25 mol%) and MEMA (45, 25 mol%) as mono-vinyl monomers. For internally degradable nanogels, degradable crosslinker PEGPLADMA (10, 50 mol%) and non-degradable mono-functional monomers were used. For externally degradable nanogels, crosslinker (PEGDMA) was non-degradable but one of the side-chain monomers was degradable (HEMAPLA). For internally-externally degradable nanogels, both crosslinker (PEGPLADMA) and one of the side-chain monomers (HEMAPLA) were degradable. For all of the nanogels, we used: AIBN (1 wt% relative to monomer mass) as thermal initiator, 1-dodecanethiol (15-30 mol%) as chain transfer agent, and 8-10 fold excess of MEK (relative to monomer mass) as the solvent. Higher volume of solvent, 10-12 fold excess was used for internally-externally degradable nanogels to avoid macrogellation due to copolymerization of higher molecular weight monomers. Also, for PEG_{4600} nanogel series, 30 mol% of chain transfer agent was used instead of 15 mol%, to control nanogel size and avoid macrogellation. Reaction temperature was 80 ^{o}C, and reflux condenser was utilized to maintain the initial solvent amount during the reaction. Stirring rate was set to

200 rpm. The reaction was carried out isothermally for 3 hours, and reached almost complete conversion (> 90%) for all nanogels.

For post-functionalizing the nanogel with methacrylate groups, IEM (equimolar to half of HEMA or HEMAPLA content) was added to the reaction mixture after it was cooled down to room temperature, then 3 drops of catalyst (dibutyltin dilaurate) (0.2 wt% relative to monomer mass) was added and reaction was carried out at ambient condition for two days. After disappearance of isocyanate peak, drop-wise precipitation step in 10-fold excess of hexane (relative to mixture volume) was performed. The precipitate (active nanogel) was re-dispersed in acetone and inhibitor amount of BHT was added to the acetone-nanogel solution before removing acetone under high vacuum. An opaque viscous fluid was obtained after complete removal of acetone. Active nanogel is considered as a multi-functional crosslinker for creating final macroscopic network.

3.2.5. Macroscopic Network Formation

Mixtures of active-nanogel : solvent with 50:50 wt% ratio were prepared (acetone and DCM were used to disperse PEG_{600}-PEG_{2000} and PEG_{4600} nanogel series, respectively). DMPA (0.2 wt% relative to total mass) was added to each mixture. A thin disc mold was placed between two glass slides (Diameter = 5 mm; Thickness = 1.5 mm) and nanogel mixtures were injected into the mold. The disc-shaped macroscopic network was formed after photo polymerization with UV light (365 nm; irradicance = 15.5 mW/cm^2) (all disc samples displayed conversions greater than 90%).

3.2.6. Macroscopic Swelling and Degradation

The discs (n = 3) were weighed subsequent to drying under house vacuum in desiccator for 7-14 days at ambient temperature. Their weights were then measured on

analytical balance to insure complete solvent removal. Samples lost half of their weights due to solvent evaporation. The weights were also monitored during hydrolytical degradation at room temperature in buffer (pH = 3.0), by carefully blotting the samples to remove the excess water on the surface. The percent water uptake (%W) was measured for each sample by using (Eq 3.1) (Lester 2003; Wu 2010):

$$\%W = (M_S - M_i / M_S) \times 100 \quad (3.1)$$

M_S : Mass after Swelling

M_i : Initial Dry Mass

We calculated the average density of each network by using sample dry mass and volume of the mold ($\pi \times (\text{diameter}/2)^2 \times \text{thickness}$), assuming no significant shrinkage or equal shrinkage after drying for all networks. For mass loss study, PEG_{4600} nanogels were chosen due to shorter degradation time, and their mass loss was monitored at room temperature in DI water. The % Mass Loss was calculated gravimetrically by measuring the initial and final dry mass of the polymer specimen (polymer samples were dried at room temperature under house vacuum for 2-3 weeks) and using (Eq 3.2):

$$\%\ \text{Mass Loss} = ((M_i - M_f)/M_i) \times 100 \quad (3.2)$$

M_i : Initial Dry Mass

M_f : Final Dry Mass

3.2.7. Measurements

Mid-IR spectroscopy (Nexus 670, Nicolet, Madison, WI) was used to calculate the conversion of the methacrylate carbon-carbon double bond (815 cm^{-1}) during nanogel synthesis, and isocyanate group (2270 cm^{-1}) conversion during nanogel post-

functionalization. Triple-detection gel permeation chromatography (GPC; Viscotek) with differential refractive index, viscosity, and light scattering detectors was employed for the analysis of nanogel weight and number averaged molecular weights, $\bar{M}_w$ (g/mol) and $\bar{M}_n$ (g/mol), polydispersity index (PDI = $\bar{M}_w/\bar{M}_n$), and average hydrodynamic radius $\bar{R}_h$ (nm). Tetrahydrofuran (THF) was used as diluent with a flow rate of 1 mL/min at 35 °C in a series of three columns spanning molecular weight of 10^4 – 10^7 calibrated with a 65 kg/mol poly(methyl methacrylate) standard.

Proton nuclear magnetic resonance (^{1}H NMR; Varian 500 MHz) and MestReNova 5.2.4 software were employed to determine and analyze the structural composition of the nanogel. DMA (Dynamic Mechanical Analysis) tests were performed using a TA instruments (DMA 8000, Perkin Elmer) to determine the glass transition temperature (T_g) of the nanogel. Nanogel (10-15 mg) (n = 2) was placed inside a steel pocket and was tested between the clamps. The glass transition temperature was determined as the position of the maximum on the tan δ vs. temperature plot. The temperature range was from -150 °C to 100 °C with a ramping rate of 3 °C/min at a frequency of 1 Hz and tan δ were recorded as a function of temperature. A preheating cycle was applied with a ramping rate of 10 °C/min.

The compressive modulus of the photopolymerized nanogel network before (dry) and after swelling in buffer solution pH = 3.0 were measured at room temperature using a mechanical testing machine (MTS; MiniBionix II). Disc samples (n = 3) were compressed with 10 N load at a constant rate of 1 mm/min. The modulus (K) was calculated from the slope of the linear region of the stress vs. strain curve. StatPlus v5.9.91 (AnalystSoft Inc) was used for statistical analysis. After passing normality

(Shapiro-Wink W), one-way Analysis of Variance (ANOVA) and *post hoc test* (Tukey B) was performed, and null hypothesis was rejected if the *p*-value was less than 0.05.

3.3. Results and Discussion

3.3.1. Nanogel GPC Analysis

The $\bar{M}_w$, $\bar{M}_n$, $\bar{R}_h$, PDI, and the degree of branching/crosslinking portrayed by Mark Houwink exponent measured by GPC, are important determinants of physical and mechanical properties of nanogel particles (Table 3.1-5). In this study, we observed when PEG length was constant, increasing the concentration of crosslinker from 10 to 50 mol% increased the molecular weight and hydrodynamic radius of the nanogels. This effect was expected due to increased number of pendant double bonds on the backbone and overall addition of higher number of monomers to the nanogel structure. Also, by keeping the crosslinker concentration constant while increasing the PEG molecular weight from 600 to 2000 g/mol, the molecular weight of the nanogel increased. At a constant PEG length, polydispersity index decreased when the concentration of the crosslinker increased from 10 to 50 mol%, due to larger M_n values (Table 3.1). When crosslinker concentration increases, M_n increases accordingly, due to higher molecular weight species (M_i) and their higher mole fractions (x_i). As it was mentioned before, we used 10-fold excess of solvent to synthesize the internally-externally degradable nanogels, increasing the solvent increases the extent of intra-molecular crosslinking and cyclization rather than intermolecular crosslinking, consequently creates more compact particles with relatively lower molecular weights (Table 3.4). By increasing the crosslinker concentration, we expected to see lower MH-*a* values due to increased branching/crosslinking and more hard-sphere like behavior, yet GPC results showed the opposite trend mainly in non-

degradable and internally degradable nanogels (Table 3.1-2), which might be due to the change in solvent-particle interaction, arising from increased hydrophilicity character with higher concentration of hydrophilic crosslinker. The MH-*a* can take up different values depending on the quality of the solvent, 0 < MH-*a* < 0.5, MH-*a* =0.5 (theta solvent), and MH-*a* ≥ 0.8 represent semi-rigid sphere (highly branched), an unperturbed Gaussian chain (flexible random coil), and flexible chain (less branched), respectively (Hiemenz, 2007). The NG_{11} (Table 3.2) had the lowest molecular weight among all the nanogels synthesized in this study, which might be related to water/THF ensemble, causing hydrolytic degradation during GPC sample preparation and overnight runs (Lyu, 2009).

Table 3.1. GPC Results for Non-Degradable Nanogels: copolymers of PEGDMA (PEG molecular weight = 600, 2000 g/mol) and HEMA (NG_1-NG_4); copolymers of PEGDMA, HEMA, and MEMA (NG_5-NG_8).

	Nanogel Name	$\bar{M}_n$	$\bar{M}_w$	$\bar{M}_w/\bar{M}_n$	$\bar{R}_h$	MH-*a*
NG_1	**PEG_{600}DMA/HEMA(10:90)**	5,700	**12,000**	**2.1**	**2.4**	**0.35**
NG_2	**PEG_{600}DMA/HEMA(50:50)**	32,000	**32,000**	**1.0**	**3.7**	**0.81**
NG_3	**PEG_{2000}DMA/HEMA(10:90)**	5,900	**20,000**	**3.4**	**3.5**	**0.37**
NG_4	**PEG_{2000}DMA/HEMA(50:50)**	37,000	**41,000**	**1.1**	**5.7**	**0.49**
NG_5	**PEG_{600}DMA/HEMA/MEMA(10:45:45)**	4,200	**15,000**	**3.6**	**2.8**	**0.42**
NG_6	**PEG_{600}DMA/HEMA/MEMA(50:25:25)**	25,000	**27,000**	**1.1**	**3.8**	**0.82**
NG_7	**PEG_{2000}DMA/HEMA/MEMA(10:45:45)**	11,000	**25,000**	**2.2**	**4.3**	**0.54**
NG_8	**PEG_{2000}DMA/HEMA/MEMA(50:25:25)**	42,000	**46,000**	**1.1**	**5.7**	**0.50**

Table 3.2. GPC Results for Internally Degradable Nanogels: crosslinker structure contains degradable PLA linkages; copolymers of PEGPLADMA (PEG molecular weight = 600, 2000 g/mol) and HEMA (NG_9-NG_{12}).

	Nanogel Name	$\bar{M}_n$	$\bar{M}_w$	$\bar{M}_w/\bar{M}_n$	$\bar{R}_h$	MH-*a*
NG_9	**PEG_{600}PLADMA/HEMA(10:90)**	8,600	**36,000**	**4.2**	**3.3**	**0.41**
NG_{10}	**PEG_{600}PLADMA/HEMA(50:50)**	39,000	**62,000**	**1.6**	**6.0**	**0.61**
NG_{11}	**PEG_{2000}PLADMA/HEMA(10:90)**	800	**2,000**	**2.4**	**1.5**	**0.21**
NG_{12}	**PEG_{2000}PLADMA/HEMA(50:50)**	41,000	**41,000**	**1.0**	**5.5**	**0.83**

Table 3.3. GPC Results for Externally Degradable Nanogels: one of the side-chain monomers contain degradable PLA linkages; copolymers of PEGDMA (PEG molecular weight = 600, 2000 g/mol), HEMAPLA, and MEMA (NG_{13}-NG_{16}).

	Nanogel Name	$\bar{M}_n$	$\bar{M}_w$	$\bar{M}_w/\bar{M}_n$	$\bar{R}_h$	MH-*a*
NG_{13}	**PEG_{600}DMA/HEMAPLA/MEMA(10:45:45)**	3,000	**24,000**	**7.2**	**2.2**	**0.51**
NG_{14}	**PEG_{600}DMA/HEMAPLA/MEMA(50:25:25)**	5,900	**9,400**	**1.6**	**1.9**	**0.33**
NG_{15}	**PEG_{2000}DMA/HEMAPLA/MEMA(10:45:45)**	4,900	**19,000**	**3.9**	**3.6**	**0.44**
NG_{16}	**PEG_{2000}DMA/HEMAPLA/MEMA(50:25:25)**	42,000	**46,000**	**1.1**	**5.9**	**0.52**

Table 3.4. GPC Results for Internally-Externally Degradable Nanogels: crosslinker and one of the side-chain monomers contain degradable PLA linkages; copolymers of PEGPLADMA (PEG molecular weight = 600, 2000 g/mol), HEMAPLA, and MEMA (NG_{17}-NG_{20}).

	Nanogel Name	$\bar{M}_n$	$\bar{M}_w$	$\bar{M}_w/\bar{M}_n$	$\bar{R}_h$	MH-*a*
NG_{17}	**PEG_{600}PLADMA/HEMAPLA/MEMA(10:45:45)**	1,800	**6,000**	**3.4**	**2.1**	**0.38**
NG_{18}	**PEG_{600}PLADMA/HEMAPLA/MEMA(50:25:25)**	3,000	**6,000**	**1.8**	**2.3**	**0.23**
NG_{19}	**PEG_{2000}PLADMA/HEMAPLA/MEMA(10:45:45)**	1,400	**3,000**	**2.2**	**1.8**	**0.28**
NG_{20}	**PEG_{2000}PLADMA/HEMAPLA/MEMA(50:25:25)**	5,700	**8,000**	**1.4**	**3.0**	**0.13**

Table 3.5. GPC Results for PEG_{4600} Nanogel Series: non-degradable (NG_{21}), internally degradable (NG_{22}), externally degradable (NG_{23}), and internally-externally degradable (NG_{24}).

	Nanogel Name	$\bar{M}_n$	$\bar{M}_w$	$\bar{M}_w/\bar{M}_n$	$\bar{R}_h$	MH-*a*
NG_{21}	**PEG_{4600}DMA/HEMA/MEMA(50:25:25)**	13,000	**15,000**	**1.2**	**3.3**	**0.71**
NG_{22}	**PEG_{4600}PLADMA/HEMA/MEMA(50:25:25)**	19,000	**24,000**	**1.3**	**3.4**	**-**
NG_{23}	**PEG_{4600}DMA/HEMAPLA/MEMA(50:25:25)**	13,000	**16,000**	**1.2**	**3.2**	**0.74**
NG_{24}	**PEG_{4600}PLADMA/HEMAPLA/MEMA(50:25:25)**	6,700	**18,000**	**1.1**	**3.2**	**-**

3.3.2. Nanogel ^{1}H NMR Analysis

^{1}H NMR spectra of nanogels help to verify the structures particularly for low M_w particles. We calculated the ratio of di-vinyl group $C{=}CH_2$ (peak at 5.7 or 6.2) to PEG length PEG-OCH_2CH_2O- (peak at 3.64) for PEG_{600} and PEG_{2000} series (Table 3.6-9). This ratio is correlated with functional group density of the active nanogel. Increasing the PEG concentration from 10 to 50 mol% reduces this ratio. This trend was observed for all nanogel groups except for NG_2 and NG_{16}, due to unreacted residual IEM trapped in the

precipitated nanogel. We also observed a decreasing effect on (peak 6.2/peak 3.64) ratio, when PEG molecular weight increased from 600 to 2000 g/mol, while concentration of the crosslinker remained constant. In all four nanogel categories, the nanogel with highest concentration of crosslinker and highest molecular weight of PEG had the lowest functional group density (NG_4, NG_8, NG_{12}, and NG_{20}), except for NG_{16} (Table 3.6-9).

Table 3.6. ^{1}H NMR Results for Non-Degradable Nanogels (NG_1-NG_8).

	Nanogel Name	Peak 6.2 ppm/Peak 3.64 ppm
NG_1	**PEG_{600}DMA/HEMA(10:90)**	0.0359
NG_2	**PEG_{600}DMA/HEMA(50:50)**	0.0370
NG_3	**PEG_{2000}DMA/HEMA(10:90)**	0.0255
NG_4	**PEG_{2000}DMA/HEMA(50:50)**	0.0036
NG_5	**PEG_{600}DMA/HEMA/MEMA(10:45:45)**	0.0368
NG_6	**PEG_{600}DMA/HEMA/MEMA(50:25:25)**	0.0108
NG_7	**PEG_{2000}DMA/HEMA/MEMA(10:45:45)**	0.0201
NG_8	**PEG_{2000}DMA/HEMA/MEMA(50:25:25)**	0.0063

Table 3.7. ^{1}H NMR Results for Internally Degradable Nanogels (NG_9-NG_{12}).

	Nanogel Name	Peak 6.2 ppm/Peak 3.64 ppm
NG_9	**PEG_{600}PLADMA/HEMA(10:90)**	0.1862
NG_{10}	**PEG_{600}PLADMA/HEMA(50:50)**	0.0587
NG_{11}	**PEG_{2000}PLADMA/HEMA(10:90)**	0.0089
NG_{12}	**PEG_{2000}PLADMA/HEMA(50:50)**	0.0064

Table 3.8. ^{1}H NMR Results for Externally Degradable Nanogels (NG_{13}-NG_{16}).

	Nanogel Name	Peak 6.2 ppm/Peak 3.64 ppm
NG_{13}	**PEG_{600}DMA/HEMAPLA/MEMA(10:45:45)**	0.0594
NG_{14}	**PEG_{600}DMA/HEMAPLA/MEMA(50:25:25)**	0.0094
NG_{15}	**PEG_{2000}DMA/HEMAPLA/MEMA(10:45:45)**	0.0129
NG_{16}	**PEG_{2000}DMA/HEMAPLA/MEMA(50:25:25)**	0.0169

Table 3.9. ^{1}H NMR Results for Internally-Externally Degradable Nanogels (NG_{17}-NG_{20}).

	Nanogel Name	Peak 6.2 ppm/Peak 3.64 ppm
NG_{17}	**PEG_{600}PLADMA/HEMAPLA/MEMA(10:45:45)**	0.0293
NG_{18}	**PEG_{600}PLADMA/HEMAPLA/MEMA(50:25:25)**	0.0141
NG_{19}	**PEG_{2000}PLADMA/HEMAPLA/MEMA(10:45:45)**	0.0210
NG_{20}	**PEG_{2000}PLADMA/HEMAPLA/MEMA(50:25:25)**	0.0029

3.3.3. Nanogel DMA Characterization

All of the nanogels in this study had T_g at or below room temperature (Fig A.1-10) and Tan δ less than unity, which is an indication of elastic behavior (Mahlin, 2009). The highest (25.2 ± 0.71 °C) and lowest (-77.7 ± 0.07 °C) average glass transition temperatures belonged to externally degradable PEG_{600}DMA/HEMAPLA/MEMA(10:45:45) (NG_{13}) (Fig A.7) and non-degradable PEG_{2000}DMA/HEMA(50:50) (NG_3) (Fig A.2) nanogels, respectively. The flexibility of the backbone and the T_g of constituent monomers were the dominant factors in nanogel T_g values. Increasing the crosslinker concentration from 10 to 50 mol% decreased the T_g 21.2 ± 0.41 °C between NG_1 and NG_2 (Fig A.1), as opposed to increase it, and 41.3 ± 0.85 °C between NG_3 and NG_4 (Fig A.2), which is due to the increased fraction of the lower T_g monomer (PEG) compared to higher T_g monomer (HEMA) in the co-polymer composition (Verhoeven, 1989; Fernandez-Garcia, 2000). This trend was also observed between NG_5 and NG_6 with decreasing T_g of 14.9 ± 0.55 °C (Fig A.3), and NG_7 and NG_8 difference was 21.8 ± 19.1 °C (Fig A.4). Furthermore, in non-degradable nanogel category of PEG/HEMA, increasing PEG molecular weight from 600 to 2000 g/mol at constant crosslinker concentration, resulted in a T_g reduction of about 47.3 ± 0.92 °C and -67.3 ± 0.22 °C at 10 and 50 mol% crosslinker concentration, respectively. The same trend was observed for PEG/HEMA/MEMA non-degradable nanogel category. Glass transition temperature of PEGs decreases with increasing their molecular weight, as a result of increased flexibility of the longer PEG length. Consequently, nanogels with longer PEGs in their backbone had lower T_gs. Replacing half of HEMA with MEMA in the nanogel structure, while keeping the crosslinker concentration constant at 10 mol% (45

mol% MEMA content), had a mixed effect on T_g. The T_g difference between NG_1 and NG_5 was 5.35 ± 0.55 °C, and between NG_3 and NG_7 was 6.1 ± 1.1 °C. On the other hand, the T_g difference when crosslinker concentration was 50 mol% (25 mol% MEMA content) (Fig A.1-4) increased 0.9 ± 0.41 °C from NG_2 to NG_7, and 13.4 ± 19.1 °C between NG_4 and NG_8, which is an indication of dominant effect of higher PEG concentration on reducing T_g. Addition of PLA to the backbone and side chain of the nanogel structure had an overall increasing effect on the T_g compared to controls. In internally degradable nanogel category, there was statistically significant difference between the T_g of NG_9 and NG_{10}, but when PEG molecular weight increased from 600 to 2000 g/mol in NG_{11} and NG_{12}, there was a -12.2 °C reduction in T_g (Fig A.5-6). Furthermore, the dependency of T_g on nanogel molecular weight did not exhibit a conventional trend, due to the dominant effect of nanogel composition. The effect of PLA addition to both crosslinker and side-chain monomer, had more dominant effect on raising the T_g compared to control, when PEG was longer (PEG molecular weight = 2000 g/mol) (Fig A.9-10).

3.3.4. Equilibrium Swelling Analysis

The amount of water uptake of a polymeric material is correlated with its free volume and chain polarity (Simon, 1998). The amount of unbound water, which is correlated with free volume in the network only contributes to mass gain as opposed to swelling, but what causes swelling is the amount of bound water, which is directly correlated with the polarity of the polymer chains. Water uptake measurement is based on mass gain during swelling, therefore volume change data is needed to decouple the effect of free volume and chains polarity. In common crosslinked systems, where a crosslinker is directly mixed with a monofunctional monomer and polymerized to form a

macroscopic network, increasing the crosslinker concentration decreases free volume available in the bulk and decreases water uptake. Equilibrium degree of swelling is considered where water uptake vs. time curve plateaus for a long period of time, which its value is solvent and temperature dependent, and is obtained from balancing the osmotic drive to dilute the polymer and the entropic resistance to chain extension (Hiemenz, 2007; Hoffman, 2013). Equilibrium degree of swelling of a polymer provides valuable information regarding biomedical and pharmaceutical applications including: the solute diffusion coefficient, surface properties and surface molecule mobility, mechanical properties, and optical properties (contact lens) (Hoffman, 2013). In our systems, we have to consider two types of free volumes: first, the intra-particle free volume associated with nanogel particle itself and is governed by concentration of the primary crosslinker and its functional group density; second, the inter-particle free volume affected by the concentration of the nanogel (secondary crosslinker) and its functional group density.

Concentration of nanogel in the medium determines the distance between dispersed particles and the level of network confluency (nanogel loading ≥ 20 wt%) (Moraes, 2011). Functional group density of nanogel particle is determined with the ratio of number of attached methacrylate groups on the particle surface to nanogel molecular weight. The post-functionalization of all nanogels in this study was performed by addition of IEM to more accessible hydroxyl groups on side-chains (equimolar to half of HEMA or HEMAPLA). It is clear that by increasing the concentration of HEMA or HEMAPLA, the number of functional groups surrounding the nanogel particle do increase. Based on this initial knowledge, we are able to look further into the swelling behavior of nanogel networks in this study:

3.3.4.1. Non-Degradable Networks

In non-degradable networks, increasing the concentration of hydrophilic primary crosslinker (PEGDMA) from 10 to 50 mol% had an overall increasing effect on water uptake (Fig 3.1 A-B), although the primary mesh size had significantly decreased. The simultaneous increase in hydrophilic character of the backbone (more PEG content) counter-balances the tighter mesh size, yet draws more water molecules into polymer network. It is important to note, when the concentration of the primary crosslinker increases, concentration of side-chain monomer(s), HEMA and MEMA decreases, leading to lower secondary functional group density, and consequently lower secondary mesh size. The lower concentration of polar side-chains (HEMA and MEMA) was entirely shielded by higher concentration of PEG. At the same time, nanogel molecular weight increased due to higher concentration of crosslinker, as a result, secondary functional group density decreases furthermore, which creates much larger secondary mesh size.

The larger secondary void volume and higher hydrophilicity of the nanogel have dominant collective impact on raising the equilibrium water uptake than reverse effect of smaller primary mesh size and lower polar side chain content. The amount of water uptake also increased when PEG molecular weight increased from 600 to 2000 g/mol at constant crosslinker concentration. The longer PEG crosslinkers possess amplified hydrophilicity due to greater oxygen content, more primary free volume due to larger distance of active chains, and less resistance to extension relative to shorter PEG (a polymer chain can be stretched by nearly a factor of $N^{1/2}$; N is the number of repeat units) (Hiemenz, 2004; Dill, 2010). Comparing two non-degradable control groups, PEGDMA/HEMA and PEGDMA/HEMA/MEMA indicated that, replacing half of HEMA with

MEMA slightly decreased equilibrium water uptake when PEG length was shorter (PEG_{600}), yet did not have a significant effect in cases of longer PEGs (PEG_{2000}).

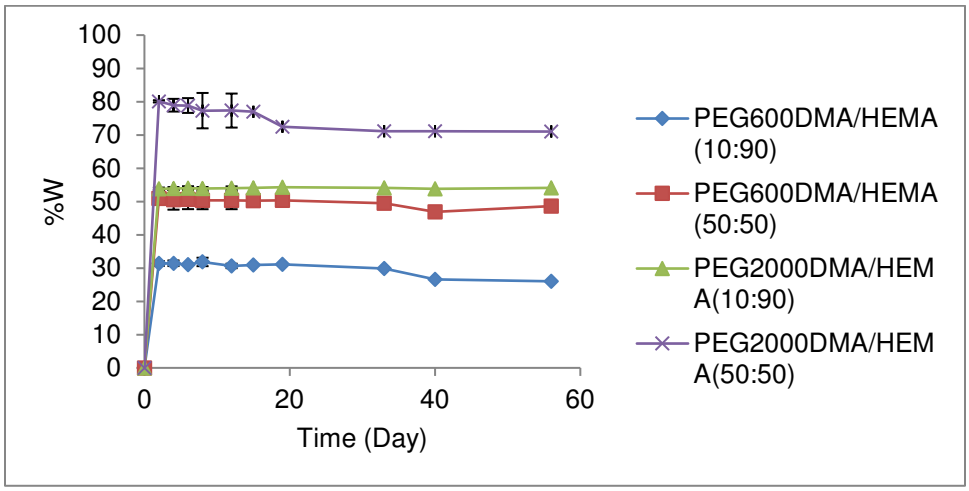

(A)

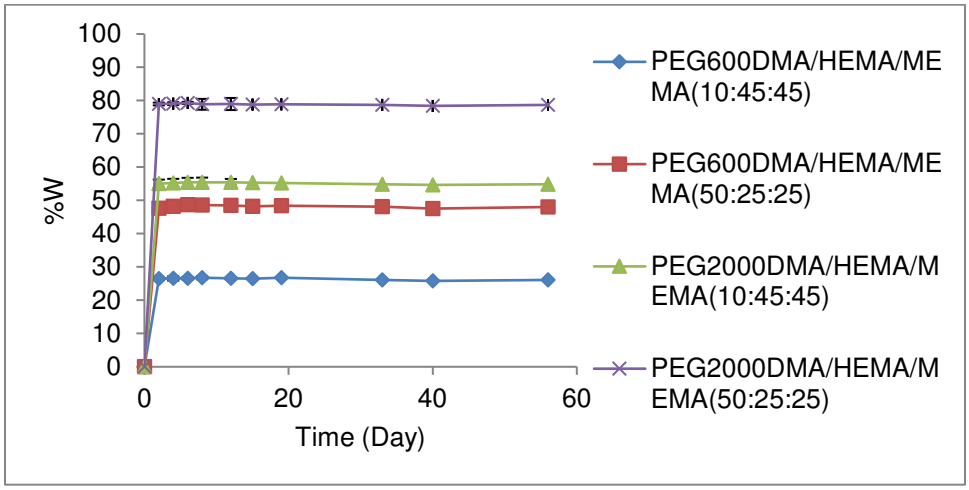

(B)

Figure 3.1. Water uptake vs. time for non-degradable nanogel networks; (A) NG_1-NG_4, (B) NG_5-NG_8; PEG molecular weight = 600, 2000 g/mol.

3.3.4.2. Internally Degradable Networks

Adding hydrophobic PLA linkages to both sides of PEG in internally degradable networks (Fig 3.2) decreased the degree of swelling (day 56) compared to non-degradable counterparts, except for PEG_{2000}PLADMA/HEMA(50:50) (NG_{12}), which water uptake did not change compared to the control (*p*-level = 0.52). Adding PLA on both sides

of PEG increases primary void volume yet decreases the polarity of polymer backbone. In addition, increasing the degradable crosslinker concentration lowered swelling in a greater extent compared to control when core PEG segment was shorter (600 g/mol). The value of equilibrium water uptake for PEG_{600}PLADMA/HEMA(10:90) (NG_9) and PEG_{600}PLADMA/HEMA(50:50) (NG_{10}) on day 2 was statistically the same (*p*-level = 0.25), which shows that these two systems are equivalent in terms of total void volume and chain polarity.

On the other hand, the value of water uptake was 20.9% higher in PEG_{2000}PLADMA/HEMA(50:50) (NG_{12}) than in PEG_{2000}PLADMA/HEMA(10:90) (NG_{11}). Although unchanged total void volume also seems like a reasonable assumption here, yet polarity increase is the main contributor to invite more water inside the former network NG_{12} than the latter NG_{11}. Also, for NG_{11} we observed a 6.6% reduction in W (*p*-level = 0.006), and there was a visual indication of mass loss, therefore we can conclude that the degraded mass did not leave the sample as a result of high secondary crosslinking density.

In NG_{12}, the water uptake increased about 5.0% from day 2 to 56 and never reached a plateau. This observation is an indication of gradually increasing void volume due to degradation and being occupied simultaneously by more penetrated water molecules. For NG_{11}, the opposite trend (deswelling) was observed, since W decreased from 51% (day 2) to 44.5% (day 56). As it was discussed before, the secondary mesh size in this nanogel is much tighter than in NG_{12} due to higher HEMA content and consequently higher secondary crosslinker, therefore the impenetrable and non-degradable outer shell is able to trap the degraded species inside the network and shift

the osmotic drive. NG_9 and NG_{10} remained at equilibrium level of water content until the end of study, which shows a mass balance between water entering the network and degraded mass leaving the network.

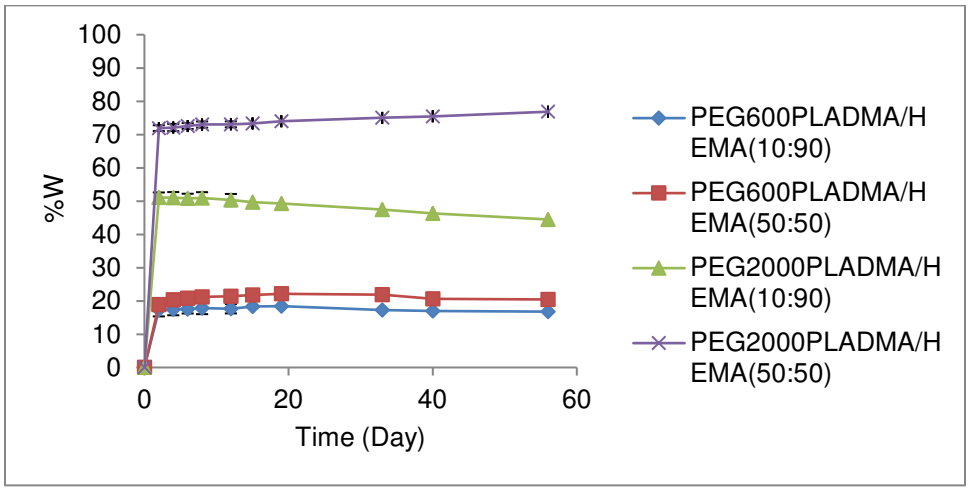

Figure 3.2. Water uptake vs. time for internally degradable nanogel networks, NG_9-NG_{12}; PEG molecular weight = 600, 2000 g/mol.

3.3.4.3. Externally Degradable Networks

The amount of water uptake of PEG_{600}DMA/HEMAPLA/MEMA(10:45:45) (NG_{13}) decreased about 10% compared to the control (NG_5). On the other hand, in PEG_{600}DMA/HEMAPLA/MEMA(50:25:25) (NG_{14}), we observed a 13% increase in W compared to its non-degradable counterpart (NG_6), also NG_{14} had 45% more water content than NG_{13} (Fig 3.3). The reason for higher W in NG_{14} than in NG_6 might be related to hard sphere behavior of NG_{14} particles (MH-a = 0.33 < 0.5) (Table 3.3), which lowers the packing density and increases the void volumes between particles. PEG_{2000}DMA/HEMAPLA/MEMA(10:45:45) (NG_{15}) and PEG_{2000}DMA/HEMAPLA/MEMA(50:25:25) (NG_{16}) networks, had 5% decrease and no change in water uptake compared to their controls, respectively. Comparing these

nanogels within the group showed that decreasing the concentration of HEMAPLA increased swelling in a greater extent when molecular weight of PEG was lower (600 g/mol). Based on these observations, the more dominant factor in reducing water sorption is, to what extent the hydrophilicity of the backbone is affected by shielding effect of PLA on the side-chains. All the nanogel networks in this group remained at equilibrium state until day 56.

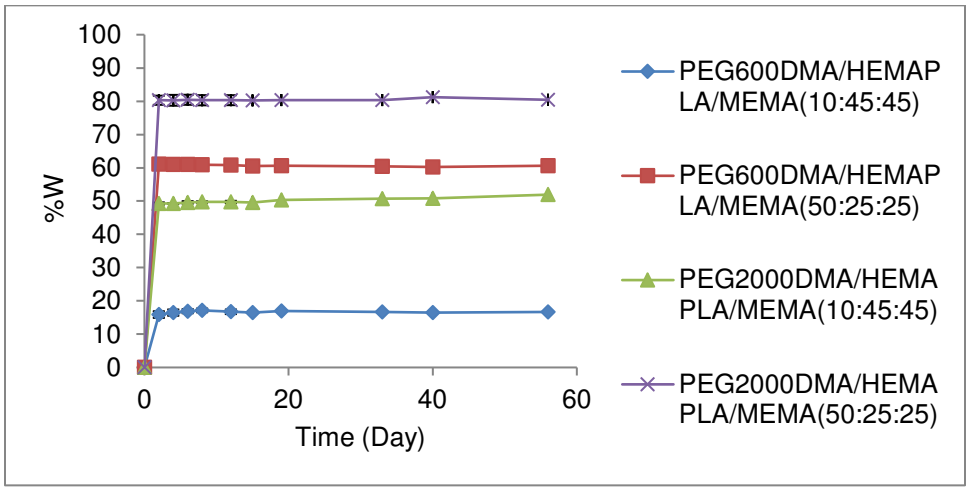

Figure 3.3. Water uptake vs. time of externally degradable nanogel networks, NG_{13}-NG_{16}; PEG molecular weight = 600, 2000 g/mol.

3.3.4.4. Internally-Externally Degradable Networks

In internally-externally degradable networks, we observed different trends not only compared to controls but also to other types of degradable groups. The initial water content (day 2) of PEG_{600}PLADMA/HEMAPLA/MEMA(10:45:45) (NG_{17}) was 10%, which was the lowest among all other groups, yet it continued swelling linearly with lower rate than the initial rate without reaching equilibrium plateau until the end of the study (day 56), with final W of 32% (Fig 3.4). The initial low water uptake is due to significant increase of PLA content both in the backbone and side-chains, and the linear increase of W from day 2, is a result of higher inward diffusion rate of water than outward diffusion rate of

degraded species. In PEG_{600}PLADMA/HEMAPLA/MEMA(50:25:25) (NG_{18}), initial water uptake reached 31% (day 2) and gradually decreased to 17% (day 56). Higher initial swelling compared to NG_{17} is a result of enhanced polarity (more PEG_{600} content), yet the reduction in W overtime represents the underlying degradation process and the actual reduction in mass. In this type of network, more PLA units must be cleaved for erosion of the network and consequently more water concentration is needed based on hydrolysis kinetics. The initial water uptake of PEG_{2000}PLADMA/HEMAPLA/MEMA(10:45:45) (NG_{19}) was 47%, which immediately reached equilibrium. The NG_{19} samples sustained their equilibrium state at 47% water content until day 56, this behavior indicates a continuous mass balance between degradation and diffusion, in other words, the residence time of degraded polymers approaches zero due to larger secondary mesh size. We also can recall from equilibrium swelling of non-degradable samples that larger secondary mesh size had the dominant effect on water diffusion. PEG_{2000}PLADMA/HEMAPLA/MEMA(50:25:25) (NG_{20}) network had the highest initial water content of 84% among all the networks in this study, water continued diffusing into the network until day 12 when blotting/weighing (mechanical stress) turned the sample into several pieces. All the pieces were transferred into the water but it was clear after this point on the erosion would be enhanced due to smaller sample size. On day 20 very small residual pieces were left from the whole sample, which made gravimetric measurement no longer feasible. The continuation of swelling after day 2 is an indication of uninterrupted and rapid primary and secondary crosslinker bond cleavage, due to higher initial water content and high concentration of PLA. The microscopic reverse gelation happened after day 20 when the original network was completely dissolved in

water. As it was mentioned before, we consider this as a premature reverse gelation due applying external stress to the network during weight measurement.

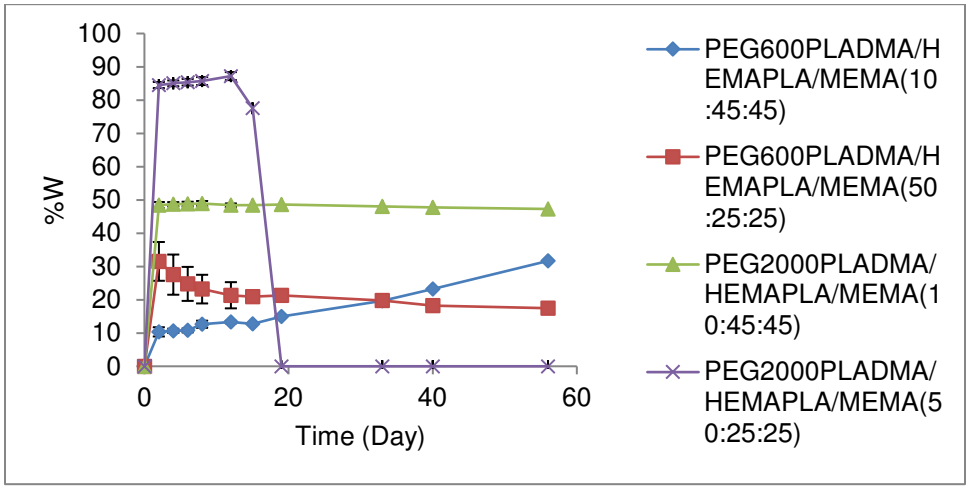

Figure 3.4. Water uptake vs. time of internally-externally degradable nanogel networks, NG_{17}-NG_{20}; PEG molecular weight = 600, 2000 g/mol.

3.3.5. Compressive Modulus Analysis

For understanding the mechanical strength of a swollen hydrogel network we need to consider two independent contributing factors: i) crosslinking density and ii) polymer volume fraction. The compressive modulus of a polymer network is directly proportional to crosslinking density, polymer volume fraction, and inversely proportional to the molecular weight between crosslinks ($\bar{M}_c$) (Eq 3.3-5). Also the polymer volume fraction (ϕ_2) is inversely proportional to the degree of swelling (Q_v) (Eq 3.3-5) (Metters, *Polym* 2000). Based on this knowledge, for hydrogels composed of nanogel particles in this study, the macroscopic compressive modulus should be inversely correlated with the number averaged molecular weight between primary and secondary crosslinks ($\bar{M}_x$). For a network composed of crosslinked Gaussian chains this relationship is determined through rubber elasticity theory and correlation between Young's modulus (E), macroscopic compressive modulus (K), and shear modulus (Eq 3.3-5) (Metters, *Polym*

2000; Hiemenz, 2007). These equations are valid under the following assumptions: i) no defects in the network (no loops, no dangling ends, and no multiple crosslinks), ii) crosslinked Gaussian chains are still Gaussian, iii) each junction point moves in proportion to the macroscopic deformation (affine junction assumption), iv) free energy gradient is purely entropic (ideal elastomer), and v) conservation of volume during deformation. In fact assumption (v) meets the experimental condition in this study, since we measured the modulus in the linear regime of stress-strain curve, where extension ratio approaches 1 ($\lambda \rightarrow 1$).

$$3K\ (1-2\nu) = \ 2G\ (1+\ \nu) \tag{3.3}$$

$$K = \left(\frac{2\ (1+\nu)}{3\ (1-2\nu)}\right)\frac{\rho RT}{\bar{M}_x} \tag{3.4}$$

$$K = \ \left(\frac{2\ (1+\nu)}{3\ (1-2\nu)}\right)\ \frac{\rho RT}{\bar{M}_x}\ (\phi_2)^{1/3} \tag{3.5}$$

In Eq 3.3, v is the Poisson's ratio and its value is strongly dependent on packing and connectivity of the material (Greaves, 2011). Eq 3.4 and Eq 3.5 are used for dry and swollen hydrogels, respectively, Eq 3.5 indicates that compressive modulus of a swollen network is reduced by a factor of $(\phi_2)^{1/3}$ compared to dry network. The other parameters in Eq 3.4-5 are density of dry macroscopic network (ρ), gas constant (R), and temperature (T). The same level of packing in dry state of macroscopic nanogel networks in this study is a safe assumption due to confluent nature of these networks, yet they differ in degree of crosslinking (connectivity), therefore the real values of Poisson's ratio in dry state of each network is different. Additionally v_{dry} and $v_{swollen}$ is different for each sample due to the effect of swelling on packing, therefore assumption of constant v ($v_{dry\ polymer}$ ~ 0.3; $v_{isotropic\ hydrogel}$ ~ 0.45) (Kloxin, 2010; Greaves, 2011) for all samples in dry and equilibrium

swollen state is a poor assumption, however it is an inevitable alternative due to lack of shear modulus (G) or Young's modulus (E) data (Hiemenz, 2007). In addition, we assumed that dry and swollen networks are both isotropic due to quasi-homogeneous distribution of crosslinks. Polymer volume fraction (ϕ_2) can be obtained gravimetrically by using Eq 3.6-8 (Metters, 2006).

$$Q_m = \frac{M_s}{M_d} \tag{3.6}$$

$$Q_v = 1 + \frac{\rho_p}{\rho_s}(Q_m - 1) \tag{3.7}$$

$$\phi_2 = \frac{1}{Q_v} \tag{3.8}$$

Here, Q_m is mass swelling ratio, M_s network swollen mass, M_d network dry mass, ρ_p polymer density (equal to ρ in Eq 3.4 and 3.5), and ρ_s water density (1 g/cm^3). We also evaluated $\bar{M}_x$ for swollen hydrogels based on equilibrium swelling theory or Flory-Rehner equation (Eq 3.10) (Hiemenz, 2007) by assuming: i) isotropic swelling, ii) no contribution of network in ΔG_m ($N \rightarrow \infty$) using Flory-Huggins theory (Eq 3.9), and iii) free energy gradient of mixing and distortion are purely entropic, or in other words $\chi = 0$ and $\Delta G_{el} = -T\Delta S_{el}$, respectively.

$$\frac{\Delta G_m}{kT} = \phi_1 \ln \phi_1 + \frac{\phi_2}{N} \ln \phi_2 + \phi_1 \phi_2 \chi \tag{3.9}$$

$$\bar{M}_x = \frac{\rho \hat{V}_1 \left(\frac{\phi_2}{2} - \phi_2^{1/3}\right)}{\ln(1-\phi_2) + \phi_2 + \chi \phi_2^2} \tag{3.10}$$

In Eq 3.7, *k* is Boltzmann constant, (ϕ_1) solvent volume fraction, and χ solvent-polymer interaction parameter. In Eq 3.10, $\hat{V}_1$ is molar volume of the solvent (18 cm^3/mol for water). The value of $\bar{M}_x$ for dry network using Eq 3.10 is mathematically undefined, since

($\phi_2 = 1$), and also it violates the underlying thermodynamics concepts of this relationship, since neither mixing nor distortion occur in dry sample, thus Eq 3.10 is not the best model to evaluate $\bar{M}_x$ history from dry state all the way to degraded state in hydrogel systems, therefore our analysis is predominantly based on $\bar{M}_x$ values using Eq 3.4-5 and compressive modulus measurements.

3.3.5.1. Non-Degradable Network

In non-degradable hydrogels, the decrease of compressive modulus from dry to swollen state is due to $(\phi_2)^{1/3}$ factor (the larger the value of Q_m the lower the ϕ_2), not increasing $\bar{M}_x$ (Fig 3.5 A-D). The first observation is that, K values of dry samples in all four categories of nanogel network in this study are two orders of magnitude higher than the compressive modulus of networks obtained by radical polymerization of functionalized PEG-*co*-PLA macromer only (Metters, *Polym* 2000; Clapper, 2007). Samples with lower primary crosslinking (10 mol%) and higher secondary crosslinking had higher dry modulus, although this trend was less pronounced and even reversed when PEG length changed from 600 to 2000 g/mol. For PEG_{2000}DMA/HEMA/MEMA(50:25:25) (NG_8) and PEG_{2000}DMA/HEMA/MEMA(10:45:45) (NG_7), the difference in modulus was $\Delta K \approx 71.5$ MPa with former having higher modulus than the latter. These trends reveal the dominant effect of primary crosslinking, when PEG length is long, and that of secondary crosslinking, when PEG is short. Another contributor to high modulus of nanogel networks with lower primary crosslinking (higher secondary crosslinking) might be due to higher level of chain entanglements in the overlapped regions. In addition, K values for NG_7 did not change statistically all throughout the experiment (*p*-level between groups = 0.31). NG_7 networks had average water uptake of 50%, therefore, based on Eq 3.5, constant K

after swelling with no degradation involved, may be related to the microstructure of these gels, which under compressive stress squeeze the water out. Replacing half of HEMA with MEMA had mixed effects on dry K values.

In PEG_{600} nanogel series in this group (Fig 3.5 A-B), adding MEMA increased the modulus as opposed to PEG_{2000} series (Fig 3.5 C-D). The increasing modulus effect might be due to more reactivity of MEMA monomers compared to HEMA during nanogel synthesis, since MEMA radicals are relatively more stable than HEMA (due to less electron withdrawing effect of methoxy compared to hydroxyl), as a result MEMA monomers are consumed at early stages of particle formation due to less stability, and HEMAs at later stages. Consumption of HEMAs at later stages of reaction creates more distribution of HEMA towards the surface of the nanogel, thus after functionalization with IEM, methacrylate groups are more accessible for crosslinking. The reducing effect on modulus by addition of MEMA to nanogel formulation happened when PEG length increased. PEG_{2000}DMA/HEMA/MEMA(10:45:45) (NG_7) had significantly lower modulus than PEG_{2000}DMA/HEMA(10:90) (NG_3) ($\Delta K \approx 104$ MPa), this is due to lower secondary crosslinking density in NG_7 than in NG_3. On the other hand, PEG_{2000}DMA/HEMA/MEMA(50:25:25) (NG_8) and PEG_{2000}DMA/HEMA(50:50) (NG_4) had the same dry moduli (*p*-level = 0.52), which is due to higher density of former compared to latter by factor of 3. All samples showed decrease in modulus after immersion in water (day 3), although the difference between dry and wet modulus ($\Delta K_{dry\text{-}wet}$) was different for each group. Fig 3.5A does not show a difference in $\Delta K_{dry\text{-}wet}$ after PEG_{600}DMA concentration increases from 10 to 50 mol%, even though water uptake is 20% higher in PEG_{600}DMA/HEMA(50:50) (NG_2) compared to PEG_{600}DMA/HEMA(10:90) (NG_1), also the

same trend was observed for PEG_{600}DMA/HEMA/MEMA(10:45:45) (NG_5) and PEG_{600}DMA/HEMA/MEMA(50:25:25) (NG_6). This observation might be due to increase in v (less packing), $(\phi_2)^{1/3} < 1$ is also an important factor. More swelling decreases the value of $(\phi_2)^{1/3}$ but increases v, therefore several parameters such as ϕ_2, v_{dry}, $v_{swollen}$, ρ, and $\bar{M}_x$ have to change simultaneously to keep $\Delta K_{dry\text{-}wet}$ constant between two networks. On the other hand, when PEG length increased the $\Delta K_{dry\text{-}wet}$ value increased for the networks with higher primary crosslink density. The $\Delta K_{dry\text{-}wet}$ in PEG_{2000}DMA/HEMA(10:90) (NG_3) and PEG_{2000}DMA/HEMA(50:50) (NG_4) was 101.4 MPa and 153 MPa, respectively. Furthermore, the $\Delta K_{dry\text{-}wet}$ of PEG_{2000}DMA/HEMA/MEMA(10:45:45) (NG_7) and PEG_{2000}DMA/HEMA/MEMA(50:25:25) (NG_8) were 12 MPa and 152 MPa, respectively. This observation indicates that in longer PEG length, reduction of $(\phi_2)^{1/3}$ is the dominant factor in changing K. The isotropic range of Poisson's ratio is -1 ≤ v ≤ ½ at small strains, the upper limit v = ½ indicates that deformation causes no volume change and stress is a result of shape change. The lower limit v = -1 corresponds to network structure (i.e. foam, sponge) with high compressibility (Greaves, 2011). In all groups $K_{swollen}$ remained relatively constant until the end of study.

(A)

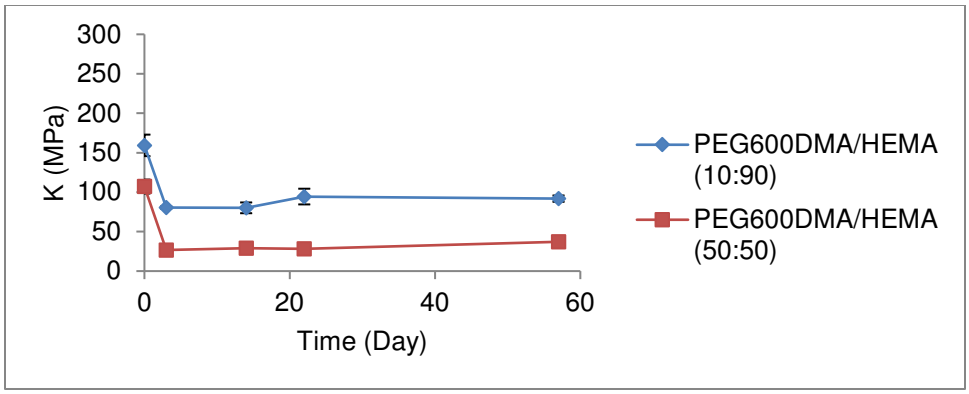

(B)

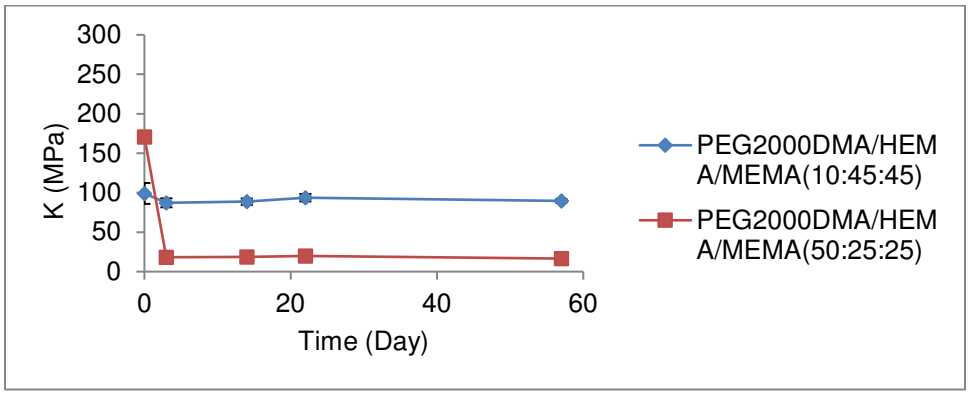

(C)

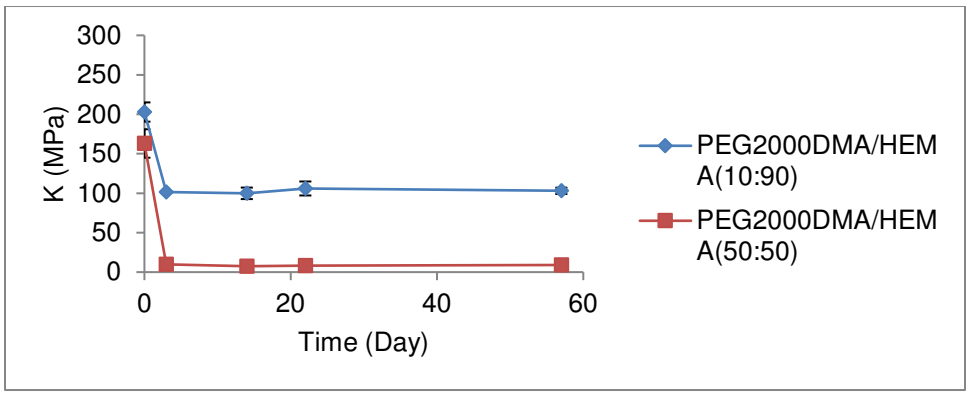

(D)

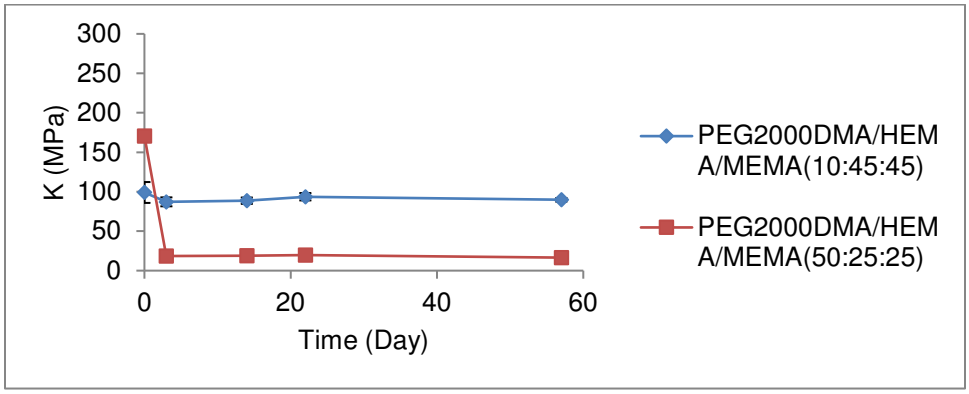

Figure 3.5. Compressive modulus (K) vs. time for non-degradable nanogel networks (NG_1-NG_8).

3.3.5.2. Internally Degradable Networks

In internally degradable networks with PEG_{600}PLADMA as crosslinker, when the primary crosslinker concentration increased from 10 to 50 mol% there was no significant effect on dry compressive modulus (*p*-level = 0.98) (Fig 3.6A). The minimum difference between dry and wet modulus was observed for the network with lowest degree of swelling (PEG_{600}PLADMA/HEMA(10:90)) (NG_9). In addition, K of values NG_9 from day 0 until 47 are statistically the same (*p*-level between groups = 0.15). Based on this information and swelling trend for NG_9 we can say there was no significant degradation was happening during the time of experiment.

There was a reduction of 80.7 MPa in K for (PEG_{600}PLADMA/HEMA(50:50)) from day 0 to day 47 (*p*-level = 0.00024), and 21 MPa from day 4 to day 47 (*p*-level = 0.00146), therefore K reduction in NG_{10} was the result of both swelling and degradation simultaneously, although its swelling data showed a plateau throughout the swelling experiment (day 4 to day 56). The K values on day 0 and day 47 for PEG_{2000}PLADMA/HEMA(10:90) (NG_{11}) were statistically the same as well (*p*-level = 0.33), similar to NG_7 (Fig 3.5 D), we also observed a 6.6% deswelling for this network, therefore we can say trapped degraded species (lactic acid and PEG_{2000}) not only reversed the osmosis effect but also were entangled inside the network and maintained the modulus.

Comparing NG_{11} and NG_7 in terms of possessing similar microstructure opens up a whole new topic, which is beyond the focus of our research. The Poisson's ratio is defined as the ratio of transverse strain (e_t) to longitudinal strain (e_l) (Eq 3.11), therefore when an isotropic polymer network swells, its behavior shifts toward incompressible

rubber ($\nu \rightarrow 0.5$) with smaller longitudinal strain, yet any conclusion about changes in ν for this case needs more pieces of information such as shear modulus or young's modulus (Eq 3.3).

$$\nu = -\frac{e_t}{e_l} \tag{3.11}$$

Keeping the primary crosslinker concentration constant at 10 mol% while PEG length increased from 600 to 2000 g/mol, decreased the dry compressive modulus from NG_9 to NG_{11} (ΔK_{dry} = 140.7 MPa) (*p*-level = 0.0013), although K_{dry} did not statistically changed for 50 mol% crosslinker while PEG length changed. This result shows that functional group density reduction of primary crosslinker has more detrimental effect on compressive modulus when primary crosslinker concentration is lower. Furthermore, in nanogels with PEG_{2000}PLADMA as the primary crosslinker, when concentration increased from 10 to 50 mol%, dry compressive modulus increased about 50%. This implies that when the crosslinker is longer due to longer PEG, increasing the primary crosslink density is more dominant in increasing the mechanical property than the adverse effect of secondary crosslink density reduction. The maximum difference between dry and wet modulus was observed for PEG_{2000}PLADMA/HEMA(50:50) (NG_{12}), which had the highest equilibrium water uptake, also its average K value on day 47 was 10.8 MPa lower than that of on day 4 with marginal *p*-level of 0.0499. The decrease in K indicates that $\bar{M}_x$ has increased due to hydrolytic degradation (shown by swelling data as well).

(A)

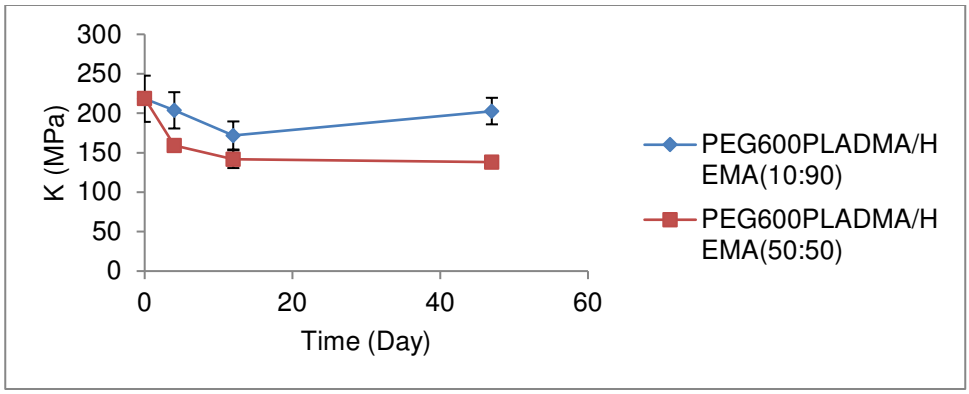

(B)

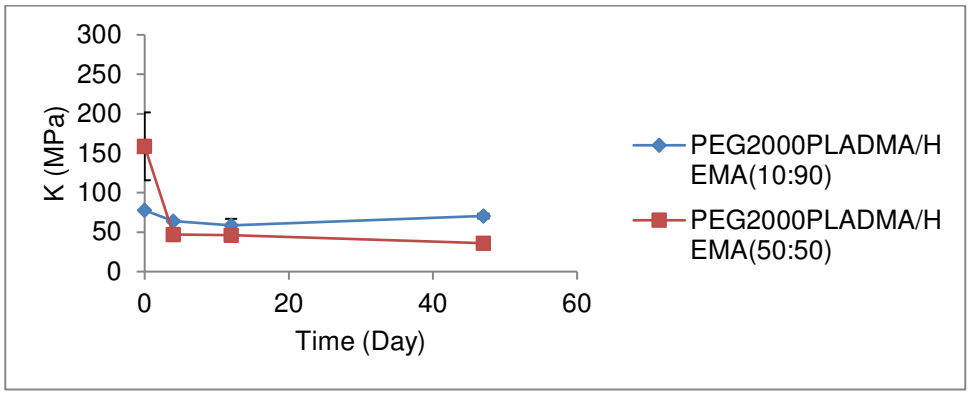

Figure 3.6. Compressive modulus (K) vs. time for internally degradable nanogel networks (NG_9-NG_{12}).

3.3.5.3. Externally Degradable Networks

Increasing the primary crosslinker ($PEG_{600}DMA$) concentration from 10 to 50 mol% (Fig 3.7A) decreased the dry compressive modulus (ΔK_{dry} = 113 MPa). This result confirms the effects of higher secondary crosslinking density and degree of entanglements in nanogels with lower concentration of primary crosslinker. The $K_{swollen}$ from day 4 until the end of experiment (day 47) for $PEG_{600}DMA$/HEMAPLA/MEMA(10:45:45) (NG_{13}) (*p*-level = 0.38) and $PEG_{600}DMA$/HEMAPLA/MEMA(50:25:25) (NG_{14}) (*p*-level = 0.15) remained the same, therefore we can conclude that the cleaved chains during this time were not able to change the integrity of the network. This is due to the fact that cleaved nanogel particles in the bulk are trapped and not able to leave the network unless their neighboring

nanogels have already dissociated themselves from the surface. The same result was also observed for PEG_{2000}DMA/HEMAPLA/MEMA(10:45:45) (NG_{15}) and PEG_{2000}DMA/HEMAPLA/MEMA(50:25:25) (NG_{16}). One more time we observed that when PEG length is larger (2000 g/mol), increasing the concentration of primary crosslinker, considerably increases the dry modulus (Fig 3.7B).

The maximum difference between dry and swollen modulus was related to the networks with highest amount of water uptake, (PEG_{2000}DMA/HEMAPLA/MEMA(50:25:25) (NG_{16}) and PEG_{600}DMA/HEMAPLA/MEMA(50:25:25)) (NG_{14}), they also had the lowest $K_{swollen}$ from day 4 until the end. When we compared the final K values of NG_{12} and NG_{16}, we noticed a 21.9 MPa difference (*p*-level = 0.04) with former having higher modulus, which indicates that cleavage of secondary crosslinks has more detrimental effect on decreasing the modulus compared to cleavage of primary crosslinks. This also indicates that most effective crosslinks including the entanglements to absorb elastic energy lies between the nanogels not within their core, which goes back to the concept of decreased heterogeneity in crosslinked nanogels due to absence of sol fraction, loops, and dangling naogels. An important trend was revealed when we compared the final K values of internally degradable and externally degradable systems. This trend shows that compressive modulus of externally degradable networks on day 47 was significantly lower than final K values of internally degradable gels in the following fashion, the ΔK between NG_9-NG_{13}, NG_{10}-NG_{14}, NG_{11}-NG_{15}, and NG_{12}-NG_{16} were 73.8 MPa (*p*-level = 0.0033), 104.3 MPa (*p*-level = 0.00068), 13.7 MPa (*p*-level = 0.017), and 29.0 MPa (*p*-level = 0.00025), respectively. These results indicate: i) the most effective crosslinks including

entanglements lie between the nanogels not in their cores, ii) the compressive modulus reduces more when the primary crosslinker concentration increases, or more importantly when the secondary crosslinker concentration decreases, which confirms the fact that entanglements in the overlapped volume contribute to modulus more effectively when the secondary crosslinking density is lower, iii) K reduction at constant crosslinker concentration is higher when PEG is shorter, and iv) K reduction is higher when concentration of secondary crosslinker is lower (the same as (ii)). The reason for conclusion (iii) is due to higher functional density of the crosslinker when PEG is shorter, and increased heterogeneity of crosslinks distribution.

(A)

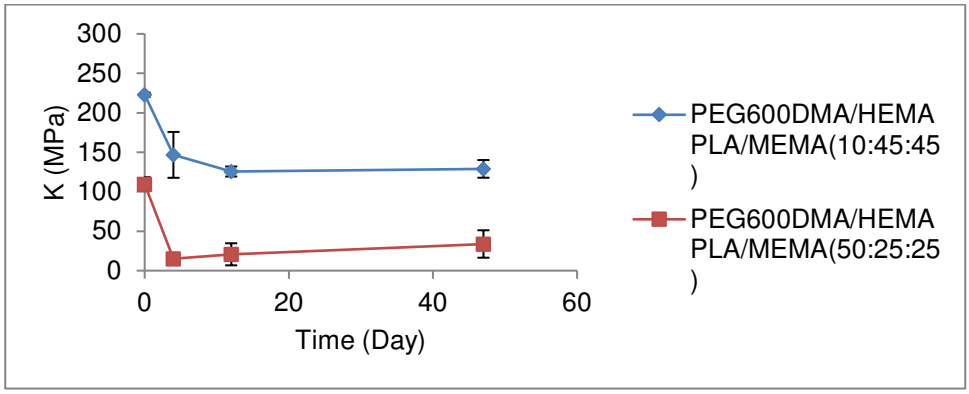

(B)

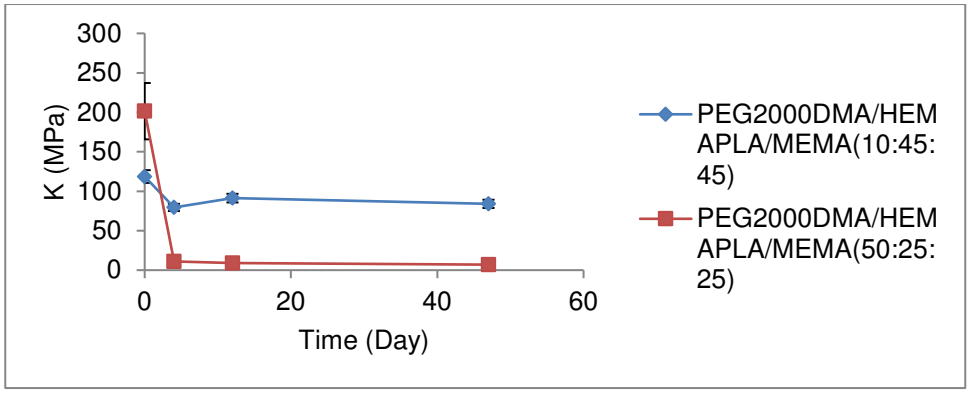

Figure 3.7. Compressive modulus (K) vs. time for externally degradable nanogel networks (NG_{13}-NG_{16}).

3.3.5.4. Internally-Externally Degradable Networks

The internally-externally networks had an overall lower compressive modulus (Fig 3.8 A-B) compared to other three groups, as a result of increased flexibility and average mesh size, due to the addition of PLA (Clapper, 2007) to both primary and secondary crosslinkers. The maximum difference between dry and swollen modulus belonged to the network with the highest amount of water uptake (PEG_{2000}PLADMA/HEMAPLA/MEMA(50:25:25)) (NG_{20}) and faster degradation rate with no mechanical integrity after day 4. Looking back to equilibrium swelling results we notice that, this is the same hydrogel that turned into pieces after weighing on day 12 (Fig 3.4). The compressive modulus results indicate that the network had started loosing its effective crosslinks long before day 12. There was 70 MPa difference between K_{dry} (day 0) and $K_{swollen}$ (day 4) in PEG_{600}PLADMA/HEMAPLA/MEMA(50:25:25) (NG_{18}), the $K_{swollen}$ was statistically the same on day 4 and day 47 (*p*-level = 0.16). This is the network with declining water content, which we predicted it was due to mass loss, but now based on K values, this prediction is not valid anymore, therefore we can conclude that the degraded mass was still trapped in the gel and contributed to entanglement and deswelling. The K value of PEG_{600}PLADMA/HEMAPLA/MEMA(10:45:45) did not change from day 0 to day 4 and onwards, we can recall from swelling observation (Fig 3.4) that this network had the lowest initial swelling, yet water uptake linearly increased until the end of experiment and our conclusion was that degraded species were not able to leave the network due to tight secondary crosslinks, but now based on K evolution, we can clearly conclude that $\bar{M}_x$ and consequently packing (Poisson's ratio) have not changed in this network, which indicates no significant hydrolytic bond cleavage has happened in this network during

swelling. The fact that water concentration is a crucial factor in defining hydrolysis reaction rate manifests itself in NG_{17} modulus plot.

(A)

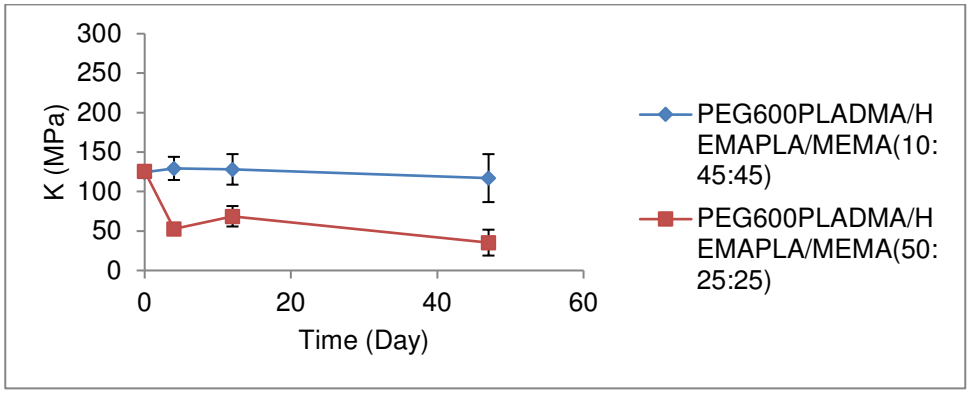

(B)

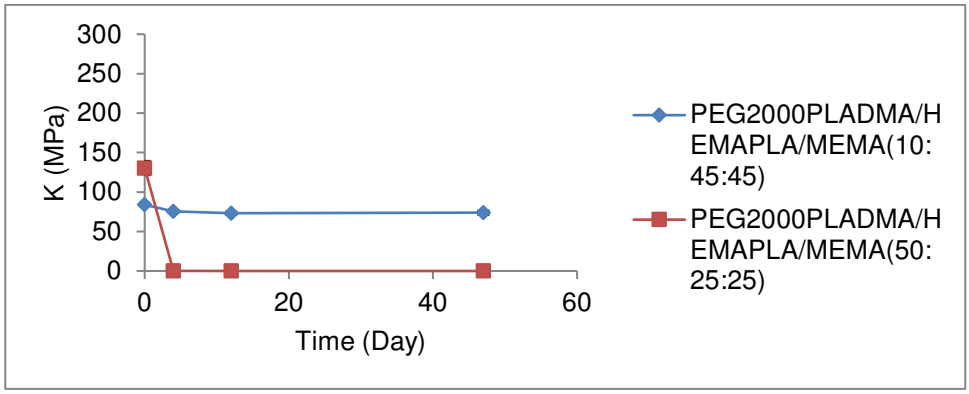

Figure 3.8. Compressive modulus (K) vs. time for internally-externally degradable nanogel networks.

3.3.6. Evaluation of $\bar{M}_x$ based on Gaussian Chain Assumption

3.3.6.1. Non-Degradable Networks

First we start our analysis by comparing the $\bar{M}_x$ values we obtained from compressive modulus measurements and using Eq 3.4 for dry samples and Eq 3.5 for swollen samples. There was an increase in $\bar{M}_x$ on day 3 for all the nanogels in this category. The lower $\bar{M}_x$ values associated with dry hydrogels is due to higher modulus in dry state, and it is related to the crosslinking density of each network and also entanglement effect in overlapped volume between nanogels. Crosslinking permanently

traps the overlapped volume, which particularly behaves similar to trapped entanglements (temporary physical crosslinks) between single chains at low secondary crosslinking density and enhances the modulus. After swelling, polymer-polymer interactions in the overlapped regions are replaced by polymer-water (good solvent) interactions, as a result the equilibrium swollen modulus has much lower value compared to dry modulus even though $\bar{M}_x$ has not changed. Fig 3.9 A-B show that $\Delta\bar{M}_x$ between dry and wet state is larger for networks with lower secondary crosslink density and higher concentration of more hydrophilic segments. Higher hydrophilicity increases swelling, as a result polymer chains in the overlapped area become more disentangled. At higher concentration of secondary crosslinking we observed that the effect of overlapping on increasing the modulus was diminished (similar to the effect of trapped entanglements in high crosslinked chains). PEG_{2000}DMA/HEMA(50:50) (NG_4) and PEG_{2000}DMA/HEMA/MEMA(50:25:25) (NG_8) had highest values of $\bar{M}_x$ at equilibrium swollen state due to higher degree of swelling, and consequently less polymer-polymer interactions. The $\bar{M}_x$ values of NG_2 on day 3 and day 57 are statistically the same (*p*-level = 0.066). The average $\bar{M}_x$ for all the networks remained constant after day 3, due to absence of hydrolytic degradation. All the $\bar{M}_x$ values were less than 2500 g/mol.

(A)

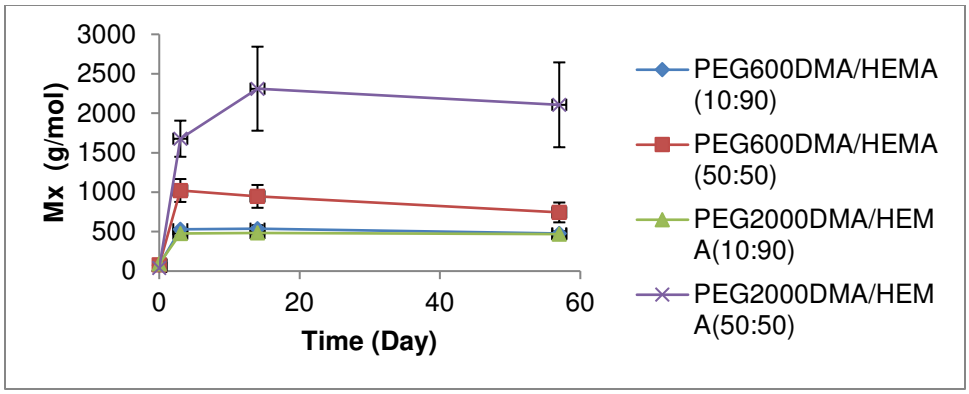

(B)

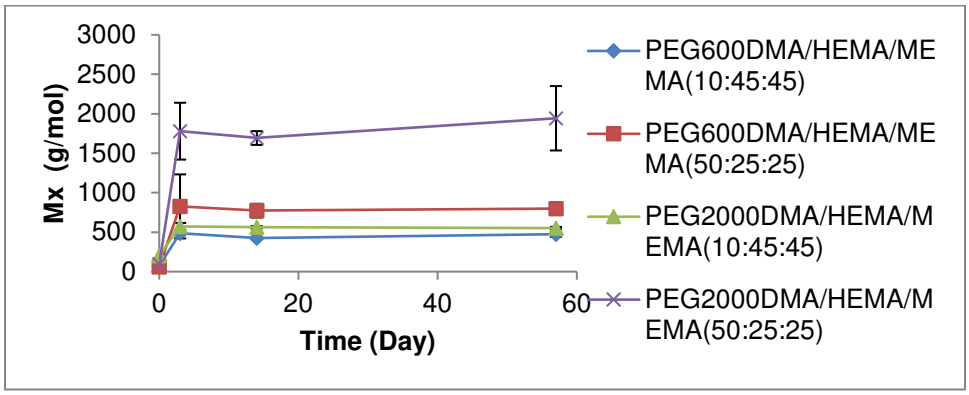

Figure 3.9. Molecular weight between crosslinks ($\bar{M}_x$) vs. time for non-degradable nanogel networks; $\bar{M}_x$ calculated based on Rubber Elasticity Theory (Eq 3.4 and Eq 3.5) and Gaussian distribution assumption for polymer chain conformations.

Figure 3.10 A-B show $\bar{M}_x$ values evaluated based on swelling equilibrium theory (Eq 3.10), since the dry values of $\bar{M}_x$ are irrelevant due to lack of fundamental theory supporting Eq 3.10, we only consider the swollen values of $\bar{M}_x$, which are dependent on ϕ_2 and polymer density (we assigned $\bar{M}_x$ = 0 for dry state). The higher the ρ_p and/or the lower the ϕ_2 are, the higher the $\bar{M}_x$ will be. The density of PEG_{2000}DMA/HEMA(10:90) (NG_3) calculated based on dry mass and mold volume had the highest value among all four networks in this plot (Fig 3.10A). The higher value of NG_3 density compared to that of NG_4 contradicts the theoretical expectation, since the higher density monomer (PEG_{2000}) is more concentrated in NG_4. The reason behind this discrepancy may be due to non-homogeneous mixture of nanogel and solvent (acetone), which can be the result

of solvent-solute incompatibility. In addition, any small changes in ϕ_2 is able to cause a much larger impact on $\bar{M}_x$ in Eq 3.10 than in Eq 3.5, therefore Flory-Rehner equation tends to overestimate the $\bar{M}_x$ if only ϕ_2 is concerned. The basis of this overestimation is the contribution of free energy of mixing for $\bar{M}_x$ evaluation in Eq 3.10. Fig 3.10B, on the other hand, shows that the $\bar{M}_x$ at equilibrium swollen state is higher for PEG_{2000}DMA/HEMA/MEMA(50:25:25) (9000 g/mol) than PEG_{2000}DMA/HEMA/MEMA(10:45:45) (4000 g/mol), which was expected. The discrepancy between the values of $\bar{M}_x$ based on Eq 3.5 and Eq 3.10 may also be related to: i) invalid assumption of Gaussian chain behavior, ii) different dry and swollen Poisson's ratios for each network, and iii) different χ values for each nanogel-water system. The $\bar{M}_x$ values in Fig 3.10A are all less than 1400 g/mol, but in Fig 3.10B are less than 7000 g/mol.

(A)

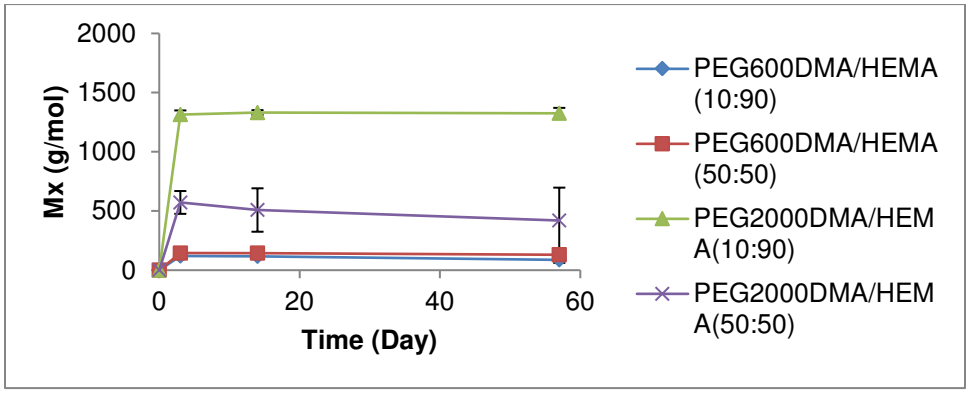

(B)

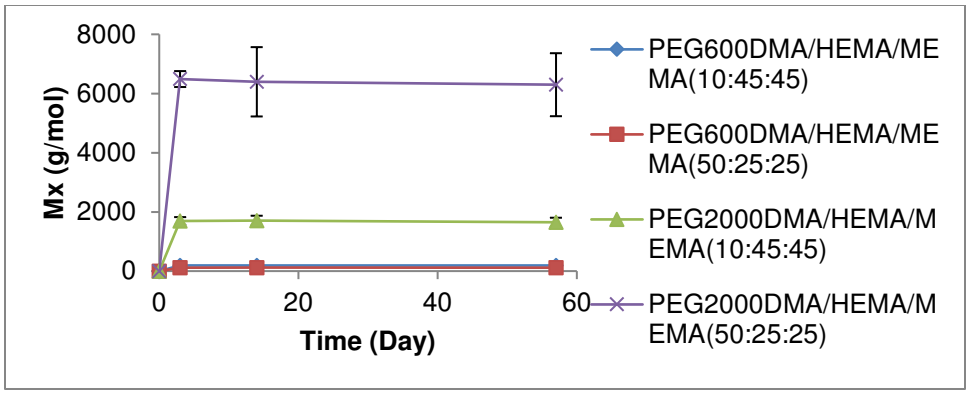

Figure 3.10. Molecular weight between crosslinks ($\bar{M}_x$) vs. time for non-degradable nanogel networks; $\bar{M}_x$ calculated based on Equilibrium Swelling Theory (Eq 3.10) and Gaussian distribution assumption for polymer chain conformations.

3.3.6.2. Internally Degradable Networks

The trends observed for $\bar{M}_x$ based on compressive modulus data show an initial increase in $\bar{M}_x$ values from day 0 to 4 in internally degradable networks due to the coupled effect of decreased level of chain entanglements in the overlapped volume (similar to non-degradable networks) and also the cleavage of ester bonds. The greater increase in $\bar{M}_x$ from dry to swollen state (day 4) belonged to PEG_{2000}PLADMA/HEMA(10:90) (NG_{11}) and PEG_{2000}PLADMA/HEMA(50:50) (NG_{12}), which had the higher level of water uptake compared to their PEG_{600} counterparts. There was no statistical difference between $\bar{M}_x$ of PEG_{600}PLADMA/HEMA(10:90) (NG_9) on day 4 and day 47 (*p*-level = 0.96). In NG_{10} network, there was a 64 g/mol difference (*p*-level = 0.00085) between $\bar{M}_x$ on day 4 and day 47, with latter having higher value. The final values of $\bar{M}_x$ on day 47 were different for each network (*p*-level between groups << 0.05), in the following order: PEG_{2000}PLADMA/HEMA(50:50) > PEG_{2000}PLADMA/HEMA(10:90) > PEG_{600}PLADMA/HEMA(50:50) > PEG_{600}PLADMA/HEMA(10:90), that follows the exact same order as water uptake values. The $\bar{M}_x$s on day 4 and day 47 for NG_{11} and NG_{12} were statistically the same with *p*-level values of 0.093 and 0.069, respectively. Although,

there was a marginal difference between compressive modulus of NG_{12} on day 4 and day 47, yet based on evaluated $\bar{M}_x$, we conclude that there was no significant degradation in this network. All the $\bar{M}_x$ values in Fig 3.11 A were less than 1000 g/mol.

The trends in $\bar{M}_x$ from equilibrium swelling data followed the same trends observed based on K data except that it predicted much higher values for swollen $\bar{M}_x$ for networks with higher ϕ_2s (NG_{11} and NG_{12}) (Fig 3.11 B). Furthermore, it showed that the $\bar{M}_x$ increased 868 g/mol for NG_{12} and decreased 276 g/mol for NG_{11} from day 4 to day 47 with *p*-levels of 0.007 and 0.02, respectively. The reduction in $\bar{M}_x$ in PEG_{2000}PLADMA/HEMA(10:90) is due to the increase in ϕ_2 during this time (recall from swelling data) and entanglement of degraded species (PEG_{2000}). Also, low crosslinking density in internally degradable nanogels, leads to release of longer chains by only cleaving few crosslinks, therefore released chains spend more time inside the network before they diffuse to the surrounding solvent. The surprising observation was that Eq 3.8 predicted higher $\bar{M}_x$ on day 47 for NG_{12} than on day 4, which is an indication of degradation and mesh size increase, although Eq 3.5 did not show the same result.

(A)

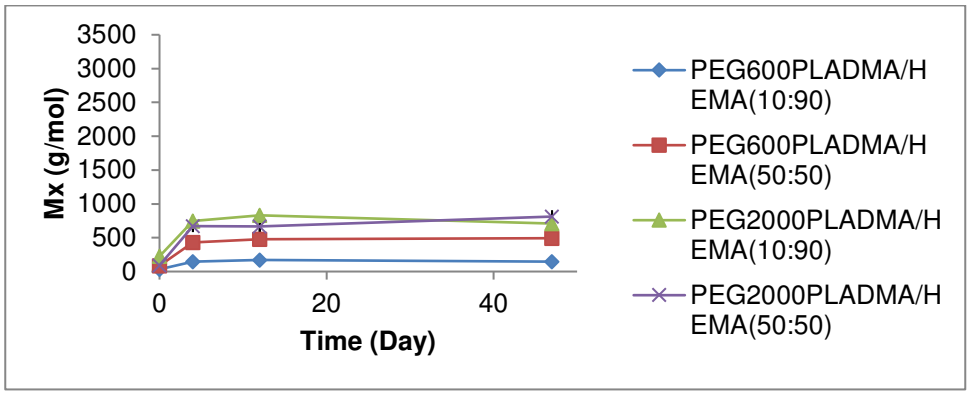

(B)

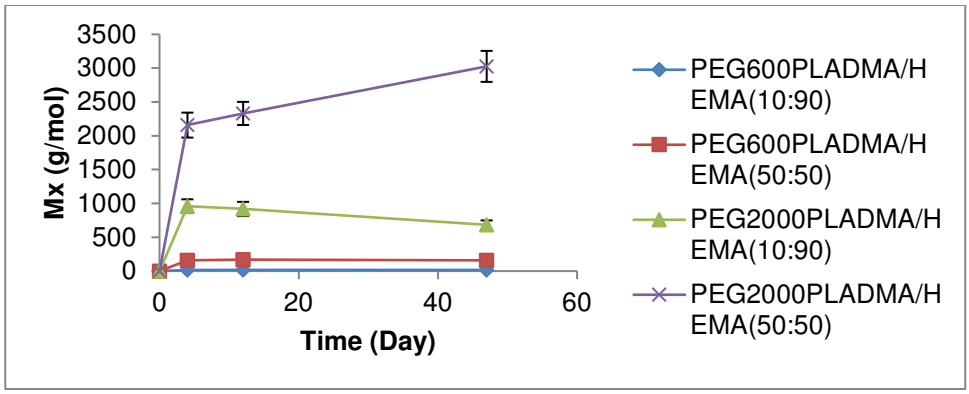

Figure 3.11. Molecular weight between crosslinks ($\bar{M}_x$) vs. time for internally degradable nanogel networks based on: (A) Rubber Elasticity Theory, and (B) Equilibrium Swelling; All chains are assumed to possess Gaussian Distribution of Conformations.

3.3.6.3. Externally Degradable Networks

The observation highlights in $\bar{M}_x$ trends based on rubber elasticity theory (Eq 3.4-5) in externally degradable networks are as follows: the initial increase in $\bar{M}_x$ value is a combination of decreased entanglement in the overlapped area along with hydrolytic degradation of PLA linkages surrounding the nanogels. The initial increase in $\bar{M}_x$ is greater for networks with lower secondary crosslinking densities and higher content of hydrophilic crosslinker, similar to what we observed for non-degradable networks. The $\bar{M}_x$ values on day 4 and day 47 were statistically the same for $PEG_{600}DMA/HEMAPLA/MEMA(10:45:45)$ (NG_{13}) (*p*-level = 0.38), $PEG_{600}DMA/HEMAPLA/MEMA(50:25:25)$ (NG_{14}) (*p*-level = 0.15), and $PEG_{2000}DMA/HEMAPLA/MEMA(10:45:45)$ (NG_{15}) (*p*-level = 0.32) networks, yet it increased for $PEG_{2000}DMA/HEMAPLA/MEMA(50:25:25)$ (NG_{16}) (*p*-level = 0.04), which is an indication of enlarging secondary mesh size. The NG_{13} and NG_{15} both had the lowest $\bar{M}_x$ value (480 g/mol) (Fig 3.12 A), with W of 16.7% and 52%, respectively. The highest $\bar{M}_x$ (4393 g/mol) belonged to NG_{16}, which had the highest water content (80%).

The $\bar{M}_x$ values based on swelling equilibrium (Fig 3.12 B) were higher for NG_{16} (7642

g/mol) and NG_{14} (1725 g/mol), and it remained constant from day 4 until day 47. NG_{13} (66 g/mol) and NG_{15} (824 g/mol) had the lowest $\bar{M}_x$. It is clear that Eq 3.10 tends to evaluate relatively larger values for $\bar{M}_x$ except for NG_{13}.

(A)

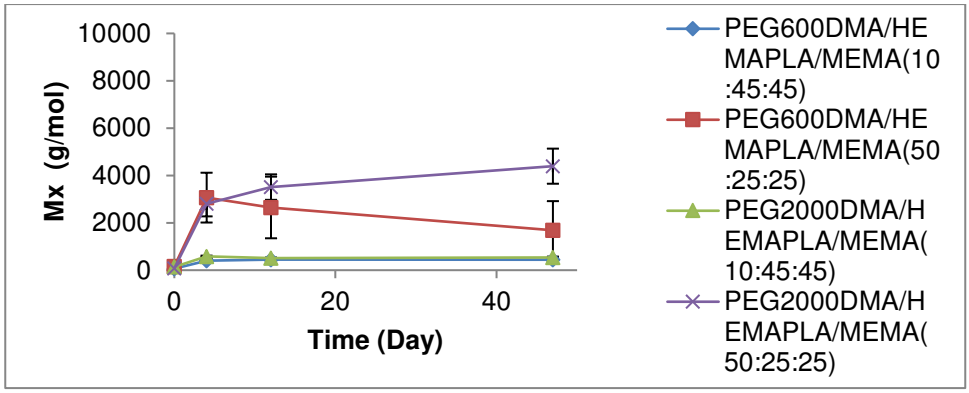

(B)

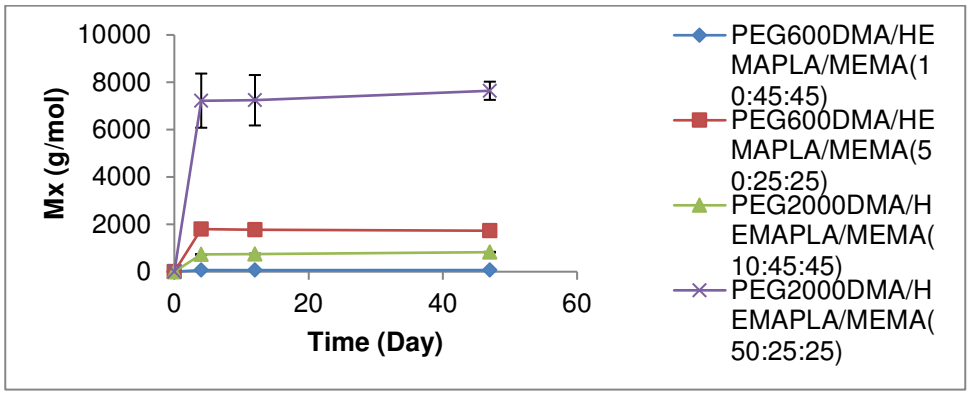

Figure 3.12. Molecular weight between crosslinks (M_x) vs. time for externally degradable nanogel networks based on: (A) Rubber Elasticity Theory, and (B) Equilibrium Swelling; All chains are assumed to possess Gaussian Distribution of Conformations.

3.3.6.4. Internally-Externally Degradable Networks

The $\bar{M}_x$ based on compressive modulus results for this category is shown in Fig 3.13 A-B. The sharp increase of $\bar{M}_x$ to 35,700 g/mol in PEG_{2000}PLADMA/HEMAPLA/MEMA(50:25:25) (NG_{20}) is an indication of rapid hydrolytic degradation (Fig 3.13 A), which was previously predicted based on swelling result as well. The PEG_{600}PLADMA/HEMAPLA/MEMA(10:45:45) (NG_{17}) and PEG_{2000}PLADMA/HEMAPLA/MEMA(10:45:45) (NG_{19}) had slight initial increase in $\bar{M}_x$,

yet there was no change until the end, also their final $\bar{M}_x$ values were 396 and 604 g/mol, respectively. The $\bar{M}_x$ for PEG$_{600}$PLADMA/HEMAPLA/MEMA(50:25:25) (NG$_{18}$) remained statistically the same on day 4 and day 47 (*p*-level = 0.24).

We also observed one-order of magnitude lower $\bar{M}_x$ for NG$_{20}$ on day 4, evaluated based on swelling data than from compressive modulus data (Fig 3.13 C), which is surprising. As it was shown in swelling results, we were able to measure the intact swollen mass up until day 12 but then after that on day 15 the gel turned into pieces while trying to measure its weight. This discrepancy between these results as it was predicted before in external compressive modulus analysis section may arise from the fact that majority of effective crosslinks reside in the outer layer of nanogels (secondary crosslinks), where they also share a high level of entanglements, therefore losing simultaneous connectivity from outer and inter layers has detrimental effect on sustaining mechanical integrity, even though the gel keeps swelling without dissolving. This is an evidence for systematic degradation even when the network can no longer store elastic energy. Another important conclusion is rubber elasticity seems to be able to more accurately predict the events at molecular level during degradation, when degraded chains are no longer entrapped or entangled inside the network.

(A)

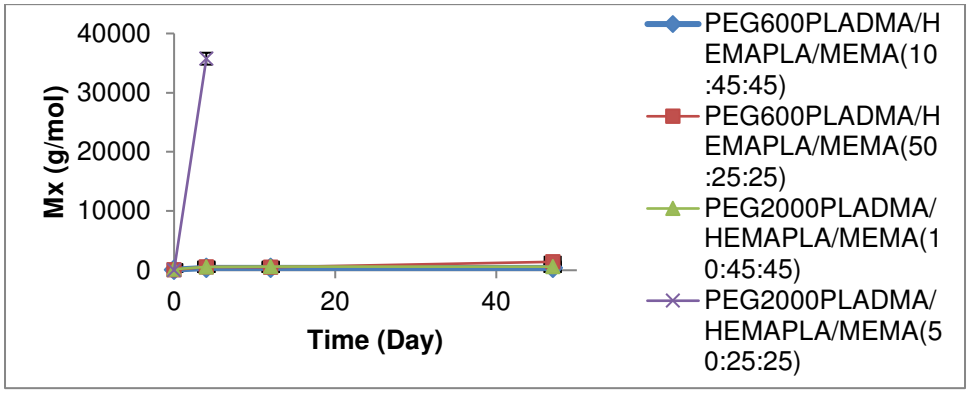

(B)

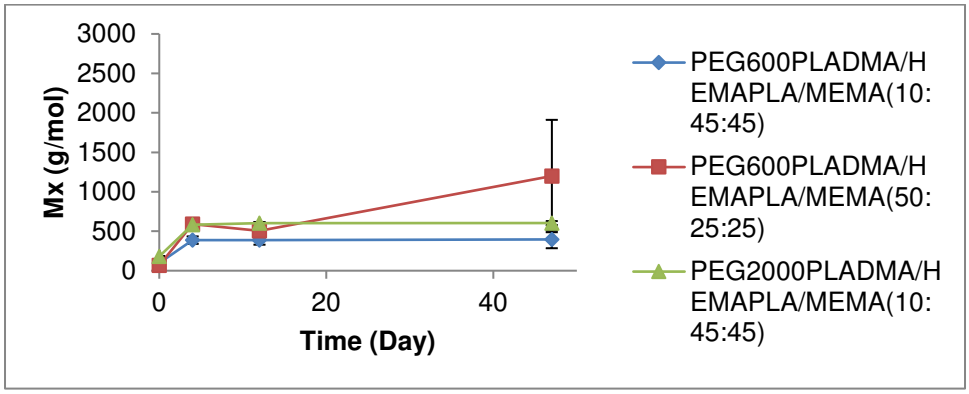

(C)

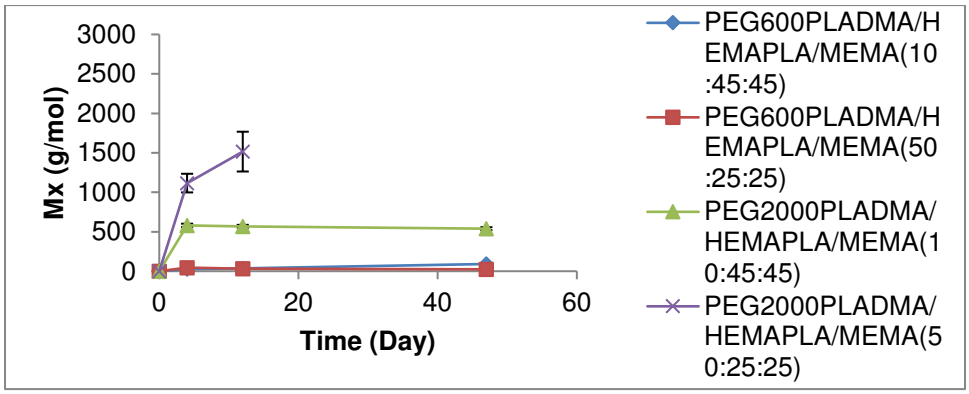

Figure 3.13. Molecular weight between crosslinks $\bar{M}_x$ vs. time for internally-externally nanogel networks based on: (A-B) Rubber Elasticity Theory, and (C) Equilibrium Swelling; All chains are assumed to possess Gaussian Distribution of Conformations.

3.3.7. Evaluation of $\bar{M}_x$ based on Non-Gaussian Chain Assumption

Based on $\bar{M}_x$ values of all networks in dry state evaluated by Eq 3.4, they were all less than 140 g/mol. For Gaussian distribution assumption to be valid, the minimum number of bonds per repeat unit should be N ≈ 10 (Hiemenz, 2007), in addition, the minimum number of such units has to be about 100 (Pohorecki, 2010), therefore Gaussian $\bar{M}_x$ has to be at least equal to or greater than 10 x 14 g/mol x 100 = 14,000 g/mol (molecular weight of the repeat unit CH_2 in $\bar{M}_x$ = 14 g/mol). Another definition of Gaussian chain was introduced by Tobita (1992):

"*In order for the conformation of the chain to be Gaussian, at least 50 carbon atoms between crosslinking points would be necessary*."

Based on this statement, $\bar{M}_x$ should be equal to or greater than 50 x 14 g/mol = 700 g/mol, thus based on either of these cutoffs, the assumption of Gaussian distribution of conformations for the backbone chain segment between crosslinks in nanogel networks seems invalid. To derive a relationship between compressive modulus and $\bar{M}_x$ in a crosslinked network of non-Gaussian chains, we can use expanded version of Kuhn and Grün distribution function, which the Gaussian result is the first term in the series (Treloar, 1954; Hiemenz, 2007) (Eq 3.12-13) (derivation is in Apendix A.2).

$$\boldsymbol{K = \left(\frac{2(1+\nu)}{3(1-2\nu)}\right)\frac{\rho RT}{\bar{M}_x}\left(1 + \frac{3}{5\bar{N}_x} + \frac{11}{175\bar{N}_x^2}\right)} \tag{3.12}$$

$$\boldsymbol{K = \left(\frac{2(1+\nu)}{3(1-2\nu)}\right)\frac{\rho RT}{\bar{M}_x}\left(1 + \frac{3}{5\bar{N}_x} + \frac{11}{175\bar{N}_x^2}\right)\left(\phi_2^{1/3}\right)} \tag{3.13}$$

Furthermore, by applying Flory-Rehner equation, we can determine $\bar{M}_x = 14\,\bar{N}_x$ based on equilibrium swelling data for non-Gaussian network (Treloar, 1954) (Eq 3.14) (Apendix A.2).

$$\boldsymbol{\bar{M}_x = \frac{\rho\bar{V}_1\left(\frac{\phi_2}{2} - \phi_2^{1/3}\right)\left\{1 + \frac{39\phi_2^{-2/3} + 3 + ln\phi_2^{-1} - 9\phi_2^{2/3}}{10\bar{N}_x} + \frac{11\left(3\phi_2^{-2/3} - 3 - ln\phi_2^{-1}\right)^2}{175\bar{N}_x^2}\right\}}{\ln(1-\phi_2) + \phi_2\left(1 - \frac{1}{\bar{N}_x}\right) + \chi\phi_2}} \tag{3.14}$$

3.3.7.1. Non-Degradable Networks

There was no difference in $\bar{M}_x$ trends between Gaussian and non-Gaussian assumptions in by rubber elasticity and equilibrium swelling theories for non-degradable networks. Swelling equilibrium theory with Gaussian and non-Gaussian assumptions predicted the same values for $\bar{M}_x$ (Fig 3.10 A-B, and Fig 3.15 A-B), although rubber

elasticity predicted lower values for $\bar{M}_x$ with non-Gaussian assumption compared to Gaussian (Fig 3.9 A-B, and Fig 3.14 A-B).

(A)

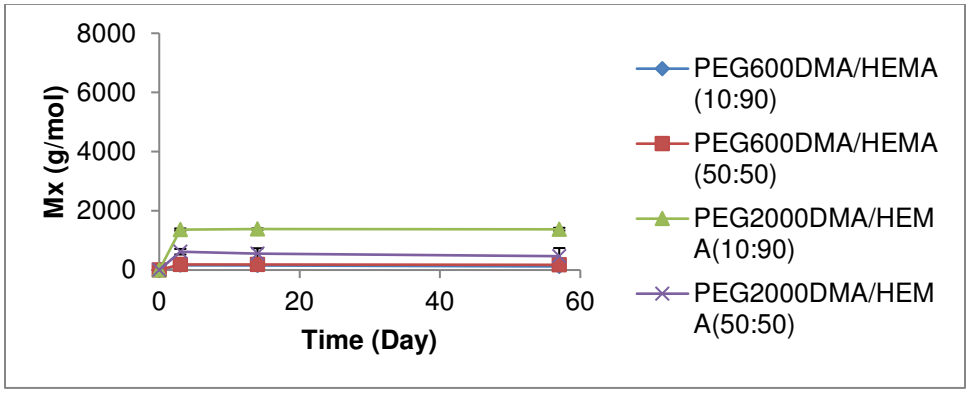

(B)

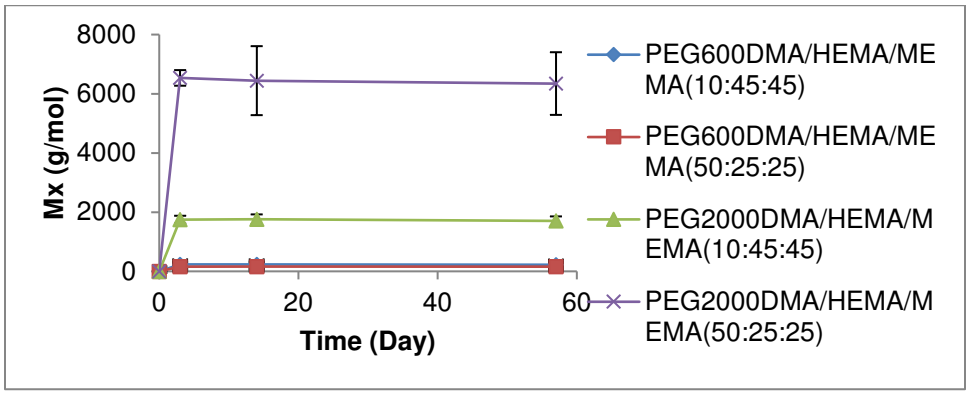

Figure 3.15. Molecular weight between crosslinks ($\bar{M}_x$) vs. time for non-degradable nanogel networks; $\bar{M}_x$ calculated based on Equilibrium Swelling Theory (Eq 3.14) and Non-Gaussian Distribution of Conformations.

3.3.7.2. Internally Degradable Networks

The same trends and values were observed for $\bar{M}_x$ (< 3500 g/mol) based on equilibrium swelling theory with both assumptions, Gaussian and non-Gaussian (Fig 3.11 B, and Fig 3.16 B), although rubber elasticity theory predicted lower $\bar{M}_x$, when non-Gaussian assumption was applied (< 500 g/mol) compared to values with Gaussian assumption (< 1000 g/mol) (Fig 3.11 A, and Fig 3.16 A).

(A)

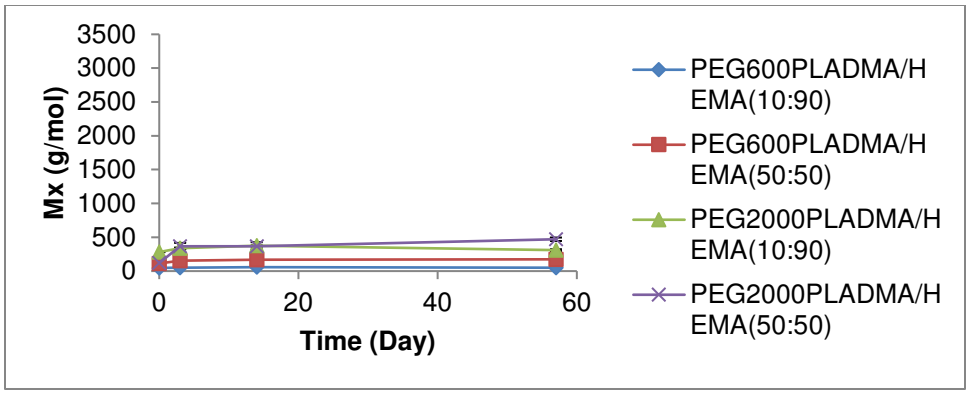

(B)

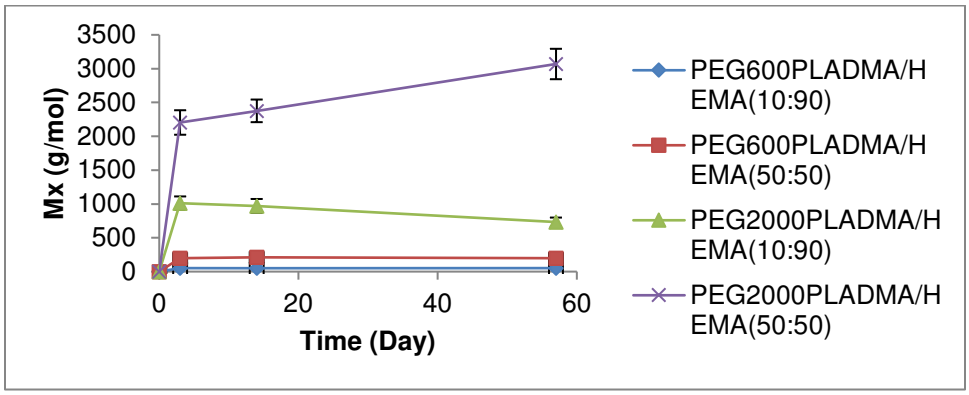

Figure 3.16. Molecular weight between crosslinks ($\bar{M}_x$) vs. time for internally degradable nanogel networks based on: (A) Rubber Elasticity Theory, and (B) Equilibrium Swelling; All chains are assumed to possess Non-Gaussian Distribution of Conformations.

3.3.7.3. Externally Degradable Networks

Once more, rubber elasticity theory predicted lower $\bar{M}_x$ with non-Gaussian assumption (< 3500 g/mol), as opposed to Gaussian assumption (< 5000 g/mol), also the trends were identical based on both assumptions (Fig 3.12 A, and Fig 3.17 A). The equilibrium swelling theory predicted the same trends and values with both assumptions (Fig 3.12 B, and Fig 3.17 B).

(A)

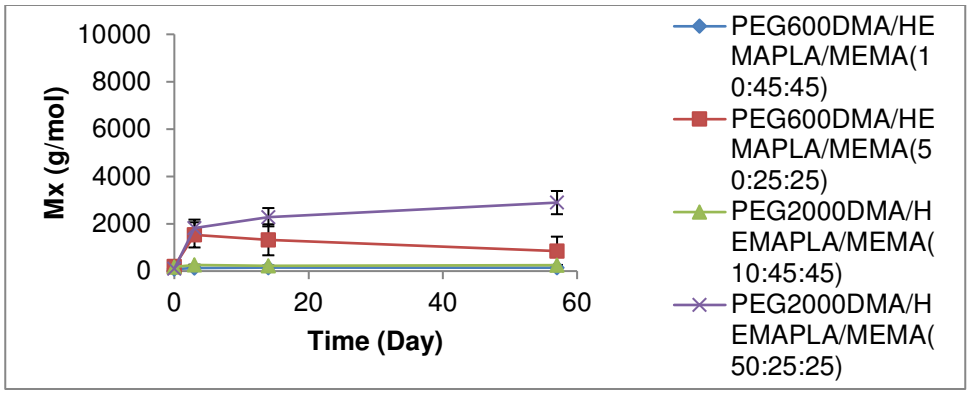

(B)

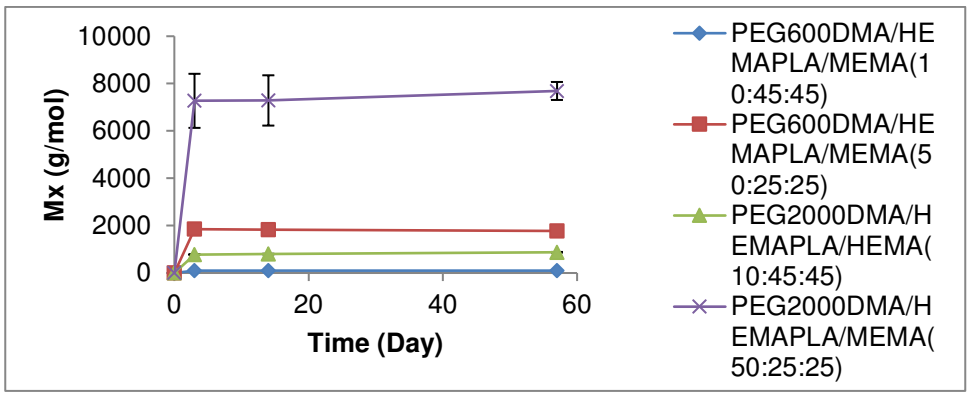

Figure 3.17. Molecular weight between crosslinks (M_x) vs. time for externally degradable nanogel networks based on: (A) Rubber Elasticity Theory, and (B) Equilibrium Swelling; All chains are assumed to possess Non-Gaussian Distribution of Conformations.

3.3.7.4. Internally-Externally Degradable Nanogel Networks

In this category, the results followed the same conclusions as the other networks. The rubber elasticity theory one more time predicted lower $\bar{M}_x$ with non-Gaussian assumption with a factor of 2 in the denominator. We have to note that the non-Gaussian assumption for short polymer chains is applied when the end-to-end distance of the chain under deformation is approaching its maximum value ($N_x b$), where chain can no longer extend beyond it. The fact that swelling equilibrium predicted same values for $\bar{M}_x$ with either assumption indicates that the extent of chain deformation during swelling did not approach the contour length, therefore non-Gaussian treatment was not necessary, although the same argument does not apply to rubber elasticity predictions. Implementing

non-Gaussian distribution evaluated lower $\bar{M}_x$ value for the same compressive modulus, which is a more precise assessment of a macroscopic nanogel network.

(A)

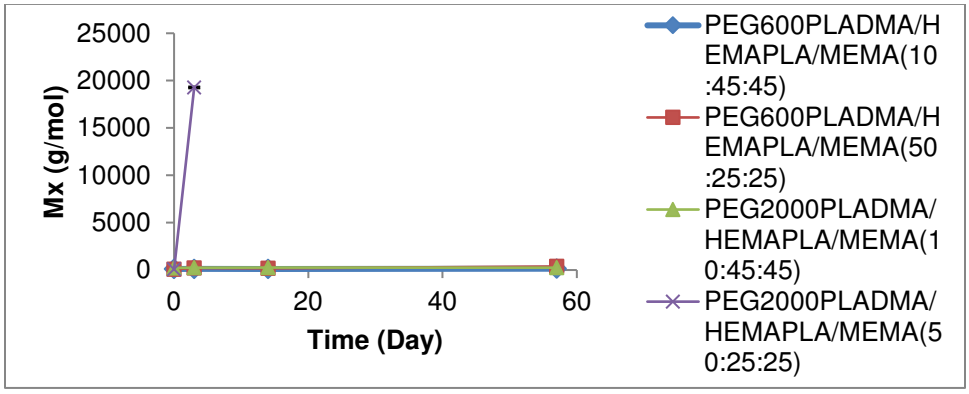

(B)

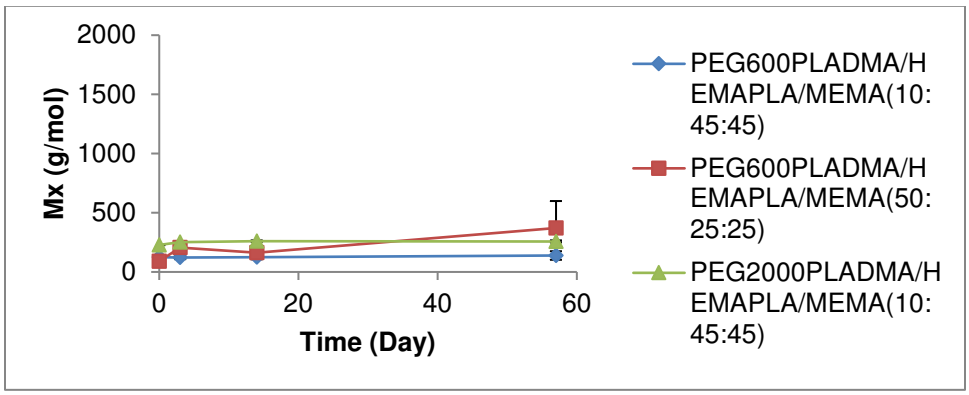

(C)

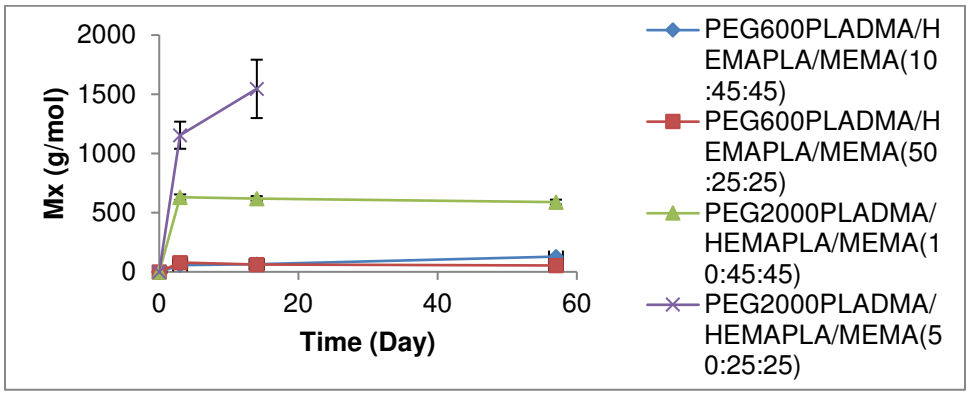

Figure 3.18. Molecular weight between crosslinks $\bar{M}_x$ vs. time for internally-externally nanogel networks based on: (A-B) Rubber Elasticity Theory, and (C) Equilibrium Swelling; All chains are assumed to possess Non-Gaussian Distribution of Conformations.

3.3.8. Mass Loss Analysis

Hydrolytic degradation is a process that starts with water uptake by amorphous regions within the network followed by hydrolytic cleavage of hydrolytically labile bonds (e.g. ester), which finally transforms the polymer into oligomers and monomers (Fu, 2010). For further investigation of macroscopic degradation in a more reasonable time scale, we chose PEG_{4600} as crosslinker core segment, a substantially hydrophilic oligomer relative to PEG_{600} and PEG_{2000} in high concentration (50 mol%). The same four categories of nanogel structures: non-degradable, internally degradable, externally degradable, and internally-externally degradable were prepared with PEG_{4600} in their backbones. The hydrolysis of hydrophobic PLA segments begins as soon as they become in contact with water at a rate governed by hydrolysis kinetic (Eq 3.15), (Metters, *Polym* 2000):

$$\frac{d\,[E]}{dt} = -k\,[E][H^+]\,[H_2O] \qquad (3.15)$$

In this equation [E] is the concentration of ester bonds, $[H_2O]$ is the concentration of water within the swollen network, which can be assumed constant when considering highly swollen gels (volumetric swelling ratio $Q_v > 4$) (Fig 3.24) (Metters, *Polym* 2000), and $[H^+]$ is the concentration of hydronium ion in the surrounding water, which in this case is the hydronium ion concentration associated with DI water plus the acidic species leaching out from the degradable sample (hydrolysis product) during the course of degradation, therefore $[H^+]$ is not constant, since buffer was not used here.

Eq 3.15 can be simplified to Eq 3.16, a pseudo second-order kinetic rate law, by combining constant values. After integration we obtain [E]/[H^+] as an exponential function of time (Eq 3.17) (Rawlings, 2015).

$$\frac{d\,[E]}{dt} = -k'\,[E][H^+] \tag{3.16}$$

$$\frac{[E]}{[H^+]} = \frac{[E]_0}{[H^+]_0}\, e^{-([H^+]_0 - [E]_0)kt} \tag{3.17}$$

k' is the new rate constant that has the water concentration value lumped into it, $[E]_o$ and $[H^+]_o$ are initial concentrations of ester groups and hydronium ion, respectively. Measuring swollen weights of PEG_{4600} hydrogel series was not feasible due to their highly swollen character and sticking to Kimwipes during excess water removal from the surface, therefore water uptake data for these hydrogels is not available. By keeping Eq 3.17 in mind and following the macroscopic behavior of the networks including rate of mass loss, pH of the surrounding water, and also visually following the samples during degradation, we try to explain the microscopic behavior in nanogel networks during degradation.

Eq 3.17 indicates: i) [E]/[H^+] and rate of [E]/[H^+] reduction decreases with time, and ii) higher [H^+], increases the rate of [E] reduction due to autocatalysis. Based on these kinetic information, we expect to see a decreasing trend for mass loss vs. time if degradable macromers (PEGPLADMA, HEMAPLA) were unconnected chains. From the mass loss data (Figure 3.23) and the pH values during degradation (Table 3.10), it is evident that mass loss increases with time, and consists of two distinct stages, first stage is from day 0 to 60, and second stage is from day 60 to 90.

3.3.8.1. Non-Degradable Networks

No mass loss and no degradation by-products were predicted for this system due to lack of hydrolytically labile groups. Fig 3.19 A-B show schematic structures of non-degradable active nanogel and macroscopic network created by polymerizing overlapped nanogel particles. Oligomeric poly(methacrylate) chains are connected to each other via primary non-degradable crosslinks (PEGDMA) and polymeric poly(methacrylate) chains connect nanogel particles together and create the final network. The pH value of surrounding water remained constant at 4.5 during the 90-day study (Table 3.10).

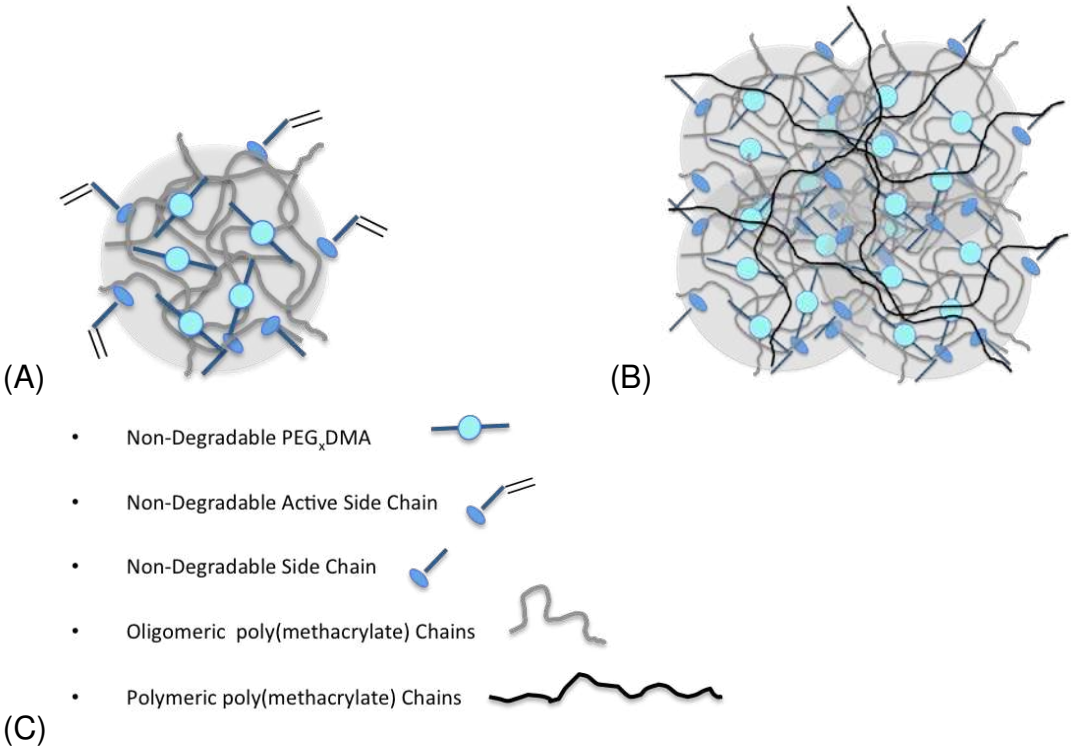

Figure 3.19: (A) Non-degradable active nanogel structure; (B) Polymerized overlapped nanogels create non-degradable network; (C) Sub units: PEGDMA (solid line represents non-degradability), non-degradable active side chain (methacrylate functionalized HEMA), non-degradable side chains (non-functionalized remaining HEMA and MEMA), oligomeric poly(methacrylate) chains connecting PEGDMA primary crosslinkers together to create primary network, polymeric poly(methacrylate) chains connecting nanogels (secondary crosslinker) together creating final macroscopic network.

3.3.8.2. Internally Degradable Networks

In degradable nanogel based networks, based on the location of the cleavable linkages, we predicted different mass loss behaviors. In internally degradable system, the PLA linkages were attached to both sides of the PEG block, and next to PLA chains on both sides, methacrylate functionalities were covalently attached, which all together assembled the degradable primary crosslink. The oligomeric polymethacrylate chains (non-degradable), were created during nanogel synthesis through the connection of these methacrylate functional groups to active chains, the degradable network was then formed through the connection of these short poly(methacrylate) chains via the degradable crosslinks. In addition, non-degradable side chains (HEMAs) were also attached to the oligomeric poly(methacrylate) chains in a random fashion, where the most accessible ones were post-functionalized with methacrylate groups. In the larger scale the overlapping nanogels were crosslinked during photopolymerization by connecting polymeric poly(metacrylate) chains, which had been originated from reaction between post-nanogel dangling methacrylate groups. At the molecular level, as soon as water (acidic water in this case) is in contact with the hydrolyzable PLA linkages, the acid-catalyzed hydrolytic bond cleavage starts either on one side or both sides of the PEG blocks, followed by the release of PEG units and lactic acid from the interior regions of nanogels, and start diffusing out into the free volume between the nanogels, and ultimately to the surrounding water. The rate of pH reduction in surrounding water is governed by the rate of degradation and the rate of diffusion, on the other hand, the rate of degradation is dictated by Eq 3.17 and microstructure of the network. The rate of diffusion according to reptation model developed by de Gennes for a single, flexible chain

trapped in a permanent network, is dependent on diffusion path length, degree of entanglement, friction factor of each segment, average mesh size, and temperature. When enough crosslinks are cleaved and diffused into the solvent, then the free oligomeric poly(methacrylate) chains with their dangling side chains (or dangling one sided crosslink) that are not connected to polymeric poly(methacrylate) chains start diffusing out, but since their molecular weight is not large due to their short length, this transition should be smooth without a significant effect on the rate of mass loss. Based on Table 3.10, the pH of water gradually reduced from 4.5 (day 30) to 3.5 (day 90), so clearly this was accelerated hydrolysis period, which manifested itself in Fig 3.23 by increased rate of mass loss after day 60. At later stages of degradation when enough number of nanogels are degraded, then the polymeric poly(methacrylate) chains can release themselves from the network either as a plain chain or with dangling oligomeric poly(methacrylate) chains attached to it. Even under accelerated condition, on day 90 with average mass loss of 92%, 2/3 of samples still had undissolved residual pieces. This observation confirms the systematic degradation and delaying the microscopic reverse gelation (primary burst effect), which is a characteristic of heterogeneous degradable networks, the microscopic reverse gelation in conventional heterogeneous networks starts at 78% mass loss. Fig 3.23 A-B show the structure of internally degradable active nanogel and the macroscopic network formed by crosslinking the overlapped nanogels. Fig 3.23 C shows schematic structure of degradation by-products of internally degraded nanogel network. Based on Eq 3.17, $[E]/[H^+]$ ratio decreases with higher rate in an exponential decay regime, when the difference the number in the parenthesis $([H^+]_0 - [E]_0)$ becomes larger. The pH of the surrounding solution remained constant at 4.5 from day 0

until day 30 (Table 3.10) and Fig 3.23 shows a linear mass loss of 14% during this time. The mass loss continued with the same rate until day 60, and then it became much faster with a rate of 1.98% per day due to increased $[H^+]_0$.

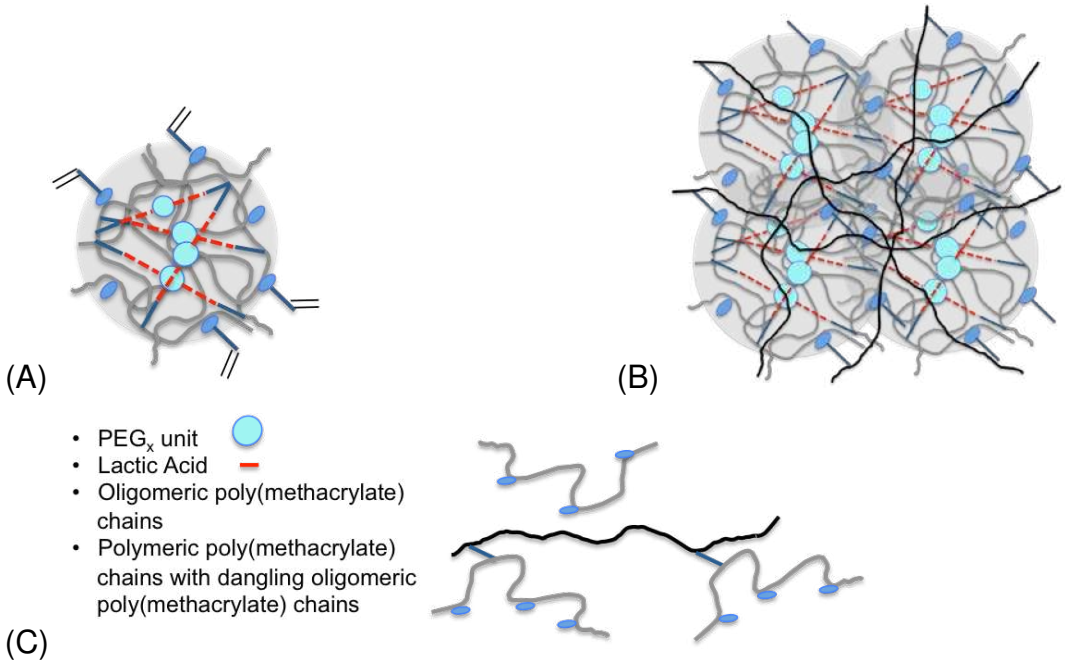

Figure 3.20: (A) Internally degradable active nanogel (red dashed lines represent degradable linkages (PLA) on both sides of PEG$_x$ units); (B) Degradable macroscopic network formed via polymerizing of overlapped internally degradable nanogels; (C) By-products of hydrolysis degradation of internally degradable nanogel network.

3.3.8.3. Externally Degradable Networks

Fig 3.21 shows the structure of externally degradable active nanogel and the macroscopic network formed after photopolymerization. In this system the degradable PLA linkages are attached to HEMA, which are randomly attached to the oligomeric polymethacrylate chains in the nanogel structure, and some of them are also connected to the final network through polymeric poly(methacrylate) chains. In this type of network, at early stages of degradation only low molecular weight acidic species are released. We did not observe significant mass loss from day 0 to day 60. The effect of released acidic

molecules manifested itself one more time through decreased pH value of the surrounding water from day 30 to 90, and accelerated hydrolysis effect after day 60. Since other structural elements in the nanogel and the polymeric poly(methacrylate) chains connecting the nanogels are all non-degradable, it was predictable to have a prolonged stable mass until majority of the degradable side chains were cleaved. At this point we can imagine the network of attached nanogels is transformed into cleaved nanogels trapped within the secondary network. From this stage onwards we can expect to see a rise in the rate of mass loss due to losing individual cleaved nanogels from the surface, since the other cleaved nanogels inside the bulk of the samples are still trapped. This stage of erosion is followed by the release of individual polymeric poly(methacrylate) chains free of dangling nanogels and this cycle continues systematically until the entire mass is eroded (surface erosion). Final pH on day 90 was 4.0, which is higher than that of internally degradable samples on this day, which is due to less PLA content. This gear shifting in degradation behavior from bulk erosion to surface erosion happened only by changing the location of the labile linkages and keeping other parameters the same. In this type of network we completely by-pass the primary and secondary reverse gelations and the entire sample is eroded layer by layer.

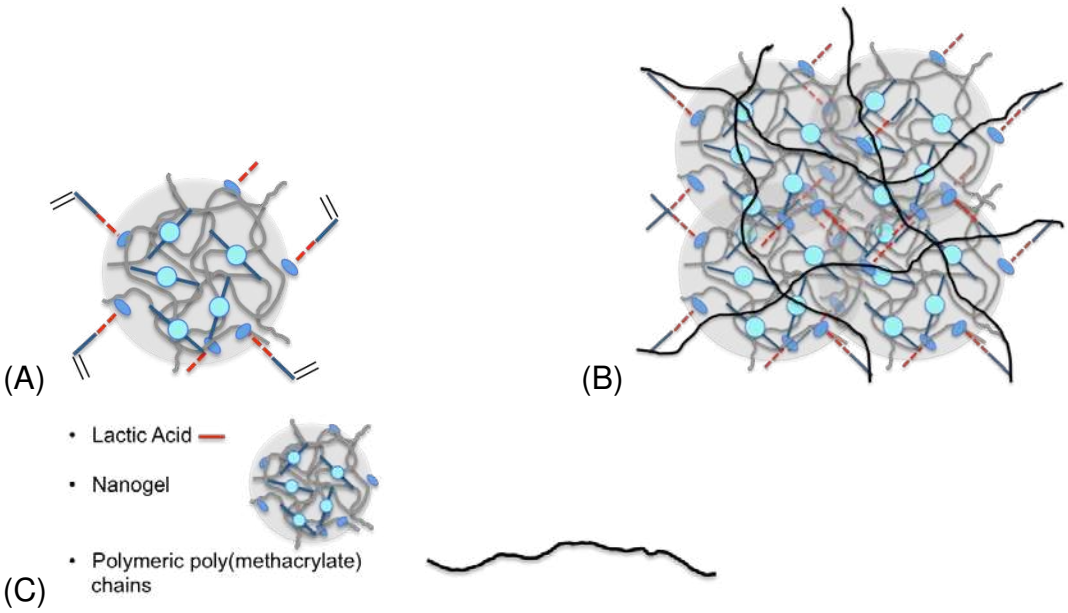

Figure 3.21: (A) Externally degradable active nanogel; (B) Macroscopic network formed by polymerizing overlapped externally degradable nanogels; (C) Schematic structures of degradation by-products.

3.3.8.4. Internally-Externally Degradable Networks

In this system internal and external degradable linkages are cleaved simultaneously, initially releasing lactic acid and PEG segments followed by oligomeric poly(methacrylate) chains and further the release of plain polymeric poly(methacrylate) chains, as shown in Fig 3.22 C. The rate of mass loss in internally-externally degradable samples followed the same trend as internally degradable gels, with accelerated hydrolysis effect showing after day 60, and one out of three samples had still residual pieces. The final conclusion is that the overall mass loss rate is governed by internal degradability rather than external. The pH of water remained constant at 4.5 from day 0 until day 30 and decreased to 3.0 (Table 3.10) between day 30 and 90. The higher $[H^+]$ on day 90 in this case is due to higher concentration of PLA in internally-externally degradable nanogels. The average mass loss on day 90 was 85%, and there was no statistical difference between the final mass loss of NG_{22} and NG_{24} (p-level = 0.68).

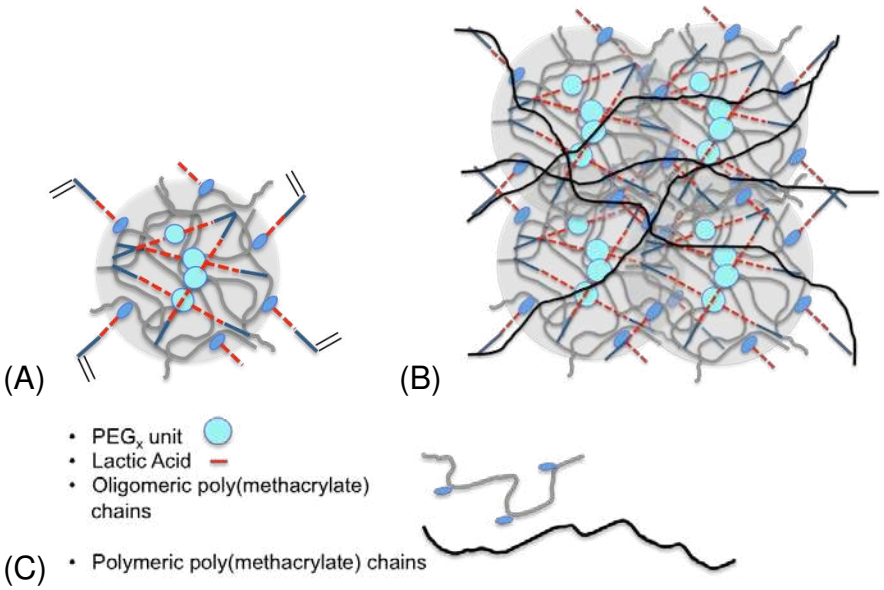

Figure 3.22: (A) Internally-externally degradable active nanogel; (B) Macroscopic network of polymerized overlapped nanogel; (C) Schematic structures of hydrolysis degradation by-products.

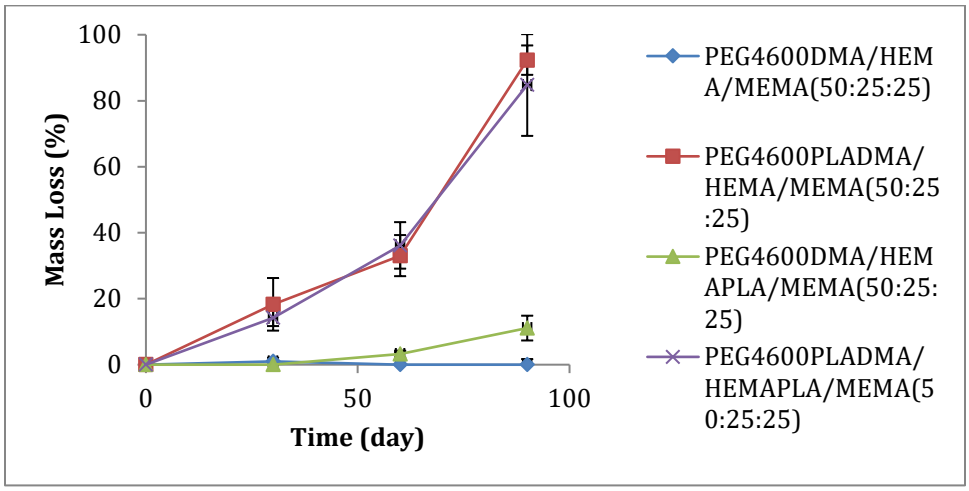

Figure 3.23. Mass loss (%) vs. time in DI water and ambient condition for non-degradable, internally degradable, externally degradable, and internally-externally degradable nanogel networks of PEG$_{4600}$ series.

Table 3.10. pH values of surrounding water solution during hydrolysis of PEG_{4600} hydrogel series; t=0 shows pH value of neat DI water.

Time [Day]	pH Non-Degradable Network	pH Internally Degradable Network	pH Externally Degradable Network	pH Internally-Externally Degradable Network
0	4.5	4.5	4.5	4.5
2	4.5	4.5	4.5	4.5
30	4.5	4.5	4.5	4.5
90	4.5	3.5	4	3

3.3.8.5. Visual Analysis

We also visually followed the degradation process for 20 days in all four nanogel networks in PEG_{4600} series. The photopolymerized discs had white color before being submerged in water, which is an indication of semi-crystallinity and it is due to micro scale alignment of PEG_{4600} segments (the critical lowest molecular weight for PEG to crystallize in crosslinked networks is 1000) (Qiao, 2004). In all samples the diameter of the discs almost doubled after spending 1 day in DI water and the swollen network had opaque (white) color. In non-degradable samples, the swollen gel lost a slight degree of opacity due to water penetration into the network but overall stayed white during the 20 days of observation. In internally degradable case, the samples became transparent after spending 20 days in DI water, which is an indication of increased mesh size that allows more water penetrating into the bulk and as a result less scattering. The addition of PLA to both sides of the PEG increases the crosslinker length and consequently opens up the primary mesh size. In externally degradable networks, the samples were initially opaque but the opacity started to slightly decrease after day 1 and remained the same until day 20, which confirms that mesh size does not increase further and sample lose mass by free nanogels leaving the network surface. In internally-externally degradable samples, opacity decreased dramatically between day 1 and day 7, which shows a larger mesh

size created. Between day 7 and day 20 the sample was extremely swollen and it turned into pieces while trying to take it out of the vial for actual picture, therefore we do not have picture of the sample due to macroscopic burst effect.

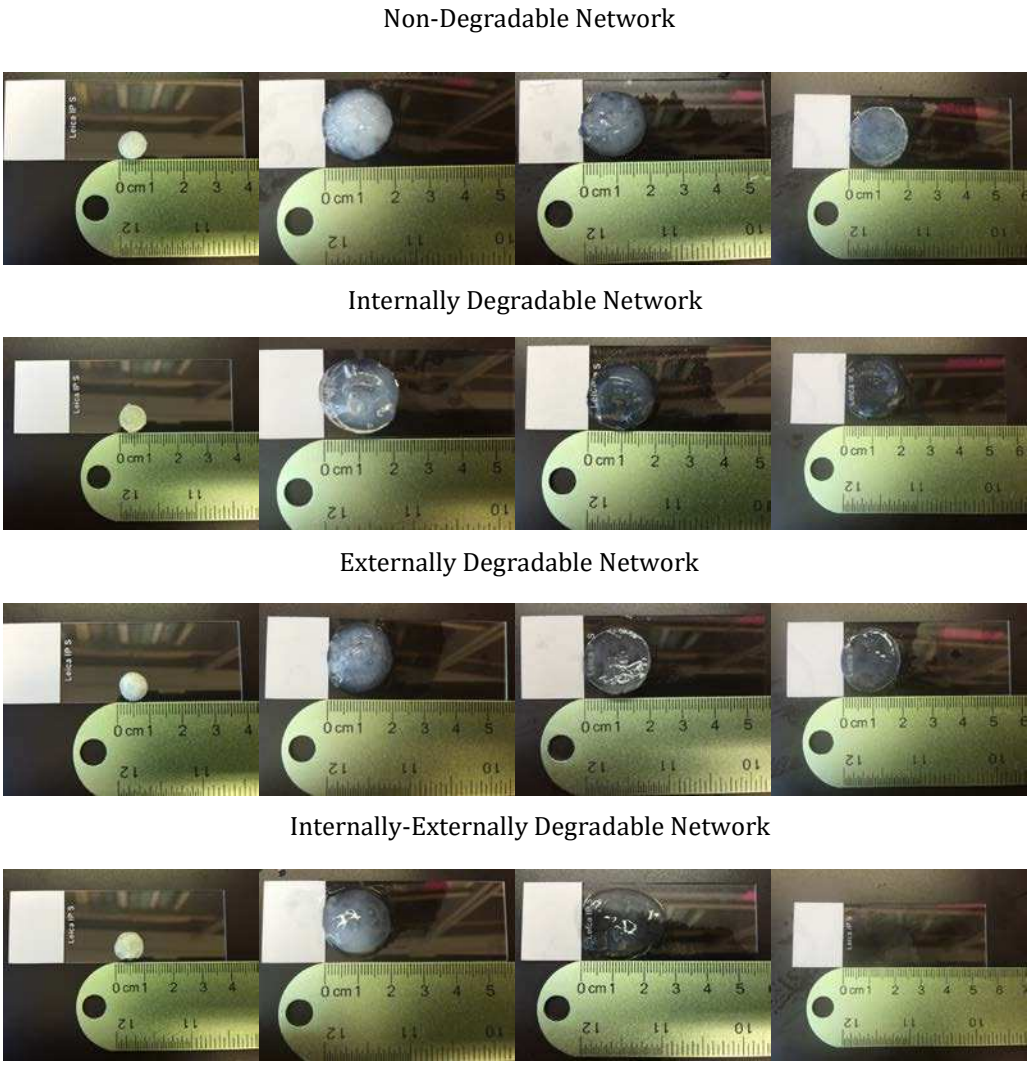

Figure 3.24. Visual observation of swelling nanogel networks of PEG_{4600} series (NG_{21}-NG_{24}) in DI water from t=0 (dry state) to t=1, 7, and 20 days (swollen state).

3.4. Conclusions

Regio-specific degradable nanogels were successfully prepared via free-radical solution polymerization of PEG-*co*-PLA with HEMA-*co*-PLA and MEMA. Their weight-averaged molecular weights were less than 65 kg/mol with hydrodynamic radius of less than 6.0 nm and 1.0 < PDI < 7.2. The glass transition temperature of bulk nanogels was at or below room temperature. The photopolymerized macroscopic networks of these nanogels exhibited dramatic high dry-state moduli depending on chain flexibility and crosslink density. The swollen-state moduli were lower than that of dry-state depending on the hydrophilicity of the network. The molecular weight between crosslinks evaluated based on rubber elasticity theory showed lower values of $\bar{M}_x$ by applying non-Gaussian conformation distribution assumption, yet equilibrium swelling theory predicted same values for $\bar{M}_x$ regardless of the type of implemented distribution. The incorporation of hydrolytically labile linkages to the backbone and side-chain of the nanogel led to bulk and surface type erosions, respectively. The mass loss trends in these novel networks showed a sustained release of degraded species even under autoaccelerated acid-catalyzed hydrolysis by delaying or completely bypassing reverse gelation. The investigated nanogels in this study offer tremendous control and versatility in hydrolytic degradation for variety of biomaterial applications such as controlled-drug delivery and scaffold engineering.

CHAPTER 4

SUPPRESSION OF HYDROLYTIC DEGRADATION IN LABILE POLYMER NETWORKS VIA INTEGRATED STYRENIC NANOGELS

4.1. Introduction

The most common monomers used in dental composites have hydrophilic linkages such as esters/hydroxyls in Bis-GMA (bisphenol A glycidyl methacrylate), esters/urethanes in UDMA (urethane dimethacrylate), and esters/ethers in TEGDMA (triethylene glycol dimethacrylate) (Santerre, 2001; Ferracane, 2006; Drummond, 2008). All of these linkages have the capability to attract water molecules through hydrogen bonding either as hydrogen bond donor or acceptor. Also, ester groups inherent in methacrylate structures are prone to bond cleavage through acid or base catalyzed hydrolysis as well as enzymatic attack, which lead to degradation of polymer networks composed of these monomers (Santerre, 2001; Finer, 2004; Ferracane, 2006; Bettencourt, 2010; Liu, Y. 2011) The combination of water uptake and network swelling in dental composite restoratives can facilitate leaching of unreacted monomers and degradation by-products into the oral environment as well as plasticizing the network, which deteriorate mechanical properties and promote more invasive microbial challenge that can result in secondary caries adjacent to the restoration. These processes not only affect the surfaces of composite restoratives but also involve the methacrylate-based adhesive layer, which compromises the critical bond between the tooth and restoration

(Malacarne, 2006; Liu, Y. 2011). Esterases and other enzymes present in saliva and within dentin are able to promote surface degradation of dense hydrophobic networks to reduce surface hardness/wear resistance and the probability of network degradation is increased in less crosslinked, more hydrophilic polymer networks that are representative of the dental adhesives (Ferracane, 2006; Bettencourt, 2010). In these amphiphilic adhesive resins, even a small amount of water present during polymerization may cause nano-phase separation of the hydrophilic and hydrophobic segments, which not only weakens mechanical properties but also creates a suitable gap for enzymatic attack in the bulk as well as at the surface (Malacarne, 2006; Drummond, 2008; Liu, Y. 2011).

These concerns associated with the durability of methacrylate-based polymeric dental materials have led to various approaches to eliminate or minimize the adverse effects of salivary water and enzymes on dental restoratives. Incorporation of fillers into the monomer resin have served important purposes of increasing mechanical properties and reducing shrinkage, but the hidden advantage of adding fillers to the resin is reducing the overall volume of the labile polymer. On the other hand, most of the fillers are functionalized with coupling agents such as silane, which after reacting with water creates labile silanol groups. Another approach is to increase the degree of conversion. Elevated crosslinking density has two advantages: i) reduced free volume, and ii) decreased amount of unreacted monomer (Liu, Y. 2011). Minimizing free volume via increasing crosslink density can reduce the amount of unbound water as well as bound water through increased resistance to swelling. The degree of conversion can be enhanced by choice of the resin formulation, use of a more efficient initiating system or emplying more aggressive photocuring conditions. However, this strategy has shortcomings in that resin

systems that promote higher conversion typically achieve this by use of monomers with lower reactive concentrations that limit the potential network density and modulus that can be attained. Further, enhanced conversion with dense network structure would also produce greater polymerization shrinkage and stress that can introduce other challenges to restorative longevity (Stansbury, 2000; Liu, Y. 2011; Ferracane, 2016).

On the other hand, the level of conversion via photo-polymerization has an upper limit under ambient condition due to the onset of vitrification (Tg of the curing polymer reaches the cure temperature) of the polymeric network (Sideridou, 2002; Gonçalves, 2009). Addition of enzyme inhibitors prior to application of adhesives or use of bulky/branched monomers have also been proposed to minimize enzymatic attack in dental adhesives (Liu, Y. 2011). The issue here again is the leaching of these additives to the oral cavity. Wet bonding is another approach that sequentially replaces water with ethanol during the application of the adhesive to allow more hydrophobic and densely crosslinking monomers to be introduced into demineralized dentin but this is a time-consuming, technique sensitive method with limited clinical practicality. Biomimetic re-mineralization of collagen is a physiological dehydration mechanism that replaces the unbound water with apatite. This approach can be utilized to eliminate water from resin-dentin interface but it is a slow in-vivo process.

A central consideration in the design of polymer restorative materials is to increase their life span in the oral environment by maintaining their strength, modulus and fracture toughness (Drummond, 2008). Towards this goal, the potential for aqueous swelling and hydrolysis/enzymatic attack can be related to: i) degree of hydrophilicity, ii) solubility difference between polymer and solvent, and iii) crosslinking density (Ferracane, 2006;

Liu, Y. 2011). While there are prior and ongoing examples of the development of entirely new classes of resin monomers through novel chemistries that avoid methacrylates, this strategy involves extensive work that cannot be rapidly implemented into clinical practice.

In this study, we are designing inert and reactive additives that are capable of addressing the major concerns regarding hydrolysis and enzymatic degradation. Our group has previously developed (meth) acrylate-based nanogel structures, which are highly crosslinked globular polymeric particles well below 100 nm in diameter. These functional nanogels have been applied to photocured resins and composites to control polymerization shrinkage stress reduction (Moraes, *Dent Mater J* 2011; Liu, J. *Eur Polym J* 2012, *Dent Mater J* 2014), delay gelation/stress development (Liu, J. *Polym Chem* 2014) (Chen, 2014) and enhance mechanical properties (Liu, J. *Dent Mater J* 2014). We have also demonstrated that the addition of nanogels to dental adhesive resins can limit water uptake and reduce water solubility relative to the nanogel loading. Further, the incorporation of nanogel into a model adhesive enhanced the dry/wet mechanical properties of the network without the need to change the basic monomer formulation (Moraes, *J Dent Res* 2012). Here, we have prepared nanogel formulations constructed entirely from aromatic hydrocarbon monomers that offer no heteroatoms to either promote hydrophilicity, or undergo degradative processes (Kaczmarek, 2004). Styrene-divinylbenzene copolymers, typically with quite low crosslinker content, have been widely used in size exclusion chromatography and as polymer reagents/catalyst (Rabelo, 1994), and recently in biological applications such as heart valve and blood purification (Gallocher, 2006; Harm, 2014; Brubert, 2016). These styrenic copolymers also have been used as immobilization substrate for mass production of enzymes (Sandwick, 1987;

Dizge, 2009; Hernandez, 2011). In the current study, we have produced highly crosslinked all-styrenic nanogels from a free radical solution polymerization process to test the hypothesis that dispersion and swelling of these nondegradable nanogels with hydrolytically labile resins can reduce water uptake and mass loss of the resulting polymers without negative impact on mechanical properties.

4.2. Materials and Methods

The monomers (oligomers) used in this study are, 3,6-dimethyl-1,4-dioxane-2,5-dione (Lactide; Sigma Aldrich), polyethylene glycol (Mw = 2000 g/mol) (PEG2000; Sigma Aldrich), 2-isocyanatoethyl methacrylate (IEM; TCI), divinyl benzene (DVB; Sigma Aldrich, Technical Grade 80%), and styrene (ST; Sigma Aldrich). The chain transfer agent was 2-mercaptoethanol (ME; Sigma Aldrich). The solvents are dichloromethane (DCM; Fisher Scientific), hexane (Fisher Chemical, Certified ACS), toluene (Fisher Scientific, Certified ACS), and tetrahydrofuran (THF; VWR Analytical, for HPLC ≥ 99.9%). Dibutyltin dilaurate (DBTD; Sigma Aldrich), 2,6-di-tert-butyl-4-methylphenol (BHT; Sigma Aldrich), azobisisobutyronitrile (AIBN; Sigma Aldrich), and 2,2-dimethoxy-2-phenylacetophenone (DMPA; Sigma Aldrich) are the catalyst, inhibitor, thermal initiator, and photo initiator, respectively. All the materials were used as received.

4.2.1. Degradable Macromer Synthesis

A model hydrolytically degradable dimethacrylate macromer designated as PEG_{2000}PLADMA was synthesized via ring-opening oligomerization of lactide with PEG_{2000} (Sawhney, 1993) with 4.5 to 1 molar ratio, respectively. The reaction was run under nitrogen purge (30 min prior to and throughout the reaction) to avoid lactide oxidation. Three drops of DBTD (0.2 wt% relative to monomer mass) was added when all

the lactide melted. The temperature was held constant at 140 ºC for 4 hours. After the reaction mixture reached room temperature, the unreacted lactide was removed via Kugelrohr Distillation Apparatus (BÜCHI) under high vacuum at 180 ºC. After the mixture reached ambient temperature, IEM was added with molar ratio of 2 (IEM) to 1 (PEG_{2000}PLADMA) to functionalize the degradable oligomer with methacrylate functionalities on both ends. Three drops of DBTD and 4-fold excess of DCM were also added. The sealed mixture was stirred under ambient temperature (48 h) until the isocyanate conversion reached 100% as determined by mid-IR spectroscopy (Nexus 670, Nicolet, Madison, WI, USA) using the isocyanate group absorption at 2270 cm-1. Dimethacrylate functionalized macromer (PEG_{2000}PLADMA) was precipitated from the clear solution by dropwise addition into 6-fold excess of hexane (relative to solution volume). The precipitate was filtered and redispersed in DCM. Trace amount of BHT was added before removing DCM under high vacuum. The product structure (Fig 4.1), PEG_{2000}PLADMA was confirmed by ^{1}H NMR (Apendix A Fig A.12).

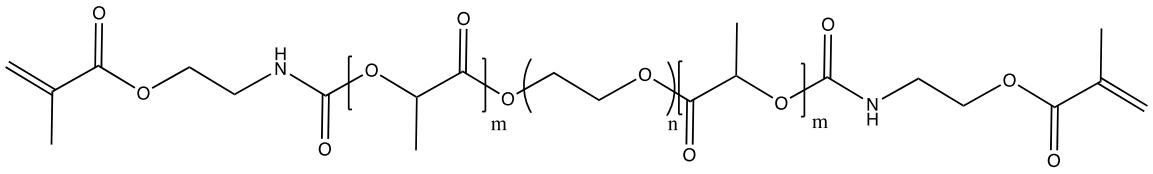

Fig 4.1. Chemical structure of PEG_{2000}PLADMA

4.2.2. Nanogel Synthesis

Different nanogels in terms of conversion, crosslinker concentration, and type of final reactive groups were synthesized via free radical solution polymerization in an isothermal (80 ºC) batch reactor (100 mL round bottom flask). DVB (20 and 50 mol%) and

ST (80 and 50 mol%) were used as the divinyl (crosslinker) and monovinyl monomers, respectively. ME (15-30 mol%) was added as chain transfer agent. The amount of ME was increased from 15 mol% to 30 mol% when the concentration of crosslinker increased from 20 mol% to 50 mol%, respectively. The chain transfer agent shortens the kinetic chain length and thereby avoids macrogelation during nanogel synthesis. AIBN (3 wt% relative to monomer mass) was added as thermal initiator.

The mixture was dispersed in 6-10 fold excess of toluene (relative to monomer mass). The 6X and 10X amount of solvent were used for 20 mol% and 50 mol% crosslinker concentration, respectively. Increasing the solvent concentration promotes cyclization rather than addition of free monomer to the growing particle as another tactic to control particle size and avoid macrogellation. In the first category, the nanogel was synthesized until it reached a high conversion (> 80%) with no post-functionalization. This category is considered as essentially inert nanogel due to relatively low concentration of pendant C=C bonds (Fig 4.2A). The second category involves the similar reached a high conversion nanogel (> 80%) that was post-functionalized with methcrylate reactive groups by addition of IEM (equimolar to ME). The OH group of ME reacts with the isocyanate group of IEM to form urethane methacrylate chain-end functionality (Fig 4.2B). Mid-IR spectroscopy was used to monitor the isocyanate bond conversion. The third category is the nanogel in which the synthesis was stopped at ~50% conversion. In this case, the pendant styrenic C=C bonds left from dangling DVB are considered the active sites (Fig 4.2C). Near-IR spectroscopy (Nicolet 6700, Thermo Scientific, West Palm Beach, FL, USA) was used to calculate the conversion of the styrenic C=C bonds based on the absorption at 4720 cm^{-1}. Nanogel was precipitated from the clear reaction mixture

by dropwise addition into a 6-fold excess of hexane (relative to reaction solution volume). The precipitate was redispersed in acetone and trace amount of BHT was added before removing the solvent under high vacuum.

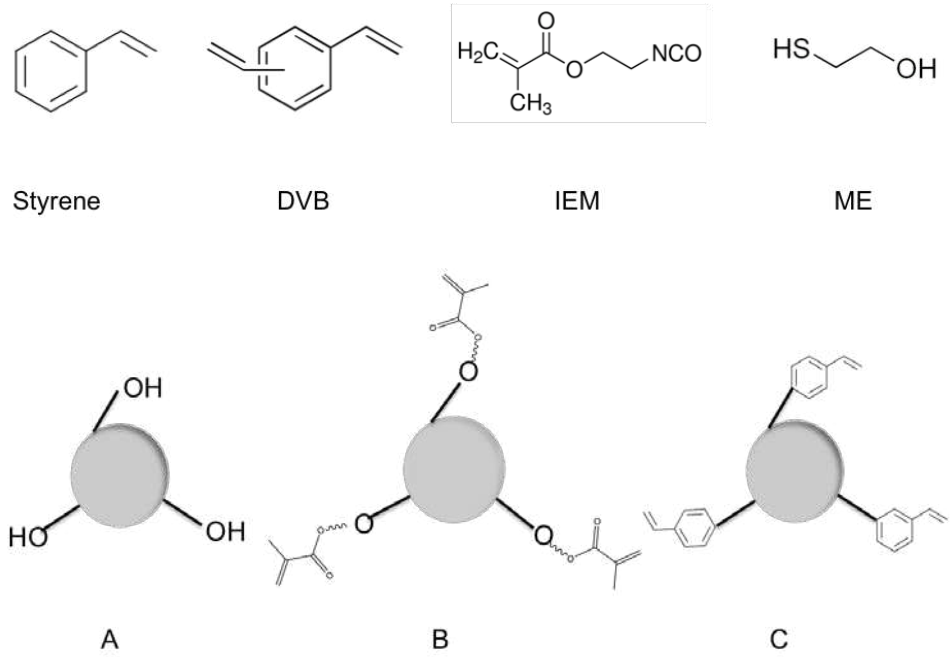

Figure 4.2. Chemical structures of monomers and reagents; (A) Structure of inert nanogel (no C=C bond functionality), (B) Structure of reactive nanogel with methacrylate C=C functionality, (C) Structure of active nanogel with pendant styrenic C=C.

4.2.3. Nanogel Particle Characterization

Triple-detection gel permeation chromatography (GPC; Viscotek, Houston, TX, USA) with differential refractive index, viscosity, and light scattering detectors was employed for the analysis of nanogel molecular weight, polydispersity (PDI), average hydrodynamic radius (Rh), and Mark Houwink exponent (MH-*a*). Tetrahydrofuran (THF) was used as eluant with a flow rate of 1 mL/min at 35 °C in a series of three columns spanning molecular weight of 104 – 107 and calibrated with a 65 kDa poly(methyl methacrylate) standard. Proton nuclear magnetic resonance (1H NMR; Varian 500 MHz)

and MestReNova 5.2.4 software were employed to determine the structural composition of the isolated nanogels. DMA (Dynamic Mechanical Analysis) tests were performed using a TA instruments (DMA; Perkin Elmer 8000, Waltham, MA, USA) to determine the glass transition temperature (T_g). Dry nanogel powder (10-15 mg) (n=2) was sandwitched inside a thin steel pocket and was subjected to single cantilever cyclic displacement 0.05 mm at 1 Hz during heating/cooling cycles.

The glass transition temperature was determined as the position of the maximum on the tan δ vs. temperature plot. The temperature range was from -20 to 120 °C with a ramping rate of 3 °C/min and tan δ were recorded as a function of temperature. A preheating cycle was applied with a ramping rate of 10 °C/min. For evaluation of the T_g of bulk-polymerized nanogel, acetone (50 wt%) was added to dry nanogel powder (50 wt%) and DMPA (0.2 wt% relative to total mass). The clear liquid nanogel dispersion was placed between two glass slides in a rectangular mold (Length, Width, Thickness) of 24.08 mm x 5.36 mm x 1.5 mm and was irradiated with UV light (365 nm) at an incident irradiance of 250 mW/cm^2. The polymerized network was ground to powder form, was dried under house vacuum for complete removal of solvent, and its T_g was determined as described previously.

4.2.4. Imaging

Formulations of DVB:ST(20:80) (high conversion with methacrylate functionality) nanogel in acetone (50/50) wt%, DVB:ST(20:80) (high conversion with methacrylate functionality) nanogel in TEGDMA (50/50) wt%, DVB:ST(20:80) (low conversion with just pendant styrenic C=C) nanogel in TEGDMA (50/50) wt%, and pure TEGDMA were

prepared. For photopolymerization, DMPA (0.2 wt% relative to total mass) was added to each mixture. A disc shape sample (D = 10 mm, H = 3 mm) was prepared by photopolymerizing via UV (365 nm) light at 10 mW/cm2. All the samples reached > 90% conversion based on near-IR 6165 cm^{-1} peak (methacrylate C=C). The samples were cut into rectangular pieces and scanning electron microscopy (SEM; JEOL 6500F, Tokyo, Japan) was performed on the cut cross-section area. The samples were secured on the carbon tape and were gold sputter coated (Denton Vacuum Desk II; Au Sputter Deposition System, Moorestown, NJ, USA). The SEM images were obtained at 30,000-70,000X magnification. ImageJ (NIH image processing software) was used to convert the 2D SEM images into pseudo-3D surface plots based on the intensity (z-axis) of grey value (black = 0, white = 255).

4.2.5. Hydrolytic Degradation

Mixtures of nanogel (33.3 wt%), degradable dimethacrylate macromer (PEG2000PLADMA) (33.3 wt%), acetone (33.3 wt%), and DMPA (0.2 wt% relative to monomers mass) were prepared for all nanogel categories. Another mixture was prepared by adding high conversion, methacrylate post-functionalization DVB:ST(20:80) nanogel (15 wt%), PEG_{2000}PLADMA (42.5 wt%), and acetone (42.5 wt%) with DMPA (0.2 wt% relative to monomers mass) to study the effect of styrenic nanogel concentration on the macroscopic swelling and degradation behavior.

The mixtures were shaken on vortex mixer (VWR; Radnor, PA, USA) to achieve complete dispersion as determined by visual inspection of optical clarity. A rubber disc mold with thickness of 1.5 mm and diameter of 5.0 mm was filled with the mixture and then sandwiched between two glass slides. Sample discs were photopolymerized under

UV irradiation (365 nm) at 250 mW/cm^2. All discs reached 100% conversion based on near-IR 6165 cm^{-1} peak within 4-20 min of irradiation. After removing the discs from the mold, they were placed in desiccator under house vacuum to remove trapped acetone from the network. After acetone removal (as assessed by stable disc weight), the overall ratio of the degradable monomer to the nanogel became 50/50 wt% for the mixture with 33.3/33.3/33.3 wt% ratio and 75/25 wt% for the 15/42.5/42.5 wt% ratio.

The initial dry weight of the discs (n=3) was measured on an analytical balance (M_i). Then the dics were submerged in DI water (10 mL) at ambient temperature. At different time intervals during degradation dics were taken out of the water solution and were lightly blotted to allow measurement of the final swollen mass (M_s) for that specific time interval. Following attaining a stable weight, the discs were placed in the desiccator under vacuum to remove water and determine the final dry mass (M_f). The equilibrium mass swelling ratio (Q_m) and weight percent mass loss were calculated based on Eq 4.1-2, respectively:

$$Q_m = (M_s/M_i) \times 100 \quad (4.1)$$

$$\% \text{ Mass Loss} = ((M_i - M_f)/M_i) \times 100 \quad (4.2)$$

4.2.6. Post-Degradation Residual Mass Characterization

Diffuse Reflectance Infrared Fourier Transform Spectroscopy (DRIFTS) was used on non-degraded and hydrolytically degraded solid samples of DVB:ST(50:50) inert nanogel/PEG2000PLADMA(50/50) wt%. For DRIFTS experiment the sample was ground and mixed with KBr powder. Mid-IR spectra was collected using KBr absorption spectra

as background. Two peaks were followed in this region at t = 0, 3, 5, 7, and 9 weeks: i) 1720 cm^{-1} peak for carbonyl (C=O) embedded in ester linkages, and ii) 1123 cm^{-1} peak representing ether (R-O-R') linkages; both peaks were normalized based on 1600 cm^{-1} peak for aromatic C=C.

4.2.7. Contact Angle

Mixtures of 50 wt% low conversion DVB:ST(20:80) nanogel, 50 wt% acetone, 1.0 wt% of DMPA (relative to total mass) (sample 1); and 50 wt% DVB:ST(20:80) high conversion with methacrylate functionality nanogel, 50 wt% acetone, 1.0 wt% DMPA (relative to total mass) (sample 2) were added into two separate 20 mL vials and were stirred on vortex shaker to achieve homogeneity. A thin layer (couple of microns) of each mixture coated a separate glass slide (area of ~10 cm^2) using spin coater (Laurell Technologies Corporation; Model WS-650MZ-23NPPB, North Wales, PA, USA,) with 1000 rpm for 30 s. The spin coated glass slides were placed under house vacuum for a week to ensure that all solvent was removed. The near-IR spectroscopy was performed to generate spectra of the samples before and after photopolymerization with UV (365 nm) irradiation at 100 mW/cm^2 intensity. The conversion of thin layer of sample 1 and sample 2 reached 35% and 57% after 90 min irradiation, respectively. The conversions were calculated based on the area under 4720 cm^{-1} (normalized over aromatic C=C 1600 cm^{-1}) and 6165 cm^{-1} (normalized over 1720 cm^{-1}) peaks depending on the type of reactive groups. A goniometer (Rame'-Hart; Model 250-F1, Succasunna, NJ, USA) was used to measure the contact angle before and after photo-polymerization by placing a water droplet (2 µL) on the thin layer surface.

4.2.8. Viscosity

The viscosity of nanogel-modified TEGDMA was measured using a cone-plate digital viscometer (CAP2000+; Brookfield, Middleboro, MA, USA) at 25 °C and 50 rpm with run time of 25 s. The methacrylate functionalized DVB:ST(20:80) (50 wt%) was used to modify TEGDMA (50 wt%).

4.2.9. Mechanical Properties

A mixture of methacrylate functionalized DVB:ST(20:80) nanogel (50 wt%), TEGDMA (50 wt%), and DMPA (0.2 wt% relative to total mass) was photopolymerized using UV irradiation (365 nm) at 50 mW/cm^2 intensity. Bar samples were prepared by encapsulating the mixture inside a mold (L x W x H: 26.5 mm x 2.0 mm x 2.0 mm) between two glass slides. The conversion was 80% after 8 min irradiation. Flexural modulus and ultimate strength were obtained using bar samples (n = 5) on a universal testing machine (Mini-Bionix II, MTS, Eden Prairie, MN, USA) using three-point bending mode and a span of 20 mm with a cross-head speed of 1 mm/min.

4.2.10. Statistical Analysis

Data from each evaluation were submitted to one-way analysis of variance (ANOVA) followed by Tukey B as post-hoc test. All analyses were performed at a global level of significance of 95%.

4.3. Results and Discussion

4.3.1. Nanogel Particle Characterization.

The weight average molecular weight (M_w) of the nanogels was between 5,000 and 400,000 g/mol (Table 4.1). The lowest M_w (5300 g/mol) and R_h (1.66 nm) belonged to DVB:ST(20:80) nanogel with low conversion and no post-functionalization. This

nanogel also had the highest PDI (8.453), which is an indication of a large degree of heterogeneity at relatively early stages of reaction (50% conversion) due to the co-existence of oligomers in various sizes and nanogel particles in the reaction medium. Post-functionalization of the nanogels with methacrylate groups increased M_w and R_h except for DVB:ST(20:80) because the methacrylate functionalized nanogel was separately synthesized in higher concentration of solvent (8-fold excess instead of 6-fold). Increasing the solvent concentration promotes cyclization rather than addition of reactive monomers to the nanogel particle. With increasing crosslinker concentration, a rise in molecular weight is expected since there should be more pendant active sites on the growing chains; however, in this case, we observed the opposite trend, which is due to the increased level of chain transfer agent (30 mol%) and solvent ratio (10-fold excess of toluene relative to monomer mass) to avoid macrogelation during synthesis. Increasing the concentration of chain transfer agent shortens the active chain length and produces smaller particles. The Mark-Houwink exponents of these nanogels were well below ~0.7 that is associated with random coil linear polymer structures (Gaussian) (Hiemenz, 2007). The MH-$a \leq 0.3$ is a characteristic of highly branched globular particles in a good solvent.

Glass transition temperature of nanogel particles (dry powder) is shown in Fig 4.3. The T_g of low conversion DVB:ST(20:80) showed two tan δ peaks at 39 and 98 °C. The two T_gs associated with this nanogel are the result of difference between reactivity ratios of DVB and ST before the compositional drift takes over and partially balances the nanogel particles in terms of composition. The peak at 39 °C belongs to less crosslinked/styrene-rich particles and the peak at 98 °C represents the more crosslinked/DVB-rich particles. Increasing crosslinker concentration (DVB) from 20 to 50

mol% decreased the glass transition temperature, which is the opposite of what we normally expect and it is due to the reduced primary chain length and the increased level of chain ends created by higher concentration of chain transfer agent (30 mol%). There was a ~20 °C reduction in T_g of DVB:ST(20:80) after methacrylate functionalization, which is due to a large decrease (an order of magnitude) in molecular weight from 232,500 g/mol for non-functionalized to 34,000 g/mol for functionalized nanogel. Also, addition of IEM molecules to the chain ends increases the mobility of the chain ends and decreases the T_g. Addition of IEM to DVB:ST(50:50) high conversion nanogel increased the M_w, which is expected due to the high concentration of ME used during synthesis.

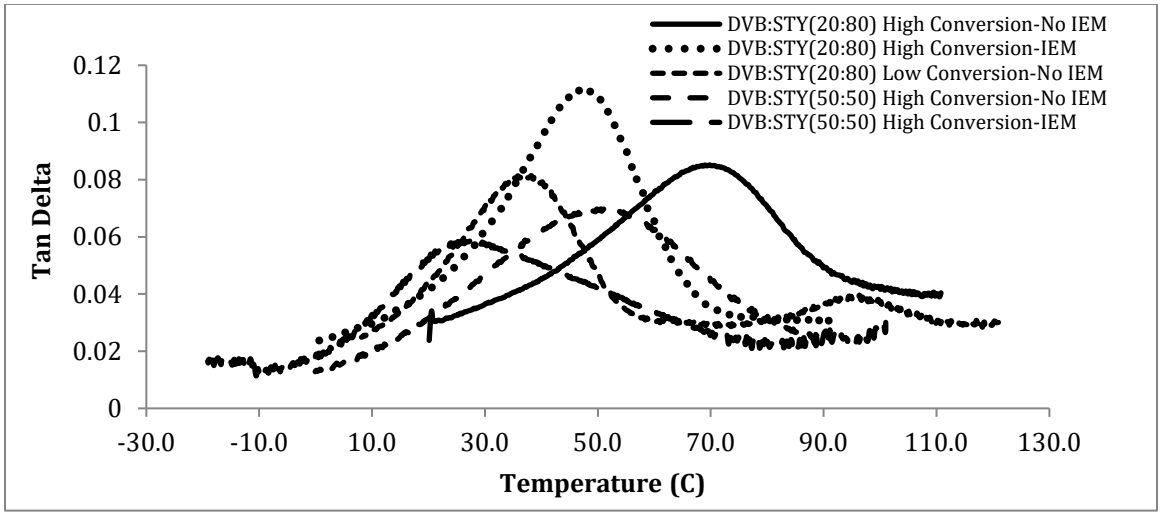

Figure 4.3. Glass transition temperature of nanogel particles: The temperature associated with tan δ peak shows the glass transition temperature.

Table 4.1. Nanogels GPC Characterization

Nanogel	DVB/Styrene (20:80) High Conversion-No IEM	DVB/styrene (20:80) Low Conversion-No IEM	DVB/Styrene (20:80) High Conversion-With IEM	DVB/Styrene (50:50) High Conversion-No IEM	DVB/Styrene (50:50) High Conversion-With IEM
Mn (g/mol)	110100	600	16600	34300	226500
Mw (g/mol)	232500	5300	34000	117800	380400
Mw/Mn	2.111	8.453	2.051	3.44	1.679
Rh (nm)	8.36	1.66	3.05	4.37	7.66
MH-a	0.347	0.311	0.167	0.253	0.523

4.3.2. Macroscopic Network Characterization

Functionalized nanogels are able to contribute to the formation of macroscopic polymerized network either as reactive filler or as sole precursor (Dailing, 2013; Liu, J. *Polym Chem*, 2014). At this point, it is important to determine the ability of the synthesized nanogels to participate in network formation, which can be probed by spectroscopic and thermomechanical analyses. Fig A.16 (Apendix A) shows the near-IR spectra of methacrylate functionalized DVB:ST(20:80) nanogel photopolymerized in acetone at a 50/50 wt% ratio. The rapid, near complete disappearance of methacrylate carbon-carbon double bonds at 6165 cm^{-1} peak in first overtone region, disappearance of 4743 cm^{-1} and growth of 4681 cm^{-1} in combination band region (Stansbury, 2001) are indications of very efficient intra- and inter-particle reactivity that produces macroscopic network structure. Another important observation was the constant concentration of pendant styrenic C=C bonds (4720 cm^{-1}) (Grunden, 2003) under radical attack. Furthermore, we followed the methacrylate and styrenic C=C bonds consumption when low conversion DVB:ST(20:80) nanogel was mixed with PEG_{2000}PLADMA (Apendix A Fig A.17). In this case, also the methacrylate double bonds were consumed but pendant styrenic double bonds remained unreacted. For the same reason we could not form a macroscopic network of only low

conversion DVB:ST(20:80) in acetone even after 2 hours of irradiation and increased amount of photo-initiator. These results indicate that the pendant styrenic double bonds in the nanogel structure either do not exist or are inaccessible for radical growth. Divinylbenzene has a short distant between its two reactive double bonds, which are connected by a stiff aromatic group, as a result incorporation of DVB as crosslinker into the nanogel structure brings the short kinetic chains very close to each other and creates a highly dense network. This dense and rigid structure with high level of steric hindrance might be accountable for inaccessibility of pendant styrenic double bonds (Leicht, 1981; Anseth, 1994). On the other hand, polymerization of pendant methacrylate C=C bonds on the periphery of nanogel particles was readily feasible.

The glass transition temperature of macroscopic network of DVB:ST(20:80) nanogel with methacrylate functionality was 98 °C (Fig 4.4), which shows 48 °C increase compared to the nanogel powder T_g. The higher T_g in polymerized network of nanogel particles is due to restricted conformational rearrangements and decrease in chain-end density. It is important to note that the T_g of polymerized bulk nanogel is obtained after removal of 50 wt% solvent, which certainly limits the T_g that can be achieved compared with neat monomers, neat liquid nanogels, or higher T_g nanogels. Also, the tan δ peak width at half height increased from 26 °C for nanogel powder to 42 °C for polymerized nanogel network, which is due decreased number of chain ends. The increased level of heterogeneity is due to the formation of long (relative to nanogel primary chains) polymethacrylate chains connecting the naogel particles to each other.

Figure 4.5 shows 2D SEM and pseudo-3D images of cross-sectioned photopolymer networks obtained from the solvent-dispersed methacrylate functionalized nanogel (A), a methacrylate functionalized nanogel swollen with TEGDMA (B), the low conversion nanogel in TEGDMA (C), and neat TEGDMA (D). The cross-sectioned surfaces of the macroscopic polymers display a range of surface roughness as evident in the pseudo-3D surface plots. The uniform, pore-free structure of the polymerized methacrylate functionalized nanogel polymerized in solvent (A1-A2) presents relatively low surface roughness, and clearely shows the confluent structure obtained by dense-packing of nanogels. Polymer surface roughness is dramatically enhanced when overlapping reactive nanogels were swollen by TEGDMA (B1-B2). This is likely due to the increased level of localized crosslinking, which leads to alteration in the direction of the minimum energy pathway of a propagating crack relative to the direction of the applied force. Fig 4.5 C1-C2 shows the polymerized network of TEGDMA modified with the low conversion nanogel, which practically acts as inert nano-filler due to lack of pendant styrenic double bonds (Fig S.4.6). It is evident that in this case nanogel particles have practically no effect on reducing the heterogeneity, which in terms of void size, we do not see any significant difference between this network and neat TEGDMA network (Fig 4.5 C1-C2 and D1-D2).

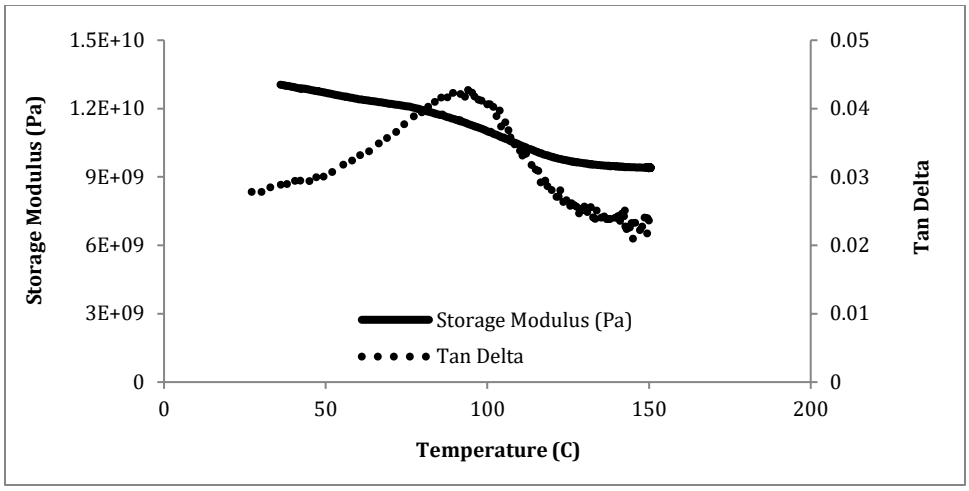

Figure 4.4. Tan δ vs. temperature for polymerized network of high conversion DVB:ST(20:80) nanogel with methacrylate functionality.

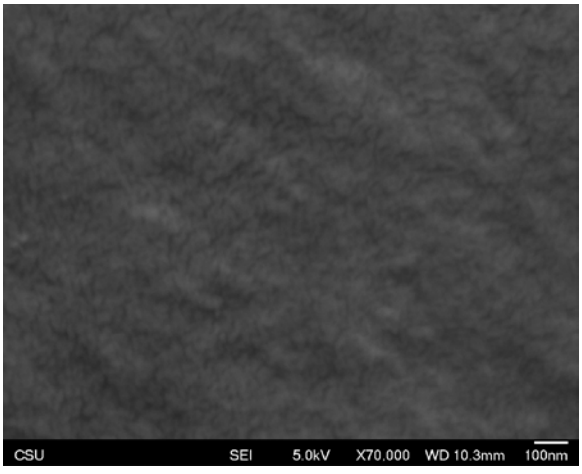

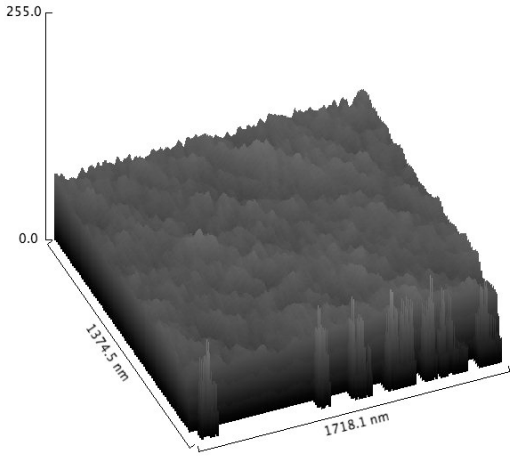

A1 A2

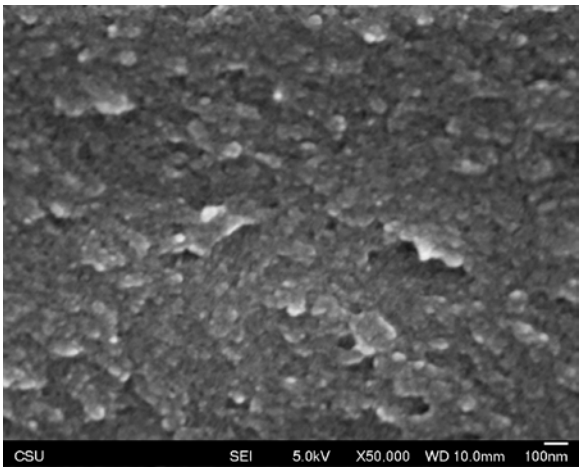
CSU SEI 5.0kV X50,000 WD 10.0mm 100nm

B1

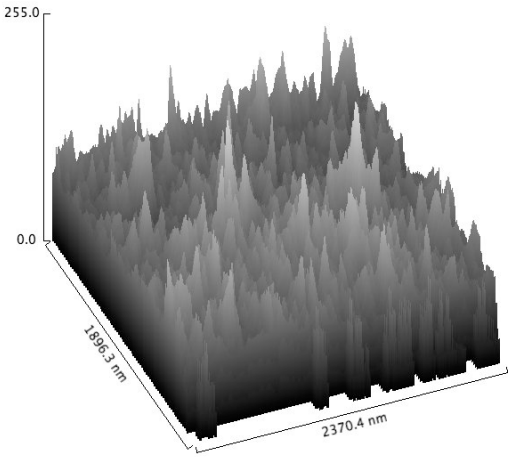
255.0
0.0
1896.3 nm
2370.4 nm

B2

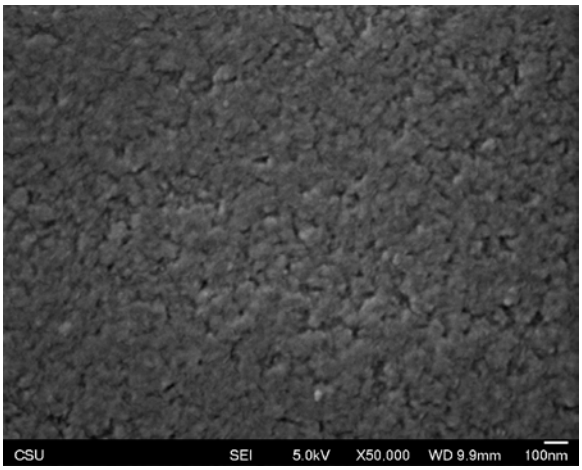
CSU SEI 5.0kV X50,000 WD 9.9mm 100nm

C1

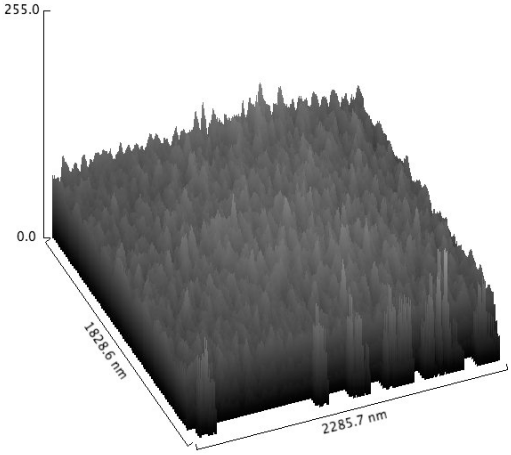
255.0
0.0
1828.6 nm
2285.7 nm

C2

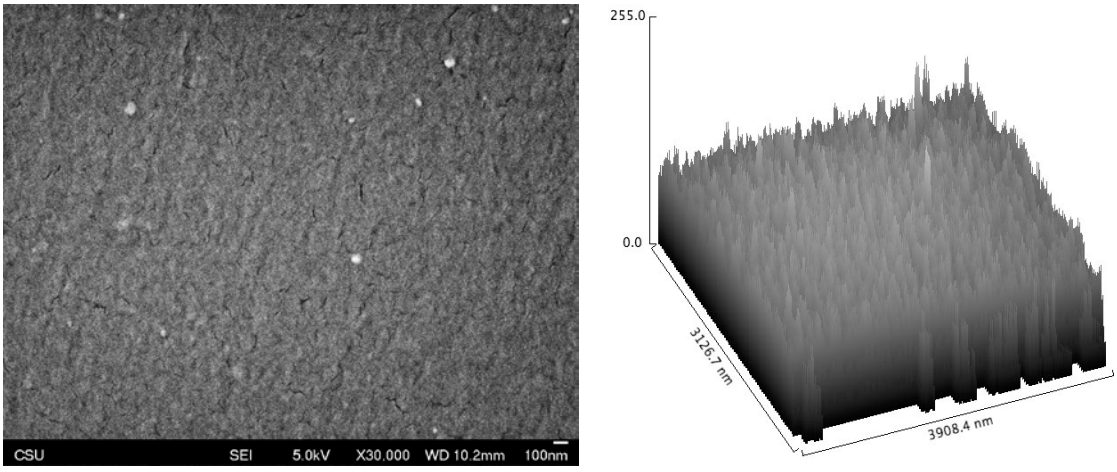

D1 D2

Figure 4.5. SEM 2D image and pseudo-3D surface plot of cross-sectional area of photopolymerized macroscopic network; A1,A2 = Polymerized DVB:ST(20:80) high conversion with methacrylate functionality nanogel, B1,B2 = DVB:ST(20:80) high conversion with methacrylate functionality nanogel/TEGDMA(50/50) wt%, C1,C2 = DVB:ST(20:80) low conversion nanogel/TEGDMA(50/50) wt%, and D1,D2 = TEGDMA (control).

4.3.3. Equilibrium Swelling

The extent and rate of water uptake into polymer networks are predominantly controlled by two main factors: resin polarity dictated by the number of polar sites available to form hydrogen bonding with water molecules and network topology. Non-polar polymers with low cohesive energy densities permit water molecules to move freely through voids as “unbound” water. Since this unbound water is only filling free volume it is not expected to cause significant dimensional changes of the polymer.

In contrast the water molecules that interact with polymer chains via solvation hydrogen bonding (quasichemical interactions) are referred to as “bound” water and this altered structure can disrupt the inter-chain packing and induce swelling as well as plasticization of the polymer (Malacarne, 2006). Also, water sorption follows Fickian diffusion kinetics (Smith, 2003; Ferracane, 2006). Networks or gels are often able to absorb more than their own weight in solvent, which is due to the balance between the

osmotic drive to dilute the polymer and the entropic resistance to chain extension or loss of conformational entropy (Hiemenz, 2007).

The chemical potential gradient drives solvent into the network until the state of equilibrium is reached via elastic resistance of the network to further deformation. The amount of solvent absorbed by the network at the equilibrium (plateau region of Q_m vs. time plot) is correlated to the chemical nature of the polymer chains, their flexibility, and also the crosslinking density. The polymeric equilibrium swelling in water of different hydrolytically sensitive samples was assessed based on: i) crosslinking density in the nanogel network, ii) loading level of nanogel in the labile macromer, and iii) post-functionality with ester-containing methacrylate linkages. The control group was pure crosslinked network of the macromer (PEG_{2000}PLADMA). Mass swelling ratio measurement does not allow us to distinguish between unbound and bound water but it is still a useful bulk quantification of water influx into the network. We observed (Fig 4.6) that the network with highest loading level of nanogel (50 wt%) and highest level of crosslinker concentration (50 mol%) and no methacrylate post functionalization had the lowest degree of equilibrium mass swelling ratio (Q_m ~ 110%). The control network had the highest overall level of swelling (Q_m ~ 300%). After normalizing against Q_m of 300% for hydrophilic labile macromer, it is apparent that adding highly crosslinked hydrophobic nanogel decreases the water uptake an additional 90% compared to a normalized swelling value of 200%. This non-linear decrease in Q_m is the result of: i) dramatic decrease in void volume, which is correlated with crosslinking density and nanogel particles degree of overlapping, and ii) shielding the labile macromer by hydrophobic chains of nanogel particles. Increasing the crosslinker concentration from 20 to 50 mol%

and addition of methacrylate post functionalization did not have a significant effect on Q_m profile, but decreasing the nanogel loading level from 50 to 25 wt% increased the overall Q_m value by almost 30% due to less shielding. Even lower amount of nanogel loading could hinder water penetration in a non-linear fashion (100% lower than the normalized value of 250%). This result shows that increasing the nanogel loading from 25 wt% to 50 wt%, which corresponds to a transition from a percolated nanogel loading configuration to an essentially confluent swollen nanogel distribution (Liu, Y. *Eur Polym J* 2012) have a significant effect on lowering the swelling mass ratio. The percolation threshold is where particle-particle interactions begin to dominate over resin-particle interactions (Moraes, *Dent Mater J* 2011).

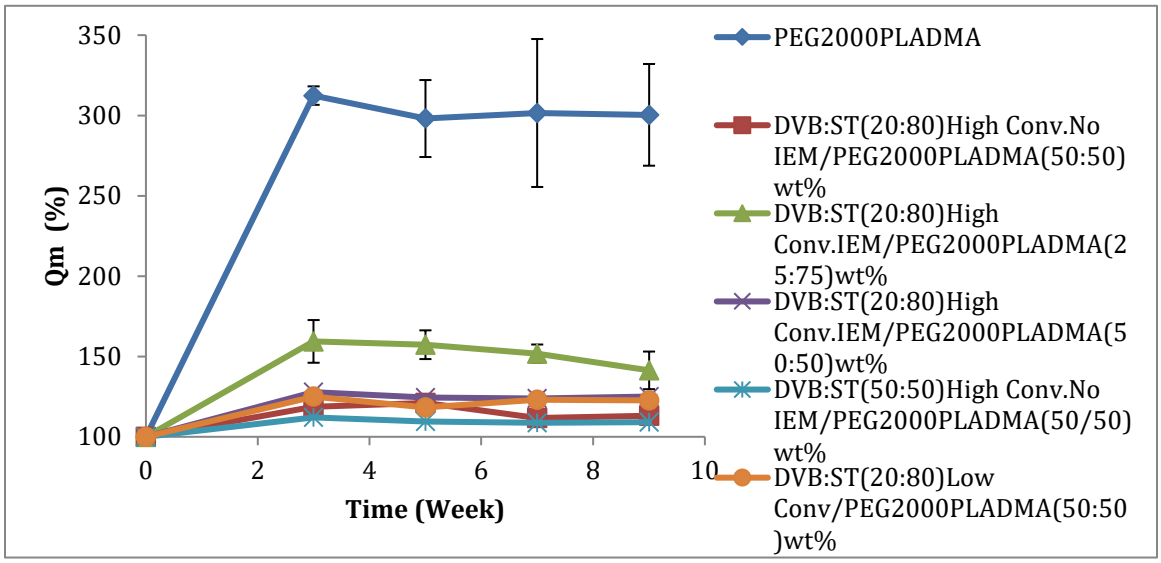

Figure 4.6. The equilibrium water uptake Qm vs. time for nanogel incorporated degradable network of PEG_{2000}PLADMA.

4.3.4. Mass Loss

Figure 4.7 shows the mass loss profile of the hydrolytically degradable polymer obtained from the PEG_{2000}PLADMA macromer as the control along with different categories of added DVB:ST(20:80) nanogel in terms of type of functionality and loading level. The positive control group (PEG_{2000}PLADMA) had the highest average mass loss of 55% after 9 weeks, which was expected due to its high mass swelling ratio and degradation potential. The second highest mass loss (40% at week 9) belonged to the network with methacrylate-functionalized nanogel with lowest level of loading (25 wt%). After being normalized against the mass loss of control group at 9 weeks and considering the nanogel loading level, the extent of mass loss did not change compared to the control. In other words, assuming the styrenic nanogel is non-degradable and not water leachable, a 55% mass loss of PEG_{2000}PLADMA occurred even at the 25% nanogel loading level, which might be due to the higher amount of localized water. The samples with 50 wt% loading all had the same profile with average mass loss of 10-15%. This shows an almost 30% difference between the mass loss of 25 and 50 wt% loaded networks, which is in agreement with 30% higher overall mass swelling ratio for samples with lower level of loading. We also tested the polymerized network of only high conversion DVB:ST(20:80) nanogel with methacrylate functionality as a negative control. There was no significant mass loss (< 2.0 %) associated with this network through the end of the 9-week study. Based on aqueous swelling and mass loss results, we can clearly see the effect of incorporation of styrenic nanogel on suppressing water penetration and network degradative mass loss. In addition, the hydrophobic effect and lack of water have beneficial advantages in dental application such as decreasing the

number of effective enzyme collisions and reducing enzyme activity (Sandwick, 1987; Dizge, 2009; Hernandez, 2011). Fig 4.7 shows the mass loss vs. time of degradable networks with 50 wt% loading of DVB:ST(20:80) and DVB:ST(50:50) nanogels. Based on this result, we did not observe a significant difference in degradation when the nanogel crosslinker concentration was increased, which again is in agreement with the mass swelling data.

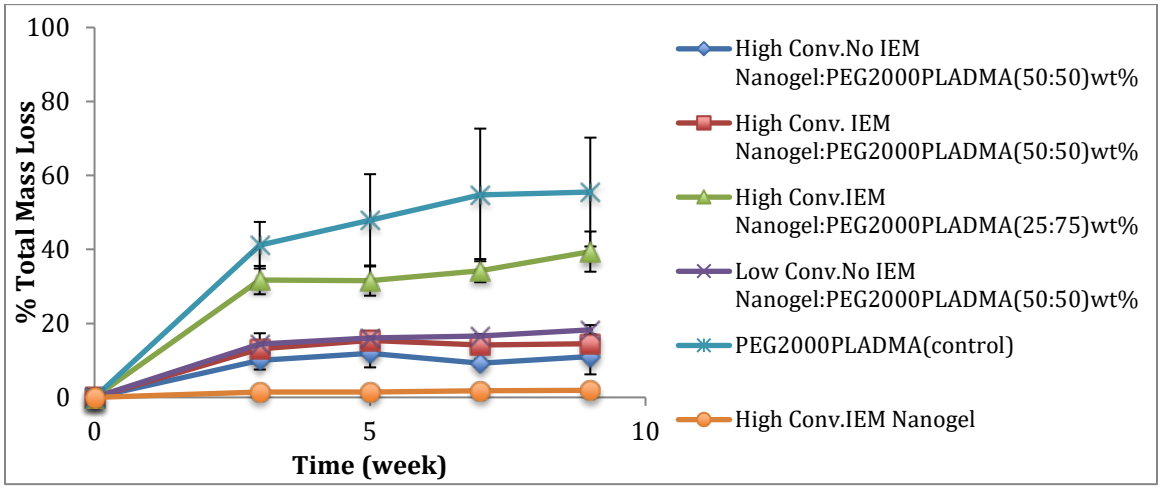

Figure 4.7. Mass loss profile vs. time for DVB:ST(20:80) nanogel series incorporated into degradable network of PEG_{2000}PLADMA.

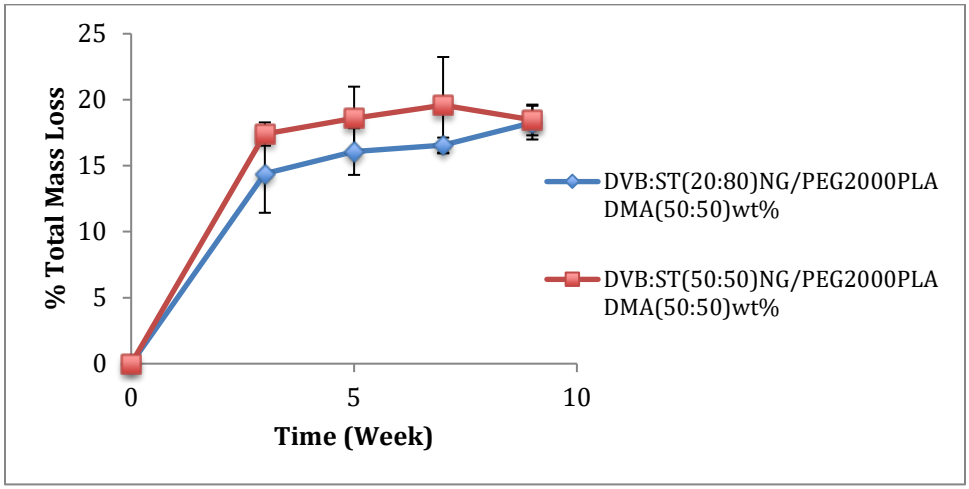

Figure 4.8. Comparing the mass loss profile for 50 wt% nanogel loaded degradable network with different crosslinker concentrations (25 and 50 mol%).

4.3.5. Residual Mass Analysis

During the course of hydrolytic degradation, the macromer network can be cleaved at the polyester linkages releasing lactic acid, PEG_{2000}, and polymethacrylate chains. To confirm this process more quantitatively, we followed two peaks in mid-IR spectra, 1720 cm^{-1} (C=O) and 1123 cm^{-1} (R-O-R') (both were normalized based on the styrenic nanogel derived aromatic peak at 1600 cm^{-1}) at t = 3, 5, 7, and 9 weeks intervals in DVB:ST(50:50) inert nanogel/PEG_{2000}PLADMA (50/50) wt% samples (Fig 4.9) (Lin-Vien, 1991; Bruice, 2015). The normalized peak area vs. time is shown in Fig 4.10. We observed a sharp decrease during the first 3 weeks of soaking in water and then both curves plateaued to relatively constant values. The decrease in 1720 cm^{-1} peak is an indication of loss of lactic acid and methacrylate chains, which ultimately results in the release of PEG_{2000} units with a corresponding decrease in the 1123 cm^{-1} ether peak. Fig 4.10 also shows that ether groups have decreased in a greater extent than the carbonyl group, which is due to the higher number of repeat units in PEG_{2000} (~45 ethylene oxide repeat units per chain) than in PLA (~8 lactyl repeat units per chain). The pattern of both curves follows the mass loss curve for this network (Fig 4.7), which after a sharp increase during the initial 3 weeks reaches a plateau at average value of 18%. The constant value of mass loss (constant 1720 and 1123 cm^{-1} peaks) indicates that either diffusion of cleaved species was dramatically hindered or the hydrolytic cleavage has effectively stopped. Based on water uptake data, which showed a dramatic reduction with 50 wt% naogel loading, we can conclude that the cleavage process was slowed significantly especially in the shielded areas by nanogel particles due to lack of diffused water.

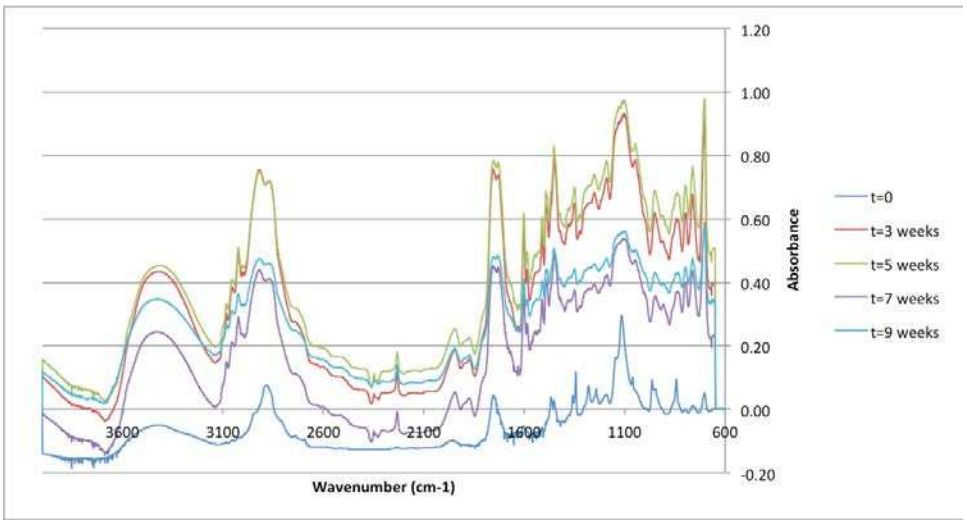

Figure 4.9. Mid-IR spectra of residual mass before and after hydrolytic degradation of DVB:ST(50:50) inert nanogel/PEG2000PLADMA(50/50) wt% at four time intervals (t = 3, 5, 7, and 9 weeks).

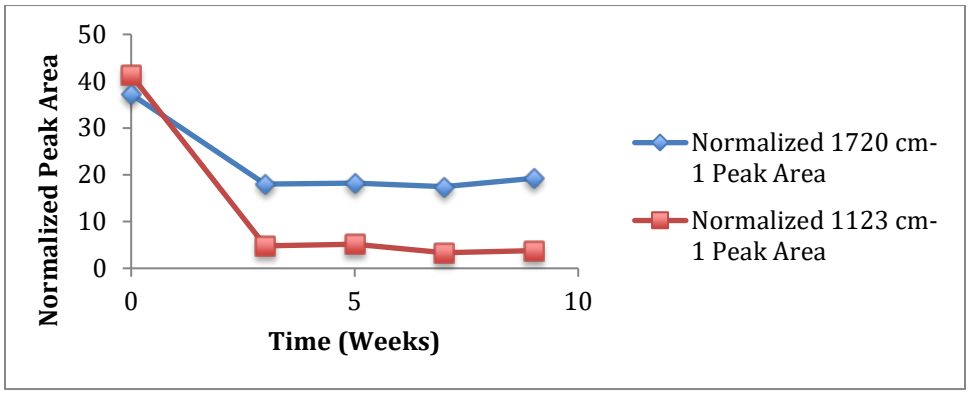

Figure 4.10. Normalized near-IR peak area of carbonyl (1720 cm^{-1}) and ether (1123 cm^{-1}) bonds for DVB:ST(50:50) inert nanogel/PEG2000PLADMA(50/50) wt% degradable network.

4.3.6. Contact Angle Analysis

The average water contact angle of DVB:ST(20:80) nanogel with methacrylate functionality before and after UV irradiation was 78° and 90° (p-level = 0.00014), respectively (Fig 4.11-12). The 90° contact angle is typically taken as a threshold above which truly hydrophobic material character is displayed. The increase in contact angle after polymerization and the transition to a more hydrophobic surface is due to the formation of polymethacrylate chains consisting of only hydrocarbon atoms along the

backbone and also due to the increased crosslinking density of the surface after polymerization. On the other hand, the contact angle of low conversion DVB:ST(20:80) nanogel before and after polymerization did not change (p-level = 0.61929) (Fig 4.13-14). This result was expected due to lack of pendant styrenic double bonds. By comparing the average contact angle value of both nanogels before polymerization, we observed that high conversion DVB:ST(20:80) with methacrylate functionality had a lower value (78.4°) than low conversion DVB:ST(20:80) (83.8°) (p-level = 0.00971). This is probably due to lack of ester and urethane groups on the side chains of low conversion DVB:ST(20:80) nanogel. Also, the average contact angle after polymerization was higher for DVB:ST(20:80) nanogel with methacrylate functionality compared to low conversion DVB:ST(20:80) nanogel (p-level = 0.00231), which is likely due to the higher level of crosslinking density in the former network (nanogel-nanogel crosslinking), also the contact angles in these nanogels are in the same range as the contact angle of polystyrene (Li, 2007).

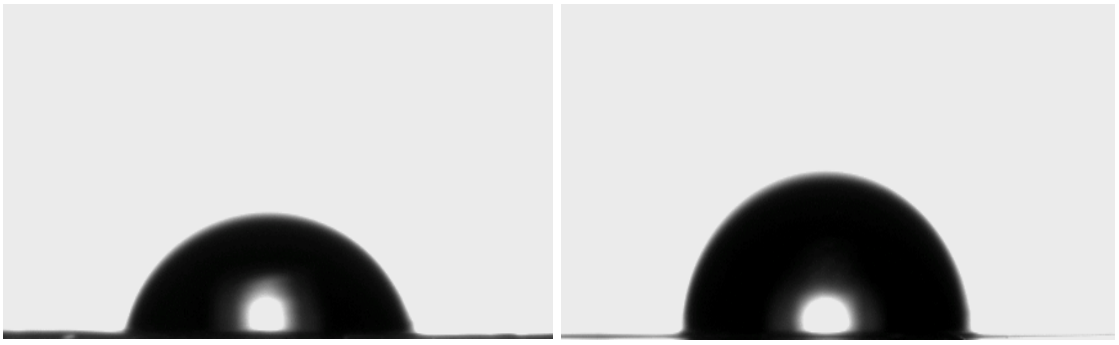

(a) (b)

Figure 4.11. The water contact angle measured on thin film of DVB:ST(20:80) with methacrylate functionality (a) before photo-polymerization and (b) after photopolymerization.

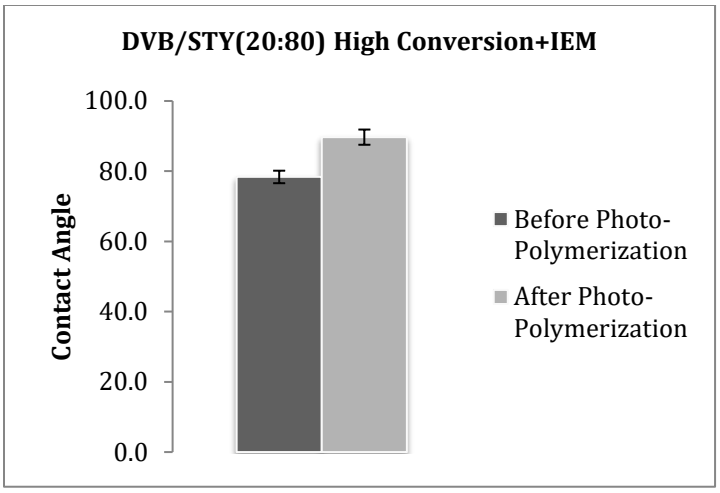

Figure 4.12. The water contact angle values before and after photo-polymerization (p-level = 0.00014).

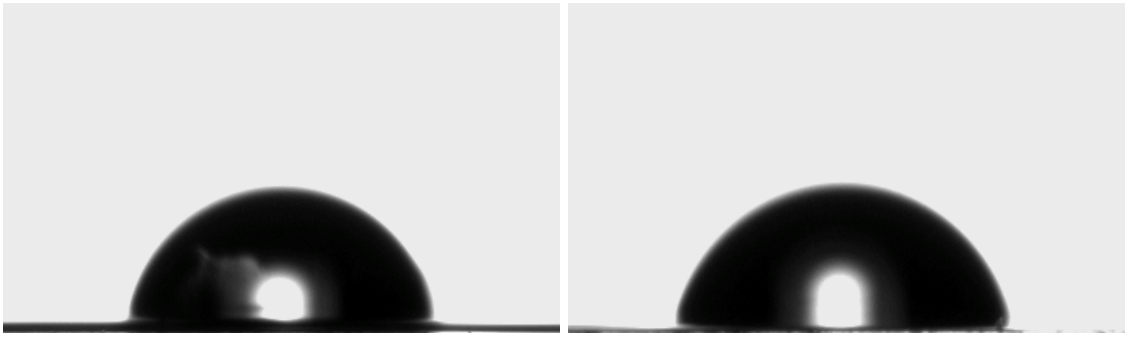

Figure 4.13. The water contact angle measured on thin film of low conversion DVB:ST(20:80) with pendant styrenic C=C bonds (a) before photo-polymerization and (b) after photo-polymerization.

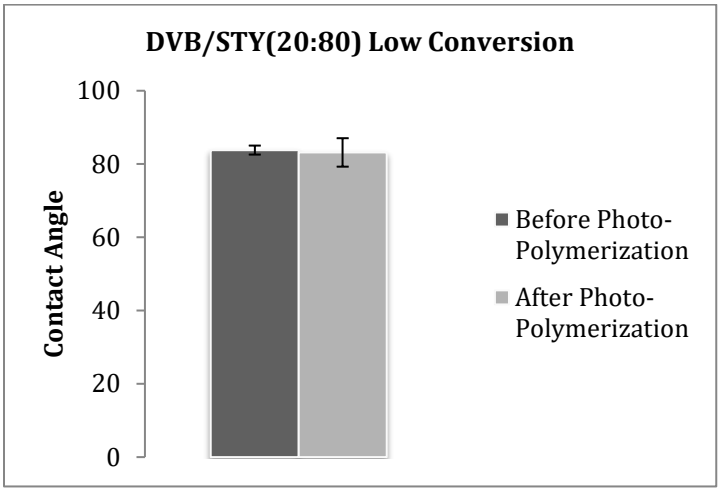

Figure 4.14. Water contact angle values of low conversion DVB:ST(20:80) before and after photo-polymerization (p-level = 0.62).

4.3.7. Viscosity and Flexural Modulus Analysis

The viscosity value of the nanogel-modified TEGDMA was 58.2 ± 3.1 Pa.s @ 25 °C, which is almost two orders of magnitude higher than that of TEGDMA alone (η = 0.05 Pa.s @ 30 °C), moderately higher than that of UDMA (η = 28 Pa.s @ 30 °C), and almost two orders of magnitude lower than that of BisGMA (η = 1369 Pa.s @ 30 °C) as examples of widely used commercial dental monomers. An exponential increase of viscosity in nanogel-modified TEGDMA relative to neat TEGDMA is due to the dominant nanogel-nanogel entanglements (immobilization effect) compared to that of between TEGDMA linear chains. It is also an indication of continuous TEGDMA-swollen nanogel phase (Dickens, 2003; Moraes, *Dent Mater J*, 2011). From the dental application point of view, the nanogel-modified TEGDMA even at 50 wt% loading still provides a practically workable viscosity.

The flexural modulus and ultimate strength of polymerized TEGDMA and nanogel-modified TEGDMA did not change statistically (Fig 4.15-16). The p-value between groups for flexural modulus and strength were 0.29 and 0.92, respectively. This result is an indication of unaltered number of efficient crosslinks in nanogel-modified TEGDMA despite the fact that functional group density is dramatically lowered when replacing TEGDMA with nanogel due to higher molecular weight of nanogel particles. The more efficient crosslinking in nanogel-modified resin is due to replacement of microgel-cluster formation during photopolymerization in pure TEGDMA by introducing nano-sized pre-crosslinked overlapping particles swollen by TEGDMA, which creates a more homogeneous network due to increased number of effective crosslinks.

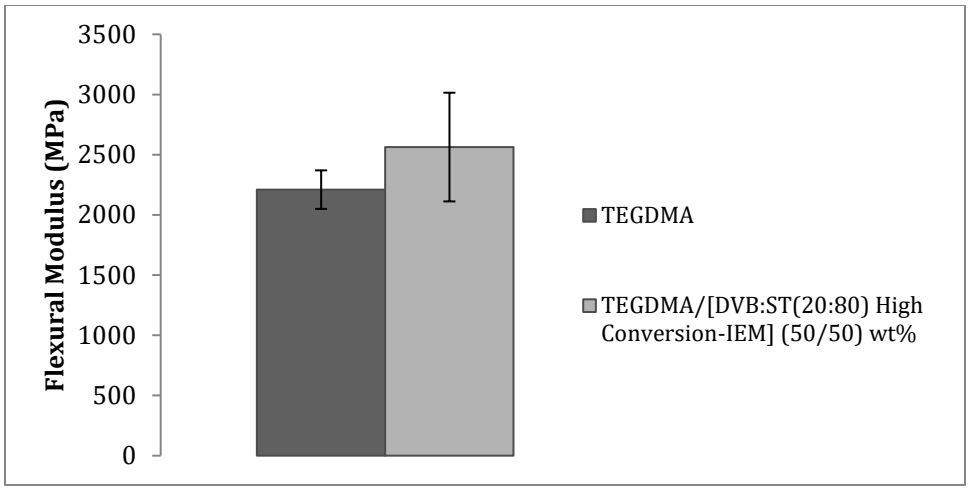

Figure 4.15. The flexural modulus of photo-polymerized TEGDMA (control) and DVB:ST(20:80) (high conversion nanogel with methacrylate functionality)/TEGDMA (50/50) wt% (p-level = 0.29).

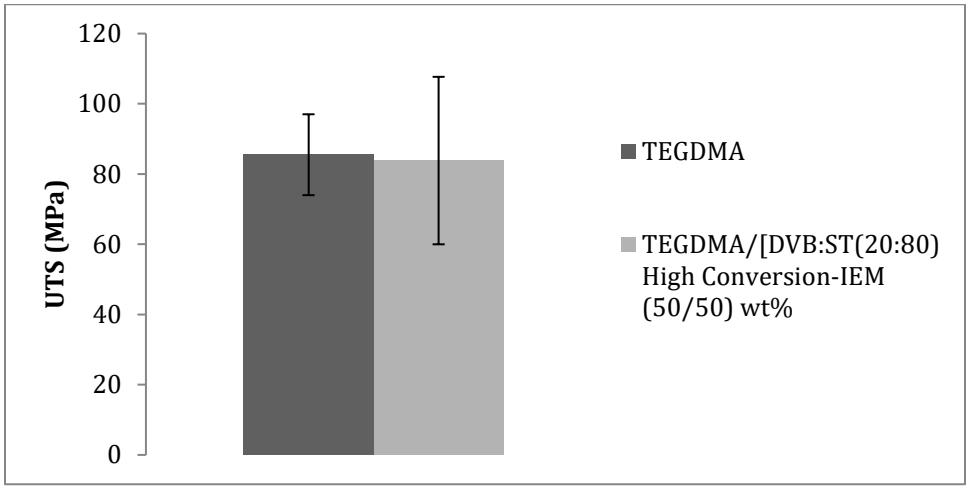

Figure 4.16. The ultimate tensile strength (UTS) of photo-polymerized TEGDMA (control) and DVB:ST(20:80) (high conversion nanogel with methacrylate functionality)/TEGDMA (50/50) wt% (p-level = 0.92).

4.4. Conclusions

Controlling water uptake and hydrolytic degradation in common methacrylate-based dental composites and potentially in dental adhesives would be expected to provide longer clinical service time while minimizing the release of leachable species. Regarding this challenge, most attention has been focused on creating a water-free environment before and during the polymerization with little effort in suppressing effects

post-polymerization. A model hydrolytically susceptible polymer network was used in this demonstration to accentuate the challenge in providing protection from aqueous swelling and degradation. Introducing hydrophobic all-hydrocarbon nanogels into the labile network without changing resin formulation opens a practical route for controlling hydrolytic degradation and presumably for physically restricting access for enzymatic attack in the oral cavity. Highly crosslinked styrenic nanogels were incorporated into a hydrolytically degradable monomer either as inert or reactive additives at various loading levels. The equilibrium mass swelling ratio and percent mass loss were dramatically reduced in nanogel-modified networks regardless of their functional groups. The loading level of nanogel played an important role in suppressing both water uptake and hydrolytic degradation without impractical increase of viscosity. This enhanced shielding property is a result of nanogel particle-particle overlapping beyond percolation threshold. This approach can be applied to variety of polymeric systems prone to hydrolytic degradation including dental restorations, engineered tissues, and surface coatings.

CHAPTER 5

NANOGELS WITH HIGH GLASS TRANSITION TEMPERATURE

5.1. Introduction

There are several classes of thermosets and thermoplastics that are considered high performance/high temperature polymers with numerous industrial applications such as aerospace, electronics, fire resistance materials, membranes, coatings, and polymeric structural components (Critchley, 1983; Imai, 1995; Hergenrother, 2003) These polymers are generally formed or processed at high temperatures with the potential to be used in relatively high temperature applications. Therefore they need to conform to at least one of the following specifications: i) strong inter-chain interactions often involving high aromatic content and rigid segments, exhibiting high glass transition temperatures (T_g > 200 °C) and high mechanical properties, ii) thermal decomposition temperature > 450 °C (temperature of 50.0% mass loss at a heating rate of 2.5 °C/min). These exceptional macroscopic properties are achieved by integration of several factors at molecular level such as high primary bond strength, resonance stabilization, rigid intra-chain structure, high molecular weight, homogeneity, strong intermolecular attraction (i.e. hydrogen bonding), crystallinity, and high crosslinking (only for thermosets) (Critchley, 1983; Imai, 1995; Hergenrother, 2003). In thermoplastics, prepolymers are heated to reach the flowable state, then they are formed in a mold or by other means and then solidified upon cooling, thus there is no crosslinking involved in the final polymer structure.

On the other hand, thermosets are cured at high temperatures, therefore a fixed solid-state shape is achieved by high level of crosslinking (Biron, 2013). An unfavorable competition between polymer cure and degradation introduces a critical challenge in the curing processes applied to high Tg thermosets, in addition to high cost of heating (T_{cure}) (Gillham, 1986; Imai, 1995; Biron, 2013). Based on Time-Temperature-Transformation (TTT) of the isothermal cure diagram, the onset of vitrification during the transformation of a liquid monomer to an amorphous solid, is when the T_g of the polymer reaches to the isothermal T_{cure} (Gilham, 1986). Depending on the breadth of the tan delta peak associated with thermoset polymers, polymer Tg is limited to an approximation of T_{cure} typically by ~30 °C for heterogeneous highly crosslinked methacrylate polymers. The significance of high T_{cure} for thermoset development resides in delaying the onset of vitrification to higher conversions and ultimately higher T_gs, since elevated T_{cure} retain the liquid/rubbery state of the polymeric macromolecules for an extended period of time, in addition to enhancing radical diffusion (Gilham, 1986). Villegas *et al.* (2015) have demonstrated the effect of reducing the heating time to fractions of a second on suppressing the potential thermal degradation process during thermoplastic composite (TPC)/thermoset composite (TSC) ultrasonic welding. The TPC and TSC used in that study were carbon fiber (CF)/polyether-ether ketone (PEEK) and carbon fiber (CF)/epoxy, respectively.

The drawbacks of the ultrasonic welding are the need for higher force and amplitude to achieve short heating time, thus higher stress is a self-evident outcome; also the proposed method can only be applied to thin films, since the temperature gradient is much higher between the welding interface and top/bottom layers for higher film

thicknesses, leading to compromised final structure. Another issue with conventional thermosets especially in free-radical crosslinked networks is the induced heterogeneity in spatial distribution and composition of crosslinks (hard vs. soft) due to the kinetic nature of network evolution (Di Lorenzo, 2015). Additional inhomogeneity emerges from the low solubility and high viscosity of the starting macromolecule blends, which is evident in more than one glass transition temperatures and low conversions at gelation/vitrification onsets, respectively (Dušek, 1996).

In this work, we aim to find an alternative approach to polymeric materials with high glass transition temperature and high thermal stability. Here, the design of prepolymer networks is counter-intuitively reduced to nano-scale, which critically offers the advantage of nanoparticle dispersion in common solvents and monomers. What we consider and define as nano-scale polymer (nanogel) in our lab is a highly crosslinked globular macromolecule in the range 5-20 nm in size (Dailing, 2013). These polymeric nanoparticles are synthesized via free-radical solution polymerization by employing at least one di-vinyl and one mono-vinyl monomer. Nanogels have been used in variety of applications such as shrinkage and stress reduction in dental composites and resins, water percolation control in dental adhesives, gradient and mechanical property control, precursors for water-based networks, and drug delivery (Moraes, 2011, 2012; Liu, J. 2012, *Polym Chem* 2014, *Dent Mater J* 2014; Chen, 2014; Dailing, 2015; Saraswathy, 2016; Gotti, 2016). We also employed photopolymerization at ambient condition as the cure process due to distinct advantage of light as an energy source such as: i) processes that are unable to occur energetically on reasonable timescales at ambient temperature occur readily through photopolymerization, ii) energy in a mole of photons at different light

wavelengths particularly in UV region have two-orders of magnitude higher energy than thermal energy at 25 ^{o}C, and iii) spatial and temporal control over the photopolymerization processes (Chatani, 2013). The design strategy adopted for high T_g nanogel synthesis is as follows: i) minimizing chain end concentration, and ii) high crosslinking density to decrease the configurational entropy as a result of departure from Gaussian behavior (Hale, 1991). Divinylbenzene (DVB) was chosen as di-functional monomer or crosslinker due to its aromatic and rigid structure, styrene (ST) and isobornyl methacrylate (IBMA) were mono-functional monomers based on the same criteria. The nanogel particles were evaluated for molecular weight, size, T_g, thermal stability, dispersion ability, polymerization kinetics, and mechanical properties.

5.2. Materials and Methods

5.2.1. Materials

Isobornyl methacrylate (IBMA) (Tokyo Chemical Industry) and styrene (ST) (Alfa Aesar) were mono-vinyl monomers. Divinylbenzene (DVB) (Sigma Aldrich, Technical Grade 80%) and triethylene glycol dimethacrylate (TEGDMA) (Tokyo Chemical Industry) were di-vinyl monomers. 2,2'-Azobisisobutyronitrile (AIBN) (Sigma Aldrich) and 2,2-dimethoxy-2-phenylacetophenone (DMPA) were used as thermal and photo initiators, respectively. Toluene (Fisher Scientific, Certified ACS), hexane (Fisher Scientific, Certified ACS), tetrahydrofuran (THF) (VWR Analytical), and acetone (Sigma Aldrich) were solvents. Butylated hydroxytoluene (BHT) (Sigma Aldrich) was used as an inhibitor. All the materials were used as received.

5.2.2. Nanogel Synthesis

Two different nanogels were synthesized via free radical solution polymerization. The first nanogel batch (NG_1) included DVB (30 mol%) as the crosslinking agent, ST (70 mol%) as mono-vinyl monomer, the second nanogel batch (NG_2) included DVB (30 mol%) and IBMA (70 mol%) as di-vinyl and mono-vinyl monomers, respectively. AIBN (4.0 wt% relative to monomer mass), and 8-fold excess of toluene (relative to monomer mass) were added to both batches. Reaction temperature was 110 ^oC, and cold-water flow rate in the reflux condenser was adjusted to maintain constant volume during the reaction. Stirring rate was set to 400 rpm.

The reaction was carried out isothermally for 1.75 h for NG_1 and 1.5 h for NG_2. Drop-wise precipitation of the clear reaction mixture in a 10-fold excess of hexane (relative to reaction volume) was performed after the solution reached room temperature. The solid nanogel precipitate was added to acetone to verify a clear dispersion of the discrete nanoparticles. An inhibitor (BHT; 0.02 wt% relative to nanogel mass) was added to the acetone-nanogel dispersion before the acetone was removed under high vacuum. The nanogel was isolated as a white powder.

5.2.3. Polystyrene (PS) Formation

Polystyrene was also synthesized via free radical solution polymerization. AIBN (4.0 wt% relative to monomer mass) was added to styrene and 8-fold excess of toluene (relative to monomer mass). Reaction temperature and stirring rate were 110 ^oC and 400 rpm, respectively. Conversion reached 43.8% after 2 h of reaction. Upon cooling to room temperature, the clear solution was added dropwise to 10-fold excess of hexane (relative to solution volume), which resulted in precipitation of the PS as a solid. The precipitate

was then isolated and redispersed in acetone. The acetone was removed under high vacuum to leave PS as white powder.

5.2.4. Macroscopic Network Formation

TEGDMA was chosen as a model dimethacrylate resin that produces a glassy polymer network. A homogeneous mixture of nanogel/TEGDMA (50/50) wt% was prepared for each nanogel, and DMPA (0.2 wt% relative to monomer mass) was added to each mixture. Samples were mechanically agitated until all prepolymers were fully dispersed to give an optically clear dispersion, then an aliquot of each solution was injected to rectangular mold, sandwiched between two glass slides. Two types of bar specimens with dimensions (Length, Width, Thickness) of 24.08 mm x 5.36 mm x 1.5 mm or 25.32 mm x 2.21 mm x 2.04 mm were photopolymerized at room temperature under UV light (365 nm filter) at an irradiance of 60 mW/cm^2 to obtain samples for T_g (1.5 mm thick; n=2) and uniaxial flexural modulus measurements (2.04 mm thick; n=3). We also prepared a bulk, thermally polymerized mixture of DVB (30 mol%) and ST (70 mol%) monomer blend with AIBN (4.0 wt% relative to monomer mass) for T_g measurements (n = 2). Polymerization was performed in the oven at 100 °C for 12 h with 100% conversion.

5.2.5. Nanogel Structural Analysis

Mid-IR (Nexus 670, Nicolet, Madison, WI) and near-IR (Thermo Scientific, Nicolet 6700) spectroscopy were used to calculate the methacrylate carbon-carbon double bond conversion based on 815 cm^{-1} peak and styrenic carbon-carbon double bond conversion based on 4720 cm^{-1} peak, respectively. Triple-detection gel permeation chromatography (GPC; Viscotek) with differential refractive index, viscosity, and light scattering detectors was employed for the analysis of linear polymer and nanogel molecular weight,

polydispersity (PDI), and average hydrodynamic radius (R_h). Tetrahydrofuran (THF) was used as diluent with a flow rate of 1 mL/min at 35 °C in a series of four columns spanning molecular weight of 10^4 – 10^7 calibrated with a 65 kDa poly(methyl methacrylate) standard.

5.2.6. Dynamic Mechanical Analysis (DMA)

DMA testing was performed using a TA instruments (DMA 8000, Perkin Elmer) to determine T_g of bulk nanogels (powder) (n=2) and macroscopic network of photopolymerized mixture of TEGDMA/nanogel (n=2). Nanogel powder (10-15 mg) was placed inside a thin metallic pocket, which was secured between the clamps, and then subjected to single cantilever cyclic displacement of 0.05 mm at a frequency of 1 Hz in nitrogen gas.

The glass transition temperature was determined as the position of the tan δ maximum vs. temperature plot. The temperature range was between 30 °C and 370 °C with a ramping rate of 3 °C/min. A preheating conditioning cycle was applied with a ramping rate of 10 °C/min.

5.2.7. Thermogravimetric Analysis (TGA)

TGA (Perkin Elmer – Pyris 1) was used to characterize the thermal stability of the nanogels and polymerized monomer-blends as control. The linear heating rate used in TGA was 10 °C/min under nitrogen with purging rate of 40 mL/min.

5.2.8. Refractive Index Measurement

Dispersions of nanogel in a non-volatile solvent (toluene) at different weight ratios were prepared (0, 10, and 30 wt% nanogel loading) and the refractive index of the solutions was measured with Refractometer ATAGO 2T (nD) at room temperature. The

refractive index of bulk nanogel was extrapolated from the linear fit of data for 100% nanogel weight fraction.

5.2.9. Photopolymerization Kinetics

The evolution of double bond conversion (reaction kinetics profile) during radical photopolymerization of TEGDMA and nanogel/TEGDMA mixture was carried out by near-IR spectroscopy in real time at room temperature. The peak area of the first overtone absorbance of the methacrylate $=CH_2$ group at 6165 cm^{-1} was followed for 10 min curing time under UV irradiation (365 nm filter) with 60 mW/cm^2 light intensity. The rate of polymerization (R_P) was calculated based on the slope of conversion vs. time data.

5.2.10. Flexural Strength Testing

The universal testing machine (Mini-Bionix II, MTS, Eden Prairie, MN) was employed to measure uniaxial flexural modulus of photopolymerized specimens (n=3) in three-point bending on a 20 mm span at a crosshead speed of 1 mm/min.

5.2.11. Statistical Analysis

Analysis of Variance (one-way ANOVA) was performed in conjunction with multiple pair-wise by comparisons using Tukey B Tests for assignment of significant differences between means. Null hypothesis was rejected when *p*-value was less (or equal to) 0.05 significance level.

5.3. Results and Discussion

5.3.1. Particle Size Characterization

The optical transparency of solvent dispersed nanogel solutions is the visual and first indication of discrete, single nanoparticle characteristic of NG_1 and NG_2, rather than microparticle or multi-nanogel aggregates. The conversion of DVB and ST vinyl groups

in NG_1, based on near-IR peaks at 6132 cm^{-1} and 4720 cm^{-1}, were 39.8% and 55.7%, respectively (Alfred Christy 2016). In addition, the conversion of DVB and IBMA vinyl groups, based on mid-IR peaks at 1718 cm^{-1} and 815 cm^{-1}, were 45.9 and 64%, respectively (Nyhus, 2000). It is important to note that the reactivity of pendant vinyl group decreases (2-3 orders of magnitude) for intermolecular crosslinking due to higher local concentration of pendant groups inside the active particle and their close proximity to the active center, particularly at the early stages of free radical polymerization. Therefore, it is expected that a majority of pendant double bonds undergo primary and secondary cyclizations during this time (Okay, 1995; Davankov, 2010). The conversion values indicate the overall greater consumption of vinyl groups in NG_2 than in NG_1, yet the $\bar{M}_w$ of NG_1 (613,000 g/mol) is higher than that of NG_2 (383,000 g/mol) by a factor of 1.6. This observation suggests that higher consumption of vinyl groups during NG_2 synthesis is more likely due to increased degree of cyclizations inside the growing particle, which is caused by higher concentration of pendant double bonds. The reactivity ratios of methyl methacrylate (MMA) and (*meta*-, *para*-) DVB at 70 °C are, [r_1 (MMA) = 0.41, r_2 (*m*-DVB) = 0.61; r_1 (MMA) = 0.62, r_2 (*p*-DVB) = 1.3], which confirm the preference of DVB addition to styrenic active centers (Wiley, 1968; Odian 2004). Another limiting factor on molecular weight increase in this nanogel may arise from the steric hindrance imposed by the bulky isobornyl group of IBMA, which opposes the addition of macroradicals to create a larger particle. The lower MH-*a* value (< 0.3) of NG_2 relative to NG_1 also confirms the effect of extensive cyclizations as well (Table 3.1). On the other hand, the higher $\bar{M}_w$ and relatively higher value of MH-*a* of NG_1 points out higher level of macroradical addition rate and lower degree of cyclizations, respectively. The reactivity ratios of ST and (*meta*-, *para*-)

DVB, [r_1 (ST) = 0.62, r_2 (*m*-DVB) = 0.55; r_1 (ST) = 0.2, r_2 (*p*-DVB) = 0.39] at 100 °C, show that addition of styrene and DVB to the active sites tends towards random-alternation, therefore local pendant double bond concentration in NG_1 is somewhat lower than that of in NG_2 (Hiemenz, 2007; Davankov, 2010). This effect also manifests itself in higher PDI value of NG_1 (2.37) compared to NG_2 (1.63) (Table 5.1).

GPC analysis also demonstrated one-order of magnitude higher $\bar{M}_w$ for nanogels compared to PS particles ($\bar{M}_w$ = 19,000 g/mol), which is due to crosslinker (DVB) effect. Addition of crosslinker to a pool of mono-functional monomer raises the probability of propagation steps on the growing particles by creating pendant double bonds. Therefore the number of monomer addition steps to an active particle is likely higher than that of to an active oligomer. The PDI of 2.638 for PS particles is in the range for polystyrene synthesized via conventional free radical polymerization (PDI ≥ 2.0) (Erdmenger, 2009). The hydrodynamic radius of PS was 2.98 nm.

Table 5.1. Nanogel GPC Characterization

	DVB/Styrene (30:70) (NG_1)	DVB/IBMA (30:70) (NG_2)	Polystyrene (PS)
$\bar{M}_n$ (g/mol)	259,000	235,000	7,000
$\bar{M}_w$ (g/mol)	613,000	383,000	19,000
R_h (nm)	9.58	7.79	2.98
$\bar{M}_w/\bar{M}_n$	2.367	1.628	2.638
MH-*a*	0.304	0.243	0.299

5.3.2. Bulk Nanogel T_g

The theoretical glass transition temperature for each nanogel was predicted by applying Fox equation (Eq 5.1) (Hiemenz, 2007) and homopolymer T_g of each monomer. The homopolymer T_gs used for poly(isobornyl methacrylate) (PIBMA) and polystyrene (PS) were 165 and 100 °C, respectively (Zhang, 1994; Hiemenz, 2007). There was no

numerical value associated with the T_g of polydivinylbenzene (PDVB) in the literature, due to its high crosslinking density (Wang, 2016), thus we used $T_g = \infty$ for pDVB.

$$\frac{1}{T_g} = \frac{w_1}{T_{g,1}} + \frac{w_2}{T_{g,2}} \quad (5.1)$$

The theoretical T_g values for NG_1 and NG_2 were 299.8 and 274.9 °C, respectively. We have to note that Fox equation is valid for statistical copolymers (both reactivity ratios of comonomers are close to 1) (Davis, 2002), when this assumption $\Delta C_{p,1}T_{g,1} \approx \Delta C_{p,2}T_{g,2}$ holds (ΔC_p represents the heat capacity difference between liquid and glass phases of the comonomer) and both T_gs are not too different. The off the chart value of T_g for PDVB causes these assumptions to be invalid, yet using Eq 5.1 provided a rough estimation of what might be expected without considering any other factors affecting the final T_g of nanogel particles. As it was specified in the experimental section, the nanoparticles in this study (NG_1, NG_2, and PS) were synthesized at 110 °C, therefore by analogy this temperature is equivalent to T_{cure} during nano-scale network formation. The maximum possible glass transition temperature in a bulk polymerization process is a function of cure temperature, network heterogeneity, and molecular structure (Ye, 2011). Bowman et al. have developed two important relationships $T_g \approx T_{gmax}$ and $T_g \approx T_{cure} + T_{g1/2width}$ for systems polymerized near or above their maximum possible glass transition temperature, where $T_{cure} \geq T_{gmax} - T_{g1/2width}$, and systems cured well below their T_{gmax}, where $T_{cure} < T_{gmax} - T_{g1/2width}$, respectively (Ye, 2011). The most important conclusion based on these relationships is that increasing T_{cure} forces the T_g of a comonomer system to reach its T_{gmax} (although for any system T_{cure} has an upper limit, which beyond that T_{gmax} does not change anymore). The kinetic explanation for this correlation is that at high cure temperatures, radical polymerization instead of being diffusion-controlled, it is topology-

controlled. Therefore, copolymerization can reach higher conversion. It is well known that the actual volume of a polymer network (V) is the sum of the volume occupied by the molecules (V_{occ}) and free volume (V_f), which both are functions of temperature (they both increase as kinetic energy increases) (Hiemenz, 2007). Below T_g, V_{occ} and V have almost the same linear relationship with temperature, and V_f remains almost constant at its lowest possible value, but above T_g, V starts to diverge as a result of increased V_f. Based on this knowledge, the delayed vitrification at high cure temperature keeps the final V_f at its minimum until higher conversions, thus T_g a strong function of V_f reaches to its maximum value. In our system the polymerization kinetics was forced towards topology-controlled regime by increasing both T_{cure} and agitation rate within the reaction solution. The solution-state nanogel polymerization, in addition to enabling avoidance of macrogelation effectively reduces the T_g of the evolving nanogel particles thereby allowing high conversion and a potential for high T_g upon solvent removal. The free volume occupied by solvent during the formation of the nanogel particles is expected to progressively diminish as the internal network structure densifies. Furthermore, introducing crosslinking by addition of DVB to the monomer mixture, raises the final network T_g by reducing V_f, and also increases thermal stability, depending on DVB concentration (Nakagawa, 1987; Levchik 1999; Lu, 2001; Hiemenz, 2007). The tan δ vs. temperature plot for NG_1 (Fig 5.1 A) shows a broad transition with maximum tan δ at T_g = 242.5 ^oC, which is 57.3 ^oC lower than the value predicted by Fox equation. This curve has only one peak even after de-convolution, which justifies our earlier prediction for this nanogel regarding a more homogeneous distribution of comonomers among particles, yet it is a broad peak with a transition between 25 and 350 ^oC, which is due to broad

distribution of relaxation times and mobilities stemming from heterogeneous distribution of crosslinks (high concentration of crosslinker) and large PDI of particle sizes (Lu, 2001). For NG_2, we observed two different glass transition temperatures at 206.3 and 316.9 ^oC (Fig 5.1 B). The reason for two different T_gs goes back to the copolymer structure and the large difference between comonomers reactivity ratios, which creates DVB-rich and IBMA-rich particles. Based on these two T_g values, we can assign 206.3 and 316.9 ^oC for IBMA-rich and DVB-rich segments, respectively. The high glass transition temperatures of these nanogels from chemical structure point of view are due to different factors: i) stiff backbone (high potential barriers between conformations), ii) large rigid side-groups, iii) high crosslinking density, and iii) minimized chain-end effects. The DMA result for PS particles shows a T_g of only 53 ^oC (Fig 5.2), which is much lower than the two nanogels under study here and more importantly lower than the T_g of linear PS reported in the literature, which is due to higher number of chain-ends relative to molecular weight. The glass transition width of PS particles is between 20 and 100 ^oC, which is due to the PDI value of 2.64.

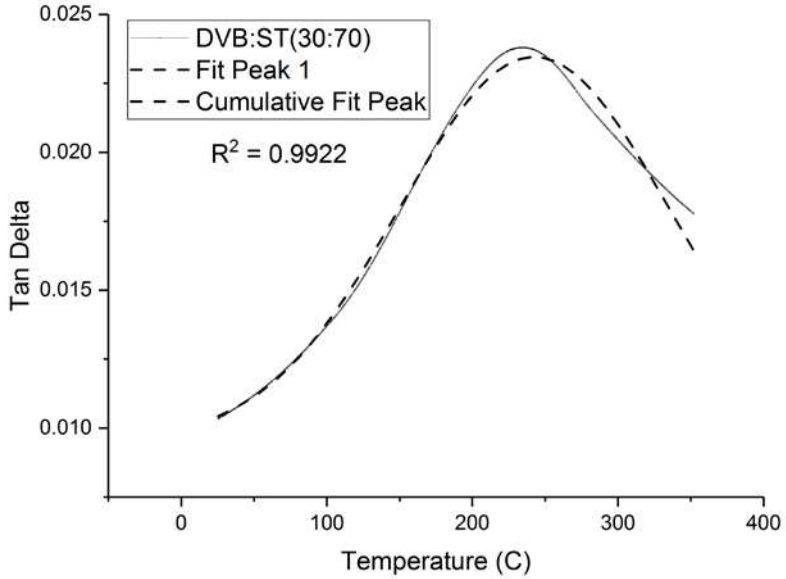

(A)

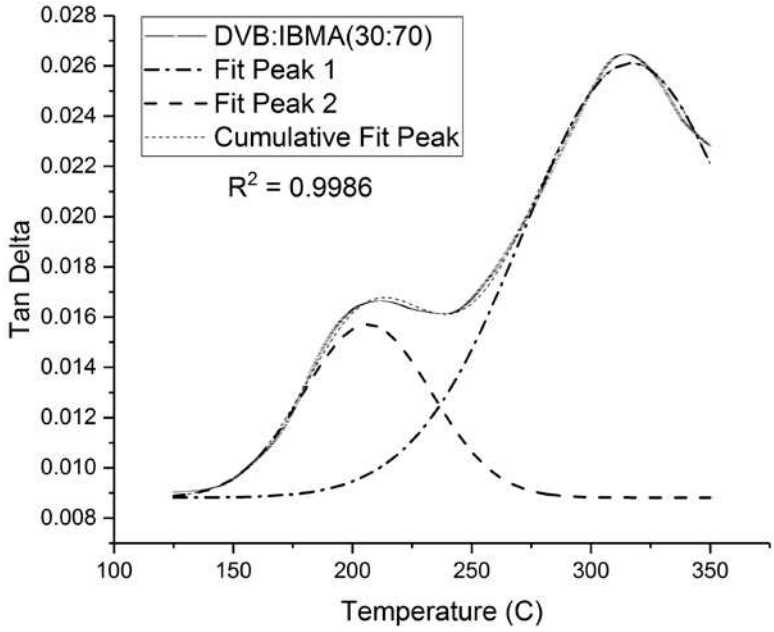

(B)

Figure 5.1. Tan δ vs. Temperature plots (de-convoluted) of bulk nanogel: (A) NG_1 (DVB:ST(30:70)) (raw data (solid line), Gaussian fitted curve (dash line)), (B) NG_2 (DVB:IBMA(30:70)) (raw data (solid line), Gaussian fitted curve 1 (dash line), and Gaussian fitted curve 2 (dash dot line)).

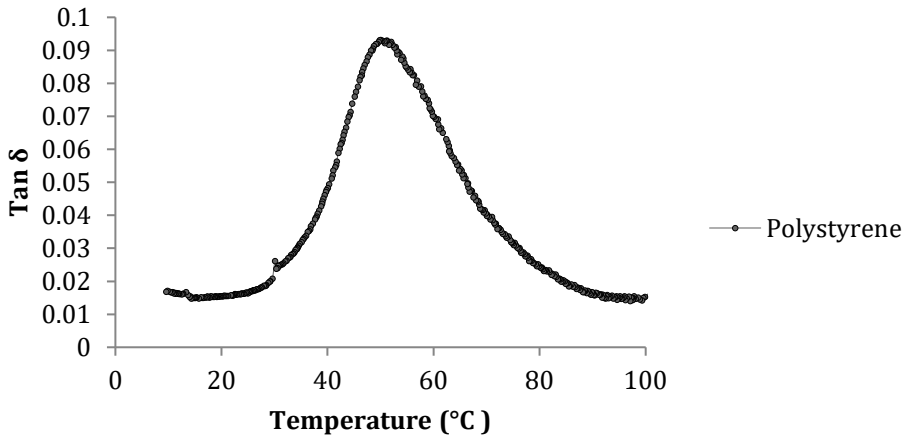

Figure 5.2. Tan δ vs. Temperature for polystyrene (PS) particles synthesized with the same reaction conditions as the nanogels.

5.3.3. Thermal Stability

The thermal decomposition of a copolymer is a hybrid process of decomposition of individual polymers (Beyler, 2002). The mechanism of thermal decomposition of PS in nitrogen starts with end-chain scission at ~250 °C, continues with unzipping and intramolecular H transfer, and ends with bi-molecular termination at 500 °C (Peterson, 2001; Beyler, 2002). The decomposition of PIBMA in vacuum occurs in two steps similar to PS, with a sharp mass loss at around 300 °C due to loss of side chains and continuous mass loss above 400 °C due to decomposition of the backbone (Ozlem, 2013). Furthermore, the addition of DVB increases the thermal stability and also increases the char formation (Shim, 2004). The reason for choosing nitrogen environment for performing our thermal stability studies is to limit the decomposition process only to heat-induced reactions, and also to eliminate the oxygen-inhibition effect, since decomposition reactions in radically polymerized materials are in fact radical de-polymerization with initiation, de-propagation, and termination steps (Beyler, 2002). To assess the thermal stability of nanogel networks and blends we use the temperature at 10% mass loss (T_{10})

as an indication of actual thermal stability and the temperature at 50% mass loss (T_{50}) as a measure of crosslinking consistency (Li, 2001). We have to note that heating rate of TGA for thermal stability assessment was 10 ^{o}C/min, which is 4-fold higher than what typically is used for thermal stability studies, and since decomposition is an endothermic reaction, higher rate of thermal energy input reduce the onsets temperatures. The T_{10} and T_{50} for NG_1 are 197 and 442 ^{o}C, respectively (Fig 5.3). This nanogel has three distinct onsets, the mass loss in 70-360 ^{o}C, 360-490 ^{o}C, and > 490 ^{o}C regions. As it was mentioned before the decomposition of PS does not start below 250 ^{o}C, and the onset is shifted to higher temperatures depending on DVB concentration, therefore the mass loss of 16.6% between 70 and 360 ^{o}C is most likely due to loss of volatile compounds such as absorbed moisture, trapped solvent (hexane) residue from precipitation step, low molecular weight particles, and scission of weak links (unsaturated end groups or head-to-head linkages along the main chains) (Peterson, 2001; Beyler 2002).

The termination reactions via disproportionation or combination in vinyl radical polymerization even in the presence of chain transfer agent can produce numbers of vinylidene ends and head-to-head linkages, respectively, which are considered abnormal and weak (Kashiwagi, 1986; Levchik 1999; Uhl 2001; Hiemenz, 2007). The temperature range of 360-490 ^{o}C is associated with 64.6% mass loss due to de-propagation via random chain scission and intramolecular H transfer. The de-propagation step yields styrene monomer and oligomers (Wilkie, 1999; Uhl, 2001; Beyler, 2002). The third region T > 490 ^{o}C is where crosslinking and char formation occur, and 9.0% residual mass is a confirmation for a crosslinked residue.

For NG_2, T_{10} and T_{50} were 290 and 360 °C, respectively (Fig 5.3). Comparing the T_{10} values of NG_1 and NG_2 indicates much higher stability for NG_2, but the onset of sharp mass loss happens at lower temperature (280 °C) for this nanogel, which is compatible with PIBMA behavior. The T_{50} of NG_2 was 80 °C lower than that of NG_1, which confirms our earlier prediction about higher degree of cyclization and inefficient crosslinking in the former network. The NG_2 had four regions of thermal degradation: 100-280 °C, 280-360 °C, 360-450 °C and > 450 °C. The first region 100-280 °C with 3.3% mass loss is due to loss of volatile and low molecular weight particles similar to NG_1. The 280-450 °C sharp mass loss region consists of two onsets, first 280-370 °C with 44.0% mass loss, and second 370-450 °C with 32.0% mass loss, which is a deviation from pure PIBMA trend. The underlying reason for two different rates of mass loss is the difference between two de-propagation rates that happen along the chains at the intersection of crosslinks, which can be correlated with the inverse of reactivity ratios during copolymerization. Based on the r values for MMA and DVB described earlier, the de-propagation rate of methacrylates on active chain is higher than that of DVB segments, therefore the 280-360 °C and 360-450 °C regions represent the higher rate of mass loss due to de-propagation of PIBMA segments on backbone chains, and lower rate of mass loss due to de-propagation of DVB segments, respectively. The char formation region T > 450 °C led to lower residual mass (3.5%), which is related to the less aromatic character of this nanogel.

For the DVB/ST(30:70) bulk copolymer, T_{10} and T_{50} are 428 and 471 °C, respectively (Fig 5.4). The entire thermal decomposition of this macrogelled copolymer has two stages, the rapid mass loss of 87.0% happened between 380 and 508 °C, which follows the styrene-*co*-divinylbenzene trend, with 5.5% char residue. The

DVB/IBMA(30:70) copolymer has T_{10} and T_{50} of 325 and 365 °C (Fig 5.4), respectively. The higher T_{10} of DVB:ST(30:70) copolymer indicates higher thermal stability than DVB:IBMA(30:70) copolymer, which is due to the lower thermal stability of methacrylates. The T_{50} of the former blend shows more consistent crosslinks than that of the latter. The DVB:IBMA(30:70) monomer system shows a three-stage decomposition, with a sharp mass loss of 57.0% between 300 and 375 °C, lower rate of mass loss of 28.0% between 375 and 480 °C, there is also a 4.4% char residue remaining from this blend thermal decomposition.

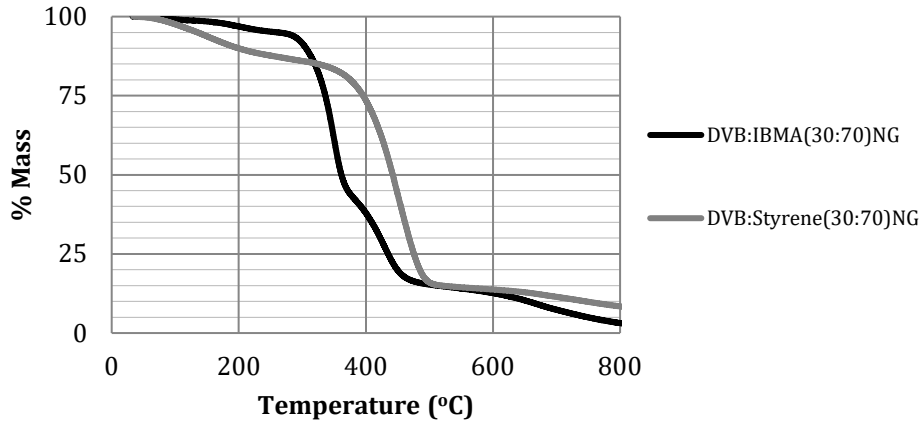

Figure 5.3. Thermogram of NG_1 (DVB:ST(30:70) and NG_2 (DVB:IBMA(30:70) in nitrogen.

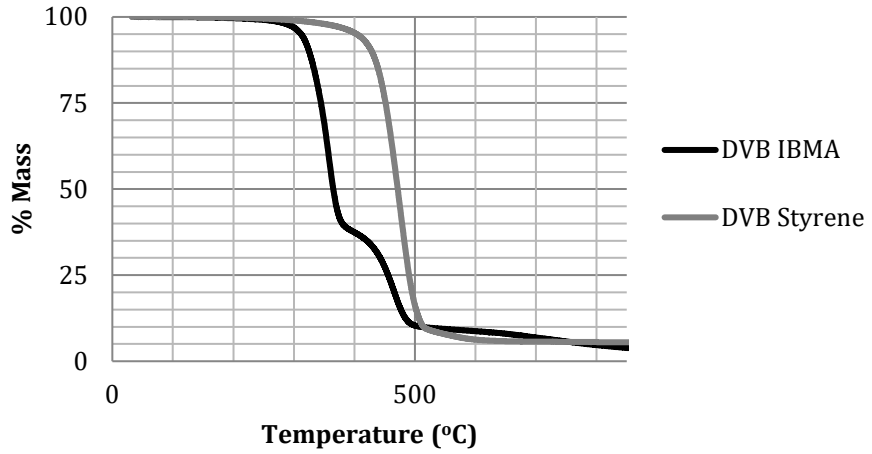

Figure 5.4. Thermogram of polymerized monomer blends of DVB/ST(30:70) and DVB/IBMA(30:70).

5.3.4. Nanogel refractive index

The classic Lorentz-Lorenz equation (Eq 5.2) is often used to predict the refractive index (RI) of a polymer, where n, R_M, and V_M represent the refractive index, molar refraction, which is the sum of atomic and group refraction of the polymer components, and molar volume, respectively (Liu, J. G. 2009). Eq 5.2 clearly indicates that polymers with high molar refraction and low molar volume substituents (i.e., aromatic groups) have high RI values. Polymers with highly polarizable π-conjugated aromatic rings can slow down the transmitting light, thus exhibit high RI (Liu, J.G. 2009; Hanemann, 2011). In this regard, the refractive indices of NG_1 and NG_2 were measured resulting in n values of 1.5915 and 1.5510, respectively (Fig 5.5). These values of n > 1.5 were expected based on the high content of aromatic rings in the nanogel structures, especially for NG_1. An additional advantage of these materials is that light scattering and loss of optical transmittance can be avoided in nanogel-dispersed media (i.e., resin, solvent) for applications that utilize light with wavelengths of at least 10-factor higher than the nanogel

size ($2R_h$ < 20 nm) (Hanemann, 2011), which obviously covers a large portion of the electromagnetic spectrum. It is also important to note that incorporating high refractive index nanogel either as inert or active filler, or as a precursor for network formation creates materials with even higher RI values due to linear and non-linear effects, and also increased density during polymerization (Liu, J. G. 2009; Howard, 2010).

$$n = \sqrt{\frac{1+2(R_M/V_M)}{1-(R_M/V_M)}} \tag{5.2}$$

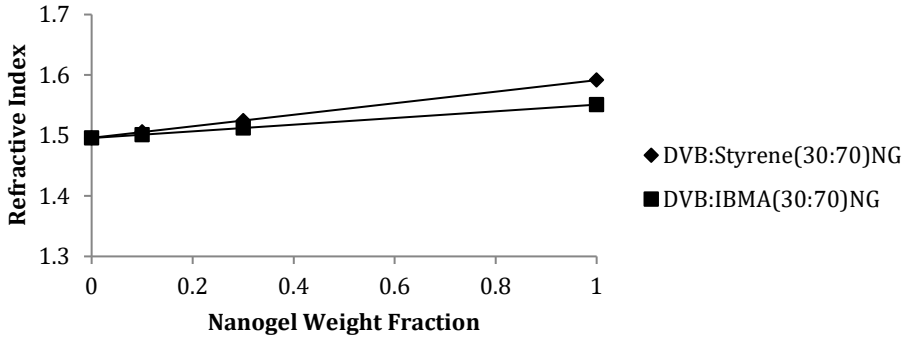

Figure 5.5. Refractive Indices of DVB:ST(30:70) and DVB:IBMA(30:70) nanogels based on linear extrapolation from measurements on toluene dispersions.

5.3.5. Photopolymerization kinetics

The effect of adding high T_g nanogel on photopolymerization kinetics of a conventional resin monomer (TEGDMA) was also investigated (Fig 5.6 A-D). At the same loading level, smaller nanogels have a higher percolation threshold than larger nanogels. This means that we may have some bulk TEGDMA with the smaller NG_2, while the larger NG_1 may be confluent at this loading level, continuous phase of monomer-swollen nanogels through near-contact and/or some degree of overlap. The TEGDMA (control), TEGDMA/NG_1 (50/50) wt%, and TEGDMA/NG_2 (50/50) wt% were photopolymerized at room temperature under UV irradiation (365 nm) with final methacrylate vinyl group

conversion of 80, 63.5, and 81% (Fig 5.6 A), respectively. Adding 50 wt% of NG_1 to the resin matrix slowed down the maximum propagation rate (autoacceleration regime) during polymerization and decreased the final conversion by 16.5% compared to the analogously photocured control. Photopolymerization rate not only depends on physical conditions such as temperature, monomer(s) viscosity, monomer(s) concentration, initiator concentration, initiator efficiency, intensity and wavelength of irradiation, but also depends on the chemical structure of the monomer(s), type and density of functional groups (Dickens, 2003; Hiemenz, 2007; Stansbury, 2012). Eq 5.3 (Hiemenz, 2007) summarizes these factors in a more comprehensive fashion:

$$R_P = k_P[M]\left(\frac{fk_d}{k_t}\right)^{1/2}[I]^{1/2} \tag{5.3}$$

In this relationship, R_P, [M], f, k_d, k_t, and [I] are the rate of polymerization, monomer concentration, initiator efficiency, initiator dissociation rate constant, termination rate constant, and initiator concentration, respectively. In addition, the onset of autoacceleration is affected by the size and mobility of macroradicals. Fig 5.6 B shows a multi-modal R_P vs. time curve for TEGDMA with a relatively delayed global R_{Pmax} at 42.4% conversion, a typical characteristic of low viscosity resin monomers, which is due to extensive cyclizations and heterogeneous network formation (Dickens, 2003; Jiu, J. 2012). By addition of NG_1, the rate of polymerization becomes unimodal and dramatically lower than control, also the onset of autoaccelaration is dramatically delayed and reduced (R_{Pmax} at 25 s = 1.5 %/s), and network reaches vitrification at lower final conversion with high fraction of unreacted monomers. The higher molecular weight of NG_1 leads to lower molar concentration of methacrylic C=C double bonds in 50/50 wt% mixture with TEGDMA, and perhaps lower overall functional group density due to lack of pendant

styrenic C=C bonds in the nanogels (recall from similar reactivity ratios of DVB and ST). There may also be a less homogeneous distribution of initiator (DMPA) inside the swollen nanogel based on the difference between non-polar NG_1 and slightly polar TEGDMA moieties, which could directly reduce R_P and consequently delay autoacceleration. Other contributing factors in lowering polymerization rate in this system can be due to ultra-high T_g characteristic of NG_1 relative to the T_g of the TEGDMA homopolymer polymerized at room temperature (60 ^oC) (Ye, 2011) (Fig 5.7) and ultra-high viscosity of the mixture due to high $\bar{M}_w$ of NG_1, which in combination can hinder diffusion of reactive species regardless of their size (Szczepanski, 2012). On the other hand, the R_P vs. time of TEGDMA/NG_2 mixture shows a multimodal plot similar to TEGDMA but with two onsets of autoaccelerations occurring sooner than the control with values of R_{Pmax1} = 8.25 %/s at 1.96 s and R_{Pmax2} = 7.89 %/s at 8.8 s, and corresponding conversions of 11.8 and 39.3%, respectively. The fast onset of autoacceleration with higher rate than the control is due to: i) increased viscosity and high T_g of NG_2, which slow down the translational diffusion of active species, yet their combination effect is still below the limiting threshold, ii) higher local functional group density (existence of pendant styrenic C=C bonds in nanogel structure) and iii) more homogeneous distribution of initiator. The interesting point is that the increased viscosity as the result of first onset does not stop the second sharp autoacceleration from happening, therefore it confirms the fact that the first onset is localized and is due to reaction between nanogel pendant double bonds and nearest TEGDMA monomers. The second onset has a similar shape to control with a more pronounced right shoulder, which is located between the R_{Pmax1} and global R_{Pmax} of TEGDMA. This suggests that the first onset may be related to crosslinking between

nanogels and nearest TEGDMAs in combination with TEGDMA-TEGDMA crosslinking, and second onset to final crosslinking between nanogel-TEGDMA-TEGDMA clusters. We have also investigated the effect of nanogel loading level on polymerization kinetics, by varying the amount of NG_2 in TEGDMA/NG_2 mixture (Fig 5.6 C-D). The final conversions of TEGDMA/NG_2 (75/25) and TEGDMA/NG_2 (90/10) wt% are 88.6 and 75.6%, respectively. As the concentration of TEGDMA increases above 50 wt%, we can see that R_{Pmax} for the first onset decreases dramatically in 75/25 and 90/10 mixtures to $1/4^{th}$ of that in 50/50, which is due to viscosity reduction. The second onset of 50/50 and 90/10 mixtures have R_{Pmax} (both at 8.8 s) of 7.89 %/s (conversion = 39.3%) and 11.58 %/s (conversion = 38.2%), respectively, yet 75/25 mixture had R_{Pmax2} of 8.66 %/s at 10.8 s with conversion of 43.1%. The highest value of R_{Pmax2} for 90/10 mixture compared to control and other ratios is due to crosslinking of spatially dispersed TEGDMA bulk with spread nanogels with higher functional density, yet the cluster-like behavior of nanogels in this particular mixture forces the network to reach pre-mature vitrification, which ultimately leads to lower conversion. On the other hand, the 75/25 mixture with lower R_{Pmax2} than 90/10 and higher R_{Pmax2} than 50/50 and control has the highest value of final conversion, which can indicate that the distribution of TEGDMA inside and outside of nanogel particles, enhances more efficient crosslinking.

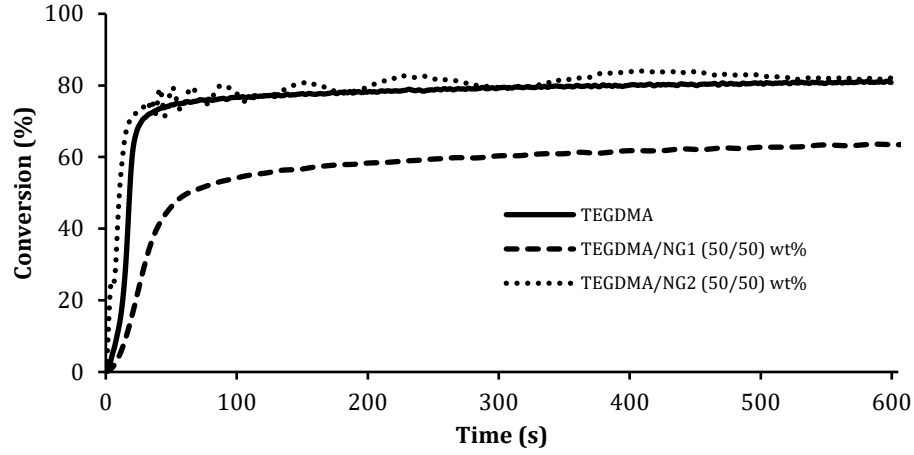
100
80
60
40
20
0
Conversion (%)
0
100
200
300
400
500
600
Time (s)
TEGDMA
TEGDMA/NG1 (50/50) wt%
TEGDMA/NG2 (50/50) wt%

(A)

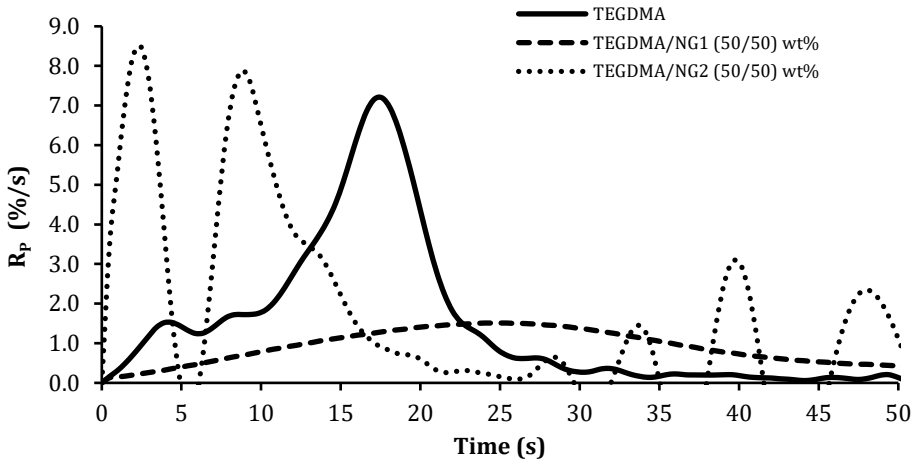
9.0
8.0
7.0
6.0
5.0
4.0
3.0
2.0
1.0
0.0
R_P (%/s)
0
5
10
15
20
25
30
35
40
45
50
Time (s)
TEGDMA
TEGDMA/NG1 (50/50) wt%
TEGDMA/NG2 (50/50) wt%

(B)

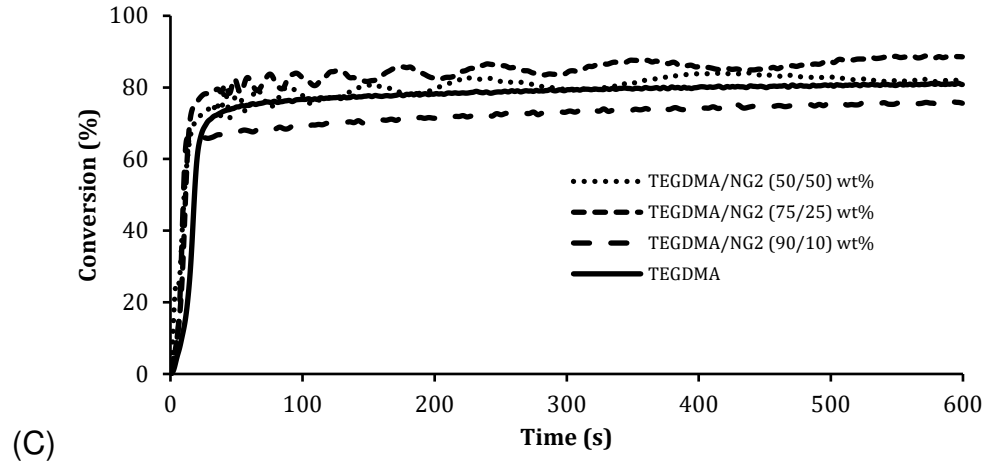

(C)

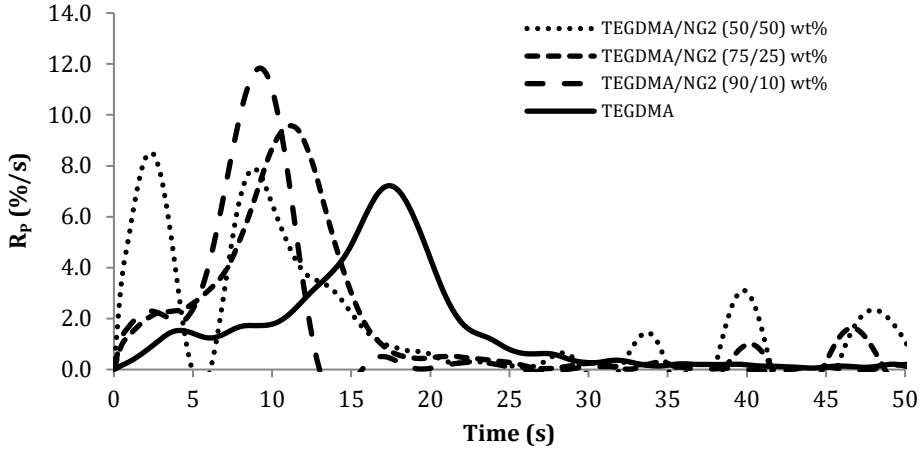

(D)

Figure 5.6. The photopolymerization kinetics: (A) Conversion vs. time for TEGDMA, TEGDMA/NG_1 (50/50) wt%, and TEGDMA/NG_2 (50/50) wt%; (B) R_P vs. time for TEGDMA, TEGDMA/NG_1 (50/50) wt%, and TEGDMA/NG_2 (50/50) wt%; (C) Conversion vs. time for TEGDMA, TEGDMA/NG_2 (50/50) wt%, TEGDMA/NG_2 (75/25) wt%, and TEGDMA/NG_2 (90/10) wt%; (D) R_P vs. time for TEGDMA, TEGDMA/NG_2 (50/50) wt%, TEGDMA/NG_2 (75/25) wt%, and TEGDMA/NG_2 (90/10) wt%. Samples were irradiated under UV (365 nm) with 60 mW/cm^2.

5.3.6. Macroscopic Network T_g

The glass transition temperature of photopolymerized networks of pure TEGDMA and TEGDMA/NG (50/50) mixtures are compared in Fig 5.7 A-C. It is important to note that based on time-temperature superposition principle polymer T_g value depends on the cooling (heating) rate during measurements. The homopolymer of TEGDMA had a T_g of

155 °C (Fig 5.7 A). After de-convolution of tan δ vs. temperature peaks by fitting Gaussian function (R^2 = 0.99), we found two T_g values of 134.2 and 189.0 °C for TEGDMA/NG_1 (50/50), and two T_g values of 110.9 and 199.8 °C for TEGDMA/NG_2 (50/50) networks, which the lower and higher values are attributed to TEGDMA-rich and nanogel-rich moieties, respectively. The global maximum T_g for TEGDMA/NG_1 and TEGDMA/NG_2 networks were 34 and 45 °C higher than that of control, respectively. The overall increase of glass transition temperature in these networks compared to control is an interesting result since it shows that higher T_g in a conventional resin is attainable by adding high T_g nanogels without changing the polymerization conditions, which otherwise is not physically possible. The tan δ_{max} for TEGDMA homopolymer, TEGDMA/NG_1 (50/50), and TEGDMA/NG_2 (50/50) are 0.10, 0.11, and 0.13, respectively. Higher damping is an indication of higher storage modulus and consequently more efficient and homogeneous crosslinking in the mixture systems (Li, 2002).

The thermally polymerized network of the bulk DVB/ST copolymer with 30/70 molar ratio was also evaluated for thermal transition. Fig 5.8 shows the tan δ vs. temperature of this network, with two T_g values of 88.1 and 211.3 °C after peak de-convolution (fitted Gaussian function with R^2 = 0.99), which represent ST-rich and DVB-rich moieties, respectively. The nanogel T_g of the same monomers (NG_1) was a single peak at 242.5 °C. The unimodal character of tan δ peak shows the compositional homogeneity of nanogel particles, but we could not precisely evaluate the breadth of tan δ peak, representing relaxation time distribution, due to the upper limit temperature of DMA.

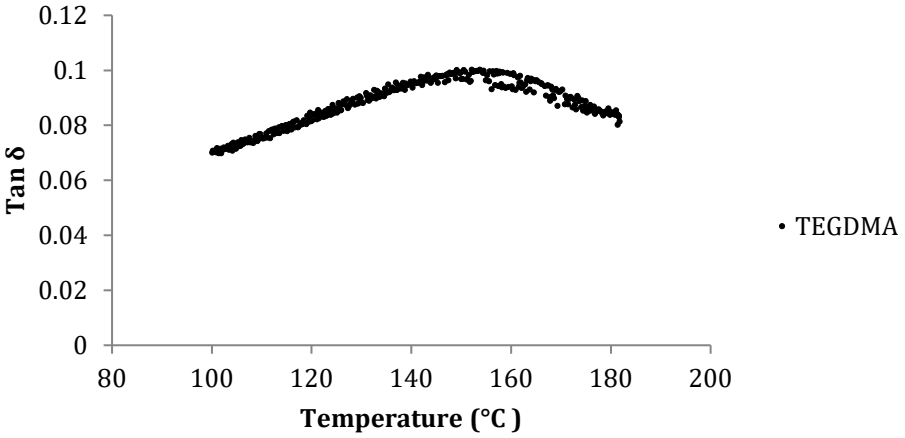
0.12
0.1
0.08
0.06
0.04
0.02
0
Tan δ
80
100
120
140
160
180
200
Temperature (°C)
• TEGDMA

(A)

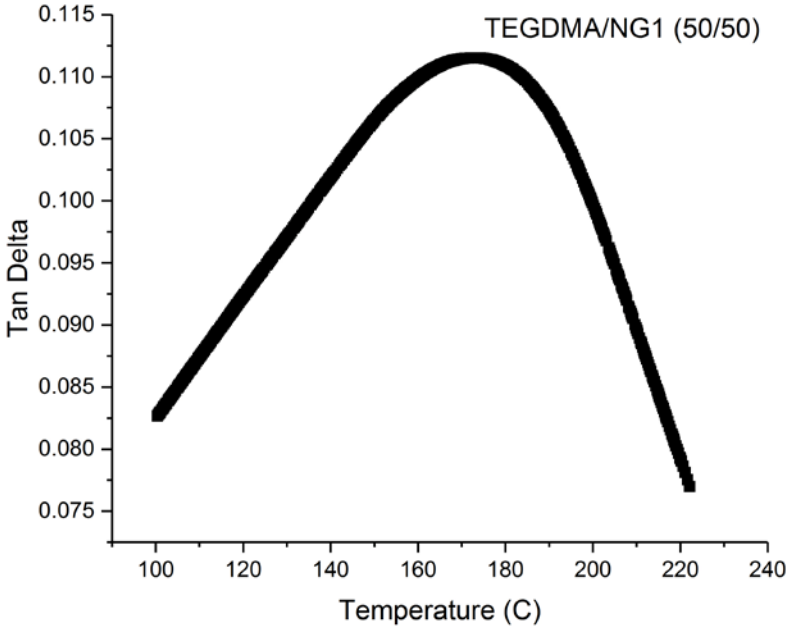
TEGDMA/NG1 (50/50)
0.115
0.110
0.105
0.100
0.095
0.090
0.085
0.080
0.075
Tan Delta
100
120
140
160
180
200
220
240
Temperature (C)

(B)

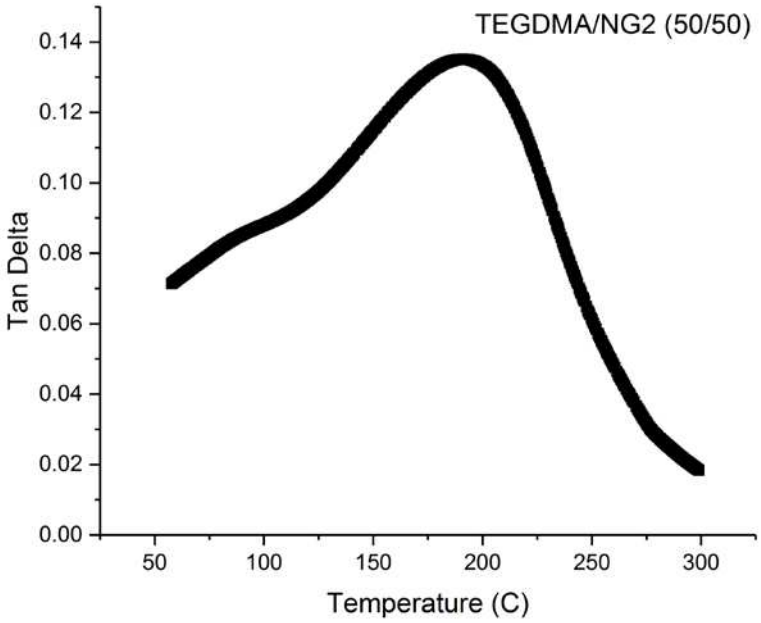

(C)

Figure 5.7. Glass transition temperature of photo-polymerized: (A) TEGDMA, (B) TEGDMA/NG_1 (50/50), and (C) TEGDMA/NG_2 (50/50).

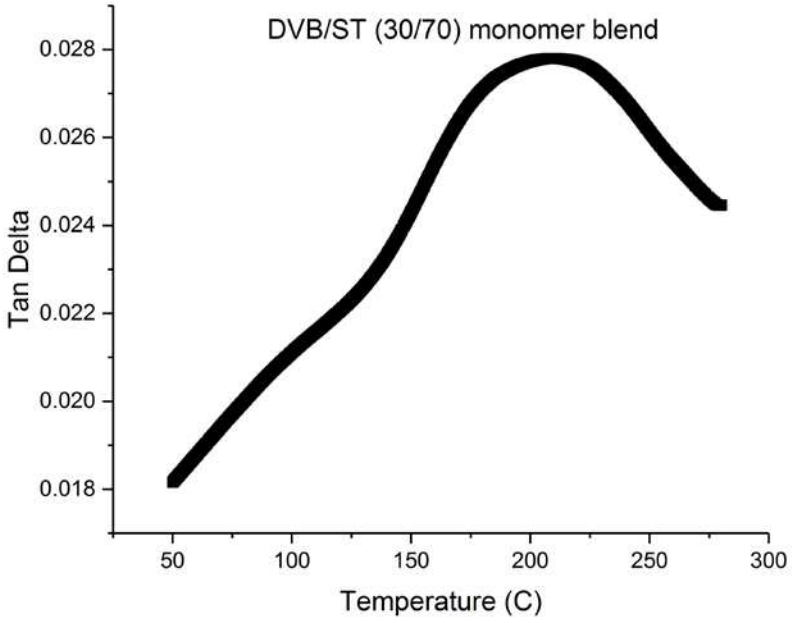

Figure 5.8. Glass transition temperature of thermally polymerized network of monomer mixture of DVB (30 mol%) and ST (70 mol%).

5.3.7. Mechanical Properties

The imposed rigidity by aromatic and bulky side groups on a polymer backbone can lead to brittle character of the materials with high content of such structures. Their low tensile strength is decreased even further in densely crosslinked networks. For the aforementioned reason, the effect of high T_g nanogels on the mechanical properties of a conventional crosslinked network (TEGDMA) was investigated in a mixture of TEGDMA/NG with 50/50 wt% ratio. The average flexural modulus for ambient photocured (with no thermal conditioning) polymer networks of TEGDMA, TEGDMA/NG_1, and TEGDMA/NG_2 (Fig 5.9), were 1.6, 1.7, and 1.8 GPa, respectively, where the difference between groups were not statistically significant (*p-level* = 0.95). Fig 5.9, also shows the corresponding average conversion values for each sample. The reason for unchanged flexural modulus in TEGDMA/NG samples with high content of aromatic and bulky groups at a temperature well below their T_gs (room temperature) can be related to the effect of high crosslink and entanglement density in an overlapped-nanogel regime. Styrene is an inherently brittle homopolymer and rigidity favors crazing and ultimately contributes to brittle fracture. However, higher crosslinking and entanglement density within these hybrid TEGDMA/nanogel-based networks and in the overlapped volume between nanogel particles, respectively, favor yielding through more homogeneous (non-localized) distribution of deformation stress. There is at least 10 crosslinking (entanglement) strands per backbone chain required for polystyrene to reach constant tensile strength (independent of its molecular weight) (Hiemenz, 2007).

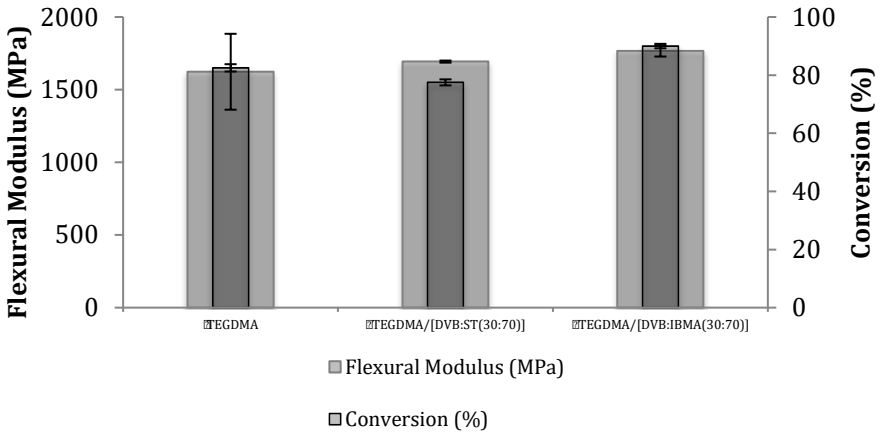

Figure 5.9. Flexural Modulus and Conversion data for photo-polymerized networks of TEGDMA, TEGDMA/[DVB:ST(30:70)] (50/50) wt%, and TEGDMA/[DVB:IBMA(30:70)] (50/50) wt%.

5.4. Conclusions

Major challenges in development of conventional high performance/high temperature polymers are due to high viscosity and insolubility of their starting materials, which ultimately make them difficult to process. A novel strategy to resolve these setbacks is to reduce the molecular weight of the starting polymers without changing their favorable properties such as high glass transition temperature (> 200 ºC), high thermal stability, and high crosslinking capability, therefore in this study we present reactive nanogel particles synthesized via free-radical solution polymerization with T_g well beyond 200 ºC threshold and refractive index close to 1.6. These materials are completely dispersible in common organic solvents and monomer resins at high loading levels without forcing the mixture to undesirable viscosity limits. The nanogels showed relatively a good thermal stability below 260 ºC, and exhibited sharp mass loss from 260 to 490 ºC, although it is believed that their thermal stability can be improved further by an extra precipitation step. The addition of high molecular weight/high T_g active nanogel (NG_1) to TEGDMA in 50/50 wt% ratio decreased the conversion due to dramatic reduction in diffusivity. The effect of

nanogel loading level on polymerization kinetics showed an interesting dependency, which defines the lower limit of the role of nanogel in enhancing homogeneity. In addition, the rigidity of nanogels backbone did not affect the flexural modulus of their blends with TEGDMA compared to control, which is due to their higher number of effective crosslinks and substantial entanglements. These materials can offer a paradigm shift in thermoplastics/thermosets and high refractive index polymers industries.

CHAPTER 6

CONCLUSIONS AND FUTURE WORK

6.1. Conclusions

The specific aims for this thesis were accomplished in the following manner:

I. *Investigate the effects of solvent, crosslinker structure, and agitation rate as synthesis parameters on the size and structural properties of the nanogels synthesized by free-radical polymerization of a divinyl monomer (EGDMA or UDMA) with a monovinyl monomer (IBMA).*

This specific aim is addressed in chapter 2. Two nanogels were synthesized with different dimethacrylate monomers, one with UDMA a hydrogen bonding donor/acceptor and the other with EGDMA where hydrogen bonding was effectively absent. The effect of stirring rate as an operational condition was investigated in free radical solution polymerization on nanogel conversion, molecular weight, hydrodynamic radius, and polydispersity. Increasing the stirring rate did not change the conversion, molecular weight or hydrodynamic radius in the IBMA:UDMA(70:30) nanogel synthesized in a hydrogen bonding promoter solvent (toluene). In MEK, which intervenes in the monomer/polymer hydrogen bonding, increasing the stirring rate decreased M_w and R_h. With the IBMA:EGDMA(70:30) nanogel prepared in toluene, increasing the stirring rate decreased the nanogel conversion rate, molecular weight, and hydrodynamic radius while the PDI and MH-*a* value did not change. Even though the effect of stirring rate in a free radical solution polymerization is generally not considered, this study showed that depending on

the choice of reactants and solvent, the potential for significant variation in critical polymer structure and properties is certainly present.

II. *Investigate the swelling properties, mechanical properties, and mass loss in amphiphilic hydrolytically degradable hydrogels, constructed from degradable active nanogel precursors differing in crosslinking density and location of the labile groups (imbedded in the crosslinker, side chains, or both). Investigate the evolution of molecular weight between crosslinks during degradation based on rubber elasticity theory and equilibrium swelling theory (Flory-Rehner equation) with Gaussian and non-Gaussian chain conformation assumptions.*

This specific aim is addressed in chapter 3. Regio-specific degradable nanogels were successfully prepared via free-radical solution polymerization of PEG-*co*-PLA with HEMA-*co*-PLA and MEMA. Their weight-averaged molecular weights were less than 65 kg/mol with hydrodynamic radius of less than 6.0 nm and 1.0 < PDI < 7.2. The glass transition temperature of bulk nanogels was at or below room temperature. The photopolymerized macroscopic networks of these nanogels exhibited dramatic high dry-state moduli depending on chain flexibility and crosslink density. The swollen-state moduli were lower than that of dry-state depending on the hydrophilicity of the network. The molecular weight between crosslinks evaluated based on rubber elasticity theory showed lower values of $\bar{M}_x$ by applying non-Gaussian conformation distribution assumption, yet equilibrium swelling theory predicted same values for $\bar{M}_x$ regardless of the type of implemented distribution. The incorporation of hydrolytically labile linkages to the backbone and side-chain of the nanogel led to bulk and surface type erosions, respectively. The mass loss trends in these novel networks showed a sustained release

of degraded species even under autoaccelerated acid-catalyzed hydrolysis by delaying or completely bypassing reverse gelation. The investigated nanogels in this study offer tremendous control and versatility in hydrolytic degradation for variety of biomaterial applications such as controlled-drug delivery and scaffold engineering.

III. *Investigate the effect of hydrophobic nanogels (styrene and divinylbenzene with two different ratios) and their loading levels on swelling ratios and mass loss of hydrolytically degradable divinyl monomer/nanogel IPN.*

This specific aim is addressed in chapter 4. Controlling water uptake and hydrolytic degradation in common methacrylate-based dental composites and potentially in dental adhesives would be expected to provide longer clinical service time while minimizing the release of leachable species. Regarding this challenge, most attention has been focused on creating a water-free environment before and during the polymerization with little effort in suppressing effects post-polymerization. A model hydrolytically susceptible polymer network was used in this demonstration to accentuate the challenge in providing protection from aqueous swelling and degradation. Introducing hydrophobic all-hydrocarbon carbon nanogels into the labile network without changing resin formulation opens a practical route for controlling hydrolytic degradation and presumably for physically restricting access for enzymatic attack in the oral cavity. Highly crosslinked styrenic nanogels were incorporated into a hydrolytically degradable monomer either as inert or reactive additives at various loading levels. The equilibrium mass swelling ratio and percent mass loss were dramatically reduced in nanogel-modified networks regardless of their functional groups. The loading level of nanogel played an important role in suppressing both water uptake and hydrolytic degradation without impractical

increase of viscosity. This enhanced shielding property is a result of nanogel particle-particle overlapping beyond percolation threshold. This approach can be applied to variety of polymeric systems prone to hydrolytic degradation including dental restorations, engineered tissues, and surface coatings.

IV. *Investigate the properties of high glass transition temperature nanogel and its effect on mechanical behavior of an interpenetrating nanogel/TEGDMA network.*

This specific aim is addressed in chapter 5. Major challenges in development of conventional high performance/high temperature polymers are due to high viscosity and insolubility of their starting materials, which ultimately make them difficult to process. A novel strategy to resolve these setbacks is to reduce the molecular weight of the starting polymers without changing their favorable properties such as high glass transition temperature (> 200 ^{o}C), high thermal stability, and high crosslinking capability, therefore in this study we present reactive nanogel particles synthesized via free-radical solution polymerization with T_g well beyond 200 ^{o}C threshold and refractive index close to 1.6. These materials are completely dispersible in common organic solvents and monomer resins at high loading levels without forcing the mixture to undesirable viscosity limits. The nanogels showed relatively a good thermal stability below 260 ^{o}C, and exhibited sharp mass loss from 260 to 490 ^{o}C, although it is believed that their thermal stability can be improved further by an extra precipitation step. The addition of high molecular weight/high T_g active nanogel (NG_1) to TEGDMA in 50/50 wt% ratio decreased the conversion due to dramatic reduction in diffusivity. The effect of nanogel loading level on polymerization kinetics showed an interesting dependency, which defines the lower limit of the role of nanogel in enhancing homogeneity. In addition, the rigidity of nanogels backbone did not

affect the flexural modulus of their blends with TEGDMA compared to control, which is due to their higher number of effective crosslinks and substantial entanglements. These materials can offer a paradigm shift in thermoplastics/thermosets and high refractive index polymers industries.

6.2. Future Work

This thesis has unveiled the great potential of overlapped nanogel particles in dense-packing regime, not only in reducing the level of heterogeneity, but also as the most economical approach to obtain a robust architectural polymeric network assembly, in terms of minimum amount of mass and energy consumption, although this does not neglect the fact that producing nanogel particles themselves is not an inexpensive procedure.

Regarding chapter 2, the particle Reynolds number would be very small ($Re_p << 1$) due to nanoscale size, even if we consider the effect of bulk Reynolds number Re_b on Re_p (i.e. $Re_p \sim Re_b$. (Normalized Particle Size)^n), particle size can be normalized based on either the impeller diameter or the vessel diameter. With this treatment, particles are assumed to experience laminar flow regime no matter what the stirring rate is, thus from particle point of view increasing the bulk velocity has insignificant effect on the fluid viscosity that particle experiences at its periphery, therefore the change in viscosity is only governed by reaction kinetics and particle volume fraction. If we assume similar volume fractions for all three batches (0, 200, and 400 rpm), which is actually the real case only at t=0, then we can anticipate that particles would have similar sizes since the diffusion-controlled kinetics would behave similar at different stirring rates. The most comprehensive study is when we correlate the two Reynolds number scales, bulk vs.

particle (i.e. Celsius vs. Kelvin) and basically define a separate set of numbers for Re_p in different flow regimes, and then analyze particle history based on that. This task might be doable by CFD, which could be a very nice addition to this work, but we have to consider that this is a very complex analysis from every angle: dimension (3D), reaction kinetics, flow regime/velocity gradient, and nanogel size evolution.

Developing a sophisticated statistical-kinetic model based on the results of chapter 3, that projects the effects of important variables such as PEG and PLA length, crosslinker concentration, order of PEG and PLA locations, and concentration of secondary functional groups on degradation mechanisms seems necessary for better understanding and decoupling the effects of each variable, and also to avoid repeated experiments. Ultimately, an *in vivo* study is required to assess the candidacy of hydrogels developed in chapter 2 as novel alternatives to current systems.

Nanogel is a colloidal particle with dense inter core and less-dense outer shell, which in terms of properties lies between hard-sphere and soft colloid particles. It would be interesting to push the core hardness and outer shell softness to their maximum limits to find the ideal hybrid nanogel with the most paradoxical properties imagined. How can we do this? By either choosing a short crosslinker with higher functionality $f > 2$ and a relatively long side chain, or using late stage addition of long and flexible monofunctional monomer(s). For instance, a low viscosity active nanogel (low T_g) with this structure may be able to form a high modulus network (high T_g) after polymerization in a dense-packing regime. On the other hand, we may be able to create super-hydrophobic surfaces only by extending the hard-sphere character of the core to higher diameter without any change in the chemical composition of the hydrophobic nanogel. By decreasing the soft outer

shell thickness and maximizing the hard core diameter, we will be able to minimize the overlapped volume, therefore the densely packed nanogels can create rows of hills and valleys on the surface, where the volume of the valleys are filled with air. The height of the hills (or the depth of the valleys) is the determinant factor in transforming the hydrophobic surface to super hydrophobic (Cassie-Baxter State), which further depends on the diameter of the hard core and the thickness of the soft outer shell.

Another exciting area to explore is the effect of nanogel dense-packing on the refractive index of the final polymerized network. As the overlapped nanogels go through radical crosslinking, they minimally shrink since the chains have been previously cyclized, and the extent of cyclization in overlapped regime is minimal. The densification of the network in portions between the overlapped volumes is a result of relatively constant mass in reduced volume, but the densification inside the overlapped volumes is the result of increased mass in a relatively constant volume, therefore the degree of densification can adopt different values depending on where it is measured. Mathematically, densification is a discrete function of mass and volume. On the other hand, in the overlapped volume the close proximity of molecules can raise non-linear effects such as non-linear increase in molar refraction, therefore the final macroscopic refractive index might be a linear combination of non-linear effects.

REFERENCES

The following list represents references used in **chapter 1:**

- Ahmed, E. N. Hydrogels: preparation, characterization, and applications: A review. *Journal of Advanced Research* **2015,** *6*, 105-121.
- Albertsson, A. C.; Varma, I. K. Recent developments in ring opening polymerization of lactones for biomedical applications. *Biomacromolecules* **2003,** *4*, 1466-1486.
- Anselmo, A. C.; Mitragotri, S. Impact of particle elasticity on particle-based drug deliverysystems. *Advanced Drug Delivery Reviews* **2017,** *108*, 51-67.
- Anseth, K. S.; Metters, A. T.; Bryant, S. J.; Martens, P. J.; Elisseeff, J. H.; Bowman, C. N. In situ forming degradable networks and their application in tissue engineering and drug delivery. *Journal of Controlled Release* **2002,** *78*, 199-209.
- Azagarsamy, M. A.; McKinnon, D. D.; Alge, D. L.; Anseth, K. S. Coumarin-based photodegradable hydrogel: design, synthesis, gelation, and degradation kinetics. *ACS Macro Letters* **2014,** *3* (6), 515-519.
- Bohdanecký, M.; Gordon, M.; Koningsveld, R.; Kratochvíl, P.; Dušek, K. *Macromolecules* **2000,** *33* (10), 3497-3498.
- Bryant, S. J.; Bender, R. J.; Durand, K. L.; Anseth, K. S. Encapsulating chondrocytes in degrading PEG hydrogels with high modulus: engineering gel structural changes to facilitate cartilaginous tissue production. *Biotechnology and Bioengineering* **2004,** *86* (7), 747-755.
- Brubert, J.; Krajewski, S.; Wendel, H. P.; Nair, S.; Stasiak, J.; Moggridge, G. D. Hemocompatability of styrenic block copolymers for use in prosthetic heart valve. *Journal of Material Science: Materials in Medicine* **2016,** *27*, 32.
- Cai, H.; Dave, V.; Gross, R. A.; McCarthy, S. P. Effects of physical aging, crystallinity, and orientation on the enzymatic degradation of poly(lactic acid). *Journal of Polymer Science: Part B: Polymer Physics* **1996,** *34*, 2701-2708.
- Chatani, S.; Kloxin, C. J.; Bowman, C. N. The power of light in polymer science: photochemical processes to manipulate polymer formation, structure, and properties. *Polymer Chemistry* **2014,** *5*, 2187-2201.
- Clapper,J. D.; Skeie, J. M.; Mullins, R. F.; Guymon, C. A. Development and characterization of photopolymerizable biodegradable materials from PEG-PLA-PEG block macromonomers. *Polymer* **2007,** *48*, 6554-6564.
- Cramer, N. B.; Stansbury, J. W.; Bowman, C. N. Recent advances and developments in composite dental restorative materials. *Journal of Dental Research* **2011,** *90* (4), 402-416.
- Dailing, E.; Liu, J.; Lewis, S.; Stansbury, J. Nanogels as a basis for network construction. *Macromolecular Symposia* **2013,** *329* (1), 113-117.
- Dailing, E. A.; Setterberg, W. K.; Shah, P. K.; Stansbury, J. W. Photopolymerizable nanogels as macromolecular precursors to covalently crosslinked water-based networks. *Soft Matter* **2015,** *11*, 5647-655.
- Davy, K. W. M.; Anseau, M. R.; Odlyha, M.; Foster, G. M. X-ray opaque

methacrylate polymers for biomedical applications. *Polymer International* **1997,** *43*, 143-154.
- De Munck, J.; Van den Steen, P. E.; Mine, A.; Van Landuyt, K. L.; Poitevin, A.; Opdenakker, G.; Van Meerbeek, B. Inhibition of enzymatic degradation of adhesive-dentin interfaces. *Journal of Dental Research* **2009,** *88* (12), 1101-1106.
- Di Lorenzo, F.; Seiffert, S. Macro- and microrheology of heterogeneous microgel packing. *Macromolecules* **2013,** *46*, 1962-1972.
- Di Lorenzo, F.; Seiffert, S. Tracer diffusion in heterogeneous polymer networks. *Macromolecular Chemistry and Physics* **2014,** *215*, 2097-2111.
- Di Lorenzo, F.; Seiffert, S. Nanostructural heterogeneity in polymer networks and gels. *Polymer Chemistry* **2015,** *6*, 5515-5528.
- Dizge, N.; Keskinler, B.; Tanriseven, A. Biodiesel production from canola oil by using lipase immobilized onto hydrophobic microporous styrene-divinylbenzene copolymer. *Biochemical Engineering Journal* **2009,** *44* (2-3), 220-225.
- Dobson, G. R.; Gordon, M. Theory of branching processes and statistics of rubber elasticity. *The Journal of Chemical Physics* **1965,** *43* (2), 705-713.
- Dragan, E. S. Design and applications of interpenetrating polymer network hydrogels. A review. *Chemical Engineering Journal* **2014,** *243*, 572-590.
- Drury, J. L.; Mooney, D. J. Hydrogels for tissue engineering: scaffold design variables and applications. *Biomaterials* **2003,** *24*, 4337-4351.
- Dušek, K. Size of network chains. *Macromolecules* **1984,** *17*, 716-722.
- Dušek, K.; Dušková-Smrčková, M. Network structure formation during crosslinking of organic coating systems. *Progress in Polymer Science* **2000,** *25*,1215-1260.
- Fairbanks, B. D.; Singh, S. P.; Bowman, C. N.; Anseth, K. S. Photodegradable, photoadaptable hydrogels via radical-mediated disulfide fragmentation reaction. *Macromolecules* **2011,** *44*, 2444-2450.
- Ferracane, J. L. Hygroscopic and hydrolytic effects in dental polymer networks. *Dental Materials* **2006,** *22* (3), 211-222.
- Flory, P. J. Molecular theory of rubber elasticity. *Polymer Journal* **1985,** 17 (1), 1-12.
- Funke, W.; Okay, O.; Joos-Müller, B. In *Microgels-Intramolecularly Crosslinked Macromolecules with a Globular Structure*; Advances in Polymer Science; Springer-Verlag: Berlin Heidelberg, 1998; Vol. 136.
- Gallocher, S. L.; Aguirre, A. F.; Kasyanov, V.; Pinchuk, L.; Schoephoerster, R. T. A novel polymer for potential use in a trileaflet heart valve. *Journal of Biomedical Materials Research Part B: Applied Biomaterials* **2006,** *79B* (2), 325-334.
- Gao, J.; Zhang, Z.; Zhou, N.; Cheng, Z.; Zhu, J.; Zhu, X. Copper(0)-mediated living radical copolymerization of styrene and methyl methacrylate at ambient temperature. *Macromolecules* **2011,** *44*, 3227-3232.
- Ge, J.; Trujillo, M.; Stansbury, J. Synthesis and photopolymerization of low shrinkage methacrylate monomers containing bulky substituent groups. *Dental Materials* **2005,** *21*, 1163-1169.
- Griffin, D. R.; Kasko, A. M. Photodegradable macromers and hydrogels for live cell encapsulation and release. *Journal of the American Chemical Society* **2012,** *134*, 13103-13107.
- Harm, S.; Falkenhagen, D.; Hartmann, J. Pore size-a key property for selective toxin

removal in blood purification. *International Journal of Artificial Organs* **2014,** *37* (9), 668-678.
- Hennink, W. E.; van Nostrum, C. F. Novel crosslinking methods to design hydrogels. *Advanced Drug Delivery Reviews* **2012,** *64*, 223-236.
- Hernandez, K.; Garcia-Galan, C.; Fernandez-Lafuente, R. Simple and efficient immobilization of lipase B from candida Antarctica on porous styrene-divinylbenzene beads. *Enzyme and Microbial Technology* **2011,** 49 (1), 72-78.
- Heyes, D. M.; Brańka, A. C. Interactions between microgel particles. *Soft Matter* **2009,** *5*, 2681-2685.
- Hiemenz, P. C.; Lodge, T. P. In *Polymer Chemistry*, 2nd ed.; CRC Press: Boca Raton, FL, 2007.
- Hiemenz, P. C.; Rajagopalan, R. In Principles of Colloid and Surface Chemistry, 3rd ed.; CRC Press: Boca Raton, FL, 1997.
- Hoffman, A. S.; Schoen, F. J.; Lemons, J. E. In *An Introduction to Materials in Medicine*, 3rd ed.; Ratner, B. D., Ed.; Biomaterials Science; Elsevier: Waltham, MA, 2013.
- Huang, W.; Baker, G. G. L.; Bruening, M. L. Surface-initiated thermal radical polymerization on gold. *Langmuir* **2001,** *17* (5), 1731-1736.
- Kabanov, A. V.; Vinogradov, S. V. Nanogels as pharmaceutical carriers: finite networks of infinite capabilities. *Angewandte Chemie International Edition* **2009,** *48* (30), 5418-5429.
- Kessenbrock, K.; Plaks, V.; Werb, Z. Matrix metalloproteinases: regulators of the tumor microenvironment. *Cell* **2010,** 141 (1), 52-67.
- Kim, D.; Stansbury, J. W. A photo-oxidizable kinetic pathway of three-component photoinitiator systems containing porphrin dye (Zn-tpp), an electron donor and diphenyl idonium salt. *Journal of Polymer Science: Part A: Polymer Chemistry* **2009,** *47*, 3131-3141.
- Kloxin, A. M.; Kasko, A. M.; Salinas, C. N.; Anseth, K. S. Photodegradable hydrogels for dynamic tuning of physical and chemical properties. *Science* **2009,** *324* (5923), 59-63.
- Kotani, Y.; Kamigaito, M.; Sawamoto, M. Living random copolymerization of styrene and methyl methacrylate with a Ru(II) complex and synthesis of ABC-type block-random copolymers. *Macromolecules* **1998,** *31*, 5582-5587.
- Leicht, R.; Fuhrmann, J. Network formation during styrene-divinylbenzene copolymerization investigated by the fluorescence polarization method. *Polymer Bulletin* **1981,** *4*, 141-148.
- Liotta, L. A.; Tryggvaso, K.; Garbisa, S.; Hart, I.; Foltz, C. M.; Shafie, S. Metastatic potential correlates with enzymatic degradation of basement membrane collagen. *Nature* **1980,** *284*, 67-68.
- Lipatov, Y. S.; Alekseeva, T. T. In *Phase-Separated Interpenetrating Polymer Networks*; Advances in Polymer Science; Springer-Verlag: Berlin, Heidelberg, 2007.
- Liu, J.; Howard, G. D.; Lewis, S. H.; Barros, M. D.; Stansbury, J. W. A study of shrinkage stress reduction and mechanical properties of nanogel-modified resin systems. *European Polymer Journal* **2012,** *48* (11), 1819-1828.
- Liu, J.; Rad, I. Y.; Sun, F.; Stansbury, J. W. Photo-reactive nanogels as a means to

tune properties during polymer network formation. *Polymer Chemistry* **2014,** *5*, 227-233.
- Liu, J.; Stansbury, J. W. RAFT-mediated control of nanogel structure and reactivity: Chemical, physical and mechanical properties of monomer-dispersed nanogel compositions. *Dental Materials* **2014,** *30* (11), 1252-1262.
- Loudon, R. In *The Quantum Theory of Light*, 3rd ed.; Oxford University Press: New York, 1973.
- Lü, C.; Cheng, Y.; Liu, Y.; Liu, F.; Yang, B. A facile route to ZnS-polymer nanocomposite optical materials with high nanophase content via γ-ray irradiation initiated bulk polymerization. *Advanced Materials* **2006,** *18*, 1188-1192.
- Manavitehrani, I.; Fathi, A.; Badr, H.; Daly, S.; Negahi Shirazi, A.; Dehghani, F. Biomedical applications of biodegradable polyesters. *Polymers* **2016,** *8* (1), 20-52.
- Marten, E.; Müller, R. J.; Deckwer, W. D. Studies on the enzymatic hydrolysis of polyesters. II. Aliphatic-aromatic copolyesters. *Polymer Degradation and Stability* **2005,** *88*, 371-381.
- Mason, M. N.; Metters, A. T.; Bowman, C. N.; Anseth, K. S. Predicting controlled-release behavior of degradable PLA-*b*-PEG-*b*-PLA hydrogels. *Macromolecules* **2001,** *34*, 4630-4635.
- Matricardi, P.; Di Meo, C.; Coviello, T.; Hennink, W. E.; Alhaique, F. Interpenetrating polymer networks polysaccharide hydrogels for drug delivery and tissue engineering. *Advanced Drug Delivery Reviews* **2013,** *65* (9), 1172-1187.
- Matsumoto, A. In *Free-Radical Crosslinking Polymerization and Copolymerization of Multivinyl Compounds*; Advanced in Polymer Science; Springer-Verlag: Berlin, Heidelberg, 1995; Vol. 123.
- Matsumoto, A.; Kitaguchi, Y. Approach to ideal network formation governed by Flory-Stockmayer gelation theory in free-radical cross-linking copolymerization of styrene with m-divinylbenzene. *Macromolecules* **1999,** *32*, 8336-8339.
- Matyjaszewski, K.; Davis, T. P. In *Handbook of Radical Polymerization*; Wiley-Interscience: Hoboken, NJ, 2002.
- Mayo, F. R.; Lewis, F. M. Copolymerization. I. A basis for comparing the behavior of monomers in copolymerization: The copolymerization of styrene and methyl methacrylate. *Journal of the American Chemical Society* **1944,** *66*, 1594-1601.
- Metters, A. T.; Anseth, K. S.; Bowman, C. N. Fundamental studies of a novel, biodegradable PEG-*b*-PLA hydrogel. *Polymer* **2000,** *41* (11), 3993-4004.
- Metters, A. T.; Bowman, C. N.; Anseth, K. S. A statistical-kinetic model for the bulk degradation of PLA-*b*-PEG-*b*-PLA hydrogel network. *The Journal of Physical Chemistry B* **2000,** *104* (30), 7043-7049.
- Mitragotri, S.; Burke, P. A.; Langer, R. Overcoming the challenges in administering biopharmaceuticals: formulation and delivery strategies. *Nature Reviews. Drug Discovery* **2014,** *13* (9), 655-672.
- Mochizuki, M.; Hirami, M. Structural effects on the biodegradation of aliphatic polyesters. *Polymers for Advanced Technologies* **1997,** *8*, 203-209.
- Morães, R. R.; Garcia, J. W.; Barros, M. D.; Lewis, S. H.; Pfeifer, C. S.; Liu, J.; Stansbury, J. W. Control of polymerization shrinkage and stress in nanogel-modified monomer andcomposite materials. *Dental Materials* **2011,** 27 (6), 509-519.

- Morães, R. R.; Garcia, J. W.; Wilson, N. D.; Lewis, S. H.; Barros, M. D.; Yang, B.; Pfeifer, C. S.; Stansbury, J. W. Improved dental adhesive formulations based on reactive nanogel additives. *Journal of Dental Research* **2012,** *91* (2), 179-184.
- Odian, G. In *Principles of Polymerization*, 4th ed.; Wiley-Interscience: Hoboken, NJ, 2004.
- Oh, J. K.; Bencherif, S. A.; Matyjaszewski, K. Atom transfer radical polymerization in inverse miniemulsion: A versatile route toward preparation and functionalization of microgels/nanogels for targeted drug delivery applications. *Polymer* **2009,** *50* (19), 4407-4423.
- Okano, T.; Katayama, M.; Shinohara, I. The influence of hydrophilic and hydrophobic domains on water wettability of 2-hydroxyethyl methacrylate-styrene copolymers. *Journal of Applied Polymer Science* **1978,** *22*, 369-377.
- Papadopoulos, A.; Bichara, D. A.; Zhao, X.; Ibusuki, S.; Randolph, M. A.; Anseth, K. S.; Yaremchuk, M. J. Injectable and photopolymerizable tissue-engineered auricular cartilage using poly(ethylene glycol) dimethacrylate copolymer hydrogels. *Tissue Engineering: Part A* **2011,** *17* (1-2), 161-169.
- Pascault, J. P.; Sautereau, H.; Verdu, J.; Williams, R. J. J. In *Thermosetting Polymers*; Marcel Dekker: New York, NY, 2002.
- Pattanayak, A.; Jana, S. C. Synthesis of thermoplastic polyurethane nanocomposites of reactive nanoclay by bulk polymerization methods. *Polymer* **2005,** *46*, 3275-3288.
- Qiu, J.; Charleux, B.; Matyjaszewski, K. Controlled/living radical polymerization in aqueous media: homogeneous and heterogeneous systems. *Progress in Polymer Science* **2001,** *26*, 2083-2134.
- Raemdonck, K.; Demeester, J.; De Smedt, S. Advanced nanogel engineering for drug delivery. *Soft Matter* **2009,** *5*, 707-715.
- Sandwick, R. K.; Schray, K. J. The inactivation of enzymes upon interaction with a hydrophobic latex surface. *Journal of Colloid and Interface Science* **1987,***115* (1), 130-138.
- Santerre, J. P.; Shajii, L.; Leung, B. W. Relation of dental composite formulations to their degradation and the release of hydrolyzed polymeric-resin-derived products. *Critical Reviews in Oral Biology & Medicine* **2001,** *12* (2), 136-151.
- Santerre, J. P.; Shajii, L.; Tsang, H. Biodegradation of commercial dental composites by cholesterol esterase. *Journal of Dental Research* **1999,** *78* (8), 1459-1468.
- Saraswathy, M.; Stansbury, J.; Nair, D. Water dispersible siloxane nanogels: a novel technique to control surface characteristics and drug release kinetics. *Journal of Materials Chemistry B* **2016,** *4*, 5299-5307.
- Scott, T. F.; Cook, W. D.; Forsythe, J. S. Kinetics and network structure of thermally cured vinyl ester resins. *European Polymer Journal* **2002,** *38* (4), 705-716.
- Scott, T. F.; Cook, W. D.; Forsythe, J. S. Effect of the degree of cure on the viscoelastic properties of vinyl ester resins. *European Polymer Journal* **2008,** *44* (10), 3200-3212.
- Sperling, L. H. In *Interpenetrating Polymer Networks and Related Materials*, 1st ed.;

Plenum Press: New York, NY, 1981.
- Stansbury, J. W. Cyclopolymerizable monomers for use in dental resin composites. *Journal of Dental Research* **1990,** *69* (3), 844-848.
- Tobita, H. Cross-linking kinetics in emulsion copolymerization. *Macromolecules* **1992,** *25*, 2671-2678.
- Tobita, H.; Kumagai, M.; Aoyagi, N. Microgel formation in emulsion polymerization. *Polymer* **2000,** *41*, 481-487.
- Uhrich, K.; Cannizzaro, S. M.; Langer, R. S.; Shakesheff, K. M. Polymeric systems for controlled drug release. *Chemical Reviews* **1999,** *99*, 3181-3198.
- Von Burkersroda, F.; Schedl, L.; Gopferich, A. Why degradable polymers undergo surface erosion or bulk erosion. *Biomaterials* **2002,** *23* (21), 4221-4231.
- Walta, S.; Di Lorenzo, F.; Ma, K.; Wiesner, U.; Richtering, W.; Seiffert, S. Diffusion of rigid nanoparticles in crowded polymer-network hydrogels: dominance of segmental density over crosslinking density. *Colloid and Polymer Science* **2017,** *295* (8), 1371-1381.
- Xia, L. W.,; Xie, R.; Ju, X. J.;, W.; Chen, Q.; Chu, L. Y. Nano-structured smart hydrogels with rapid response and high elasticity. *Nature Communications* **2013,** *4*, 2226.
- Yoshii, E. Cytotoxic effects of acrylates and methacrylate: Relationships of monomer structures and cytotoxicity. *Journal of Biomedical Materials Research: Part A* **1997,** *37* (4), 517-524.

The following list represents references used in **Chapter 2:**

- Asadi, H.; Rostamizadeh, K.; Salari, D.; Hamid, M. Preparation and characterization of tri-block poly(lactide)-poly(ethylene glycil)-poly(lactide) nanogels for controlled release of naltrexone. *International Journal of Pharmaceutics* **2011,** *416* (1), 356-364.
- Dailing, E.; Liu, J.; Lewis, S.; Stansbury, J. Nanogels as a basis for network construction. *Macromolecular symposia* **2013,** *329* (1), 113-117.
- Doran, P. M. In *Bioprocess Engineering Principles*, Academic Press Limited: San Diego, CA, 1995.
- Erdoğan, S.; Alpbaz, M.; Karagöz, A. R. The effect of operational conditions on the performance of batch polymerization reactor control. *Chemical Engineering Journal* **2002,** *86* (3), 259-268.
- Graham, N. B.; Cameron, A. Nanogels and microgels: The new polymeric materials playground. *Pure and Applied Chemistry* **1998,** *70* (6), 1271-1275.
- Hiemenz, P. C.; Lodge, T. P. In *Polymer Chemistry*, 2nd ed.; CRC Press Taylor & Francis Group: Boca Raton, FL, 2007.
- Jalil, R.; Nixon, J. R. Microencapsulation using poly(L-lactic acide) II: Preparative variables affecting microcapsule properties. *Journal of Microencapsulation Micro and Nano Carriers* **1990,** *7* (1), 25-39.
- Lemon, M. T.; Jones, M. S.; Stansbury, J. W. Hydrogen bonding interactions in methacrylate monomers and polymers. *Journal of Biomedical Materials Research*

Part A **2007,** *83A* (3), 734-746.

- Liu, J.; Howard, G. D.; Lewis, S. H.; Barros, M. D.; Stansbury, J. W. A study of shrinkage stress reduction and mechanical properties of nanogel-modified resin systems. *European Polymer Journal* **2012,** *48* (11), 1819-1828.
- Liu, J.; Stansbury, J. RAFT-mediated control of nanogel structure and reactivity: Chemical, physical and mechanical properties of monomer-dispersed nanogel compositions. *Dental Materials* **2014,** *30* (11), 1252-1262.
- Ma, J. K. H.; Hadzija, B. In *Basic Physical Pharmacy*, Jones & Bartlett Learning: Burlington, MA, 2013.
- McLinden, M. O. A liquid density standard over wide ranges of temperature and pressure based on toluene. *Journal of Research of NIST* **2008,** *113* (1), 29-67.
- Mintzer, M. A.; Simanek, E. E. Nonviral vectors for gene delivery. *Chemical Reviews* **2009,** *109* (2), 259-302.
- Moraes, R. R.; Garcia, J. W.; Barros, M. D.; Lewis, S. H.; Pfeifer, C. S.; Liu, J.; Stansbury, J. W. Control of polymerization shrinkage and stress in nanogel-modified monomer and composite materials. *Dental Materials* **2011,** *27* (6), (509-519.
- O'Brien, A. K.; Cramer, N. B.; Bowman, C. N. Oxygen inhibition in thiol-acrylate photopolymerizations. *Journal of Polymer Science: Part A: Polymer Chemistry* **2006,** *44*, 2007-2014.
- Rouzeau, S.; Méchin, F.; Pascault, J. P.; Magny, B. Criteria for the preparation of cross-linked poly(meth)acrylate microparticles by solution free radical polymerization. *European Polymer Journal* **2007,** *43* (10), 4398-4414.
- Sánchez, L.; Sánchez, P.; Carmona, M.; de Lucas, A.; Rodríguez, J. F. Influence of operation conditions on the microencapsulation of PCMs by means of suspension-like polymerization. *Colloid and Polymer Science* **2008,** *286* (8-9), 1019-1027.
- Sánchez Pérez, J. A.; Rodríguez Porcel, E. M.; Casas López, J. L.; Fernández Sevilla, J. M.; Chisti, Y. Shear rate in stirred tank and bubble column bioreactors. *Chemical Engineering Journal* **2006,** *124* (1-3), 1-5.
- Sinnott, R.; Towler, G. In *Chemical Engineering Design*, 5th ed.; Butterworth-Heinemann: Burlington, MA, 2009.
- Vvorakova, G.; Biffis, A. Room temperature preparation of highly crosslinked microgels. *Polymer Bulletin* **2010,** *64*, 107-114.
- Wu, W.; Shen, J.; Banerjee, P.; Zhou, S. Core-shell hybrid nanogels for integration of optical temperature-sensing, targeted tumor cell imaging, and combined chemo-photothermal treatment. *Biomaterials* **2010,** *31* (29), 7555-7566.

The following list represents references used in **Chapter 3:**

- Abraham, S.; Brahim, S.; Ishihara, K.; Guiseppi-Elie, A. Molecularly engineered p(HEMA)-based hydrogels for implant biochip biocompatibility. *Biomaterials* **2005,** *26* (23), 4767-4778.
- Asadi, H.; Rostamizadeh, K.; Salari, D.; Hamidi, M. Preparation and characterization of tri-block poly(lactide)-poly(ethylene glycol)-poly(lactide) nanogels for controlled release of naltrexone. *International Journal of Pharmaceutics* **2011,** *416*, 356-364.

- Bencherif, S. A.; Siegwart, D. J.; Srinivasan, A.; Horkay, F.; Hollinger, J. O.; Washburn, N. R.; Matyjaszewski, K. Nanostructured hybrid hydrogels prepared by a combination of atom transfer radical polymerization and free radical polymerization. *Biomaterials* **2009,** *30*, 5270-5278.
- Clapper, J. D.; Skeie, J. M.; Mullins, R. F.; Guymon, C. A. Development and characterization of photopolymerizable biodegradable materials from PEG-PLA-PEG block macromonomers. *Polymer* **2007,** *48*, 6554-6564.
- Dailing, E.; Liu, J.; Lewis, S.; Stansbury, J. Nanogels as a basis for network construction. *Macromolecular Symposia* **2013,** *329* (1), 113-117.
- Dill, K. A.; Bromberg, S. In *Molecular Driving Forces: Statistical Thermodynamics in Biology, Chemistry, Physics, and Nanoscience*, 2nd ed.; Garland Science: New York, NY, 2011.
- Di Lorenzo, F.; Seiffert, S. Particulate and continuum mechanics of microgel pastes: effect and non-effect of compositional heterogeneity. *Colloid Polymer Science* **2013,** *291* (12), 2927-2933.
- Di Lorenzo, F.; Hellwig, J.; von Klitzing, R.; Seiffert, S. Macroscopic and microscopic elasticity of heterogeneous polymer gels. *ACS Macro Letters* **2015,** *4* (7), 698-703.
- Di Lorenzo, F.; Seiffert, S. Nanostructural heterogeneity in polymer networks and gels. *Polymer Chemistry* **2015,** *6*, 5515-5529.
- Dušek, K.; Dušeková-Smrčková, M. Network structure formation during crosslinking of organic coating systems. *Progress in Polymer Science* **2000,** *25*, 1215-1260.
- Fernandez-Garcia, M.; Torrado, M. F.; Martinez, G.; Sanchez-Chaves, M.; Madruga, E. L. Free radical copolymerization of 2-hydroxyethyl methacrylate with butyl methacrylate: Determination of monomer reactivity ratios and glass transition temperatures. *Polymer* **2000,** *41*, 8001-8008.
- Foster, M. In *A Text Book of Physiology*, 3rd ed.; McMillan & Co: London, 1879.
- Fu, Y.; Kao, W. J. Drug release kinetics and transport mechanisms of non-degradable and degradable polymeric delivery systems. *Journal of Expert Opinion on Drug Delivery* **2010,** *7* (4), 429-444.
- Funke, W.; Okay, O.; Joos-Müller, B. In *Microgels-Intramolecularly Crosslinked Macromolecules with a Globular Structure*; Advances in Polymer Science; Springer: Berlin, Heidelberg, 1998; Vol. 136.
- Gotti, V. B.; Correr, A. B.; Lewis, S. H.; Feitosa, V. P.; Correr-Sobrinho, L.; Stansbury, J. W. Influence of nanogel additive hydrophilicity on dental adhesive mechanical performance and dentin bonding. *Dental Materials* **2016,** *32* (11), 1406-1413.
- Greaves, G. N.; Greer, A. L.; Lakes, R. S.; Rouxel, T. Poisson's ratio and modern materials. *Nature Materials* **2011,** *10*, 823-837.
- Hiemenz, P. C.; Lodge, T. P. In *Polymer Chemistry*, 2nd ed.; CRC Press Taylor & Francis Group: Boca Raton, FL, 2007.
- Hiemenz, P. C.; Rajagopalan, R. In *Principles of colloid and surface chemistry*, 3rd ed.; CRC Press Taylor & Francis Group: Boca Raton, FL, 1997.
- Hodge, R. M.; Simon, G. P.; Whittaker, M. R.; Hill, D. J. T.; Whittaker, A. K. Free

volume and water uptake in a copolymer hydrogel series. *Journal of Polymer Science: Part B: Polymer Physics* **1998,** *36* (3), 463-471

- Hoffman, A. S.; Schoen, F. J.; Lemons, J. E. In *Biomaterial Science: an introduction to materials in medicine*, 3rd ed.; Ratner, B. D., Ed.; Academic Press: Waltham, MA, 2013.
- Johnson, R. P.; Jeong, Y.I.; Choi, E.; Chung, C. W.; Kang, D. H.; Oh, S. O.; Suh, H.; Kim, I. Biocompatible poly(2-hydroxyethyl methacrylate)-*b*-poly(L-histidine) hybrid materials for pH-sensitive intracellular anticancer drug delivery. *Advanced Functional Materials* **2012,** *22* (5), 1058-1068.
- Kim, B.; La Flamme, K; Peppas, N. A. Dynamic swelling behavior of pH-sensitive anionic hydrogels used for protein delivery. *Journal of Applied Polymer Science* **2003,** *89*, 1606-1613.
- Kirschner, C. M.; Anseth, K. S. Hydrogels in healthcare: From static to dynamic material microenvironments. *Acta Materialia* **2013,** *61*, 931-944.
- Kloxin, A. M.; Kloxin, C. J.; Bowman, C. N.; Anseth, K. S. Mechanical properties of cellularly responsive hydrogels and their experimental determination. *Advanced Materials* **2010,** *17* (22), 3484-3494.
- Landel, R. F.; Nielsen, L.E. In *Mechanical Properties of Polymers and Composites*, 2nd ed.; Marcel Dekker: New York, NY, 1994.
- Landfester, K. The generation of nanoparticles in miniemulsions. *Advanced Materials* **2001,** *13* (10), 765-768.
- Lee, W. C.; Li, Y. C.; Chu, I. M. Amphiphilic poly(D,L-lactic acid)/poly(ethylene glycol)/poly(D,L-lactic acid) nanogels for controlled release of hydrophobic drugs. *Macromolecular Bioscience* **2006,** *6*, 846-854.
- Lester, C. L.; Smith, S. M.; Colson, C. D. Physical properties of hydrogels synthesized from Lyotropic liquid crystalline templates. *Chemistry of Materials* **2003,** *15* (17), 3376-3384.
- Lin, C. C.; Metters, A. T. Hydrogels in controlled release formulations: Network design and mathematical modeling. *Advanced Drug Delivery Reviews* **2006,** *58* (12-13),1379-1408.
- Liu, J.; Howard, G. D.; Lewis, S. H.; Barros, M. D.; Stansbury, J. W. A study of shrinkage stress reduction and mechanical properties of nanogel-modified resin systems. *European Polymer Journal* **2012,** *48* (11), 1819-1828.
- Liu, J.; Rad, I. Y.; Sun, F.; Stansbury, J. W. Photo-reactive nanogels as a means to tune properties during polymer network formation. *Polymer Chemistry* **2014,** *5*, 227-233.
- Lyu, S. P.; Untereker, D. Degradability of polymers for implantable biomedical devices. *International Journal of Molecular Sciences* **2009,** *10*, 4033-4065.
- Mahlin, D.; Wood, J.; Hawkins, N.; Mahey, J.; Royall, P. G. A novel powder sample holder for the determination of glass transition temperature by DMA. *International Journal of Pharmaceutics* **2009,** *371*, 120-125.
- Metters, A. T.; Anseth, K. S.; Bowman, C. N. Fundamental studies of a novel, biodegradable PEG-*b*-PLA hydrogel. *Polymer* **2000,** *41*, 3993-4004.

- Metters, A. T.; Bowman, C. N.; Anseth, K. S. A statistical kinetic model for the bulk degradation of PLA-*b*-PEG-*b*-PLA hydrogel networks. *Journal of Physical Chemistry B* **2000,** *104*, 7043-7049.
- Middleton, J. C.; Tipton, A. J. Synthetic biodegradable polymers as orthopedic devices. *Biomaterials* **2000,** *21*, 2335-2346.
- Moraes, R. R.; Garcia, J. W.; Barros, M. D.; Lewis, S. H.; Pfeifer, C. S.; Liu, J.; Stansbury, J. W. Control of polymerization shrinkage and stress in nanogel-modified monomer and composite materials. *Dental Materials* **2011,** *27*, 509-519.
- Moraes, R. R.; Garcia, J. W.; Wilson, N. D.; Lewis, S. H.; Barros, M. D.; Yang, B.; Pfeifer, C. S.; Stansbury, J. W. Improved dental adhesive formulations based on reactive nanogel additives. *Journal of Dental Research* **2012,** *91* (2), 179-184.
- Odian, G. In *Principles of polymerization*, 4th ed.; Wiley-Interscience: Hoboken, NJ, 2004.
- Oh, J. K.; Drumright, R.; Sirgwart, D. J.; Matyjaszewski, K. The development of microgels/nanogels for drug delivery applications. *Progress in Polymer Science* ***2008,*** *33* (4), 448-477.
- Papadopoulos, A.; Bichara, D. A.; Zhao, X.; Ibusuki, S.; Randolph, M. A.; Anseth, K. S.; Yaremchuck, M. J. Injectable and photopolymerizable tissue-engineered auricular cartilage using poly(ethylene glycol) dimethacrylate copolymer hydrogels. *Tissue Engineering: Part A* **2011,** *17* (1-2), 161-169.
- Pohorecki, R.; Brigwater, J.; Molzahn, M.; Gani, R.; Gallegos, C. In *Chemical Engineering and Chemical Process Technology: Rheology-Part I*; Encyclopedia of Life Support Systems; Eolss Publishers/UNESCO: UK, 2010; Vol. VI.
- Qiao, C.; Jiang, S.; Dong, D.; Ji, X.; An, L.; Jiang, B. The critical lowest molecular weight for PEG to crystallize in cross-linked networks. *Macromolecular Rapid Communication* **2004,** *25* (5), 659-663.
- Rawlings, J. B.; Ekerdt, J. G. In *Chemical Reactor Analysis and Design Fundamentals*, 2nd ed.; Nob Hill Publishing: Madison, WI, 2002.
- Rijcken, C. J. F.; Veldhuis, T. F. J.; Ramzi, A.; Meeldijk, J. D.; van Nostrum, C. F.; Hennink, W. E. Novel fast degradable thermosensitive polymeric micelles based on PEG-block-poly(*N*-(2-hydroxyethyl)methacrylamide)-oligolactates). *Biomacromolecules* **2005,** *6*, 2343-2351.
- Sawhney, A. S.; Pathak, C. P.; Hubbell, J. A. Bioerodible hydrogels based on photopolymerized poly(ethylene glycol)-*co*-poly(α-hydroxy acid) diacrylate macromers. *Macromolecules* **1993,** *26*, 581-587.
- Tanaka, M.; Mochizuki, A. Clarification of the blood compatibility mechanism by controlling the water structure at the blood-poly(meth)acrylate interface. *Journal of Biomaterials Science, Polymer Edition* **2010,** *21* (14), 1849-1863.
- Tessmar, J. K.; GÖpferich, A. M. Customized PEG-derived copolymers for tissue-engineering applications. *Macromolecular Bioscience* **2007,** *7*, 23-39.
- Tobita, H. Cross-linking kinetics in emulsion copolymerization. *Macromolecules* **1992,** *25*, 2671-2678.
- Tobita, H.; Kumagai, M.; Aoyagi, N. Microgel formation in emulsion polymerization.

Polymer **2000,** *41*, 481-487.

- Treloar, L. R. G. The photoelastic properties of short-chain molecular networks. *Transactions of the Faraday Society* **1954,** 881-896.
- Uhrich, K. E.; Cannizzaro, S. M.; Langer, R. S.; Shakesheff, K. M. Polymeric systems for controlled drug release. *Chemical Reviews* **1999,** *99* (11), 3181-3198.
- Verhoeven, J.; Schseffer, R.; Bouwstra, J. A.; Junginger, H. E. The physio-chemical characterization of poly (2-hydroxyethyl methacrylate-*co*-methacrylic acid): 2. Effect of water, PEG 400 and PEG 6000 on the glass transition temperature. *Polymer* **1989,** *30* (10), 1946-1950.
- Wang, A. Z.; Langer, R.; Farokhzad, O. C. Nanoparticle delivery of cancer drugs. *Annual Review of Medicine* **2012,** *63*, 1850198.
- Wu, Y. H.; Park, H. B.; Kai, T.; Freeman, B. D.; Kalika, D. S. Water uptake, transport and structure characterization in poly(ethylene glycol) diacrylate hydrogels. *Journal of Membrane Science* **2010**, *347* (1-2), 197-208.
- Yu, Y.; Ferrari, R.; Lattuada, M.; Storti, G.; Morbidelli, M.; Moscatelli, D. PLA-based nanoparticles with tunable hydrophobicity and degradation kinetics. *Journal of Polymer Science, Part A: Polymer Chemistry* **2012,** *50*, 5191-5200.

The following list represents references used in **Chapter 4:**

- Anseth, K. S.; Bowman, C. N. Kinetic gelation model predictions of crosslinked polymer network microstructure. *Chemical Engineering Science* **1994,** *49* (14), 2207-2217.
- Bettencourt, A. F.; Neves, C. B.; de Almeida, M. S.; Pinheiro, L. M.; Arantes e Oliveira, S.; Lopes, L. P.; Castro, M. F. Biodegradation of acrylic based resins: A review. *Dental Materials* **2010,** *26* (5), e171-e180.
- Brubert, J.; Krajewski, S.; Wendel, H. P.; Nair, S.; Stasiak, J.; Moggridge, G. D. Hemocompatability of styrenic block copolymers for use in prosthetic heart valves. *Journal of Materials Science: Materials in Medicine* **2016,** *27*, 32.
- Bruice, P. Y. In *Organic Chemistry*, 3rd ed.; Pearson: 2015.
- Chen, C.; Liu, J.; Sun, F.; Stansbury, J. W. Control of microstructure and gradient property of polymer network by photopolymerizable silicone-containing nanogel. *Journal of Polymer Science: Part A: Polymer Chemistry* **2014,** *52* (19), 2830-2840.
- Dailing, E.; Liu, J.; Lewis, S.; Stansbury, J. Nanogels as basis for network construction. *Macromolecular Symposia* **2013,** *329* (1), 113-117.
- Dickens, S. H.; Stansbury, J. W.; Choi, K. M.; Floyd, J. E. Photopolymerization kinetics of methacrylate dental resins. *Macromolecules* **2003,** *36* (16), 6043-6053.
- Dizge, N.; Keshinler, B.; Tanriseven, A. Biodiesel production from canola oil by usin lipase immobilized onto hydrophobic microporous styrene-divinylbenzene copolymer. *Biochemical Engineering Journal* **2009,** *44* (2-3), 220-225.
- Drummond, J. L. Degradation, fatigue, and failure of resin dental composite materials. *Journal of Dental Research* **2008,** *87* (8), 710-719.
- Finer, Y.; Santerre, J. P. Salivary esterase activity and its association with the biodegradation of dental composites. *Journal of Dental Research* **2004,** *83* (1), 22-26.

- Ferracane, J. L. Hygroscopic and hydrolytic effects in dental polymer networks. *Dental Materials* **2006,** *22* (3), 211-222.
- Ferracane, J. L.; Hilton, T. J. Polymerization stress-is it clinically meaningful? *Dental Materials* **2016,** *32* (1), 1-10.
- Gallocher, S. L.; Aguirre, A. F.; Kasyanov, V.; Pinchuk, L.; Schoephoerster, R. T. A novel polymer for potential use in a trileaflet heart valve. *Journal of Biomedical Materials Research: Part B: Applied Biomaterials* **2006,** *79B* (2), 325-334.
- Gonçalves, F.; Kawano, Y.; Pfeifer, C.; Stansbury, J. W.; Braga, R. R. Influence of BisGMA, TEGDMA, and BisEMA contents on viscosity, conversion, and flexural strength of experimental resins and composites. *European Journal of Oral Science* **2009,** *117* (4), 442-446.
- Grunden, B. L.; Sung, C. S. P. Cure Characterization of Unsaturated Polyester Resin by Near-IR and Mid-IR Spectroscopy, Macromolecules, 2003, 36, 3166-3173.
- Harm, S.; Falkenhagen, D.; Hartmann, J. Pore size-a key property for selective toxin removal in blood purification. *International Journal of Artificial Organs* **2014,** *37*, 1-11.
- Hernandez, K.; Garcia-Galan, C.; Fernandez-Lafuente, R. Simple and efficient immobilization of lipase B from *candida antarctica* on porous styrene-divinylbenzene beads. *Enzyme and Microbial Technology* **2011,** *49* (1), 72-78.
- Hiemenz, P. C.; Lodge, T. P. In *Polymer Chemistry*, 3rd ed.; CRC Press: Boca Raton, FL, 2007.
- Kaczmarek, H.; Świątek, M.; Kamińska, A. Modification of polystyrene and poly(vinyl chloride) for the purpose of obtaining packaging materials degradable in the natural environment. *Polymer Degradation and Stability* **2004,** *83*, 35-45.
- Leicht, R.; Fuhrmann, J. Network formation during styrene-divinylbenzene copolymerization investigated by the fluorescence polarization method. *Polymer Bulletin* **1981,** *4* (1-2), 141-148.
- Li, Y.; Pham, J. Q.; Johnston, K. P.; Green, P. F. Contact angle of water on polystyrene thin films: Effects of CO_2 environment and film thickness. *Langmuir* **2007,** *23* (19), 9785-9793.
- Lin-Vien, D.; Colthup, N. B.; Fateley, W. G.; Grasselli, J. G. In *The Handbook of Infrared and Raman Characteristic Frequencies of Organic Molecules*, Academic Press: San Diego, CA, 1991.
- Liu, Y.; Tjäderhane, L.; Breschi, L.; Mazzoni, A.; Li, N.; Mao, J.; Pashley, D. H.; Tay, F. R. Limitations in bonding to dentin and experimental strategies to prevent bond degradation. *Journal of Dental Research* **2011,** *90* (8), 953-968.
- Liu, J.; Howard, G. D.; Lewis, S. H.; Barros, M. D.; Stansbury, J. W. A study of shrinkage stress reduction and mechanical properties of nanogel-modified resin systems. *European Polymer Journal* **2012,** *48* (11), 1819-1828.
- Liu, J.; Rad, I. Y.; Sun, F.; Stansbury, J. W. Photo-reactive nanogels as a means to tune properties during polymer network formation. *Polymer Chemistry* **2014,** *5*, 227-233.
- Malacarne, J.; Carvalho, R. M.; de Goes, M.; Svizero, N.; Pashley, D. H.; Tay, F. R.; Yiu, C. K.; Roch de Oliveira Carrilho, M. Water sorption/solubility of dental adhesive resins. *Dental Materials* **2006,** *22* (10), 973-980.

- Moraes, R. R.; Garcia, J. W.; Barros, M. D.; Lewis, S. H.; Pfeifer, C. S.; Liu, J.; Stansbury, J. W. Control of polymerization shrinkage and stress in nanogel-modified monomer and composite materials. *Dental Materials* **2011,** *27*, 509-519.
- Moraes, R. R.; Garcia, J. W.; Wilson, N. D.; Lewis, S. H.; Barros, M. D.; Yang, B.; Pfeifer, C. S.; Stansbury, J. W. Improved dental adhesive formulations based on reactive nanogel additives. *Journal of Dental Research* **2012,** *91* (2), 179-184.
- Rabelo, D.; Coutinho, F. M. B. Porous structure formation and swelling properties of styrene-divinylbenzene copolymers. *European Polymer Journal* **1994,** *30* (6), 675-682.
- Sandwick, R. K.; Schray, K. J. The inactivation of enzymes upon interaction with a hydrophobic latex surface. *Journal of Colloid and Interface Science* **1987,** *115* (1), 130-138.
- Santerre, J. P.; Shajii, L.; Leung, B. W. Relation of dental composite formulations to their degradation and the release of hydrolyzed polymeric-resin-derived products. *Critical Reviews in Oral Biology & Medicine* **2001,** *12* (2), 136-151.
- Sawhney, A. S.; Pathak, C. P.; Hubbel, J. A. Bioerodible hydrogels based on photopolymerized poly(ethylene glycol)-*co*-poly(α-hydroxy acid) diacrylate macromers. *Macromolecules* **1993,** *26*, 581-587.
- Sideridou, I.; Tserki, V.; Papanastasiou, G. Effect of chemical structure on degree of conversion in light-cured dimethacrylate-based dental resins. *Biomaterials* **2000,** *23* (8), 1819-1829.
- Smith, J. M.; Van Ness, H. C.; Abbott, M. M. In *Introduction to Chemical Engineering Thermodynamics*, 6th ed.; Tata McGraw-Hill Publishing: 2003.
- Stansbury, J. W. Curing dental resins and composites by photopolymerization. *Journal of Esthetic and Restorative Dentistry* **2000,** *12* (6), 300-308.
- Stansbury, J. W.; Dickens, S. H. Determination of double bond conversion in dental resins by near infrared spectroscopy. *Dental Materials* **2001,** *17*, 71-79.

The following list represents references used in **Chapter 5:**

- Beyler, C. L.; Hirschler, M. M. In *Thermal Decomposition of Polymers*, 3rd ed.; DiNenno, P. J., Ed.; The SFPE Handbook of Fire Protection Engineering; Quincy: National Fire Protection Association, 2002; pp. 111-131.
- Biron, M. In *Thermosets and Composites, Material Selection, Applications, Manufacturing, and Cost Analysis*, 2nd ed.; Elsevier: Kidlington, OX, 2014.
- Chatani, S.; Kloxin, C. J.; Bowman, C. N. The power of light in polymer science: photochemical processes to manipulate polymer formation, structure, and properties. *Polymer Chemistry* **2014,** *5*, 2187-2201.
- Chen, C.; Liu, J.; Sun, F.; Stansbury, J. W. Control of microstructure and gradient property of polymer network by photopolymerizable silicone-containing nanogel. *Journal of Polymer Science Part A: Polymer Chemistry* **2014,** *52* (19), 2830-2840.
- Christy, A. A.; Fernando, N. R. Thermally induced chemical reactions in castor oil studied by infrared spectroscopy and gas chromatography: determination of

activation energy for the dehydration of ricinoleic acid. *Advances in Natural and Applied Sciences* **2016,** *10* (13), 146-157.
- Critchley, J. P.; Knight, G. J.; Wright, W. W. In *Heat-Resistant Polymers*; Technologically Useful Materials; Springer Science + Business Media: New York, NY, 1983.
- Crompton, T. R. In *Practical Polymer Analysis*; Springer: New York, NY, 1993; Vol. 2.
- Dailing, E.; Liu, J.; Lewis, S.; Stansbury, J. Nanogels as a basis for network construction. *Macromolecular Symposia* **2013,** *329* (1), 113-117.
- Dailing, E. A.; Setterberg, W. K.; Shah, P. K.; Stansbury, J. W. Photopolymerizable nanogels as macromolecular precursors to covalently crosslinked water-based networks. *Soft Matter* **2015,** *11*, 5647-5655.
- Davankov, V. A.; Tsyurupa, M. P. In *Hypercrosslinked polymeric networks and adsorbing materials*; D. Barceló, Ed.; Elsevier: Kidlington, OX, 2011; Vol. 56
- Davis, K. A.; Matyjaszewski, K. In *Advances in Polymer Science Statistical, Gradient, Block and Graft Copolymers by Controlled/Living Radical Polymerizations, Statistical Copolymers*; Springer-Verlag: Berlin, 2002.
- Dickens, S. H.; Stansbury, J. W.; Choi, K. M.; Floyd, C. J. E. Photopolymrization kinetics of methacrylate dental resins. *Macromolecules* **2003,** *36*, 6043-6053.
- Di Lorenzo, F.; Seiffert, S. Nanostructural Heterogeneity in Polymer Networks and Gels. *Polymer Chemistry* **2015**, *6*, 5515-5528.
- Dušek, K. Are Cured Thermoset Resins Inhomogeneous?. *Macromolecular Materials and Engineering* **1996,** *240*, 1-15.
- Erdmenger, T.; Becer, C. R.; Hoogenboom, R.; Schubert, U. S. Simplifying the free-radical polymerization of styrene: microwave-assisted high-temperature auto polymerizations. *Australian Journal of Chemistry* **2009,** *62*, 58-63.
- Gillham, J. Formation and Properties of Thermosetting and High T_g Polymeric Materials. *Polymer Engineering Science* **1986,** *26*, 1429-1433.
- Gotti, V. B.; Correr, A. B.; Lewis, S. H.; Feitosa, V. P.; Correr-Sobrinho, L.; Stansbury, J. W. Influence of nanogel additive hydrophilicity on dental adhesive mechanical performance and dentin bonding. *Dental Materials* **2016,** *32* (11), 1406-1413.
- Hale, A.; Macosco, C. W.; Bair, H. E. Glass transition temperature as a function of conversion in thermosetting polymers. *Macromolecules* **1991,** *24*, 2610-2621.
- Hanemann, T.; Honnef, K. Tailoring the optical and thermomechanical properties of polymer host-guest systems. *Journal of Applied Polymer Science* **2011,** *122*, 3514-3519.
- Hergenrother, P. M. The Use, Design, Synthesis, and Properties of High Performance/High Temperature Polymers: An Overview. *High Performance Polymer* **2003,** *15*, 3-45.

- Hiemenz, P. C.; Lodge, T. P. In *Polymer Chemistry*, 2nd ed.; CRC Press: Boca Raton, FL, 2007.
- Howard, B.; Wilson, N. D.; Newman, S. M.; Pfeifer, C. S.; Stansbury, J. W. Relationships between conversion, temperature and optical properties during composite photopolymerization. *Acta Biomaterialia* **2010,** *6*, 2053-2059.
- Imai, Y. Synthesis of Novel Organic-Soluble High-Temperature Aromatic Polymers. *High Performance Polymer* **1995,** *7*, 337-345.
- Kashiwagi, T.; Inaba, A.; Brown, J. E.; Hatada, K.; Kitayama, T.; Masuda, E. Effects of weak linkages on the thermal and oxidative degradation of poly (methyl methacrylates). *Macromolecules* **1986,** *19* (8), 2160-2168.
- Levchik, G. F.; Si, K.; Levchik, S. V.; Camino, G.; Wilkie, C. A. The correlation between cross-linking and thermal stability: cross-linked polystyrenes and polymethacrylates. *Polymer Degradation and Stability* **1999,** *65* (3), 395-403.
- Li, F.; Hanson, M. V.; Larock, R. C. Soybean oil-divinylbenzene thermosetting polymers: synthesis, structure, properties and their relationships. *Polymer* **2001,** *42* (4), 1567-1579.
- Li, F.; Larock, R. C. New soybean oil-styrene-divinylbenzene thermosetting copolymers-IV. Good damping properties. *Polymers for Advanced Technologies* **2002,** *13*, 436-449.
- Liu, J.; Howard, G. D.; Lewis, S. H.; Barros, M. D.; Stansbury, J. W. A study of shrinkage stress reduction and mechanical properties of nanogel-modified resin systems. *European Polymer Journal* **2012,** *48*, 1819-1828.
- Liu, J.; Rad, I. Y.; Sun, F.; Stansbury, J. W. Photo-reactive nanogels as a means to tune properties during polymer network formation. *Polymer Chemistry* **2014,** *5*, 227-233.
- Liu, J.; Stansbury, J. W. RAFT-mediated control of nanogel structure and reactivity: Chemical, physical and mechanical properties of monomer-dispersed nanogel compositions. *Dental Materials* **2014,** *30* (11), 1252-1262.
- Liu, J. G.; Ueda, M. High refractive index polymers: fundamental research and practical applications. *Journal of Material Chemistry* **2009,** *19*, 8907-8919.
- Lu, H.; Lovell, L. G.; Bowman, C. N. Exploiting the heterogeneity of cross-linked photopolymers to create high-T_g polymers from polymerizations performed at ambient conditions. *Macromolecules* **2001,** *34*, 8021-8025.
- Moraes, R. R.; Garcia, J. W.; Barros, M. D.; Lewis, S. H.; Pfeifer, C. S.; Liu, J.; Stansbury, J. W. Control of polymerization shrinkage and stress in nanogel-modified monomer and composite materials. *Dental Materials* **2011,** *27*, 509-519.
- Moraes, R. R.; Garcia, J. W.; Wilson, N. D.; Lewis, S. H.; Barros, M. D.; Yang, B.; Pfeifer, C. S.; Stansbury, J. W. Improved dental adhesive formulations based on reactive nanogel additives. *Journal of Dental Research* **2012,** *91* (2), 179-184.
- Nakagawa, H.; Matsushita, Y.; Tsuge, S. Studies on thermal degradation behavior of

anionically copolymerized styrene-divinylbenzene copolymers by high-resolution pyrolysis-gas chromatography. *Polymer* **1987,** *28*, 1512-1516.
- Nyhus, A. K.; Hagen, S.; Berge, A. Friedel-Crafts reactions of pendant vinyl groups in macroporous monosized poly(meta-divinylbenzene) and poly(para-divinylbenzene) particles. *Journal of Polymer Science Part A: Polymer Chemistry* **2000,** *38*, 1366-1378.
- Odian, G. In *Principles of polymerization*, 4th ed.; Wiley-Interscience: Hoboken, NJ, 2004.
- Okay, O.; Kurz, M.; Lutz, K.; Funke, W. Cyclization and reduced pendant vinyl group reactivity during the free-radical cross-linking polymerization of 1, 4- divinylbenzene. *Macromolecules* **1995,** *28*, 2728-2737.
- Peterson, J. D.; Vyazovkin, S.; Wight, C. A. Kinetics of the thermal and thermo-oxidative degradation of polystyrene, polyethylene and poly(propylene). *Macromolecular Chemistry and Physics* **2001,** *202*, 775-784.
- Saraswathy, M.; Stansbury, J.; Nair, D. Water dispersible siloxane nanogels: a novel technique to control surface characteristics and drug release kinetics. *Journal of Materials Chemistry B* **2016,** *4*, 5299-5307.
- Shim, S. E.; Yang, S.; Choi, H. H.; Choe, S. Fully crosslinked poly(styrene-co-divinylbenzene) microspheres by precipitation polymerization and their superior thermal properties. *Journal of Polymer Science Part A, Polymer Chemistry* **2004,** *42*, 835-845.
- Stansbury, J. W. Dimethacrylate network formation and polymer property evolution as determined by the selection of monomers and curing conditions. *Dental Materials* **2012,** *28*, 13-22.
- Szczepanski, C. R.; Pfeifer, C. S.; Stansbury, J. W. A new approach to network heterogeneity: Polymerization induced phase separation in photo-initiated, free-radical methacrylic systems. *Polymer* **2012,** *53* (21), 4694-4701.
- Uhl, F. M.; Levchik, G. F.; Levchik, S. V.; Dick, C.; Liggat, J. J.; Snape, C. E.; Wilkie, C. A. The thermal stability of cross-linked polymers: methyl methacrylate with divinylbenzene and styrene with dimethacrylates. *Polymer Degradation and Stability* **2001,** *71* (2), 317-325.
- Villegas, I. F.; Rubio, P. V. On Avoiding Thermal Degradation During Welding of High-Performance Thermoplastic Composites to Thermoset Composites. *Composites Part A* **2015,** *77*,172-180.
- Wang, Z.; Ye, W.; Luo, X.; Wang, Z. Heat-resistant crack-free superhydrophobic polydivinylbenzene colloidal films. *Langmuir* **2016,** *32*, 3079-3084.
- Wiley, R. H.; Jin, J. I. Monomer reactivity ratios for the copolymerization of methyl methacrylate with pure meta- and pure para-divinylbenzene. *Journal of Macromolecular Science Part A: Chemistry* **1968,** *2* (6), 1097-1104.
- Wilkie, C. A. TGA/FTIR: an extremely useful technique for studying polymer

degradation. *Polymer Degradation and Stability* **1999,** *66* (3), 301-306.

- Ye, S.; Cramer, N. B.; Bowman, C. N. Relationship between glass transition temperature and polymerization temperature for cross-linked photopolymers. *Macromolecules* **2011,** *44*, 490-494.
- Zhang, X. Q.; Wang, C. H. Solution characterization of poly (isobornyl methacrylate) in tetrahydrofuran. *Journal of Polymer Science, Part B, Polymer Physics* **1994,** *32*, 1951-1956.

APPENDIX A

A.1. NANOGEL GLASS TRANSITION TEMPERATURE

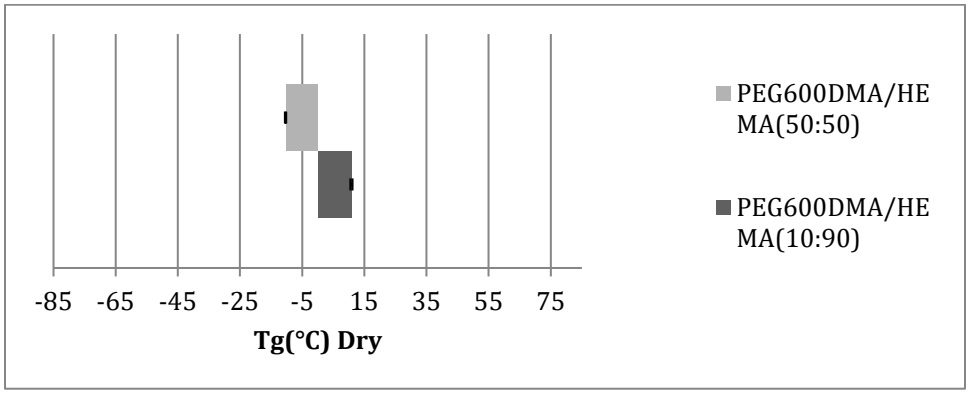

Figure A.1. Glass transition temperature of non-degradable active nanogels with $PEG_{600}DMA$ as crosslinker and HEMA as side-chain monomer; NG_1 (dark gray), NG_2 (light gray); *p*-level between groups = 0.00054.

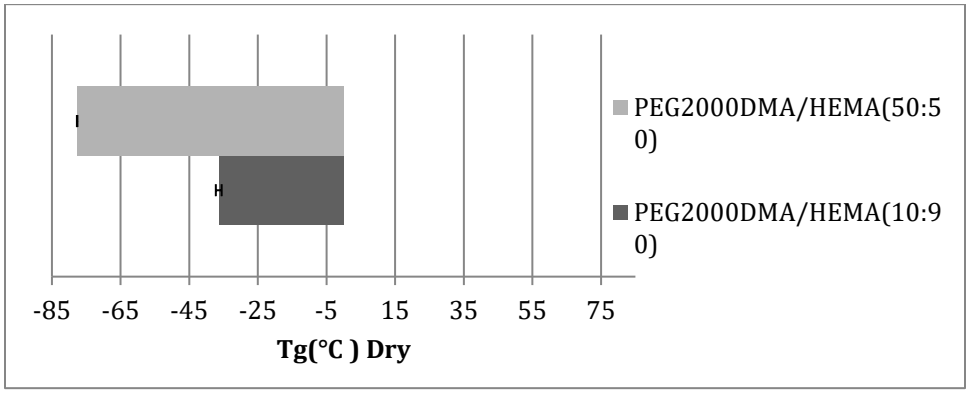

Figure A.2. Glass transition temperature of non-degradable active nanogels with $PEG_{2000}DMA$ as crosslinker and HEMA as side-chain monomer; NG_3 (dark gray), NG_4 (light gray); *p*-level between groups = 0.00056.

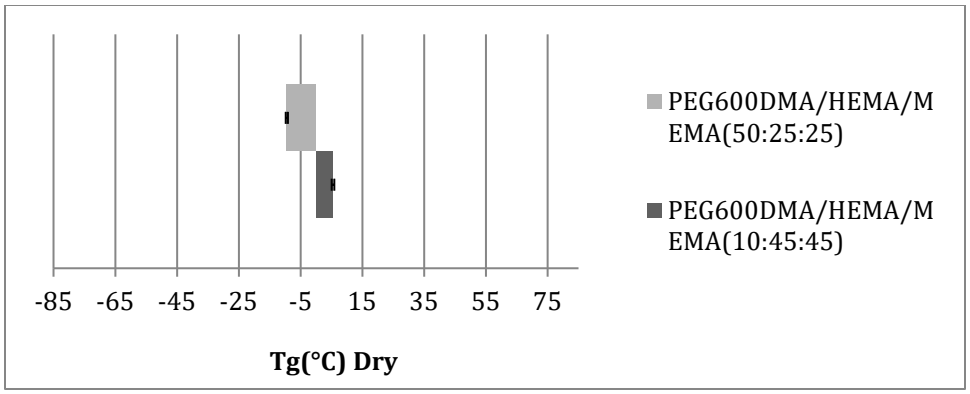

Figure A.3. Glass transition temperature of non-degradable active nanogels with $PEG_{600}DMA$ as crosslinker, HEMA, and MEMA as side-chain monomers; NG_5 (dark gray), NG_6 (light gray); *p*-level = 0.00098.

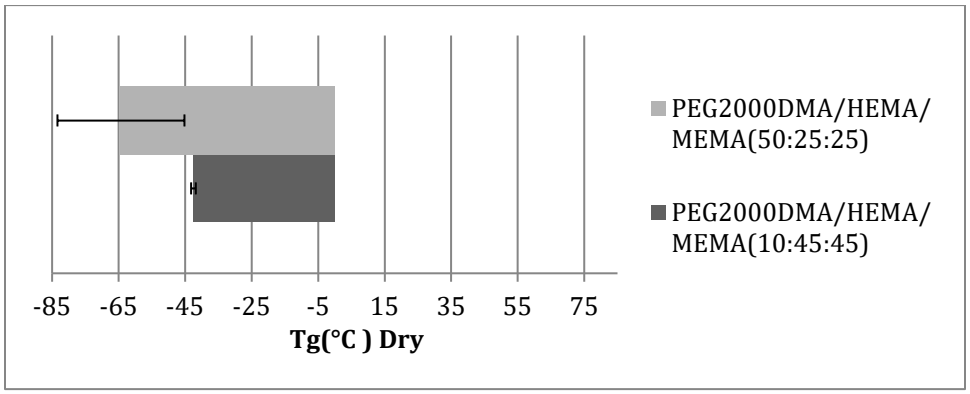

Figure A.4. Glass transition temperature of non-degradable active nanogels with $PEG_{2000}DMA$ as crosslinker, HEMA, and MEMA as side-chain monomers; NG_7 (darkgray), NG_8 (light gray); *p*-level = 0.24812.

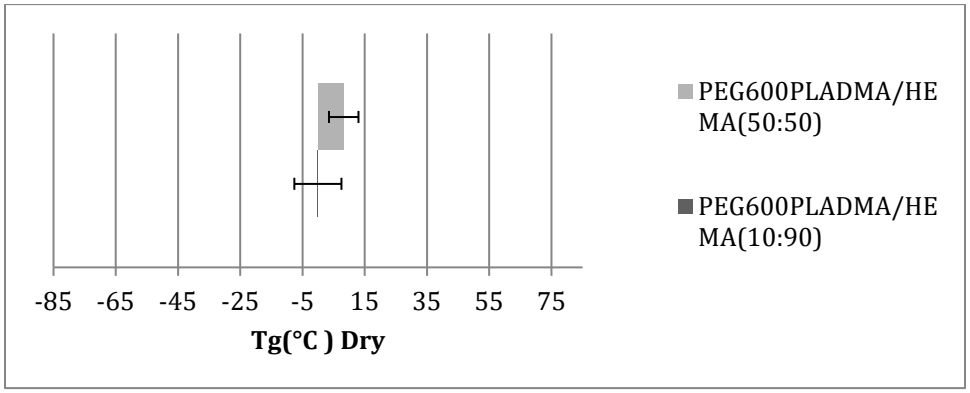

Figure A.5. Glass transition temperature of internally degradable active nanogels with $PEG_{600}PLADMA$ as crosslinker and HEMA as mono-functional monomer; NG_9 (dark gray), NG_{10} (light gray); *p*-level = 0.0559.

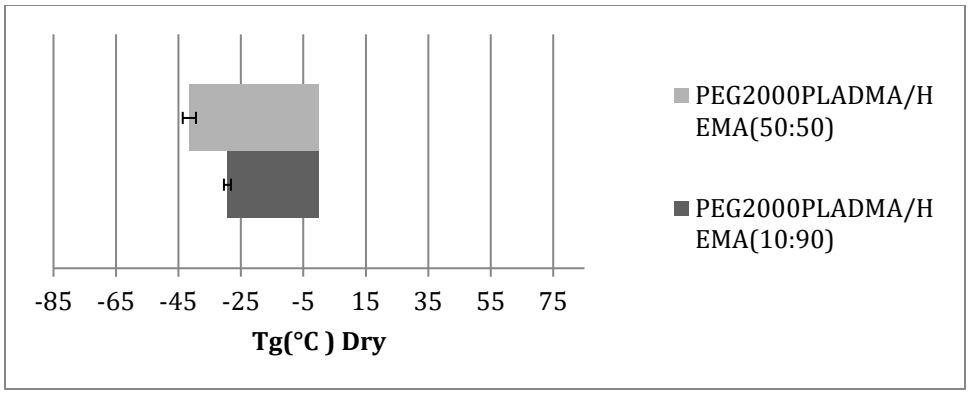

Figure A.6. Glass transition temperature of internally degradable active nanogels with PEG_{2000}PLADMA as crosslinker and HEMA as side-chain monomer; NG_{11} (dark gray), NG_{12} (light gray); *p*-level = 0.01909.

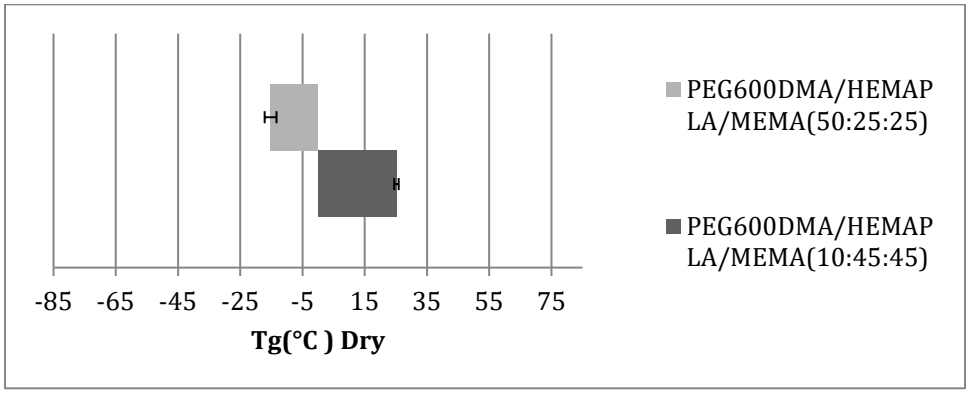

Figure A.7. Glass transition temperature of externally degradable active nanogels with PEG_{600}DMA as crosslinker, HEMAPLA, and MEMA as side-chain monomers; NG_{13} (dark gray), NG_{14} (light gray); *p*-level = 0.00154.

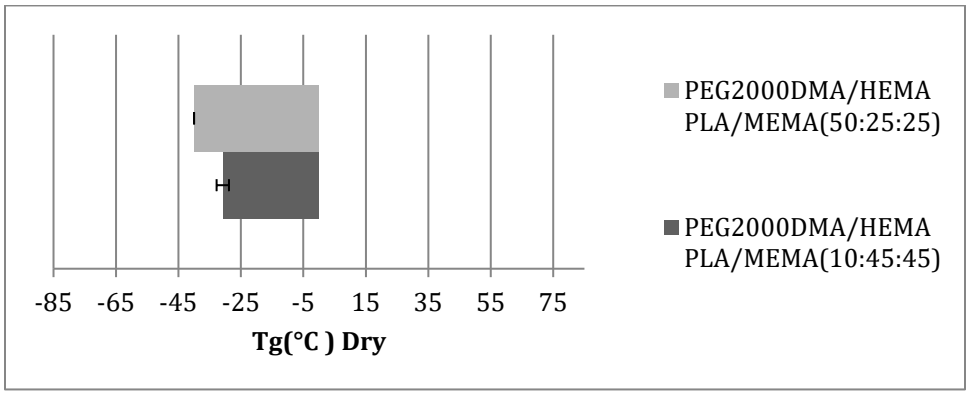

Figure A.8. Glass transition temperature of externally degradable active nanogels with PEG_{2000}DMA as crosslinker, HEMAPLA, and MEMA as side-chain monomers; NG_{15} (dark gray), NG_{16} (light gray); *p*-level = 0.02258.

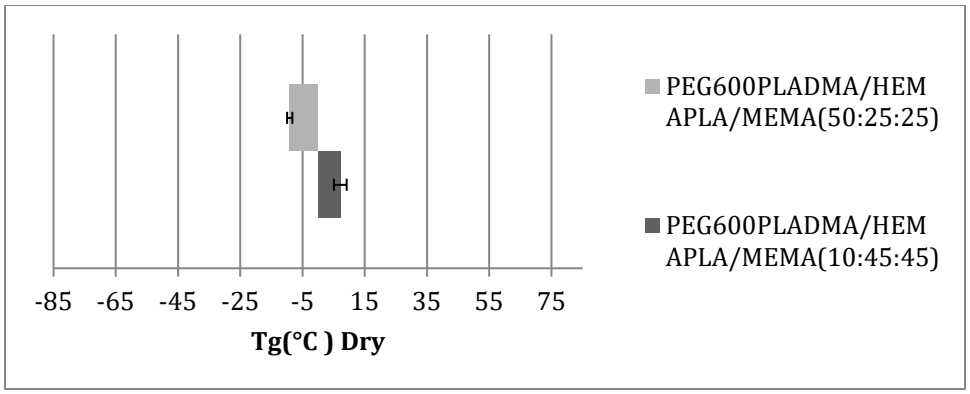

Figure A.9. Glass transition temperature of internally-externally degradable active nanogels with $PEG_{600}PLADMA$ as crosslinker, HEMAPLA, and MEMA as side-chain monomers; NG_{17} (dark gray), NG_{18} (light gray); *p*-level = 0.00942.

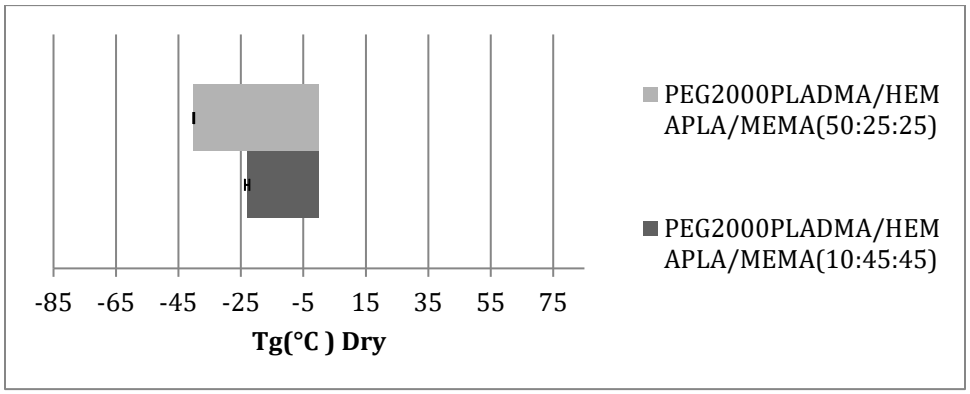

Figure A.10. Glass transition temperature of internally-externally degradable active nanogels with $PEG_{2000}PLADMA$ as crosslinker, HEMAPLA, and MEMA as side-chain monomers; NG_{19} (dark gray), NG_{20} (light gray); *p*-level = 0.00119).

A.2. DERIVATIONS

The entropy of a non-Gaussian freely jointed chain of N_x links of length b with end-to-end distance of h is defined by James and Guth:

$$S = -kN_x\left[\frac{h}{N_x b} + ln\frac{\beta}{sinh\beta}\right]$$

where the quantity β is the so-called Inverse Langevin function, $L^{-1}(x)$:

$$\beta = \mathcal{L}^{-1}\left(\frac{h}{N_x b}\right)$$

therefore S in extended power series format is written:

$$S = -kN_x\left[\frac{3}{2}\left(\frac{h}{N_x b}\right)^2 + \frac{9}{20}\left(\frac{h}{N_x b}\right)^4 + \frac{99}{350}\left(\frac{h}{N_x b}\right)^6 + \cdots\right]$$

after deformation and applying *affine junction assumption*, the end-to-end distance before deformation h_0 is changed to h after deformation, and if we assume that one end of the chain is fixed at location (0, 0, 0), then the coordinate of the other end is changed from (x_0, y_0, z_0) to (x, y, z), where $x = \lambda_x x_0$, $y = \lambda_y y_0$, $z = \lambda_z z_0$, also assume no volume change during deformation, and polymer network composed of ν_e chains, is stretched in the positive x direction, we have $\lambda_x = \lambda$, since we have $V = L_xL_yL_z = V_0 = L_0^3$, *thus* $\lambda_y = \lambda_z = \lambda^{-1/2}$.

$$\Delta S = \frac{-3k}{2N_x b^2}(h^2 - h_0^2)\left[1 + \frac{3\left(h^2 + h_0^2\right)}{10N_x^2 b^2} + \frac{33(h-h_0)^2(h+h_0)^2}{175N_x^4 b^4}\right]$$

we now note that on average $x_0^2 = y_0^2 = z_0^2 = N_x b^2/3$, therefore for a polymer network of ν_e chains the entropy change is:

$$\Delta S = \frac{-k\nu_e}{2}\left(\lambda^2 + \frac{2}{\lambda} - 3\right)\left[1 + \frac{\lambda^2 + \frac{2}{\lambda} + 3}{10N_x} + \frac{11\left(\lambda^2 + \frac{2}{\lambda} - 3\right)^2}{525N_x^2}\right]$$

$$f = -T\left(\frac{\partial \Delta S}{\partial L}\right) = -\frac{T}{L_0}\left(\frac{\partial \Delta S}{\partial \lambda}\right) = \frac{kT\nu_e}{L_0}\left(\lambda - \frac{1}{\lambda^2}\right)\left[1 + \frac{\lambda^2 + \frac{2}{\lambda}}{5N_x} + \frac{11\left(\lambda^2 + \frac{2}{\lambda} - 3\right)^2}{175N_x^2}\right]$$

$$\sigma_t = \frac{f}{area} = \frac{\lambda f}{L_0^2} = \frac{kT\nu_e}{V}\left(\lambda^2 - \frac{1}{\lambda}\right)\left[1 + \frac{\lambda^2 + \frac{2}{\lambda}}{5N_x} + \frac{11\left(\lambda^2 + \frac{2}{\lambda} - 3\right)^2}{175N_x^2}\right]$$

$$E = \lim_{\lambda \to 1}\left(\frac{\partial \sigma_t}{\partial \lambda}\right)$$

$$E = \frac{3\nu_e kT}{V}\left(1 + \frac{3}{5N_x} + \frac{11}{175N_x^2}\right)$$

$$\frac{\nu_e}{V} = \frac{\rho N_{av}}{\bar{M}_x}$$

$$G = \frac{E}{3}$$

$$2G(1 + \nu) = E = 3K(1 - 2\nu)$$

$$\boldsymbol{K = \left(\frac{2(1+\nu)}{3(1-2\nu)}\right)\frac{\rho RT}{\bar{M}_x}\left(1 + \frac{3}{5\bar{N}_x} + \frac{11}{175\bar{N}_x^2}\right)}$$

$$\boldsymbol{K = \left(\frac{2(1+\nu)}{3(1-2\nu)}\right)\frac{\rho RT}{\bar{M}_x}\left(1 + \frac{3}{5\bar{N}_x} + \frac{11}{175\bar{N}_x^2}\right)\phi^{1/3}}$$

For deriving Eq 3.14, we also assume isotropic swelling, thus $\lambda_x = \lambda_y = \lambda_z = \lambda$:

$$S = -kN_x\left[\frac{h}{N_x b} + ln\frac{\beta}{sinh\beta}\right]$$

$$\beta = \mathcal{L}^{-1}\left(\frac{h}{N_x b}\right)$$

$$S = -kN_x\left[\frac{3}{2}\left(\frac{h}{N_x b}\right)^2 + \frac{9}{20}\left(\frac{h}{N_x b}\right)^4 + \frac{99}{350}\left(\frac{h}{N_x b}\right)^6 + \cdots\right]$$

$$\Delta S = \frac{-3k}{2N_x b^2}(h^2 - h_0^2)\left[1 + \frac{3(h^2+h_0^2)}{10N_x^2 b^2} + \frac{33(h-h_0)^2(h+h_0)^2}{175N_x^4 b^4}\right]$$

we now note that on average $x_0^2 = y_0^2 = z_0^2 = N_x b^2/3$ (Hiemenz, 2007), therefore:

$$\Delta S = \frac{-3k}{2}(3\lambda^2 - 3 - ln\lambda^3)\left[1 + \frac{3\lambda^2+3+ln\lambda^3}{10N_x} + \frac{11(3\lambda^2-3-ln\lambda^3)^2}{525N_x^2}\right]$$

for and ideal elastomer, the Gibbs free energy change during deformation is purely entropic,

$$\left(\frac{\partial \Delta G_{el}}{\partial \lambda}\right) = -T\left(\frac{\partial \Delta S}{\partial \lambda}\right)$$

based on equilibrium swelling theory (Flory-Rehner equation), the change in free energy of a polymer network is:

$$\Delta G = \Delta G_m + \Delta G_{el}$$

The former and latter parts can be represented by Flory-Huggins theory expression and statistical mechanical theory of rubber elasticity, respectively (Hiemenz, 2007). At the point of swelling equilibrium, the chemical potential of the solvent inside the swollen network will equal that in the surrounding pure solvent, and so we have:

$$\left(\frac{\partial \Delta G_m}{\partial n_1}\right)_{T,p} = RT\{\ln(1-\phi_2) + \phi_2\left(1 - \frac{1}{\bar{N}_x}\right) + \chi\phi_2^2\}$$

$$\Delta\mu_1 = \left(\frac{\partial \Delta G}{\partial n_1}\right)_{T,p} = \left(\frac{\partial \Delta G_m}{\partial n_1}\right)_{T,p} + \left(\frac{\partial \Delta G_{el}}{\partial \lambda}\right)\left(\frac{\partial \lambda}{\partial n_1}\right)_{T,p} = 0$$

$$\frac{1}{\phi_2} = \frac{V}{V_0} = \lambda^3 = \frac{(V_0 + n_1 \hat{V}_1)}{V_0}$$

$$3\lambda^2 \left(\frac{\partial \lambda}{\partial n_1}\right) = \frac{\hat{V}_1}{V_0}$$

for a polymer network including ν_e chains,

$$\left(\frac{\partial \Delta G_{el}}{\partial \lambda}\right)_{T,p} = -T\left(\frac{\partial \Delta S}{\partial \lambda}\right)_{T,p} = \frac{3RT\nu_e}{N_{av}}\left(\lambda - \frac{1}{2\lambda}\right)\left[1 + \frac{39\lambda^2 + 3 + ln\lambda^3 - 9\lambda^{-2}}{10\bar{N}_x} + \frac{11(3\lambda^2 - 3 - ln\lambda^3)^2}{175\bar{N}_x^2}\right]$$

$$\bar{M}_x = \frac{\rho\hat{V}_1\left(\frac{\phi_2}{2} - \phi_2^{1/3}\right)\left\{1 + \frac{39\phi_2^{-2/3} + 3 + ln\phi_2^{-1} - 9\phi_2^{2/3}}{10\bar{N}_x} + \frac{11(3\phi_2^{-2/3} - 3 - ln\phi_2^{-1})^2}{175\bar{N}_x^2}\right\}}{\ln(1-\phi_2) + \phi_2\left(1 - \frac{1}{\bar{N}_x}\right) + \chi\phi_2^2}$$

A.3. CELL BIOCOMPATIBILITY

A.3.1. Measurements

Internally degradable PEG_{4600}PLADMA/HEMA/MEMA(50:25:25) (NG_{22}) nanogel was selected for cell biocompatibility study due to intermediate content of PLA compared to externally and internally-externally degradable nanogels of PEG_{4600} series. The promotion of biocompatibility, cell adhesion, and proliferation by higher content of PLA has been documented in the literature (Clapper, 2007). The cytocompatibility of model nanogel at different concentrations in the cell culture media was evaluated by the direct contact test with a monolayer of L929 mouse fibroblast cells according to ISO standards (ISO 10993-5, 1999). Briefly, L929 cells were sub-cultured and seeded into six-well tissue culture plates at a concentration of 50,000 cells per well. Cells were incubated for 24 h at 37 °C in 5% carbon dioxide atmosphere. Dry nanogel powder at a different concentration, 10 ug/mL, 20 ugmL, 50 ug/mL, 100 ug/mL and 200ug/mL were added and incubate for another 48 h. Cells were examined microscopically for cellular response using a phase

contrast inverted microscope (Leica, WLD MPS32, Germany). The morphology of the cells assessed in comparison with a control (media only).

A.3.2. Analysis

The L929 mouse fibroblast cells after 48 h of treatment analyzed for changes in its spindle morphology and the cell adherence nature in the culture plate. According to the observed results, there is no change in the spindle shape of cells up to 50 µg /mL of nanogel concentration and cells are strongly adhering to the culture plate. The cell morphology is comparable to that of the control. However, at higher concentration, the cells show signs of toxic effects, with some loss of the spherical morphology and an increase in detachment from the culture plate. Cells treated with 100 µg/mL nanogel concentration is seems to be mildly toxic and at 200 µg/mL, P2NG nanogel is severely toxic to L929 mouse fibroblast cells.

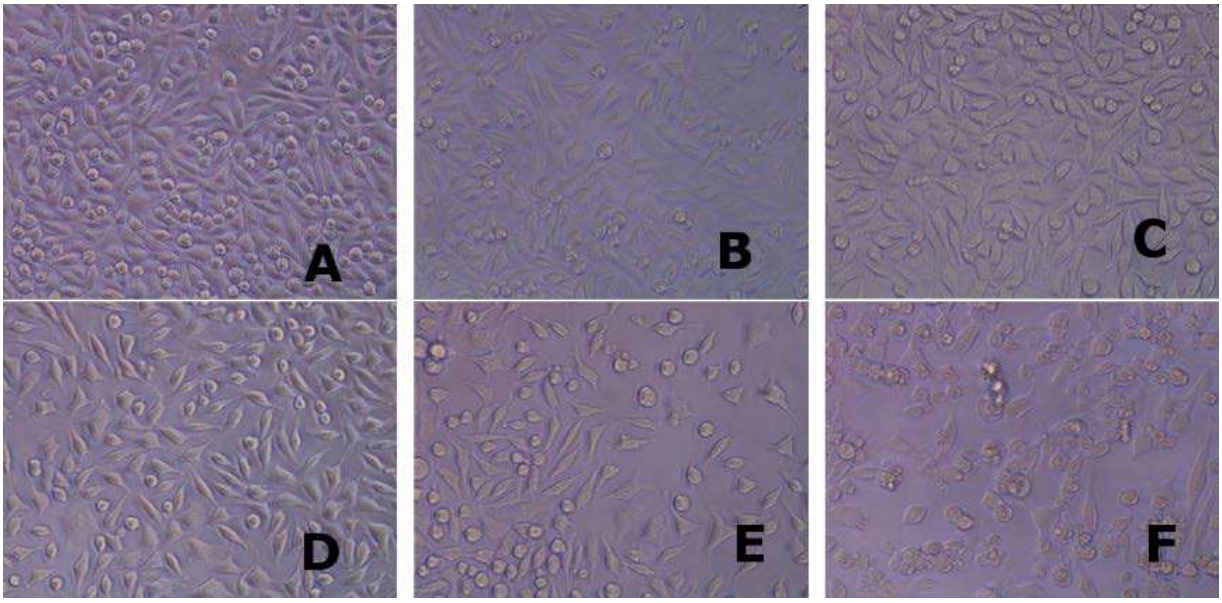

Figure A.11. The morphology of L929 mouse fibroblast cells incubating with PEG_{4600}PLADMA/HEMA/MEMA(50:25:25) (NG_{22}) nanogel (A) control (Media only), nanogel at concentration (B) 10 µg/mL (C) 20 µg /mL (D) 50 µg/mL (E) 100 µg/mL (F) 200 µg/mL.

A.4. CHAPTER 4 SUPPLEMENTARIES

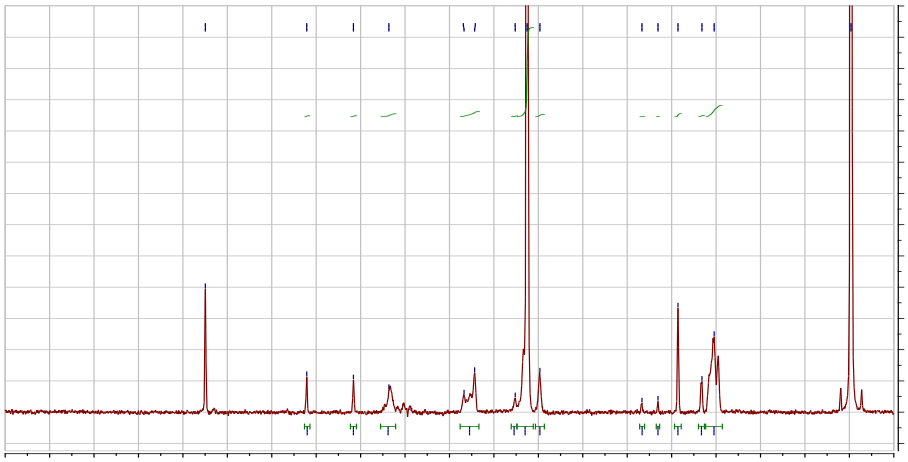

Figure A.12. Chemical structure and 1H NMR of degradable MA-PLA-b-PEG-b-PLA-MA macromer.

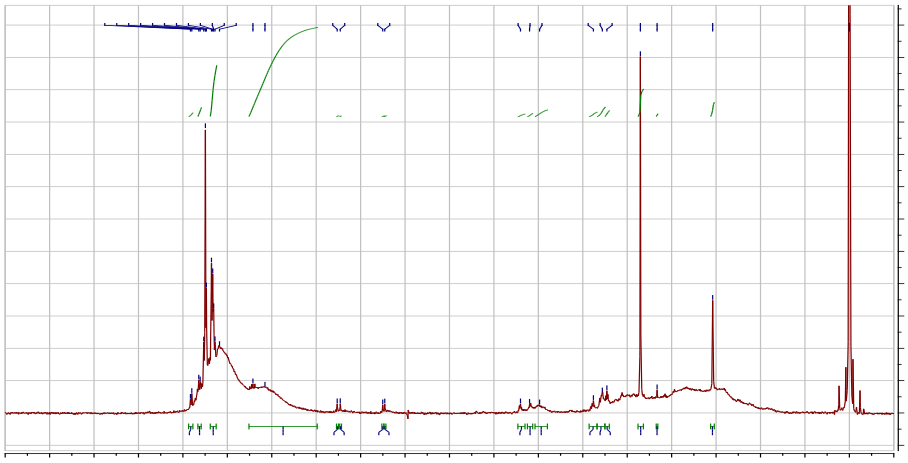

Figure A.13. DVB/Styrene (20:80)-High Conversion-No IEM

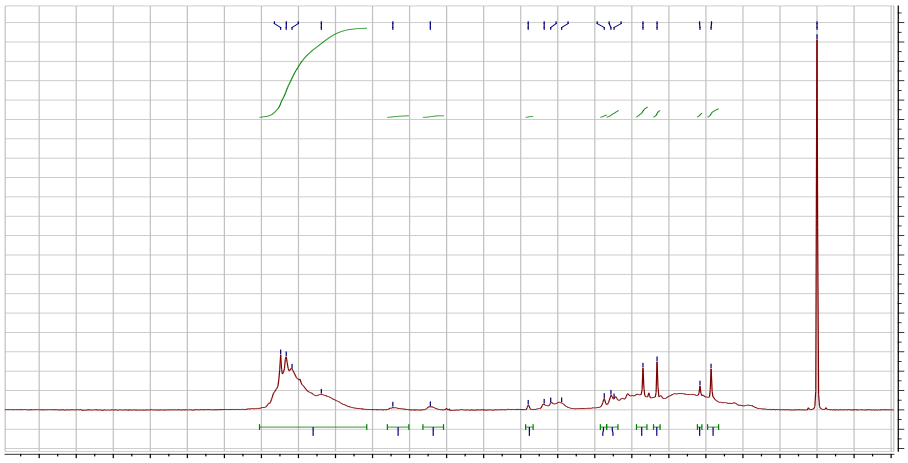

Figure A.14. DVB/styrene(20:80)-Low Conversion-No IEM

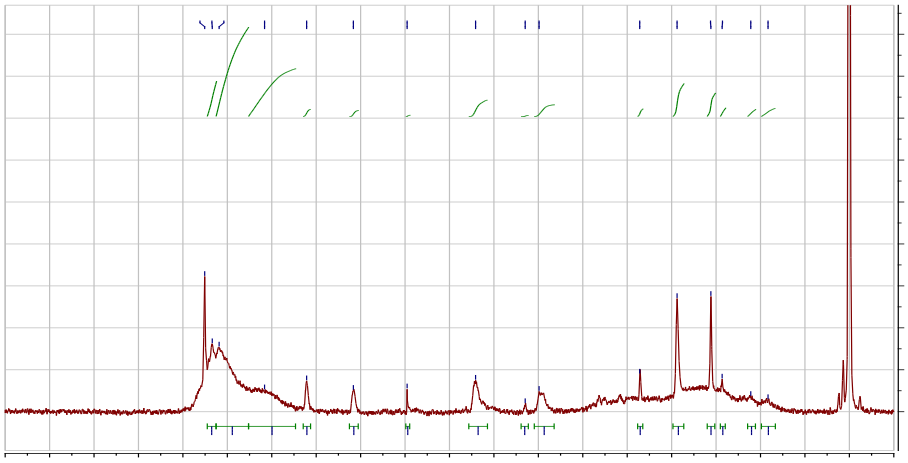

Figure A.15. DVB/Styrene(20:80)-High Conversion-With IEM

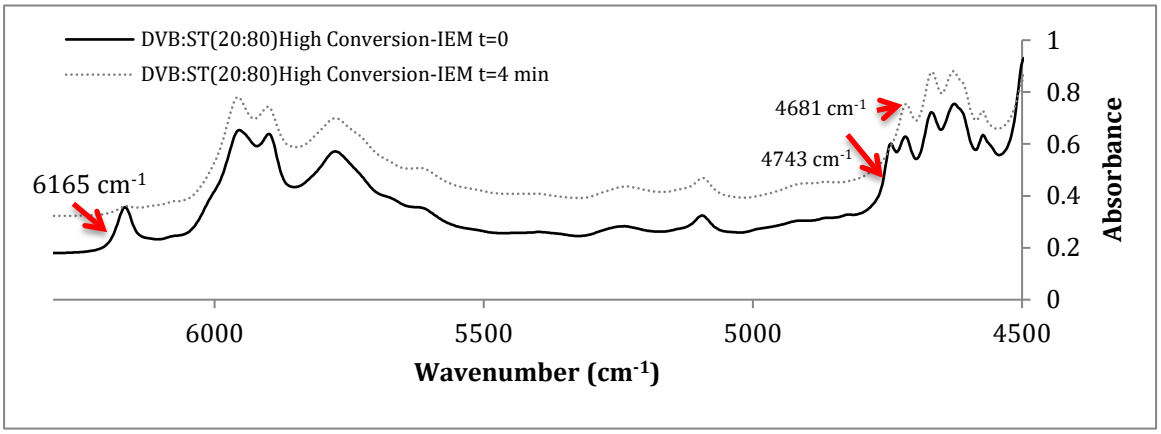

Figure A.16. FTIR spectra of methacrylate functionalized DVB:ST(20:80) nanogel before and after UV exposure shows disappearance of methacrylate C=C peak at 6165 cm^{-1}.

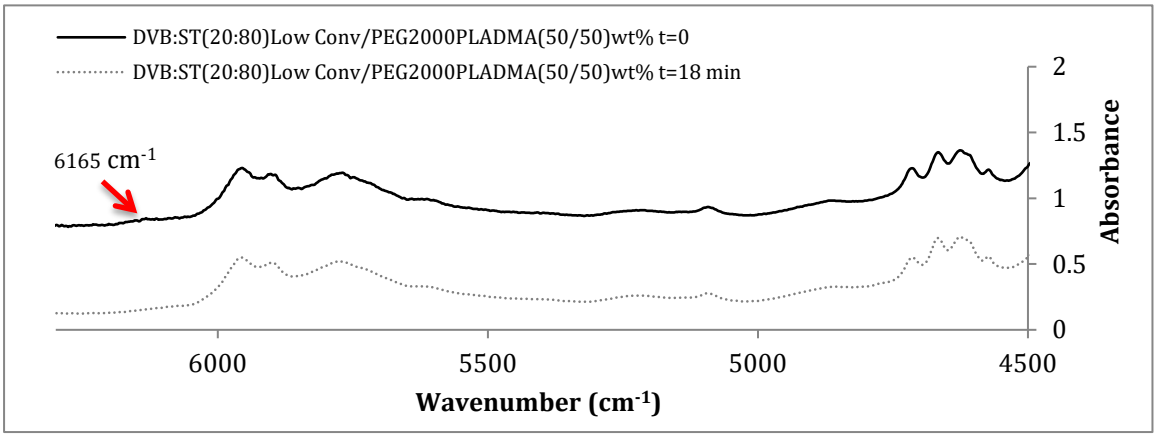

Figure A.17. FTIR spectra of the mixture of low conversion DVB:ST(20:80) and PEG2000PLADMA in 50/50 wt% before and after UV exposure shows the disappearance of methacrylate C=C peak at 6165 cm^{-1} and untouched pendant styrenic C=C peak at 4720 cm^{-1}.